BULETINUL INSTITUTULUI POLITEHNIC DIN IASI

Publicat de
UNIVERSITATEA TEHNICĂ "GH. ASACHI", IAŞI

Tomul LIII (LVII)

Fasc. 3

Secția
ŞTIINȚA ŞI INGINERIA MATERIALELOR

2007

BULETINUL INSTITUTULUI POLITEHNIC DIN IAŞI
BULLETIN OF THE POLYTECHNIC INSTITUTE OF IAŞI
Tomul LIII (LVII) 2007

MATERIALS SCIENCE AND ENGINEERING

CONTENTS	

BULETINUL INSTITUTULUI POLITEHNIC DIN IAŞI
BULLETIN OF THE POLYTECHNIC INSTITUTE OF IAŞI
Tomul LIII (LVII) 2007

STIINTA SI INGINERIA MATERIALELOR

CUPRINS

BULETINUL INSTITUTULUI POLITEHNIC DIN IAŞI
Tomul LIII (LVII), Fasc. 3, 2007
Secția
ŞTIINȚA ŞI INGINERIA MATERIALELOR

IOAN ALEXANDRU SCHOOL FOUNDER AND RESEARCH DIRECTIONS

By

ADRIAN DIMA

Abstract: The paper aims to present in a few words, some of the main achievements of a great professor and researcher, Ioan Alexandru.

Not a long time ago passed away, on February 26TH 2007, Professor Ph.D. Eng. Ioan Alexandru, Corresponding Member of the Romanian Academy of Technical Sciences, remarkable personality of the Romanian science and technique.
He was born on January the 24Th 1943 in Răcăuți, Oneşti, the County of Bacău in a family without enough financiary means.

Between 1949 and 1953 he went to the primary school in Răcăuți Oneşti and between 1953 and 1956 at the gymnasium in Oneşti.

After graduating the high school he was admitted at the Polytechnic Institute of Iaşi, the Faculty of Mechanics, the specialization Technology of Machine Building. He graduated the first, as Chief of promotion in 1969.

Due to this he was kept as teaching assistant at the Chair of Technology of Materials, the Faculty of Mechanics where he worked under the supervision of the Associate Professor Gheorghe Ailincăi, following him at the sustaining of the course of Metals Study. In his career, Ioan Alexandru also taught the disciplines of Materials Science, Study and Technology of Metals, Physical Metallurgy and Heat Treatments, Choice of Metallic Materials, at the faculties of Mechanics and Materials Science and Engineering.

He progressed in the university career step by step, teaching assistant 1969, lecturer 1974, associate professor 1991 and professor 1992.

In 1980 he sustained his Ph.D. thesis "Contributions Concerning the Influence of Heat Treatments at Cryogenic Temperatures of High Alloyed Steels on Their Cutting Properties" elaborated under the scientific direction of Professor Constantin Picoş.

In 2005 he became a Corresponding Member of the Romanian Academy of Technical sciences.

The Professor Ioan Alexandru can be considered the initiator of the implementation into the Romanian industry, starting form 1970, of the cryogenic heat treatments applied to bearing steels and cutting tools steels construction at the Politechnic Institute of Iaşi, a scientific research school, recognized in Europe, China and the USA.

From 1994 when he became adviser for doctoral programs in the field of "Materials Science and Engineering" nine doctors sustained their Ph.D. thesis under his supervision, other fourteen students being in different stages of preparation.

He was also remarked for organizing of courses and post –university schools (Materials and Modern Technologies for Hot Processing 1996, Security and Safety in Labour 2002 and Evaluation of the Risk Level and Labour Security 2004).

His scientific activity was especially rich, consisting in three treatise (one published in Handbook of Residual Stress and Deformation of Steel, Edited by G. Totten, ASM International, The Materials Information Society, Metals Park, Ohio, USA, 2002), four specialty books, 19 university handbooks, 26 articles published in magazines and proceedings from abroad, 74 articles in Romanian technical magazines and about 200 articles in volumes of scientific conferences from Romania, most of them as first or main author.

As recognition of this face of the activity of Professor Ioan Alexandru M.C. of the Romanian Academy of Technical Sciences is the fact that he was member of various scientific associations from Romania and abroad from which one can mention ASM International, Ohio, USA and ASM Heat Treating Society.

He had also leading positions in the Faculty of Materials Science and Engineering, Scientific Secretary of the Board 1996-2000, Vice-Dean 2000-2004 and he was a Member of the Faculty Board. Between 2996-2004 he was also a Member of the Senate of the Technical University "Gh. Asachi" Iaşi.

The activity of the eminent professor was happily completed by a prestigious technical activity: technical director of national and international research projects, responsible and participant at important scientific contracts, technical judiciary expert in metallurgy and expert evaluator of security and safety of labour, economico-financial expert evaluator and expert evaluator CNCSIS and Relansin.

He was also awarded with the gold and silver medal at Inventions Saloons in Brussels, Zagreb, Budapest, being also awarded with the Elite Inventor Order, the Third Class.

Certainly I could not remember here all the prestigious and complex activity, didactical, scientific and technical, developed by the eminent fellow, Professor Ph.D. Eng. Ioan Alexandru, Corresponding Member of the Romanian academy of Technical Sciences but is also certain that he will remain in our memory as an eminent personality of the Materials Science and Engineering School and of the Technical University of Iaşi, school he served with abnegation and devotion until his last seconds in life.

IOAN ALEXANDRU FONDATOR DE SCOALA SI DIRECTII DE CERCETARE

Rezumat: Lucrarea isi propune sa prezinte in cateva cuvinte cateva realizari ale unui mare profesor si cercetator, Ioan Alexandru.

BULETINUL INSTITUTULUI POLITEHNIC DIN IAŞI
Tomul LIII (LVII), Fasc. 3, 2007
Secția
ŞTIINȚA ŞI INGINERIA MATERIALELOR

THE MICROSTRUCTURE INFLUENCE ON THE CORROSION RESISTANCE OF NiCr-BASED DENTAL ALLOYS

BY

D. MARECI[*], GINA UNGUREANU[*], N. AELENEI[*], M.I. POPA[*]
JULIA CLAUDIA MIRZA ROSCA[**]

ABSTRACT. Based on the polarization curves in the case of the five commercial NiCr-based alloys (Wirolloy, Herenium, NicromalSoft, V and VeraSoft) maintained in Ringer´s type solution, it was established the intensity of the corrosion process by means of the corrosion currents value. The passivation of all the samples occurred spontaneously at the open circuit potential. For all the samples currents have values of nA order. Superior corrosion characteristics have the Herenium and Wirolloy alloys with typical dendritic microstructure The VeraSoft, V and NicromalSoft alloys presented a dangerous breakdown.

KEYWORDS: *NiCr based dental alloys, microstructure, corrosion rate, potentiometry*

1.Introduction

For more then a generation in a medicine and dentistry various materials so-called biomaterials are used with a purpose to replace or repair a body feature, tissue, organ or function. The performance of biomaterial in direct contact with living tissue is controlled by two sets of characteristics: biofunctionality and biocompatibility.

When metals and alloys are considered the central aspects of biocompatibility are the corrosion resistance of materials and the influence of corrosion products on surrounding tissue. Their biocompatibility is closely linked to the high resistance towards corrosion which is attributed to the spontaneous formation of the passive oxide film.

The integrity of the oxide film has been strongly correlated with chemical and mechanical stability of metallic materials. In spite of the chemical stability of the alloys, the release of metallic ions into the body tissue occurs by various mechanisms, including: uniform passive dissolution resulting from the slow diffusion of metal ions through the passive film and the local breakdown of the passivity as a consequence of the various types of localized corrosion, or various mechanical events such a fretting corrosion. The potential at which the passive film breaks done (transpassivation) is strictly dependent on both the chemical composition of the oxide-covering layer and the microstructure of the biomaterial.

The most commonly used base metal alloys in dentistry are Ni-Cr and Co-Cr alloys. These materials were currently used for crowns, bridges casting and denture bases. The electrochemical behavior of non-precious alloys such as Ni-Cr alloys was

the subject of a number of prior investigations [1-4]. Utilization of Ni in dental alloys is due to the fact that his properties satisfy the essential wants of dental replacements: corrosion resistance, strong, thin and cheap. The alloys oneself with chromium and cobalt provide the mechanical properties accepted by dentistry. On the other hand, the nickel is recognized as the most carcinogenic metal on Terra. Thus alloys producing nickel ions generate cancer because these ions can be absorbed readily across the cell membranes. In some cases the utilization of low concentration of Cr, up to 11%, is enough, for delaying the attack, due to the formation of a stable passive layer, which covers the alloys surface. Increasing the Cr concentration above 11% increases the corrosion protection but also increases the melting point of the alloy [5, 6]. Addition of nickel improves the protection of the alloy from corrosion in neutral and weakly oxidized media improves the ductile and formalization properties [7].

The present paper made a comparative study of five NiCr-based dental alloys: Herenium (Klutzer, Germany), Wirolloy (Bego, Germany), VeraSoft (Aalba Dent, USA), V (Vaskut, Hungary) and NicromalSoft (IMNR, Romania), regarding the corrosion behaviour in Ringer´s type solution

2. Experimental

2.1. Materials and sample preparation

Five non-precious cast NiCr-based alloys used in dental prosthetics construction were investigated. Their composition is shown in Table 1.

Table 1. Chemical composition of the NiCr-based alloys

Alloy	Main Components (%)
Herenium	59.3Ni 24Cr 10Mo 2Fe 1Nb
Wirolloy	63,5Ni 23Cr 9Fe 3Mo 0,5Mn 1Si
V	72Ni 20Cr 6Fe
VeraSoft	53,6Ni 19,5Mn 14,5Cr9,5Cu 1,6Al 1,5Si
NicromalSoft	64,6Ni 17,8Cr 9,8Cu 3,5Mn 1,8Si 1,5Al 0,5Ti 0,5Fe

The corrosion medium was an aerated Ringer´s type solution having the composition: NaCl – 6.8 g/L, KCl – 0.4 g/L, $CaCl_2$ – 0.2 g/L, $MgSO_47H_2O$ – 0.2 g/L, $Na_2HPO_4H_2O$ – 0.14 g/L, $NaHCO_3$ – 1 g/L, glucose – 1 g/L.

The pH was measured with an multiparameter analyzer CONSORT 831C. The pH of this solution was 6.8.

The electrochemical measurements were made with an assembly of three electrodes: a working electrode, a platinum counter-electrode and a reference electrode of saturated calomel (SCE). The working electrode, made from alloy sample was processed into a cylindrical shape and mounted in a Teflon support. In these conditions the surface exposed to corrosion was a one-dimensional circular surface.
Before experimental tests the samples were mechanically polished with SiC abrasive paper up to a granulation number of 2500, than polished using 1 μm alumina suspension, degreased in ethanol and rinsed with distilled water.

2.2. Microstructural characterisation

To study the microstructure of the alloys their surface was chemically treated in agreement with standard procedures. In this case, the chemical attack was realized with a (10 mL HNO_3 + 20 mL HCl + 30 mL glycerol) solution [8]. The treated surfaces were examined by optical microscopy, with an OLIMPUS PME 3- ADL apparatus.

2.3. Electrochemical measurements

Electrochemical measurements were carried out at 25^0C. All the electrochemical measurements were performed PAR 263 A potentiostat connected with a PAR 5210 lock-in amplifier controlled by PowerCorr software.

After obtained the stable value of E_{OC} (open circuit potential), the samples were subjected to the Stern Geary Tafel tests arranged from E_{OC} –150 mV to E_{OC}+150 mV at a scanning rate of 0.5 mV/s to identify the I_{corr} (corrosion current density). It was followed by the general polarization tests from –600 mV to +1200 mV to evaluate the stability of passivation. From anodic polarization curves the E_{bd} (breakdown potential) was determined.

3. Results and discussion

3.1. Microstructural characterisation

The microstructure of the four NiCr-based alloys after chemical attack is shown in Fig.1-5.

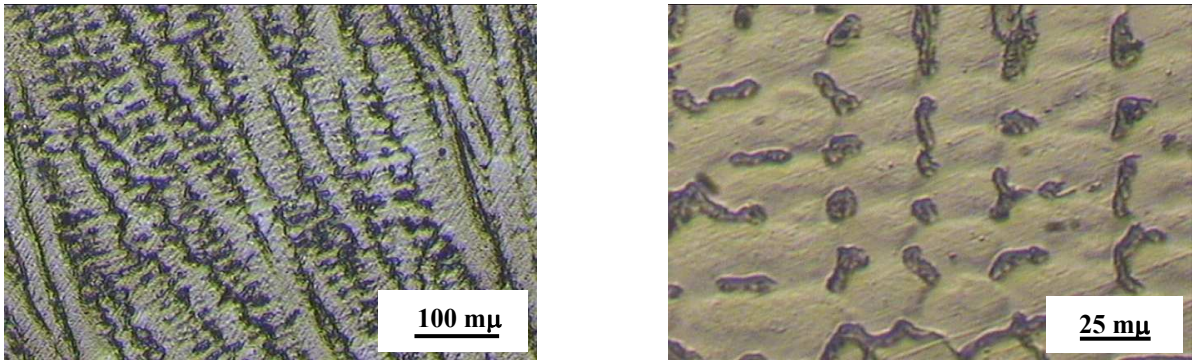

Figure 1. Optical micrographs of as-cast Wirolloy alloy

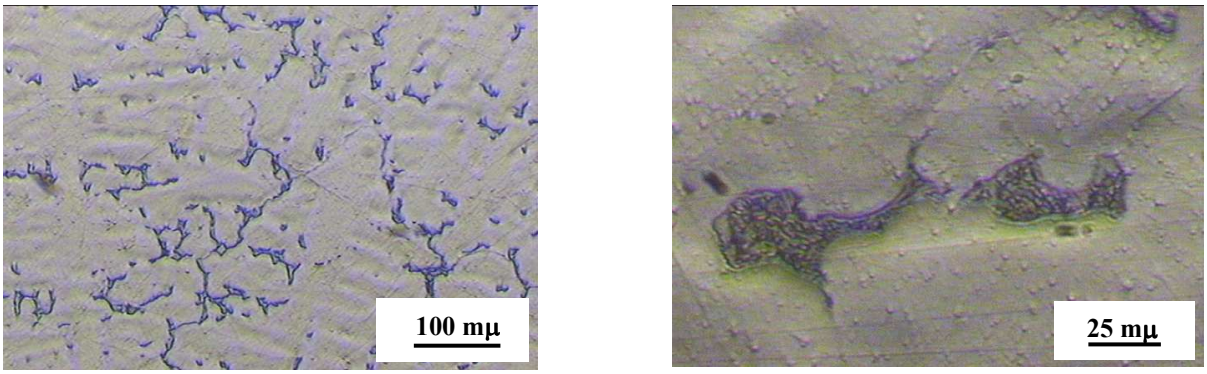

Figure 2. Optical micrographs of as-cast Herenium alloy

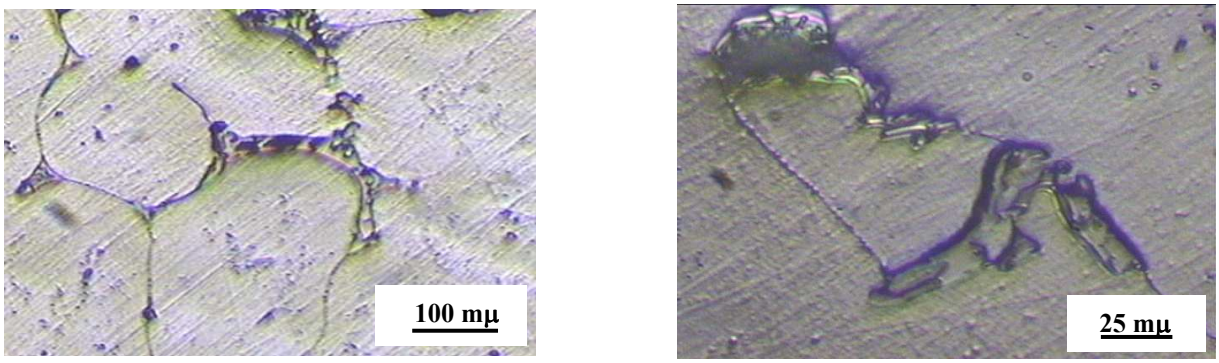

Figure 3. Optical micrographs of as-cast NicromalSoft alloy

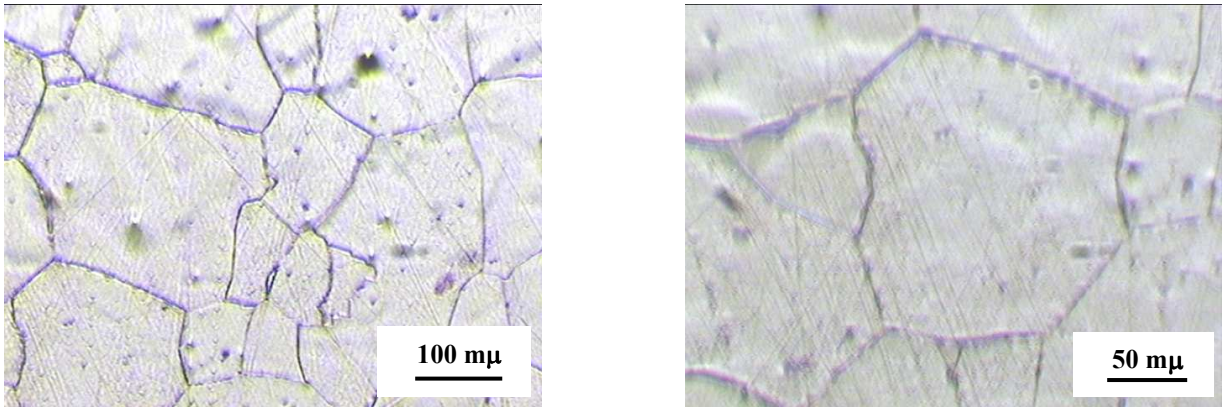

Figure 4. Optical micrographs of as-cast V alloy

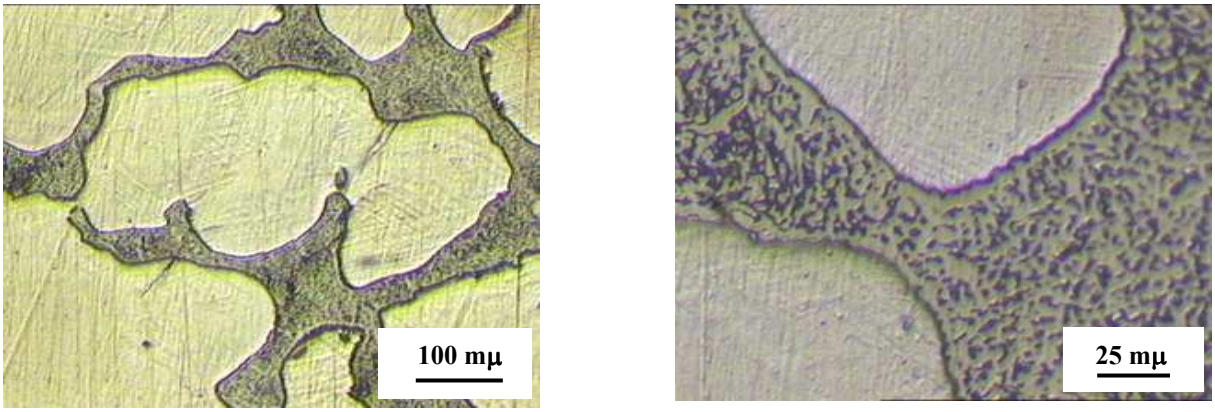

Figure 5. Optical micrographs of as-cast VeraSoft alloy

The Wirolloy cast alloy surface showed a dendritic microstructure, a rippled structure between the matrix and particle phases. Figure 2 show the microstructure of Herenium alloy, which consists of two characteristic phases – dendrites (light) and interdendritic region (dark), as that on Figure 1.

The microstructure of NicromalSoft alloy contains equiaxial grains with interdendritics particles.

V alloy s monophasic and contains only crystals of terminal solid solution with characteristic polyhedral form. The VeraSoft alloy show in Figure 5, islands structure.

The corrosion current (I_{corr}) is representative of the degree of degradation of the alloy. The corrosion currents, show in Table 2, for all the alloys were of the same order of magnitude (nA/cm^2).

Figure 6 shows in linear representation the part of the polarisation curve for all the five alloys in Ringer´s type solution, in the scale of anodic currents comprising between 0 and 500 □A/cm^2. This helps to visualise the breakdown potential E_{bd}, another electrochemical parameter, which characterises the corrosion behaviour of the alloys. The breakdown potential is the potential at which the anodic current strongly increases. The potential range situated between the zero current potential ($E_{(I=0)}$) and the breakdown potential represents the immunity zone in which corrosion is weak or even insignificant. Table 2 presents the values of the breakdown potential.

Table 2. The main parameters of the corrosion process measured and calculated for the various NiCr-based alloy in Ringer´s type solution (25^0)

Alloys	I_{corr} (nA/cm^2)	E_{bd} (mV)
Herenium	184	610
Wirolloy	166	650
V	242	380
NicromalSoft	277	160
VeraSoft	369	80

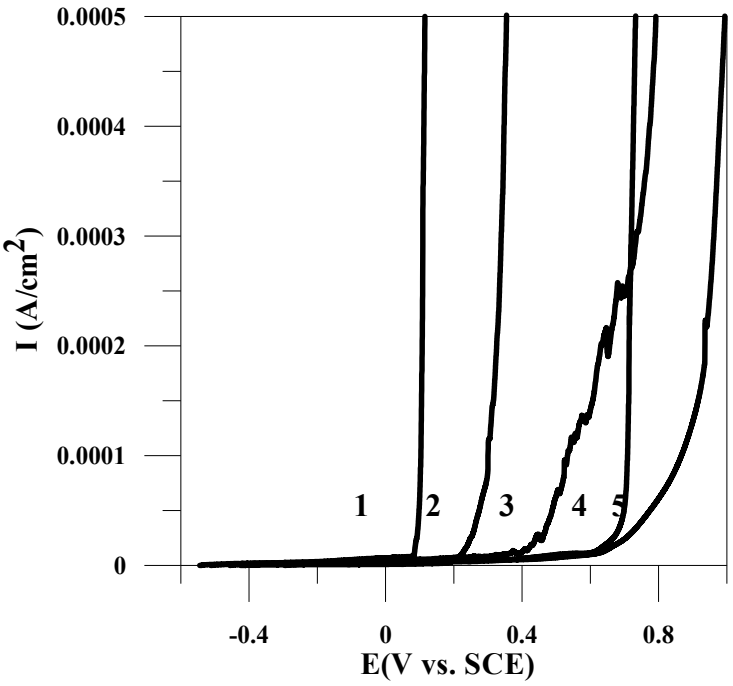

Figure 5. Potentiodynamic polarisation curves presented on linear axes in order to reveal the breakdown potential for NiCr-based alloy in Ringer´s type solution: 1 - VeraSoft alloy, 2 – NicromalSoft alloy, 3- V alloy, 4 – Wirolloy alloy, 5 – Herenium alloy

According to the values of E_{bd}, quite different corrosion behaviour can be attributed to various NiCr-based alloys. E_{bd} of VeraSoft is around 100 mV. The immunity zone is very narrow, implying that corrosion starts from 100 mV. The NicromalSoft reveals a similar behaviour with an E_{bd} smaller, around 150 mV. For the V alloy the E_{bd} is approximately 400 mV. The immunity zone from the Wirolloy alloy extends up to 650 mV. A similar behaviour is revealed by Herenium alloy with an E_{bd} of around 600 mV.

4. Conclusions

In the present study, the corrosion behavior of a five NiCr-based alloys was evaluated by use of electrochemical techniques. The passivation of all the samples occurred spontaneously at the open circuit potential. For all the samples currents have values of nA order. Using metallographic analyses has been established that only Herenium and Wirolloy alloys have dendritic solidification microstructure. For VeraSoft, NicromalSoft and V alloys a very low and dangerous breakdown potential (E_{bd}) values may be recorded. Good corrosion characteristic have only two samples of NiCr-based alloys (Herenium and Wirolloy) with typical dendritic microstructure.

Received, March, 2007

**„Gh. Asachi"Technical University of Iasi,*
*** Las Palmas de Gran CanariaUniversity,*

REFERENCES

1. J.A.Anderson, *Appl. Dent. Materials*, sixth ed., Blackwell Scientific Publications, Oxford, 1985, p. 43.
2. S.Fujimoto, K.Seddik, *Int.Dental J.,* **47**, 543 (2001).
3. M.A.Ameer, E.Khamis, M.Al-Motlaq, *Corr. Sci.,* **46**, 2825 (2004).
4. D.Mareci, Gh.Nemtoi, N.Aelenei, C.Bocanu, *European Cells and Materials*, **10**, 1 (2005).
5. L.N.Johnson, *Int.Dental J.*, **33**, 41 (1983).
6. F.A. Peyton, *Dent. Clinics of North America*, November 1985.
7. J.D. Redmond, K.H. Miska in, *The Basic of Stainless Steels in Chemical Engineering,* K.J. McNaughton, second ed., vol. 1, McGraw-Hill Publishing Co., NY, 1980, p.136.
8. ASM Intermnational, *Metalography and Microstructure Handbook*, USA, vol.**9**, 1992, 435 .

INFLUENTA MICROSTRUCTURII ASUPRA REZISTENTEI LA COROZIUNE A UNOR ALIAJE DENTARE PE BAZA DE NiCr

Rezumat: Pe baza curbele de poalrizare a fost stabilita intensitatea procesului de coroziune in solutie tip Ringer, cu ajutorul curentilor de coroziune in cazul a 5 aliaje dentare comerciale pe baza de NiCr (Wirolloy, Herenium, V, NicromalSoft si VeraSoft). La potentialul in circuit deschis toate cele 5 probe se pasiveaza spontan. Curentii de coroziune inregistrati sunt mici, de ordinul nA. Aliajele Wirolloy si Herenium care prezinta o structura de tip dendritic poseda si o mai buna rezistenta la coroziune. Aliajele VeraSoft, V si NicromalSoft prezinta potentiale de strapungere mici, deci periculoase.

BULETINUL INSTITUTULUI POLITEHNIC DIN IAŞI
Tomul LIII (LVII), Fasc. 3, 2007
Secția
ŞTIINȚA ŞI INGINERIA MATERIALELOR

THE CORROSION OF DENTAL AMALGAM IN ARTIFICIAL SALIVA

BY

D. MARECI[*], GINA UNGUREANU[*], N. AELENEI[*], JULIA CLAUDIA MIRZA ROSCA[**]

ABSTRACT. The object of this study is the electrochemical behavior of a dental amalgam in artificial saliva. The amalgam which was used is made with a spherical, high-cooper powder alloy. After mixing with mercury, it has a mercury-to-alloy ratio of approximately 50% by weight. The open circuit potential (E_{OC}) was measured during 24 hours of immersion; potentiodynamic polarization and electrochemical impedance spectroscopy were performed for corrosion behavior analysis as a function of immersion time. The breakdown potential increases with increasing of the time immersion. The EIS results show that the dental amalgam exhibits passivity at open circuit potential.

KEYWORDS: *dental amalgam*, *corrosion rate, potentiometry, EIS*

1.Introduction

Dental amalgam has been used as a restorative material for the replacement of the decayed tooth structure for more than 150 years [1]. Amalgam is a metallic alloy formed by reaction between mercury and an original alloy in powder form containing silver (40-70%), tin (15-30%), copper (10-30%), and with a very complex metallurgical structure [1]. Mercury diffuses into the alloy particles and reacts with silver, tin and copper forming various compounds. The exact compounds depend on the chemical composition of the powder and on the particle shape but are mainly phases of the system: Eut.–Ag_3Cu_2 , Cu_3Sn, η-Cu_6Sn_5 and Ag-Sn phases remaining from the reactants Ag_3Sn.

A number a factors can influence the rate of the corrosion. These include acidity of the contacting medium and temperature, which can both undergo sharp variations in a short period of time in the oral cavity, as well as the effective potential of the amalgam [2, 3].

Nevertheless, in recent years investigations of amalgam corrosion have become of great interest owing to concern deriving from toxic effects from corrosion products in the oral cavity. A further concern results from the possible release of mercury and mercury vapor [4-7] as well as the effect that mercury can have on antioxidant activity [8] and neurotoxicological activity [9].

Dental amalgam interacts in a complex manner with the oral environments and between the corrosion products can be found: $Sn^{2+} \rightarrow SnO_2$, $Sn_4(OH)_6Cl_2$, $CuCl_2$,

$3Cu(OH)_2$, CuCl and SnO. More, this interaction is subjected to electrochemical, chemical, mechanical, biological and thermal forces [10].

Numerous investigations on the corrosion behavior of the dental amalgams have been carried out using various experimental tests and methods. Nomoto et al. [11] examined the effect of hydrogen ion concentration on the electrochemical behavior of different types of amalgams in hydrochloric acid aqueous solutions. Tsujimura et al. [12] reported on the electrochemical behavior of zinc and tin on the surface of amalgams during setting. Westerhoff et al. [13] compared the corrosion behavior of 16 different commercial amalgams in artificial saliva using cyclic voltammetry. They found that the electrochemical corrosion behavior varied widely over several orders of magnitude in the corrosion medium. Horasawa et al. [14] examined using cyclic voltammetry the effect of the composition of dental amalgams on their electrochemical behavior, including reactions occurring outside of oral conditions. AgCl and Hg_2Cl_2 films were formed on all amalgams except that with only 40 wt % Ag. Lian et al [15] reported the effect of sliding wear on the corrosion behavior of two high-copper dental amalgams. The results showed that sliding wear caused a sharp reduction in the corrosion potential, a significant increase in the corrosion rate and decrease in the repasivation rate of both amalgams. Brett et al [16] have demonstrated the importance of the organic component on the rate of corrosion and adsorption phenomena on the amalgam surface.

Recently Acciari et al.[17] have been examined the corrosion of individual dental amalgam phases under in vitro conditions. The electrochemical behavior of the dental phases in 0.9% NaCl is characteristic for passive system; the mechanism involves the formation of corrosion products which protect metallic surface at lower potentials.

Electrochemical reactions are one of the most important forms of interactions between amalgam restorations and oral fluids. In the oral environment, the dental amalgam fillings corrode and often show extensive degradation, significant localized penetrations and marginal fractures [18, 19].

In this study some electrochemical methods have been used to investigate the behavior in artificial saliva of an amalgam consisting on a high-copper Tytin mixed intimately with liquid mercury (50 % w/w).

2. Experimental

Tytin dental amalgam (KerrDental, USA) was investigated. The powder alloy composition of Tytin is: 69.7% Ag, 17.7% Sn, 12% Cu and 0.9% Zn, with a mercury-to-alloy ratio of approximately 50%.

The corrosion medium was an artificial aerated saliva (Carter-Brugirard AFNOR/NF (French Association of Normalization) having the composition: NaCl – 0.7 g/L, KCl – 1.2 g/L, $Na_2HPO_4H_2O$ – 0.26 g/L, $NaHCO_3$ – 1.5 g/L, KSCN – 0.33 g/L, carbamide – 1.35 g/L, and pH 8.0.

The electrochemical measurements were made with an assembly of three electrodes: a working electrode, a platinum counter-electrode and a reference electrode of saturated calomel (SCE). The working electrode, made from alloy sample was processed into a cylindrical shape and mounted in an epoxy resin support. In

these conditions the surface exposed to corrosion was a one-dimensional circular surface.

Before experimental tests the samples were mechanically polished with SiC abrasive paper up to a granulation number of 2500 followed by an 1 □m alumina suspension, degreased in ethanol and rinsed with distilled water.

Electrochemical measurements were carried out at 25^0C. All the electrochemical measurements were performed with a PAR 263 A potentiostat connected with a PAR 5210 lock-in amplifier. The data acquisition and processing were assigned by PowerCorr software for polarization measurements and ZSimWin software for impedance measurements..

The corrosion process was characterized by several electrochemical parameters:

- The open circuit potential (E_{OC}), recorded for 24 h with the sample immersed in an natural aerated electrolyte.
- Potentiodynamic polarisation curves were registered with a scan rate of 0.5 mV/s in the potential range –600 mV to +1200 mV/SCE.
- Electrochemical impedance spectroscopy (EIS) measurements were carried out at open circuit potential in aerated solutions. The spectra were recorded in the 10^{-2} Hz to 10^5 Hz frequency range. The applied alternating potential signal had amplitude of 10 mV

3. Results and Discussions

Figure 1 shows the variation of open circuit potential (E_{OC}) with time for the amalgam in artificial saliva.

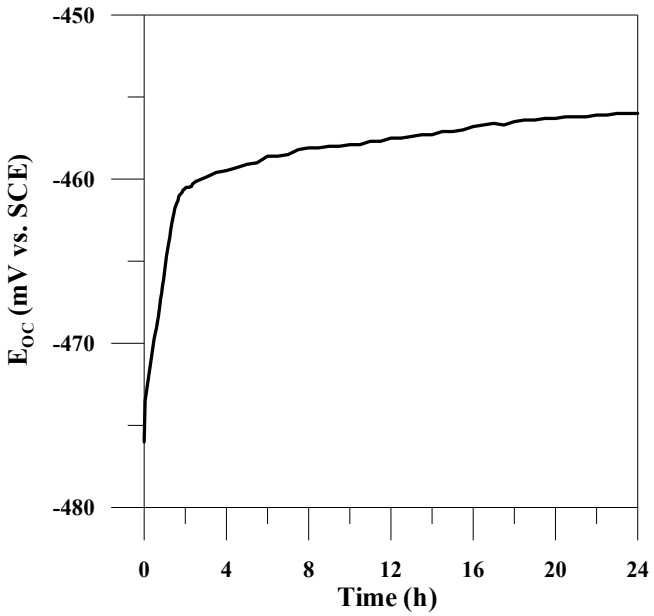

Figure 1. Variation of open circuit potential with time for Tytin dental amalgam immersed in artificial saliva

The sharp variation toward more positive values of potential was recorded during the first minutes of immersion. The change of open circuit potential with time is accompanied by the formation of a film of corrosion products seen by visual inspection and in agreement with other studies [20]. This approach is qualitative and remains insufficient for a complete analysis. More information is necessary from other technique to reach a conclusion concerning this point.

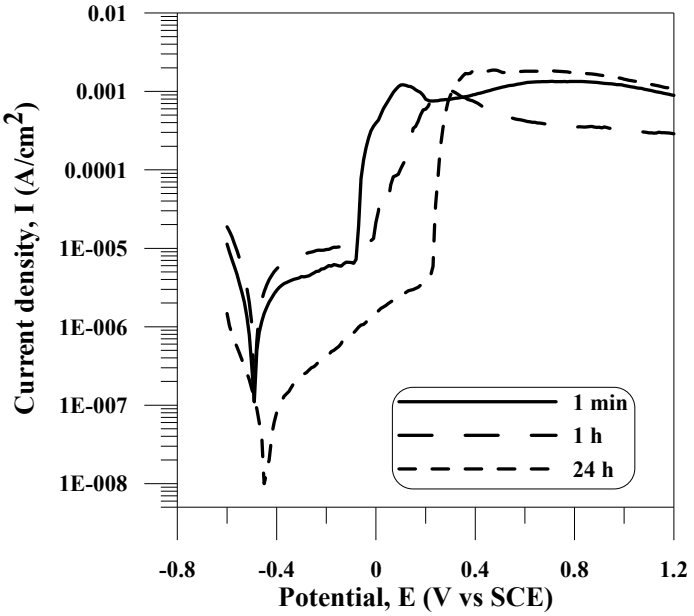

Figure 2. Polarisation curves for Tytin dental amalgam after 1min, 1 hour and 24 hours immersion in artificial saliva

Potentiodynamic polarization curves are shown in Figure 2 recorded after 1 min, 1 hour and 24 hours immersion.

The plot recorded for Tytin dental amalgam after a short immersion time (1 min) in artificial saliva shows a passive zone between potentials –0.4 and –0.1 V vs. SCE, related to the formation of a passive film. Because the Tytin dental amalgam has a complex metallurgical structure the composition of passive film is complex and is due to the: formation of SnO_2 at –0.6 V, formation of SnO at –0.4 V, formation of CuO_2 at –0.1 V, formation of AgCl and Hg_2Cl_2 at 0.2-0.3 V [14].

Up to -0.1 V the anodic current increase and the layer begins to breakdown. The amalgam translates from the "Tafel region" directly into a stable passive behavior without the traditional active-passive transition. After 1 hour of immersion the breakdown potential increase slowly, while after 24 hours immersion the anodic current decrease and the breakdown potential presented a significant increase. After 24 hours immersion is evidenced a relative passivation beginning at –0.35 V and up to 0.2 V. Above + 0.25 V. passive film breakdown take place.

Electrochemical impedance measurements have been performed to improve the understanding of the processes that take place at the amalgam electrode surface as well as the influence of surface oxide.

The experimental impedance data obtained, at E_{OC}, for different times of immersion are presented as Bode plots in Figure 3.

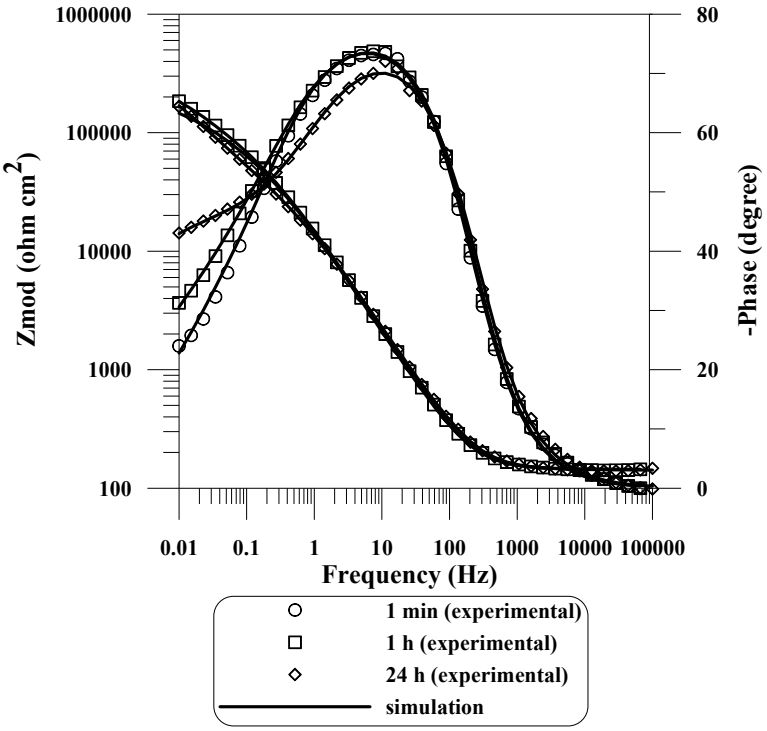

Figure 3. Impedance spectra for Tytin dental amalgam immersed in artificial saliva for various periods of time

The impedance spectra fitting was done with an equivalent circuit (EC) using series combinations of the cell resistance, R_{sol}, with two RC elements in parallel, each composed of a resistance, R, and a constant phase element (CPE) modeled by ZsimWin software as a non-ideal capacitor according to:

$$Z_{CPE} = \frac{1}{Q(j\omega)^n}$$

where Q is the combination of properties related to both the surfaces and electroactive species independent of frequency; n is related to a slope of the lgZ vs lgf Bode–plots; ω is the angular frequency and j is imaginary number ($j^2 = -1$).¨n¨ is an adjustable parameter that usually lies between 0.5 and 1.When the value of n is equal to 1, the CPE describes an ideal capacitor with Q equal to the capacitance (C). For 0.5<n<1 the CPE describes a distribution of dielectric relaxation times in frequency space, and when n is equal to 0.5 the CPE represents a Warburg impedance with diffusional character.

The impedance data were fitted with the EC presented in Figure 4 and the resultant parameters are given in Table 1.

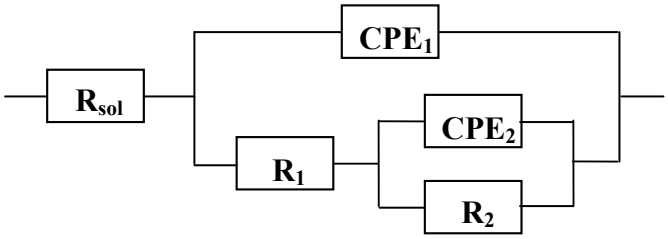

Fig. 4. Equivalent circuit (EC) used in the generation of simulated data

Table 1. Impedance parameters of the dental amalgam in Afnor saliva

R_1 ($K\Omega$ cm^2)	CPE_1 ($S\ cm^{-2}$ s^n)	n_1	R_2 ($K\Omega$ cm^2)	CPE_1 ($S\ cm^{-2}\ s^n$)	n_2
The dental amalgam maintained for 1 min in artificial saliva					
$2.9\ 10^4$	$1.3\ 10^{-5}$	0.87	$1.4\ 10^5$	$2.5\ 10^{-5}$	0.72
The dental amalgam maintained for 1 h in artificial saliva					
$5.6\ 10^4$	$1.2\ 10^{-5}$	0.87	$1.7\ 10^5$	$2.1\ 10^{-5}$	0.72
The dental amalgam maintained for 24 h in artificial saliva					
$6.5\ 10^4$	$1.2\ 10^{-5}$	0.88	$3\ 10^5$	$1.6\ 10^{-5}$	0.76

The physical meaning of the given circuit is the association of the film/electrolyte interface (R_1CPE_1) with the passive film itself (R_2CPE_2). The time constant at high frequencies is originated from the R_1CPE_1 combination while at low frequencies is initiated from the R_2CPE_2 combination. R_1 representing the charge transfer resistance and CPE_1 the double layer capacitance, as shown by the high value of the n_1 exponent. The double layer capacitances for all the samples are typical for the C_{dl} of the passive oxide layers [21-23]. The characteristics of the oxide film are reflected in the values of R_2.

The polarization resistance of the dental amalgam is equal to the sum of the R_1 (R_{ct}) and the passive film resistance, R_2. The same value for electrolyte resistance, R_{sol}, equals $35 \pm 5\ \Omega$, was observed for all of the specimens indifferent the time of immersion and was not inserted in Table 1.

Although the actual value of the dielectric constant within the passive film is difficult to estimate, a change of CPE_2 can be used as indicator of a change in the passive film thickness. Assuming that the dielectric constant does not change with the different parameters under investigation, the reciprocal capacitance of the passive film, $1/CPE_2$, is directly proportional to the thickness of the passive film. The resistance, R_2, and the thickness of the protective passive film, $1/CPE_2$, increase with the increase of the time of immersion indicating a continuous passive film growth with time until a steady state is attained. At short immersion time (1 hour) the difference between behaviors in solution are small.

For the amalgam immersed in artificial saliva the values of n_2 are small, in the range of 0.72-0.76 indicates the presence of a diffusion process within the interfacial layer of the solution. Such a diffusion process indicates a reversible dissolution process; that is, the passive film formation under open circuit condition proceeds through a dissolution-precipitation mechanism [24]. The values of n_2 increase with the increasing of the immersion time because decrease the heterogeneity and roughness of the passive layer [25].

4. Conclusions

In the present study, the electrochemical behavior of a dental amalgam was evaluated by electrochemical techniques. The amalgam translated directly into a stable passive region without exhibiting the traditional active-passive transition. The breakdown potential increases with increasing of the immersion time. The EIS results show that dental amalgam exhibit passivity at open circuit potential.

Received, March, 2007

**„Gh. Asachi"Technical University of Iasi,*
*** Las Palmas de Gran CanariaUniversity*

REFERENCES

1. R.G. Craig, *"Restorative Dental Materials, Mosby"*, St. Louis, USA, 1985.
2. M. Marek, *J. Dent. Res*., **76**, 1308 (1997).
3. M. Marek, *J. Dent. Res*., **72,** 1315 (1993).
4. M. Marek, *J. Dent. Res*., **69**, 1167 (1990).
5. M. Marek, *Dent. Mater*., **13**, 312 (1997).
6. D.B. Mahler, J.D. Adey, L.E. Simms, M. Marek, *Dent. Mater*. **18**, 407 (2002).
7. T. Okabe, B. Elvebak, L. Carrasco, J.L. Ferracane, R.G. Keanini, H. Nakajima, *Dent. Mater*. **19**, 38 (2002).
8. M. Pissichini, M. Fonzi, L. Sugherini, F. Fonzi, A. Gasparoni, M. Comporti, A. Pompella, *Sci. Total Environ.*, **184**, 19 (2002).
9. M. Sweeney, S.L. Creanor, R.A. Smith, R.H. Foye, *J. Dentistry,* **30**, 243 (2002).
10. M. Marek, Adv. *Dent. Res.,* **6,** 100 (1992).
11. S. Nomoto, N. Suzuki, Y. Ohmori, T. Yamaguchi, T. Inoue, *Nihon Univ. Dent. J.,* **60**, 404 (1986).
12. M. Tsujimura, K. Katsumata, T. Machida, A. Ohuchi, H. Honmoto, H. Onose, S. Nomoto, *Nihon Univ. Dent. J,*. **60**, 507 (1986).
13. B. Wasterhoff, M. Darwish, R. Holze, *J. Oral Rehabil,*. **22,** 121 (1995).
14. N. Horasawa, H. Nakajima, J.L. Ferracane, S. Takahashi, T. Okabe, *Dent. Mater,*. **12**, 154 (1996).
15. K. Lian, E.I. Meletis, *Dent. Mater,* **12**, 146 (1996).
16. C.M.A. Brett, I. Ioanitescu, F. Trandafir, *Corros. Sci*., **46**, 2803 (2004)
17. H.A. Acciari, A.C. Guastaldi, C.M.A. Brett, *Corros. Sci.,* **47**, 635 (2005).
18. S. Espevik, I.A. Mjor, *"Degradation of amalgam restorations in vivo. In: B.C. Syrett, A. Acharya editors. Corrosion and Degradation of Implant Materials, ASTM STP 684"*, Philadelphia: 316-327.
19. J.W. Osborne R.D. Norman, E.N. Gale*, Quintessence Int,*. **22**, 857 (1991).
20. H.A. Acciari, A.C. Guastaldi, C.M.A. Brett, *Electrochim. Acta,* **46**, 3887 (2001).
21. Moffat T.P., Latanision R.M., *J Electrochem Soc,* **139**, 1869 (1992).
22. Haupt S, Strehblow HH. *Corros Sci,* **29**, 163 (1989).
23. Castro EB, Vilche JR. *Electrochim Acta,* **38,** 1567 (1993).
24. K.M. Ismail, S.S. El-Egamy, M. Abdelfatah, *J. Appl. Electrochem,* **31,** 663-670 (2001).
25. R.M.Souto, M.Alanjali, *Corr Sci*, **42,** 2201- 2211 (2000) .

COROZIUNEA AMALGAMULUI DENTAR IN SALIVA ARTIFICIALA

Rezumat: Obiectivul acestui studiu a fost comportarea electrochimica a unui amalgam dentar in saliva artificiala.
Amalgamul a fost preparat utilizand un aliaj pulverulend avand granule de forma sferica amestecat cu mercur in proportie de 50%, procente masice. In scopul stabilirii comportarii si evolutiei in timp a coroziunii s-a inregistrat potentialul in circuit deschis timp de 24 de ore si s-au trasat curbele de polarizare potentiodinamica si respectiv spectrele de impedanta. Potentialul de strapungere creste odata cu cresterea timpului de imersare. Spectrele de impedanta indica o pasivare spontana a amlagamului in saliva artificiala la potentialul in circuit deschis.

BULETINUL INSTITUTULUI POLITEHNIC DIN IAŞI
Tomul LIII (LVII), Fasc. 3, 2007
Secția
ŞTIINȚA ŞI INGINERIA MATERIALELOR

THE CREEP BEHAVIOR AT 500^0 C FOR THE PIPE STEEL OLT65

BY

DUMITRU MIHAI, MIHAI STEFAN, ADRIAN DIMA, IBN OMER MOHAMED ABDALLA MOHAMED ABUGUSSAISSA

Abstract: The paper shows the determination of the family of creep curves by an original computer assisted method for the steel OLT 65.
Keywords: creep behavior, steel

1. INTRODUCTION

The use of steels at the construction of some installations from the energetic industry, operated for a long time at high temeperatures, imposes the handling of their behavior in creep conditions.

For designing, achieving and operating in safety conditions such installations there are necessary a great number of experimental tests. A special importance have the long duration mechanical tests, the traction creep testing being the most used. A large spreading in such installations have the pipe steels, among which is the OLT 65.

2. METHODOLOGY FOR ESTABLISHING THE FUNCTION OF A FAMILY OF CREEP CURVES

For describing the evolution in time of the accumulation of plastic deformation at constant temperature and constant tension it is proposed a function as follows:

$$\varepsilon_{plastic}(t) = Q.t + M\left(1 - e^{N.t}\right) \quad (1)$$

In which :

$\varepsilon_{plastic}$ - is the plastic specific deformation;

t - time;

Q,M,N coefficients that depend on material, tension and temperature.

The values of the coefficients Q,M,N can be determined on the basis of experimental results, by applying the methods of least squares. For this purpose it was used a calculus program. Making creep tests for several injitial tensions σ_i (at least four values), one can obtainthe functions:

$$\varepsilon_{i\ plastic}(t) = Q_i.t + M_i\left(1 - e^{N_i.t}\right) \quad (2)$$

In view of establishing a function for the creep family curves one extrapolates the results obtained for the corfficients Q_i,M_i,N_i .

$$\varepsilon_{plastic}(t) = Q.t + M\left(1 - e^{N.t}\right)$$

This relation represents the equation of a surface generatioted by the creep curves at the T temperature. By developing in Mac- Laurin series one gets:

$$e^{-N.t} = 1 - \frac{N.t}{1!} + \frac{(Nt)^2}{2!} - \frac{(N.t)^3}{3!} + ... + \frac{(-1)^n}{n!}(N.t)^n + R_n \quad (3)$$

$$\varepsilon_{plastic}(t) = A_0 + A_1.t + A_2.t^2 + A_3.t^3 + A_4.t^4 + A_5.t^5 + A_6.t^6 + A_7.t^7 \quad (4)$$

The specific plastic deformation can be computed with the relations (1) and (4), from the graphs it results they are convergent.

3. The determination of the function of the family of creep curves for the steel OLC65 at 500^0 C

The chemical composition of the studied steel, determined by the spectral method with a spectrometer, Quantovac type is shown in table 1.

Table 1. The chemical composition of OLC 65 steel

OLT 65	C %	Si %	Mn %	P% max	S % max
STAS 791-80	0,40-0,50	0,22-0,40	0,60-0,90	0,045	0,045
Sample	0,45	0,31	0,81	0,036	0,021

For the determination of the mechanical characteristics there have been made traction teste at the temperature of 20^0 C and 500^0 C. Teste were made according to the prescriptions from the standards SR EN 10002-1994 for testing at environment temperature and SR EN 10002-5 - 1995 for testing at high temperatures. The results are given in table 2.

Table 2. Mechanical properties

Material	Temperature [^{0} C]	$R_{p\,02}$ [MPa]	R_m [MPa]	$A_{11,3}$ [%]
OLT 65	20	380	650	17
	500	210	525	30

For the creep tests there were used samples having the shape and the sizes foreseen in STAS 6596-81 and there were conducted on a MF -300 installation.

The heating of the sample was achieved by using an electric furnace, the temperature being measured with three termocouples Pt – PtRh. The maintaining and the regulation of the temperature were done with an electronic regulator that ensures the nominal testing temperature with an accuracy of $\pm 2^0 C$ during the whole testing period.

The measyrement of the deformations (elongations) was done with a mechanic extensometer that ensures a precision of 1μm. There were done creep tests at the following tensions: 200 MPa, 300 MPa , 350 MPa and 400 Mpa. The results of these tests are shown in figure 1.

One can see the creep rate enhances very much at tensions bigger than 400 MPa.

The tests made at tensions of 430 MPa and 500 MPa were done until breaking. The breaking ellongations A_n and the creep necking Z, as well as the duration until breaking t_R are given in table 3 .

Tensiunea [MPa]	t_R [min]	A_n [%]	Z [%]
430	300	30	78
500	25	20	65

There were obtained the following creep curves: for $\sigma = 200 MPa$

ORIGIN = 1

$$y := \begin{pmatrix} 0 \\ 0.517\cdot10^{-3} \\ 0.812\cdot10^{-3} \\ 1.1\cdot10^{-3} \\ 1.25\cdot10^{-3} \\ 1.31\cdot10^{-3} \\ 1.517\cdot10^{-3} \\ 1.613\cdot10^{-3} \\ 1.755\cdot10^{-3} \\ 1.875\cdot10^{-3} \\ 2.145\cdot10^{-3} \\ 2.235\cdot10^{-3} \\ 2.355\cdot10^{-3} \end{pmatrix} \qquad x := \begin{pmatrix} 0 \\ 0.833 \\ 1.66 \\ 2.5 \\ 3.33 \\ 4.166 \\ 5 \\ 5.83 \\ 6.66 \\ 7.5 \\ 8.33 \\ 9.66 \\ 10 \end{pmatrix}$$

n := length(x)

m := 7

$i := 1 .. n$

$k := 1 .. 2 \cdot m + 1$

$$s_k := \sum_i \left(x_i\right)^{k-1}$$

$k := 1 .. m + 1$

$$b_k := \sum_i \left[\left(y_i\right) \cdot \left(x_i\right)^{k-1}\right]$$

$i := 1 .. m + 1$

$j := 1 .. m + 1$

$a_{i,j} := s_{i+j-1}$

$c := a^{-1} \cdot b$

$$c = \begin{pmatrix} 1.402 \times 10^{-8} \\ 8.294 \times 10^{-4} \\ -3.506 \times 10^{-4} \\ 1.405 \times 10^{-4} \\ -3.74 \times 10^{-5} \\ 5.619 \times 10^{-6} \\ -4.251 \times 10^{-7} \\ 1.257 \times 10^{-8} \end{pmatrix}$$

$$t := 0, 0.0687 .. 10$$

$$k(t) := 1.402 \times 10^{-8} + 8.294 \times 10^{-4} \cdot t - 3.506 \times 10^{-4} \cdot t^2$$

$$v(t) := 1.405 \cdot 10^{-4} \cdot t^3 - 3.74 \cdot 10^{-5} \cdot t^4 + 5.619 \cdot 10^{-6} \cdot t^5$$

$$m(t) := -4.251 \cdot 10^{-7} \cdot t^6 + 1.257 \cdot 10^{-8} \cdot t^7 \qquad w(t) := k(t) + v(t) + m(t)$$

$$C := 1.01869818391696$$

$$B := 0.71818189703541$$

$$A := 0.160557301681765$$

$$q(t) := A \cdot t + B \cdot \left(1 - e^{-C \cdot t}\right)$$

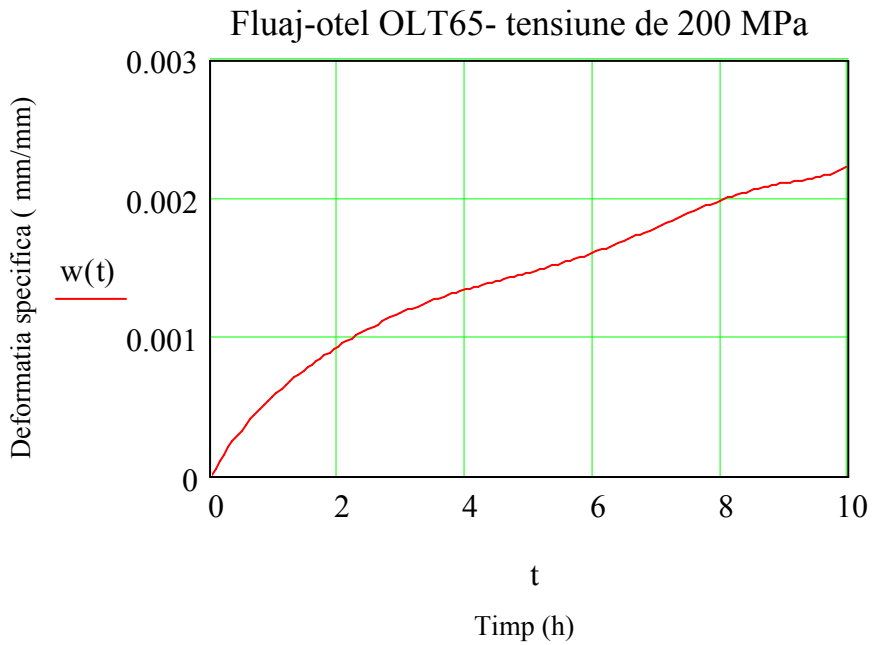

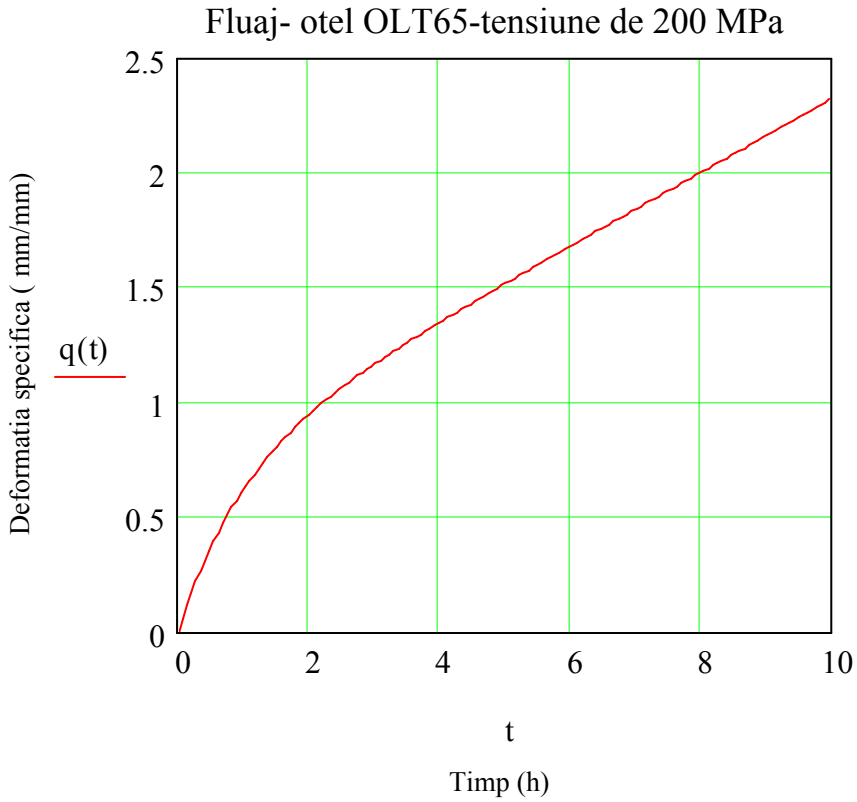

- for $\sigma = 300MPa$ ORIGIN ≡ 1

$$y := \begin{pmatrix} 0 \\ 1.915 \cdot 10^{-3} \\ 1.965 \cdot 10^{-3} \\ 2.01 \cdot 10^{-3} \\ 2.55 \cdot 10^{-3} \\ 2.74 \cdot 10^{-3} \\ 3.08 \cdot 10^{-3} \\ 3.75 \cdot 10^{-3} \\ 4.254 \cdot 10^{-3} \\ 4.74 \cdot 10^{-3} \\ 5.75 \cdot 10^{-3} \\ 5.88 \cdot 10^{-3} \\ 6.714 \cdot 10^{-3} \end{pmatrix} \qquad x := \begin{pmatrix} 0 \\ 0.833 \\ 1.66 \\ 2.5 \\ 3.33 \\ 4.166 \\ 5 \\ 5.83 \\ 6.66 \\ 7.5 \\ 8.33 \\ 9.66 \\ 10 \end{pmatrix}$$

n := length(x) m := 7

$i := 1 .. n$

$k := 1 .. 2 \cdot m + 1$

$$s_k := \sum_i \left(x_i\right)^{k-1}$$

$k := 1 .. m + 1$

$$b_k := \sum_i \left[\left(y_i\right) \cdot \left(x_i\right)^{k-1}\right]$$

$i := 1 .. m + 1$

$j := 1 .. m + 1$

$a_{i,j} := s_{i+j-1}$

$c := a^{-1} \cdot b$

$$c = \begin{pmatrix} -2.155 \times 10^{-6} \\ 5.328 \times 10^{-3} \\ -5.394 \times 10^{-3} \\ 2.624 \times 10^{-3} \\ -6.664 \times 10^{-4} \\ 9.165 \times 10^{-5} \\ -6.439 \times 10^{-6} \\ 1.807 \times 10^{-7} \end{pmatrix}$$

$$t := 0, 0.0687 .. 10$$

$$o(t) := -2.155 \times 10^{-6} + 5.328 \times 10^{-3} \cdot t - 5.394 \times 10^{-3} \cdot t^2$$

$$s(t) := 2.624 \cdot 10^{-3} \cdot t^3 - 6.664 \cdot 10^{-4} \cdot t^4 + 9.165 \cdot 10^{-5} \cdot t^5$$

$$k(t) := -6.439 \cdot 10^{-6} \cdot t^6 + 1.807 \cdot 10^{-7} \cdot t^7$$

$$w(t) := o(t) + s(t) + k(t)$$

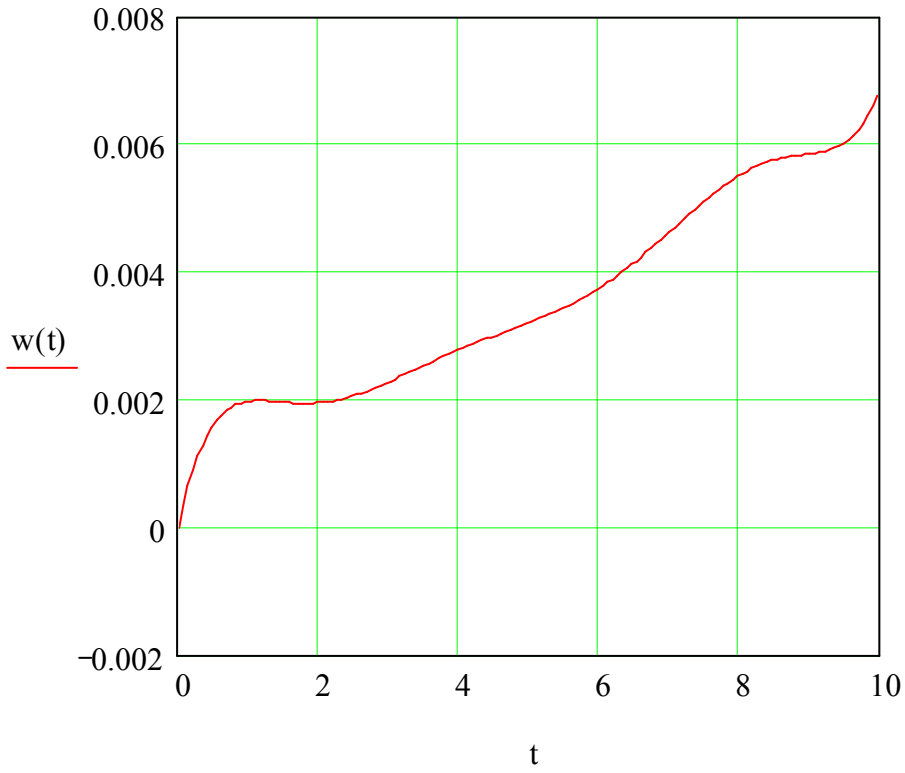

$A := 0.00053794697$

$B := 0.000841268161$ $C := 885.468079897335$

$q(t) := A \cdot t + B \cdot \left(1 - e^{-C \cdot t}\right)$

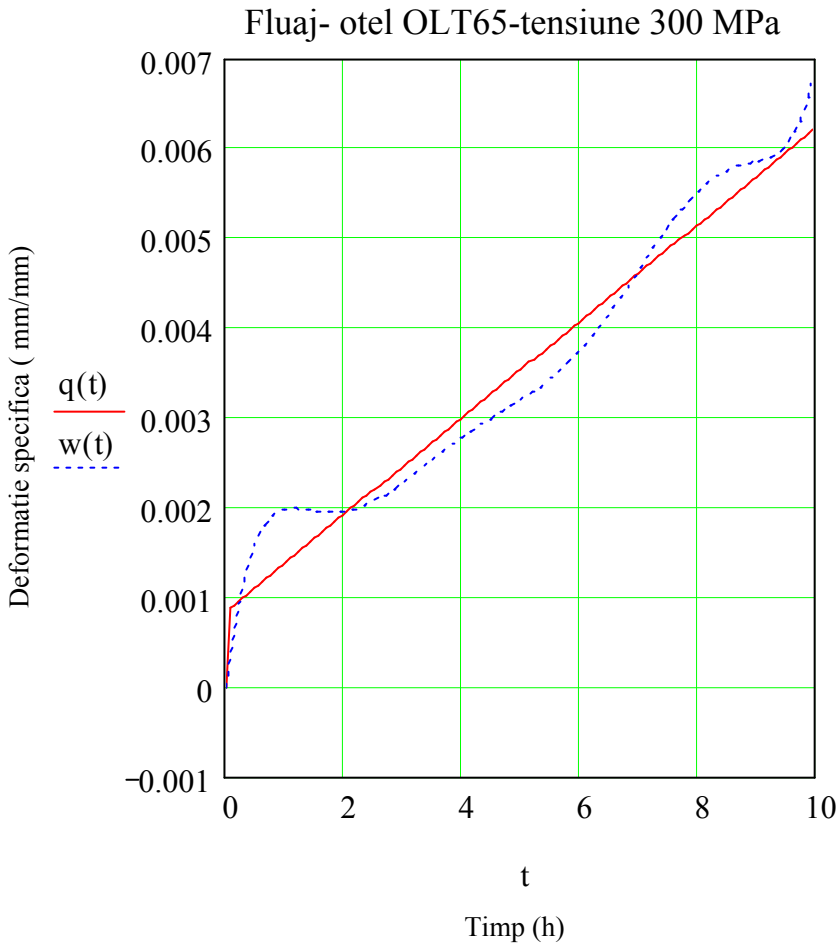

- for $\sigma = 350MPa$

ORIGIN ≡ 1

n := length(x)

m := 7

$i := 1 .. n$

$k := 1 .. 2 \cdot m + 1$

$$s_k := \sum_i (x_i)^{k-1}$$

$k := 1 .. m + 1$

$$b_k := \sum_i \left[(y_i) \cdot (x_i)^{k-1} \right]$$

$i := 1 .. m + 1$

$j := 1 .. m + 1$

$a_{i,j} := s_{i+j-1}$

$c := a^{-1} \cdot b$

$$y := \begin{pmatrix} 0 \\ 2.16 \cdot 10^{-3} \\ 2.87 \cdot 10^{-3} \\ 3.45 \cdot 10^{-3} \\ 3.96 \cdot 10^{-3} \\ 4.65 \cdot 10^{-3} \\ 5.17 \cdot 10^{-3} \\ 5.74 \cdot 10^{-3} \\ 6.01 \cdot 10^{-3} \\ 6.781 \cdot 10^{-3} \\ 7.02 \cdot 10^{-3} \\ 7.85 \cdot 10^{-3} \\ 8.22 \cdot 10^{-3} \end{pmatrix} \qquad x := \begin{pmatrix} 0 \\ 0.833 \\ 1.66 \\ 2.5 \\ 3.33 \\ 4.166 \\ 5 \\ 5.83 \\ 6.66 \\ 7.5 \\ 8.33 \\ 9.66 \\ 10 \end{pmatrix}$$

$$c = \begin{pmatrix} -1.508 \times 10^{-7} \\ 4.457 \times 10^{-3} \\ -3.138 \times 10^{-3} \\ 1.299 \times 10^{-3} \\ -2.93 \times 10^{-4} \\ 3.663 \times 10^{-5} \\ -2.387 \times 10^{-6} \\ 6.328 \times 10^{-8} \end{pmatrix}$$

$$t := 0, 0.0687 .. 10$$

$$o(t) := -1.508 \cdot 10^{-7} + 4.457 \cdot 10^{-3} \cdot t - 3.138 \cdot 10^{-3} \cdot t^2$$

$$r(t) := 1.299 \cdot 10^{-3} \cdot t^3 - 2.93 \cdot 10^{-4} \cdot t^4 + 3.663 \cdot 10^{-5} \cdot t^5$$

$$p(t) := -2.387 \cdot 10^{-6} \cdot t^6 + 6.328 \cdot 10^{-8} \cdot t^7$$

$$w(t) := o(t) + r(t) + p(t)$$

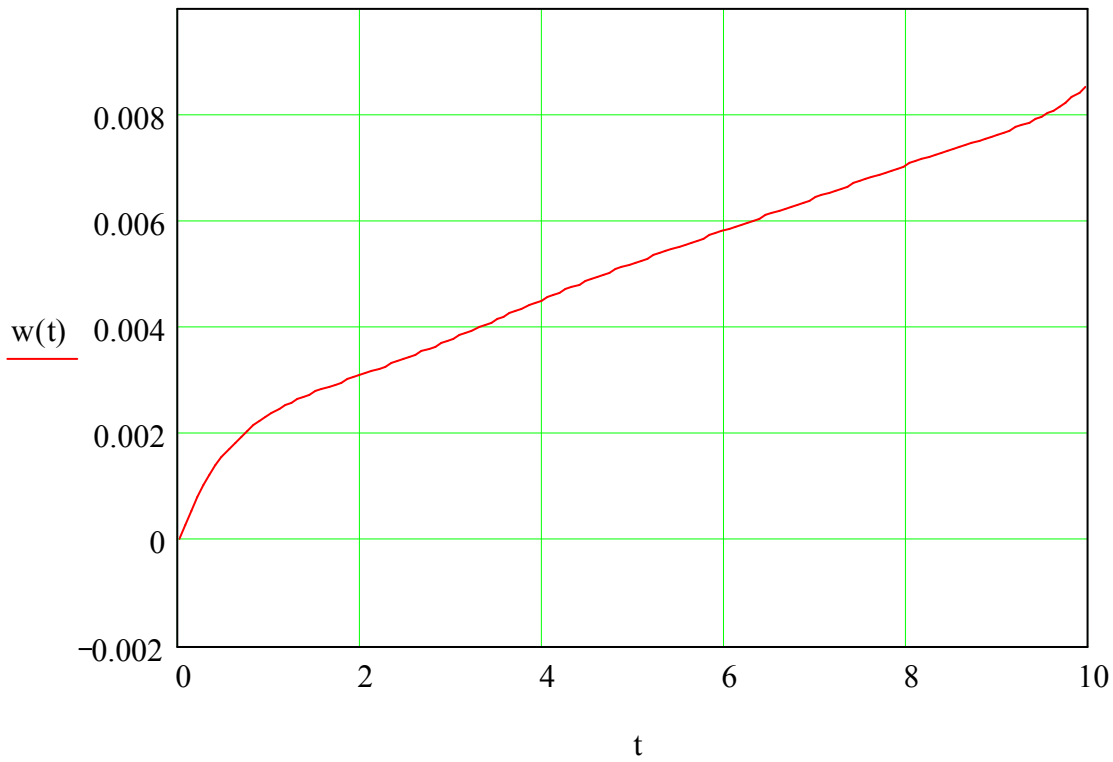

$$A := 6.186070742381458 \cdot 10^{-4}$$

$$B := 1.98724584918986 \cdot 10^{-3}$$

$$C := 1.98887859733945$$

$$q(t) := A \cdot t + B \cdot \left(1 - e^{-C \cdot t}\right)$$

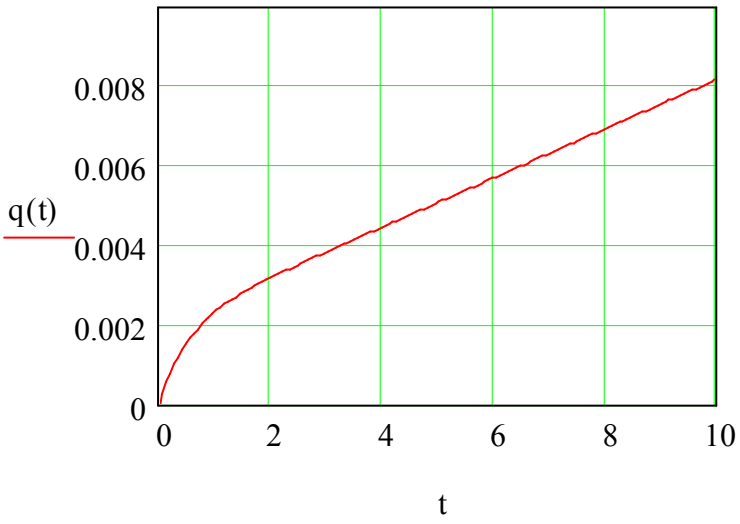

Fluaj- otel OLT65 - tensiune de 350MPa

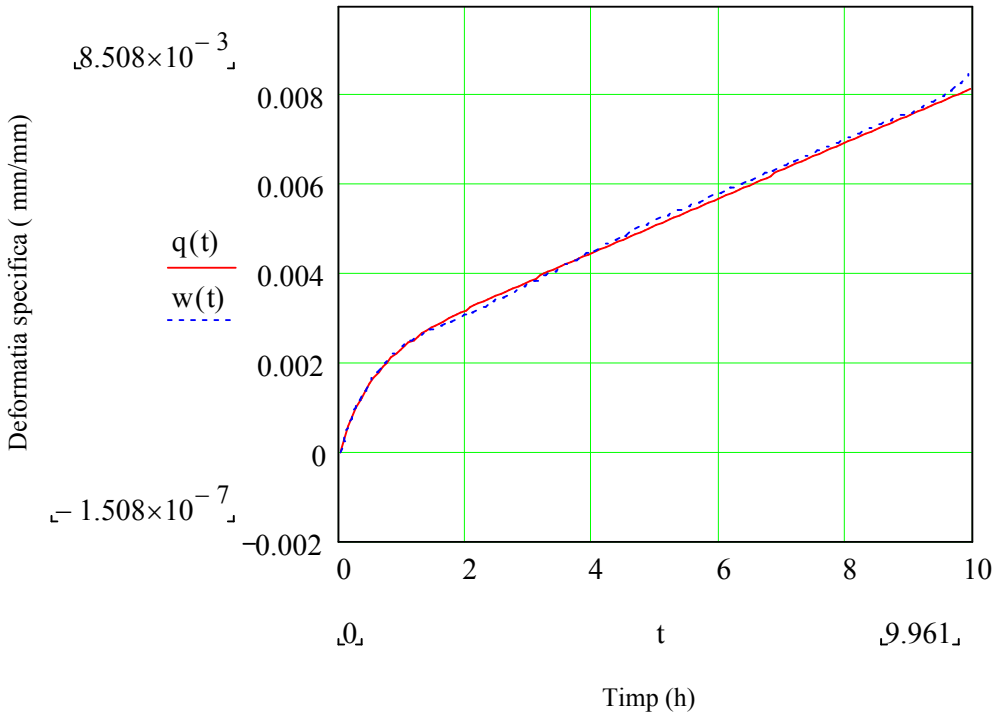

ORIGIN ≡ 1 - for - $\sigma = 400MPa$

$$y := \begin{pmatrix} 0 \\ 3.25\cdot10^{-3} \\ 4.01\cdot10^{-3} \\ 5.021\cdot10^{-3} \\ 6.21\cdot10^{-3} \\ 6.85\cdot10^{-3} \\ 7.21\cdot10^{-3} \\ 8.09\cdot10^{-3} \\ 8.75\cdot10^{-3} \\ 9.21\cdot10^{-3} \\ 10.415\cdot10^{-3} \\ 11.09\cdot10^{-3} \\ 12.75\cdot10^{-3} \end{pmatrix} \qquad x := \begin{pmatrix} 0 \\ 0.833 \\ 1.66 \\ 2.5 \\ 3.33 \\ 4.166 \\ 5 \\ 5.83 \\ 6.66 \\ 7.5 \\ 8.33 \\ 9.66 \\ 10 \end{pmatrix}$$

n := length(x)

m := 7

$i := 1 .. n$

$k := 1 .. 2 \cdot m + 1$

$$s_k := \sum_i (x_i)^{k-1}$$

$k := 1 .. m + 1$

$$b_k := \sum_i \left[(y_i) \cdot (x_i)^{k-1} \right]$$

$$c = \begin{pmatrix} 5.12 \times 10^{-6} \\ 7.748 \times 10^{-3} \\ -7.069 \times 10^{-3} \\ 3.586 \times 10^{-3} \\ -9.526 \times 10^{-4} \\ 1.353 \times 10^{-4} \\ -9.732 \times 10^{-6} \\ 2.784 \times 10^{-7} \end{pmatrix}$$

$i := 1 .. m + 1$

$j := 1 .. m + 1$

$a_{i,j} := s_{i+j-1}$

$c := a^{-1} \cdot b$

$$t := 0, 0.0687 .. 10$$

$$o(t) := 5.12 \cdot 10^{-6} + 7.748 \cdot 10^{-3} \cdot t - 7.069 \cdot 10^{-3} \cdot t^2$$

$$r(t) := 3.586 \cdot 10^{-3} \cdot t^3 - 9.526 \cdot 10^{-4} \cdot t^4 + 1.353 \cdot 10^{-4} \cdot t^5$$

$$p(t) := -9.732 \cdot 10^{-6} \cdot t^6 + 2.784 \cdot 10^{-7} \cdot t^7$$

$$w(t) := o(t) + r(t) + p(t)$$

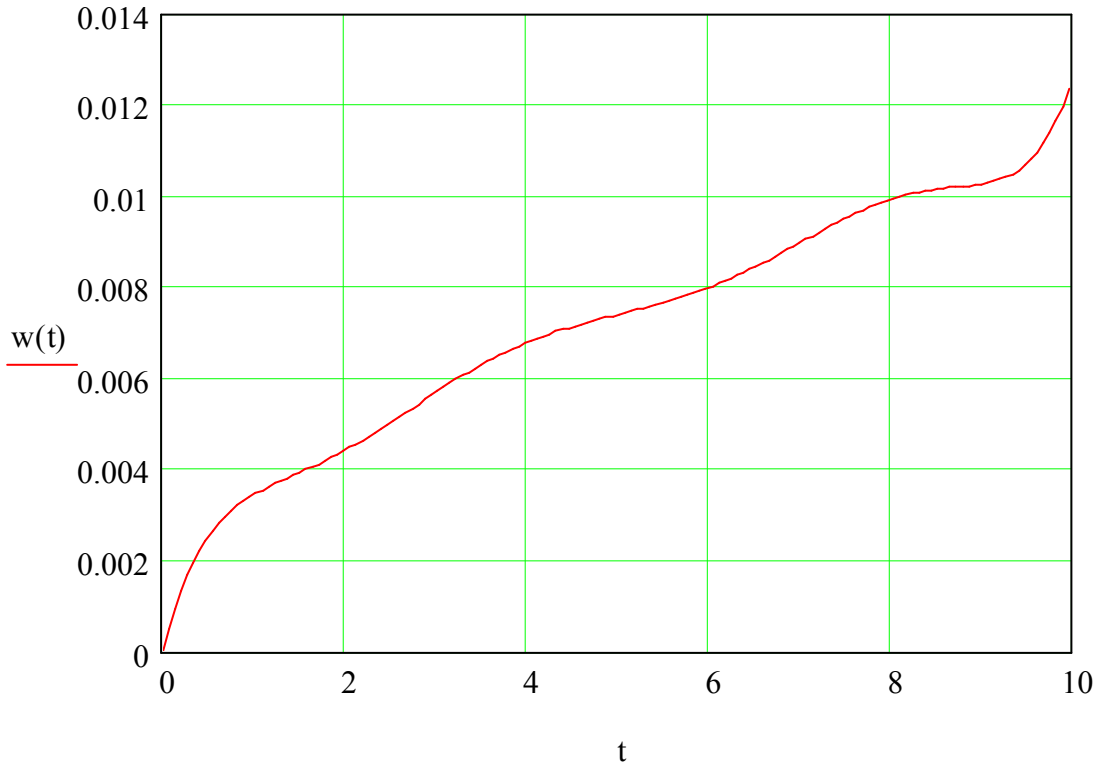

$$A := 9.18181095969481 \cdot 10^{-4}$$

$$B := 2.75960035783241 \cdot 10^{-3}$$

$$C := 2.55192973012929$$

$$q(t) := A \cdot t + B \cdot \left(1 - e^{-C \cdot t}\right)$$

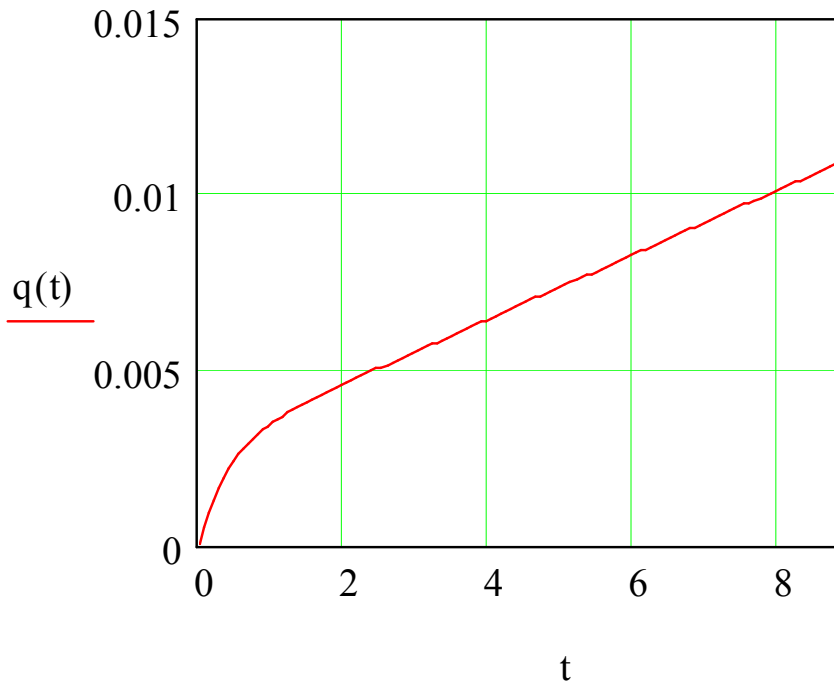

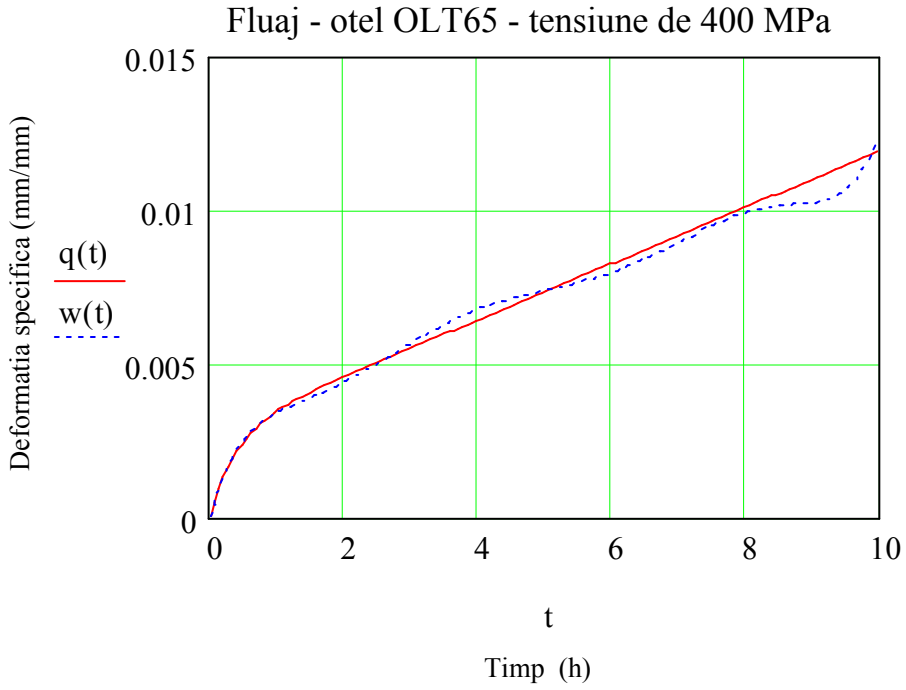

4. CONCLUSIONS

The methodology shown is especially useful for establishing a function of the family of creep curves at a certain temperature, by making a restrained number of tests.

Having in view the lack of experimental data reffering to the creep behavior of the pipe steels it is necessary to extent it to other steel brands and temperatures reccomanded for thermal plants.

REFERENCES

1. Constantinescu, A., Rothenstein, B., Lascu-Simion, N., Fluajul metalelor, Ed. Tehnica, Bucuresti, 1970
2. Mocanu, D.R.,s.a., Incercarea materialelor, vol. 1, Ed. Tehnica, Bucuresti, 1982
3. Vernon, J., Testing of Materials, McMillan Publishing House, London, 1992
4. Mihai, D., The Influence of the exposure Temperature and Time on Some Pipe Steels Used for Live Steam transport, European Journal of Mechanical and Environmental Engineering, vol. 46, nr.3, 2001, p.185, Bruxelles, Belgium
5. Mihai, D., Fiabilitatea conductelor din otel 15123 utilizate la transportul aburului viu in termocentrale, Cercetari metalurgice, Vol. IX, nr. 3, 2001

Received, Merch, 2007 Technical University „Gh. Asachi" Iasi

COMPORTAREA LA FLUAJ LA 500^0 C A OTELULUI OLT65

Rezumat: Lucrarea prezinta determinarea familiei curbelor de fluaj pentru otelul OLT 65 printr-o metoda originala, asistata de computer.

BULETINUL INSTITUTULUI POLITEHNIC DIN IAŞI
Tomul LIII (LVII), Fasc. 3, 2007
Secția
ŞTIINȚA ŞI INGINERIA MATERIALELOR

INTEGRATION OF OPERATIONAL, HEALTH AND SAFETY RISKS USING FLOW DIAGRAMS

BY

PAUL ALEXANDRU * AND SYLVIE NADEAU *

Abstract: In this article we present the developments of an instrument describing the existing socio-relational structure in autonomous and general-purpose work in uncertain environments and the implications of this structure as for the ergonomic risks and occupational safety. A socio-relational structure is described. We can note, from the literature and our design, that the experience of the workers, as well as the structure of the working team are strong indicators of health and safety risks. A preliminary validation of our model was made from observations in the case of the furniture moving industry in Quebec, Canada. A better integration and harmonization of the work organization, the type of supervision, the allocation of tasks between the workers and the type of relations established with the customer are necessary for a good prevention of the health hazards and occupational safety. The results of our study find applications in the residential and commercial removal organizations and should influence the operational, tactical and strategic decisions of the stakeholders.

Key words: integration, work teams, furniture moving industry

1. Introduction

In a working team consisting of several individuals, one finds workers more or else experimented and specialized, able to carry out simple to complex tasks and containing different degrees of health and safety risks. The risky situations are more numerous when the tasks are complex. In complex teams, the coordination of an administrator (foreman) is necessary. In teams consisting of two (2) or three (3) members only, it is the autonomy which outdoes. The teamwork, the interaction between the team-mates, the coordination between the fellow members of the team, the communication between them, the determination of whom will accomplish which task, the information on the risks and the accident prevention activities are essential elements in autonomous and general-purpose work in uncertain environments. To decrease fatigue, in a complex team of more than three (3) members, a rotation of task responsibility, respecting the capacities of the workers, their skills and the difficulty of the tasks, is planned. To avoid the accumulation of fatigue, micro-breaks, breaks and days off are planned to control the physical workload and the painfulness of the work.

2. Methodology

A case study of the 2001s estimates at 51 % the accidents recorded in the residential and commercial removal organizations (Nadeau, 2001).

In the province of Quebec (Canada), the demands of compensation for year 1998 to the Occupational Health and Safety Board (Commission de la santé et de la sécurité du travail – CSST) increased, globally, by 28 % (Allaire and Ricard, 1999). By this study, we want to validate a model integrating socio-relational structure in autonomous and general-purpose work, operations management, ergonomics and occupational prevention within the framework of this service sector. Firstly, we analyze the socio-relations of the working teams and their impacts on occupational accidents. Semi-steered interviews and direct observations of teams in action allowed us to collect the information necessary for our analysis. We then used influence diagrams and a hierarchical organization of the occupational risks identified to do our analysis.

3. Results

During the observations made in moving firms, we were able to notice that the distribution, the assignment and the division of the tasks is an important dimension of the teamwork. We were also able to note that this dimension influences the constraint of the work, notably the driving requirements of this type of service: the speed of execution of the work and the capacity to respond correctly to the requirements of the customer.

Speed is a very important factor in the fulfillment of the tasks and one of the requirements of the customer. The rhythm of work is always imposed by the administrator (foreman), generally the most experimented removal man. He takes into account the complexity of the task (dimensional characteristics of the space, furniture and their variability), the risk of wounds and the minimization of the fatigue of his team-mates. A very high working speed, in particular in certain conditions (staircases, between floors, on the banister towards the truck) is forbidden by the regulations of the administrator (foreman). This rule insures a certain occupational safety (reduction musculoskeletal injuries).

The working method for a complex team is also generally defined by the administrator (foreman). He takes into account the removal reality, the effective capacity and the aptitudes of the members of the team. The most experimented workers will firstly be consulted on this distribution, assignment and division of tasks, then the opinion of the other employees will be listened to.

The risks factors of this type of work are presented in table 1. The major risks are linked to the position the worker has to take to move the loads, to transport the loads in the space and to share the handling of loads with a partner. Some loads are complex to handle, the regularity and the dimensions of the loads vary, fatigue is accumulated, unpredictable situations are common as for errors in the execution of the tasks and in the choice of the most adequate method of handling.

Table 1: Risks factors in the residential and commercial removal sector

Risks linked to the space, loads and environment	**Risks linked to the relations with the customer**
Inadequate exterior steps ✓ the first step is commonly called "the death step'' ✓ ice, water or snow may be found on the steps ✓ some staircases do not respect Quebec's building code **Building in construction** ✓ materials may be found all over the space ✓ some staircases remain unfinished **Space architecture** ✓ some staircases are in spiral or very tight, making it almost impossible to tilt the loads in the space ✓ it is sometimes necessary to use the balconies, the emergency staircases, the windows to handle the furniture, because the doors are too small **Furniture difficult to handle (Refrigerators, marble tables, pianos, curiosity cases, etc,)** ✓ some furniture must be handle with partners ✓ the dimensions, weight or fragility of some furniture pose visibility and communication problems **Environment** ✓ Temperature (cold or hot) and humidity have an influence on the constraint of work	✓ Customer's address is unknown or not clear ✓ The truck loading didn't respect the unloading requirements of the customer ✓ Customer's invoicing is not right ✓ The relationships between the team-mates or between the team and the customer are not good ✓ Pieces of furniture must be dismantled, the team discovers it on the spot, the tools needed for disassembly are not on hand ✓ The customer interacts with the team-mates, wanting to help, but simply confuses the team-mates
The human body parts that are most exposed to the risks of wounds, according to several removers are*:*	
- Back pain; - Musculoskeletal injuries of the upper or lower limbs - Finger and hand wounds (cuts, bruises, etc) - Feet wounds	

3.2 Influence diagram

The integration of the socio-relational structure in autonomous and general-purpose work, operations management, ergonomics and occupational prevention supposes the use of asymmetric information.

In this context, the use of a tool as the influence diagrams has several advantages compared with more traditional tools (e.g. decision trees, valuation network, sequential decision diagrams) (Bielza and Shenoy, 1999). Here are some elements which give it these advantages:

- ✓ its representation is compact and qualitative;
- ✓ its understanding is simple;
- ✓ it is a pragmatic tool;
- ✓ the underlying quantitative evaluation of the variables is included by the arrows representing the flow of influence;
- ✓ it is a good communication tool;
- ✓ it is flexible in the treatment of the variables;
- ✓ the representation of uncertainty is possible;
- ✓ it is useful in the context of conditional probability.

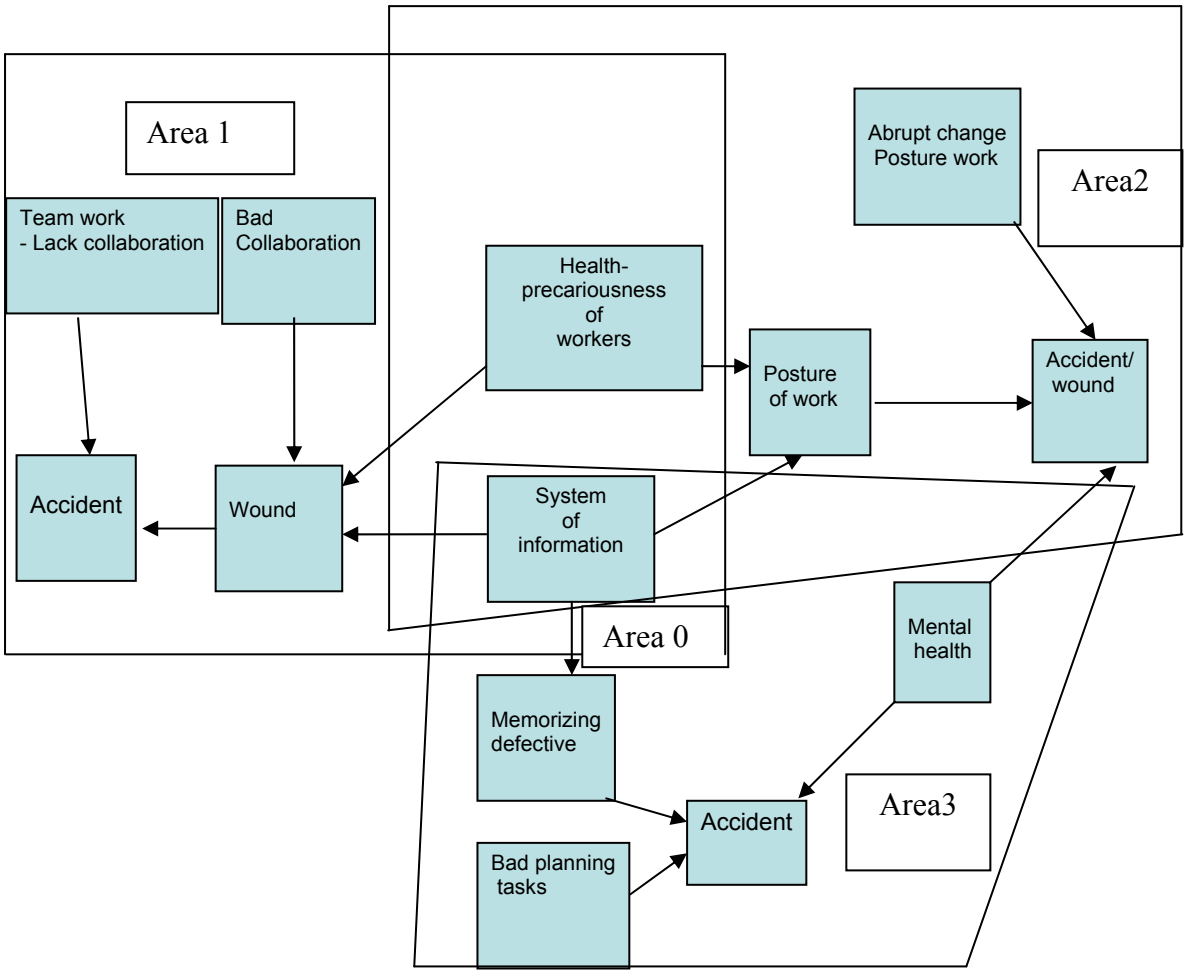

Figure.2. Influence diagram - the case of residential and commercial removal organizations (P. Alexandru, 2005).

The influence diagram (Bernard and Aubert, on 2004) is useful in identifying the interactions between elements of a system. This tool establishes the links between the piloting sub-system and the operational sub-system by putting in evidence the risks inherent in the system.

The influence diagram establishes a balanced relation between the decision variables, the unpredictable variables, the parameters and the general variables, by facilitating the determination of the marginal effects.

The risks which intervene are structured according to several levels of sophistication:

- ✓ Level 0: identification of the events; at this level it is necessary to choose all the risks, positive, or negative which are considered.
- ✓ Level 1: identification of the worst event; the identification of the worst event is made by the clear delimitation of the elements of risks in touch with the positive factors.
- ✓ Level 2: identification of the quasi-worst event
- ✓ Level 3: the estimation of the most likely event is made by a clear identification following the determination of events.

The estimation of all the scenarios, the probabilities and the uncertainties are made for the levels which integrate all the variables.

Sphere of influences (1, 2, 3) present each of the risks and the links in the same family of risks. An interaction between the families of risks is also presented.

3.3. Case study in organization 1

The service was delivered by an enlarged team of seven (7) workers. The loads to be handled were very different: school furniture, boxes, household apparels. The space, doors and staircases allowed a normal progress of the service without any supplementary measures. Part of the unloading of the moving truck was made possible using one of the rooms of the day-care center. This measure, as well as the use of trolleys for the transport of boxes, led to a considerable decrease of the efforts and the risks of wounds for the workers.

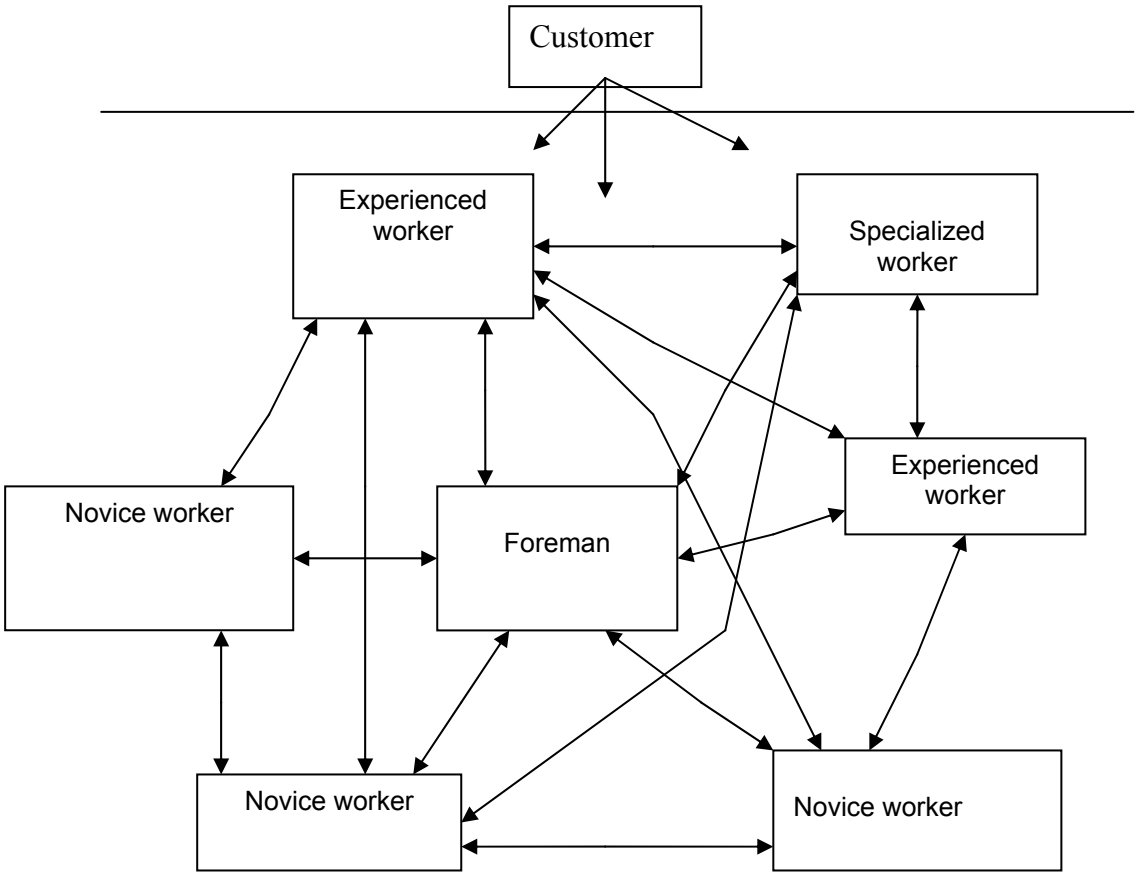

Figure 3: Socio-relational structure case study 1

Three (3) trucks, specific equipments to go up staircases and transport heavy loads, protection equipments for the handling of furniture were used. A socio-relational structure expressing the spheres of influence between the team-mates is proposed.

The administrator (foreman) is in direct relation with all the members of the team. With the experimented removal man (highly autonomous and versatile), they communicate concerning

- ✓ Operation orders
- ✓ Health and safety orders
- ✓ Information taking
- ✓ Task reassignment

With the specialized removal man (highly autonomous and versatile, specialization is needed in highly uncertain environments), they communicate concerning

- ✓ Specialized operation orders
- ✓ Health and safety orders
- ✓ Information taking
- ✓ Task reassignment

With the other removal men (autonomous, novice and low versatility), they communicate concerning

- ✓ Limited operations orders
- ✓ Detailed health and safety orders
- ✓ Precise information on the task

4. Discussion

In this context, one could say that there are privileged relations and relations with a high risk. In our diagram, there are several centers of influence. The balance which must be created, is based on the reduction of the levels of risks by experience. Our proposition at this level is to reduce the risk by increasing the influence of the administrator (foreman) and the experienced or specialized removal men. The sum and the average of the risks, in our case are influenced by the direct relation with the customer.

The supplementary information concerning the service serves for reducing the operational risks. At the same time, the new unexpected requirements of the customer may change the operational procedure, the working time, the organization of the tasks, the planned rotation of tasks, increase stress and uncertainties during the service.

It is necessary to have a good communication between the administrator (foreman), the team-mates and the customer. It is the condition which allows to keep the other parameters stable, to assure the balance of the system in case of uncertain situations of psychological or physical nature.

For the administrator (foreman), the systematic approach must be very well mastered to realize this synergy at the operational level. The risks result from the outside more often than from the inside of the system.

5. Conclusion

Several ideas were pulled from this campaign:

- ✓ the lack of qualified workers is a great problem in this sector;
- ✓ the use of specialized teams in specific situations is absolutely necessary to decrease the risks of health and safety;
- ✓ stress must be minimized;
- ✓ communication and socio-relations must be facilitated;
- ✓ the relation with the customer must be simplified by the administrator (foreman) and maintained by the workers;
- ✓ Work must be reorganized continuously.

6. Acknowledgements

This work was made possible by an NSERC grant and the collaboration of several organizations of the residential and commercial removal industry.

References

1. A. Aubert Benoit, Bernard Jean-Gregoire Bernard, 2003, *Mesure intégrée de risque dans les organisations,* CIRANO, Les Presses de l'Université de Montréal.
2. Alexandru, P. et Nadeau, S. ,2004, *Intégration des aspects de santé et de sécurité à la gestion des opérations dans le travail autonome et polyvalent en environnement incertain*, Congrès 2005 de l'AQHSST (17 to 19 mai 2005, Saint-Hyacinthe, Québec).
3. Alexandru, P. et Nadeau, S., 2005, *Modèle interrelationnel pour l'intégration des aspects de santé et de sécurité à la gestion des opérations dans le travail autonome et polyvalent,* Buletinul Institutului Politehnic din lasi, Tomul L (LIV), Fasc. 3-4. Sectia Stiinta Si Ingineria Materialelor
4. Bernard Jean –Gregoire, A. Aubert, Benoit, 2002, *Le risque: un modèle conceptuel d'intégration*, Rapport de projet, CIRANO Montréal, Canada.
5. Boreham, N., sept. 1999, *Models for the Analysis of Work Competence: A Critical Review*. Paper Presented at the European Conference on Educational Research, Lahti, Finland.
6. Boyer, R., Freyssenet, M., 1993-1999, *The World that Change the Machine*. Synthesis of GERPISA Research Programs.
7. Engstrom, T., Jonsson, D., 1996, *Alternatives to line assembly : Some Swedish examples*. International Journal of Industrial Ergonomics 17 (p 235-245)
8. Toulouse, G., Archer K. M., Imbeau, D. et Nastasia, U., 2002, *Etudes de faisabilité visant à intégrer l'ergonomie et la santé et sécurité à une démarche d'amélioration de la production*, 25e Congrès de l'AQHSST.
9. Y.Q.Liu, Y.P.Shen, Y.W.Chen, F.Gao, 2004, *The Integrated Process of Project Risk Management Based on Influence Diagrams*, International Engineering Management Conference 2004.

CONSIDERATIILE DE INTEGRARE A RISCURILOR DE MUNCA UTILIZAND DIAGRAMA DE FLUX

Rezumat : *Prin acest articol vizam gasirea unui instrument ce permite explicarea structurilor socio-relationale existente pentru munca autonoma si polivalenta si implicatiile stucturii acestor relatii asupra riscurilor ergonomice si de securitate a muncii. Preocuparile pentru o mai buna integrare a conceptelor organizarii muncii, supervizarea, repartitia sarcinilor si relatia cu clientul sunt premize pentru identificarea riscurilor sanatatii si securitatii muncii.*

Validarea demersului stiintific este realizata prin sinteza observatiilor de teren – in cazul afectiunilor din industria demenajarilor prin utilizarea ca instrument a diagramei de infuenta cu centrele aferente dezvoltate. O structura socio-relationala este descrisa in urma unui studiu de caz efectuat. Aspecte ce privesc interactuneia corelationala si experienta constituie principalele elemente ce determina conexiunile modelului nostru, considerand in acelasi timp proiectia si structura muncii pentru echipa de lucru.

Rezultatele exercitiului nostru se regasesc ca aplicabilitate in industria demenajarilor comerciale si rezidentiale la nivel operational si cu infuenta asupra deciziilor tactice si strategice ale supervizorilor.

BULETINUL INSTITUTULUI POLITEHNIC DIN IAŞI
Tomul LIII (LVII), Fasc. 3, 2007
Secția
ŞTIINȚA ŞI INGINERIA MATERIALELOR

THE EFFECT OF MECHANICAL VIBRATIONS APPLIED DURING SOLIDIFICATION OF CASTED ALLOYS

BY

GELU BARBU

Abstract: It is known that at casting of metallic materials, a positive effect is brought about by the presence of vibrations applied on the bath of liquid alloy. The methods of producing vibrations are different, being used mechanic, pneumatic, hydraulic and electric vibrators.

The mechanic vibrators can be provided with a translation element or by a rotating masses, the latter being used for large forces and at frequencies under 60 Hz.

Aluminum-Silicon and Aluminum-Copper alloys are important non-ferrous casting alloys. Different methods have been applied to improve their casting characteristics, their microstructure and consequently, their mechanical properties. Application of mechanical vibrations to the mold during solidification of the alloy is one of these methods.

This work presents the main results obtained by using vibrations, on global scale.
Keywords: solidification of casted alloys, vibrations

1. Vibrations

Vibration is the motion of the particles of an elastic body or medium in alternately opposite directions from the position of equilibrium, periodically in time.

When the vibrations are beying applied, a series of physical processes appear, like the action of count forces, the mass macroscopic transfer, cavitation phenomena, the amplification of the overcooling degree and the changing of the conditions of solid-fluid equilibrium. Thus, shearing forces appear, which act on the growing dendrits, at the solid-fluid severance limit. The macroscopical mass transfer depends on the correlation between the amplitude and the frequency of the movement, the crystalls which belong to the moving fluid will come into collision with the branch of the dendrits in the braxket, resullting a breaking effort τ_r, given by the relation:

$$\tau_r = \frac{1}{2}\rho_c W^2$$

In which ρ_c is the density of the crystals and W – the speed of the fluid.

The displacement of the alloy acomplishes in flowing regime given by the Reynolds criterion, in the expression interviening the amplitude and the casting frequency. When the relative speed between the fluid and the crystals is bigger than a critical speed, the cavitation phenomenon appears.

After the destruction of the cavitation bubble, the gases from the interior of it commpresses itself almoust adiabatic. The performing implosion is attended by an important rising of the local pressure, which may have as an impact the crashing of the crystals current growing.

But the possibility that at high amplitudes of the vibrating movements also exists, and also, to appear voids in the casted material and splashes at the exterior surface.

The mechanic-physical treatments, applied to the alloys in liquid state intensifies the vibration in the limitation layers, which conduces towards collateral currents, changes the hydrodynamical situation at the limit between the solidified layer and the walls of the shape, so it changes the conditions of the heat convector transfer and the macroscopical mass transfer; thus, the speed grows and the solidification time reduces.

The vibrations influence the superficial tension between the phasels (solid-liquid) in the purpose to reduce it, to conduce to the shrinking of the minimum radius of the nucleuses on which these do not remelt but they follow a development process.

The propitious effect on the appearance on the solid phase owes to the conglomerate processes of the subcritical germs and the activation of the heterogeneous surfaces.

Among the technological effects of the application of the vibrations at solidification: the homogenization and the finishing of the solidification structure, the amplification of the compactication of the casted material, the degasing of the alloy, the shrinking of the segregations, the expulsion of unmetallic inclusions and the increase of the capacity of yielding alloy.

It is known that through vibration, while solidification of the metallic material structure it finishes, by finishing obtaining and emending some mechanic-physic properties.

Pillai et. al. have published an extensive survey of the different methods of vibrations used on solidifying metals and their effect on the final structure (1).

Table 1 presents a summary of their survey.

Table 1. Literature survey on the use of vibrations on solidifying metals

	Aluminum Alloy	Source of Vibration	Effect of vibrations
1	Al	Ultrasonic	Degassing
2	Pure Al	Rectilinear vibrations by transforming rotary motion of a DC motor, 100 cycles/min (2Hz)	Grain refinement Reduction in pipe formation Reduced solidification time
3	Eutectic Al-Si alloy	Low frequency vibration	Coarsening of Mg and Na modified alloy Refinement of Sr modified eutectic Si
4	Al-Si alloys. AK9(hypo) and AK11 (eutectic)	Electromagnetic stirring (EM) during continuous casting	Lower porosity by the factor of 3 Higher UTS and % elongation Modified eutectic only in EM mold without modifier addition
5	Al-20Si	Low frequency	Melt agitation Significant reduction in gas content

6	Hypoeutectic Al7Si hypereutectic Al20Si	Electromagnetic stirring	Reduction in Si segregation in hypereutectic alloy Promotion of dendrite fragmentation in hypoeutectic alloy Reduced axial porosity and hence sound core of the ingot
7	Al-Ti, Al alloy, Al- Si alloy, Al-Cu alloy	Vigorous agitation of mould Vibration to the dies	Formation of fine grains Grain refinement Improved surface finish Reproduction of thin sections Dispersion of porosity and oxides Coarsening of secondary precipitating phases Segregation due to constitutional under cooling not prevented
8	Light alloy (500 kg of Al)	Ultrasonic vibration	Improves degasification Reduced degassing time of a few minutes with scavenging cum vibration against 30 min with scavenging alone Suppression of pipe Reduction in hot tearing tendency Reduction in porosity and shrinkage concentration in a spot Reduction in gravity segregation $FeAl_3$
9	Al-8.5Si-1,75Cu-0,35Mg-0,4Mn-0,55Fe	Ultrasonic at 990K	Increased hardness with decreased fluctuations in different parts of die cast parts Formation of homogeneous fine structures of _and _+Si phases Enhancement in density 0,001-0,01 g/cm^3
10	Al alloys	Magnetic field/passing AC through the melt	Grain refinement
11	Continuous cast AI-Zn-Mg-Cu ingot	Ultrasonic	Grain refinement Decreased hydrogen especially with low Fe content alloys
12	AK9 Al casting	Ultrasonic 20 KHz Ti alloy emitter immersed inside the melt at 1013K	Maximum enhancement in mechanical properties after 10 min of treatment UTS increases from 164 to 181Mpa % Elongation increases from 2,8 to 3,1 Reduction in H_2 content and size of oxide inclusions by a factor 1,5 and 3

13	Al-5Mg	Electromagnetic	field Reduced diffusion layer thickness in front of the solidification front Increased concentration of alloying elements in solid solution Decreased volume of non equilibrium eutectics Refinement of dendritic microstructure and fine distribution of non equilibrium eutectic phases
14	Al-6/11/15Cu	Mechanical vibration	Refinement and uniform distribution of primary Al Primary grains contact/connect each other forming a complicated inter twist morphology Improvement in tensile strength with increasing amplitude of Vibration
15	Al alloy	Combined effect of internal variable magnetic field and passing of AC through the molten metal	Refinement of structure Dispersion of inclusions Elimination of modifier addition
16	Al alloy with Zr oddition	Ultrasonic treatment during continuous casting	Formation of sub dendritic grains (0,1 mm) against coarser grains (0,8-1,5 mm) without treatment to enhanced plasticity
17	Al-5Mg Al-4,5%Cu	Electromagnetic generator at 30 and 150 Hz. 0,05-5,52 mm amplitude 1-120 g peak acceleration	Extensive grain refinement especially with high accelerations
18	Al-4,5Cu	Rectilinear vibration by transforming rotary motion of a DC motor, 100cycles./min (2Hz)	Elimination of most of the shrinkage Grain refinement occurs but similar to pure Al, rapid initially and slower later Reduced solidification time Si and Fe phases become less acicular
19	Al 12,3Si	Varying frequencies of 15 – 41,7 Hz and amplitude of 0,125-0,5 mm With increasing vibration time	Increasing frequency and amplitude resulted in grain refinement and reduced pipe Coarsening of eutectic silicon in unmodified and sodium modified Coarsening of primary silicon

Forced vibrations can be applied to a melt via a variety of methods including ultrasonic, electromagnetic, and mechanical methods.

2. Ultrasonic Vibrations

A number of researchers haves used ultrasonic vibrations for melt treatment.

The effect of ultrasonic treatment on light alloys is summarized by Eskin (2,3) . Works of various researchers demonstrate that ultrasonic vibrations can be used for cavitation, melt degassing, fine filtration of melts, non-dendritic solidification, improved semi-solid deformation, spatial solidification and for the production of aluminum alloys with low-solubility components.

3. Electro-magnetic vibrations

Electro-magnetic vibrations typically involve two different force fields, a stationary magnetic field and an alternating electric field. If a stationary magnetic field with a magnetic flux density B and an alternating electrical field with a frequency f and current density J is applied to a melt, a vibrating electromagnetic body force with a density F=J x B is induced inside the melt. This force sets the particles inside the melt into vibration motion with a frequency equal to the frequency of the alternating electrical field, vibrating perpendicular to the plane of J and B. Another electro-magnetic force is formed inside the me!t due to the applied magnetic force and the induced force. This force is partly rotational and stirs the melt . Figure 1 illustrates the relationship between these forces.

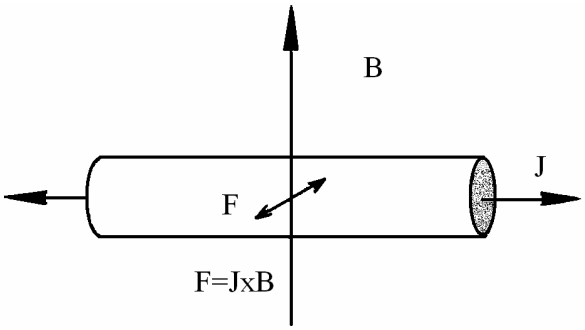

Figure 1. Direction of vibrating force F developed by the interaction of tne alternating electric field J and the stationary magnetic field B

Zong (4) reported that low frequency electromagnetic vibrations could be used to grain refine, to eliminate micro segregation, and to avoid cracks and improve the as-cast surface quality of alloys. Yoon et al (5) found that electromagnetic vibrations reduce the grain size of primary silicon. They attributed this phenomenon to the collision of primary Si particles with one another. Mizutani et al (6) imposed electro-magnetic vibrations on an Al-7wt%Si alloy and found that with increasing the intensity of the vibrations, the primary a-Al dendrites approached a globular shape of about 25 μm in size. They also foud that in Al-17wt%Si, the primary Si particles were refined to 5 μm at a frequency

nearing 1 kHz. The level of refinement increased with the frequency of vibration. They attributed this phenomenon to collapsed dendrite arms due to micro-explosions and stirring in the melt. Various researchers reported refined and uniform grain sructure, refined primary and eutectic Si, and improved surface quality of castings due to electromagnetic vibrations.

4. Mechanical Vibrations

In this method, the entire mold is set into vibration by means of a vibration source. Although the use of mechanical vibrations allows limited degrees of freedom to the operator, it is the most promising method of applying vibrations to solidifying melts due to its simplicity and the ruggedness of the equipment needed for inducing vibratons.

5. The Use of Mechanical Vibration in Casting

Sokoloff was probably the first to report on the use of mechanical vibrations for grain refinement. Campbell (7) reported that mechanical vibration causes inprovement in mechanical and corrosion properties of alloys Mechanical vibrations have also been linked to the reduction or complete removal of the tendency for pipe formation in ingots of pure metals.

6. Solidification Reactions, in an hypereutectic Alloy

The chemical composition of 390 alloy is 16-13%Si, 0,15-0,65%Mg, 0,5%max Mn, 1% max Fe, 4-5%Cu, 1,4%max Zr, Balance Al.

During solidification of 390 alloy primary Silicon forms first. As solidification progresses, Aluminum dendrites develop in the melt. The presence of Iron in the alloy promotes the formation of the Al_5FeSi phase. Manganese in the alloy suppresses the formation of this brittle phase and forms $Al_{15}(Mn,Fe)_3S_{12}$ instead. This phase is often termed “Chinese script” and has a complex morphology.

Reactions during solidification of B390 alloy :

Suggested temperature °C	Reaction
667	Formation of primary Si
657	Development of dendrite network
575	Liquid → Al +Si+ Al_5FeSi
573	Liquid → Al +Si+ $Al_{15}(Mn,Fe)_3S_{12}$
555	Liquid → Al +Si + Mg_2Si
512	Liquid + Mg_2Si → Al +Si + Al_2Cu + $Al_5Mg_8Cu_2Si_6$
507	Liquid → Al +Si + Al_2Cu + $Al_5Mg_8Cu_2Si_6$

Microstructure of 390 Alloy

The microstructure of 390 alloy consists of primary Silicon particles in a matrix of Aluminum and Silicon eutectic. The morphology of the primary Silicon greatly depends on the imposed temperature gradient, and the presence of nucleating agents and impurities. Several morphologies of primary Silicon have been identified. The most common among them are star-shaped, polyhedral, plate-like, and dendritic.

REFERENCES

1. R.M. Pillai et al Journal of Materials Processing Technology, vol 146, 2004, pp 338-348.
2. Eskin G. I. Ultrasonic Sonochemistry Vol 8, no.3, 2001, pp319-325.
3. Eskin G. I. Ultrasonic Treatment of Light Alloy Melts, Gordon and Breach, Amsterdam, 1998.
4. Zong C. J. Transactions of the Nonferrous Metals Society of China, vol.13, no.3, pp473-483, 2003.
5. Yoon E. P. et al, Materials Science Forum, vol.475-479, pp320-332, 1998.
6. Mizutani Y et al, Materials Transactions, vol.45, no.6, pp 1994-1998, 2004
7. Campbell J., International Metals reviews, Vol.26, no.2, pp71-108, 1981.
8. Jayesh Deshpande, The effect of Mechanical Mold Vibration On the Characteristics of Aluminum Alloys, Worcester Politechnic Institute, 2006.

Received, March 2007 *Technical University "Gh. Asachi" Iasi*

EFECTELE VIBRATIILOR MECANICE APLICATE IN TIMPUL SOLIDIFICARII ALIAJELOR TURNATE

Rezumat: Este cunoscut ca turnarea materialelor metalice este influentata pozitiv de prezenta vibratiilor aplicate asupra baii de aliaj lichid. Metodele de producere a vibratiilor pot fi diferite, putand fi utilizate vibratii mecanice, pneumatice, hidraulice si electrice. Vibratiile mecanice se pot obtine cu un element in translatie sau cu mase in rotatie, ultimele fiind utilizate pentru o gama larga de forte si frecvente sub 60 Hz.

Aliajele aluminiu-siliciu si aluminiu-cupru sunt dintre cele mai importante aliaje neferoase turnate. Diferite metode pot fi aplicate pentru a imbunatati caracteristicile de turnare ale aliajelor, microstructura, proprietatile mecanice.

Prezenta lucrare prezinta principalele rezultate obtinute prin utilizarea vibratiilor, pe plan mondial.

BULETINUL INSTITUTULUI POLITEHNIC DIN IAŞI
Tomul LIII (LVII), Fasc. 3, 2007
Secția
ŞTIINȚA ŞI INGINERIA MATERIALELOR

CHARACTERIZATION OF STEELS IN TERMS OF THEIR PHYSICAL AND MECHANICAL PROPERTIES

BY

STELA CONSTANTINESCU AND LUCICA ORAC

Abstract: To be able to characterize steels in terms of their physical and mechanical properties,a significant role is played by the tests.

The following mechanical characteristics are determined : ultimate strength , yielding poit standing , breaking elongation and the resilience test .

Based on the researches carried out a heat treatment technology can be determined which further lead to an optimum set of mechanical properties according to the technical conditions : A. Annealing (austenite at temperature 920^oC , exposure 2 minutes per mm , water cooling) B. Tempering (heating at temperature 680^oC , exposure 4 minutes per mm , air cooling) .

The micro – structural analysis showed the structural modification swhich tahes place when tempering within 580 – 700 ^oC .

Upon heating , the martensite out of balance structural tend to get transformed . The process is based on diffusion whose amplitude is higher when the temperature is higher too .

With smaller tempering temperatures , 580 – 700 ^oC , the martensite acs segmented .

Keywords : *ultimate strength , yielding poit , breaking elongation , resilience test,annealing,.*

I .INTODUCTION

From the piece of plates made from steel ASTM14 gade F plates were cut in order to make pull and resilience samples.

The following research schedule was designed to determinethe heat treatmentparameters :

- austenite at 900 ^{0}C , 920^{0}C ,exposure time 2 minutes / mm ;
- water cooling
- tempering temperatures : 580^{o}C, 600^{o}C, 620^{o}C, 640^{o}C, 660^{o}C, 680^{o}C, 700^{o}C , exposure time 4 minutes / mm .

From the heat treatment samples were taken to carry out analyses and tests :

- pull yests to determine : R_m, $R_{p0,2}$, A_5;
- tenacity tests to determine: KV_L
- micro-structural analysis to determine the micro-structure.

The heat treatment research schedule is given in table no. 1 .

Table no. 1

Austenite temperature [^oC]	Exposure time [min]	Cooling agent	Tempering temperature [^oC]	Exposure time [min]	Tempering agent
920	40	water	580 600 620 640 660 680 700	80	still air
920	40	water	580 600 620 640 660 680 700	80	still air

II. RESEARCHES AND EXPERIMENTAL RESULTS

To be able to characterize steels in terms of their physical and mechanical properties, a significant role is played by the pull tests .

For this purpose samples were taken transversally with respect to the rolling direction to make STAS 200 – 75 samples .

The test consists in applying slow smooth loads in ambient environment .

The following mechanical characteristics are determined :

- yielding poit standing for the ratio of the load where the length is increasing and the initial cross section area of the blank
- ultimate strength which is the ratio of the max load and initial cross section area of the sample
- breaking elongation : $A_5 = \frac{L_u - L_o}{L_o} \cdot 100$
- breaking throttle : $\Psi = \frac{S_o - S_u}{S_0} \cdot 100$

The resilience test is actually a bending test by shock and serves the purpose os assessing the material tenacity .

The test consists in brweaking by one strong hit with a pendulum hammer Charpy , a sample fitted with a V – shapedgroove in the middle which freely leans against two seats to determine the breaking energy .

The samlees are cooled in systems made of heat insulated recipients . Cooling agentsare are etilic alcohol and carbon snow .

The results obtained are given in table no.2 for the annealed and tempered samples.

Tabel no.2.

No	Austenite temperature [^oC]	Tempering temperature [^{o}]	Mechanical prorerties under annealed and tempered conditions			
			R_m [N/mm^2]	$Rp_{0,2}$ [N/mm^2]	A_5 [%]	$KV_{L-46}{}^oC$ [J]
1	900	580	1092	1005	15	54;52;53
2		600	1075	1000	16	61;62;63
3		620	1058	995	16,5	66;67;68
4		640	1030	972	16,5	74;75;73
5		660	995	944	18	93,5;95;96,5
6		680	920	848	20	112,5;115;117,5
7		700	786	786	22,5	123;125;124
8	920	580	1105	1011	15,5	51;50;52
9		600	1068	998	16,5	58;58;58
10		620	1061	990	16,5	63;62;64
11		640	1035	965	17	72;70;68
12		660	989	937	17,5	95;94;93
13		680	923	873	21	102;100;101
14		700	782	791	22	115,5;115;114,5

The value of the mechanical characteristics obtained furyher to the heat treatments applied have been statistically processed and illustrated vs heat treatment parameters , in fig. 1;.2; .3; .4.

….Austenite at 900 ^oC
….Austenite at 920 ^oC

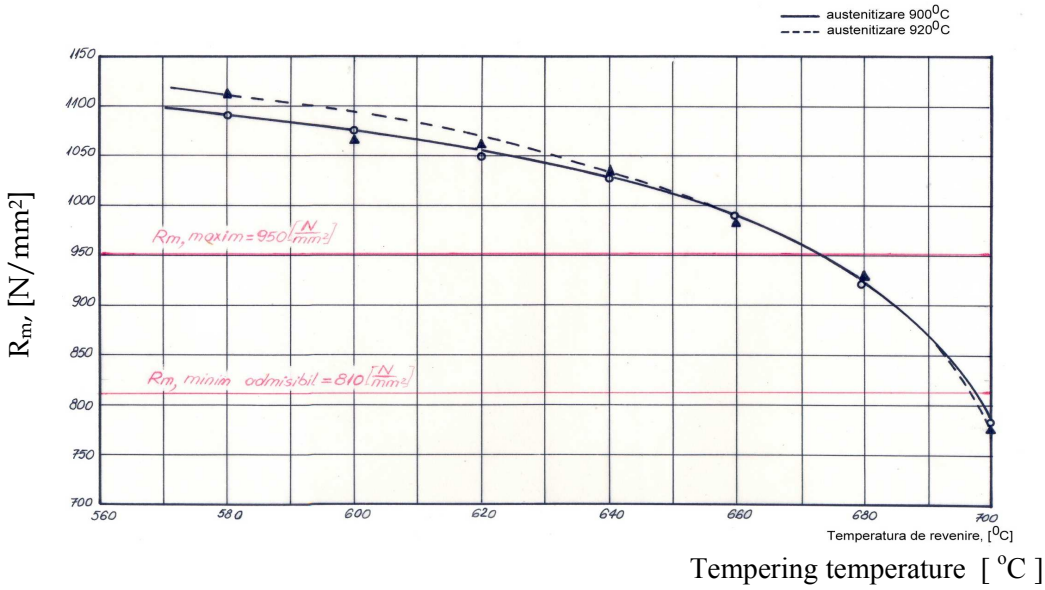

Tempering temperature [^oC]

Figure 1.Effect of tempering temperature the ultimate strenght , R_m [N/mm^2]

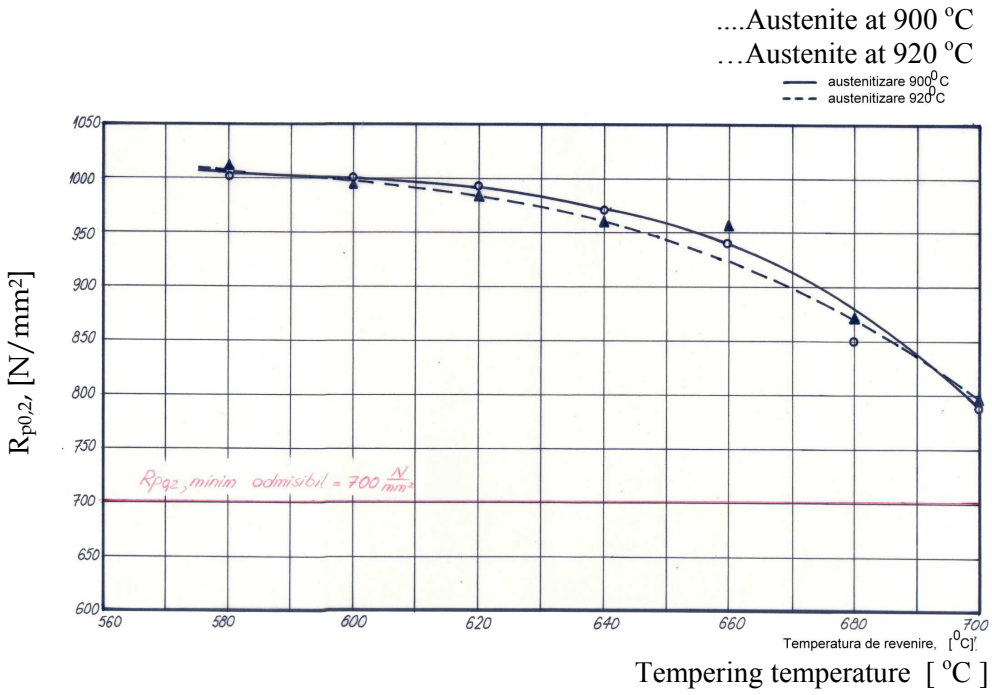

Figure 2. .Effect of tempering temperature the yielding , R_{p02} [N/mm^2]

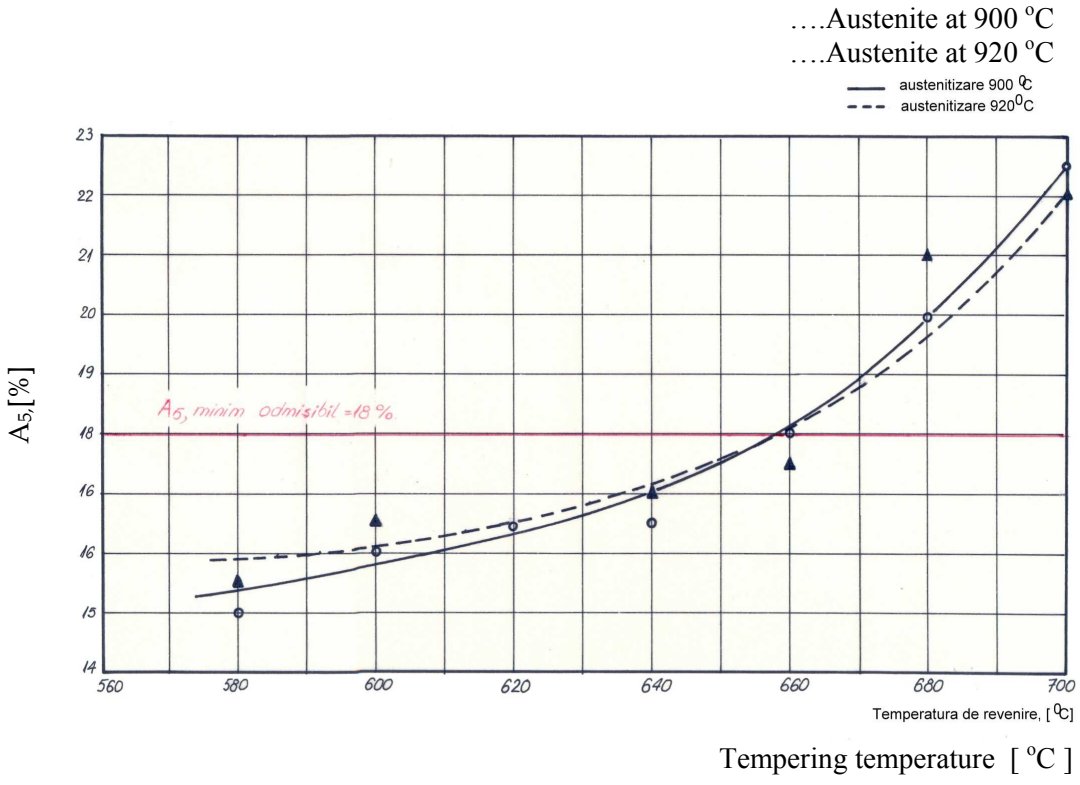

Figure 3. Effect of tempering temperature on the breaking elongation , A_5 [%]

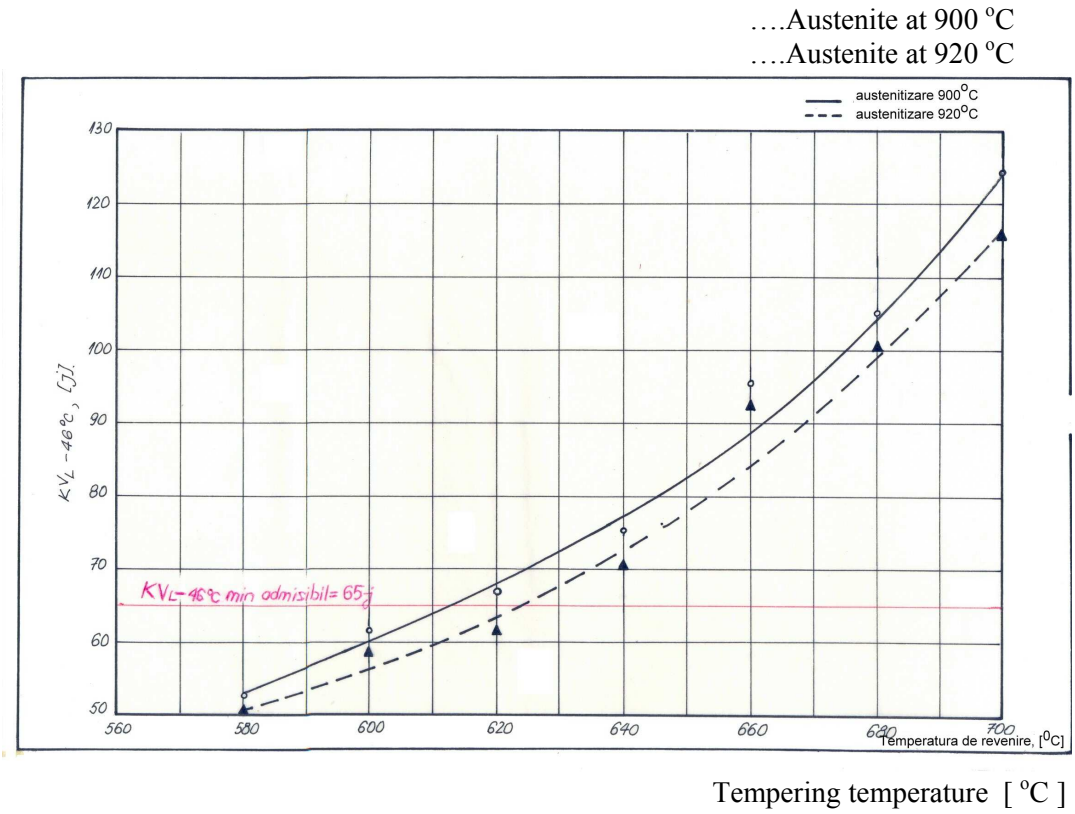

Figure 4. Effect of tempering temperature on cross resilience , KV_L [J]

Micro- structural measurements

From the heat treated material , according to the research schedule , metallographic samples were taken .

The micro- structural analysis revealed the structural transformations occurring during tempering at various temperatures within 580 – 700°C interval .

The results obtained the microstructures corresponding to the tempering temperature in the above mentioned interval are given in the figure below .

$T_{călire}=920^0C$

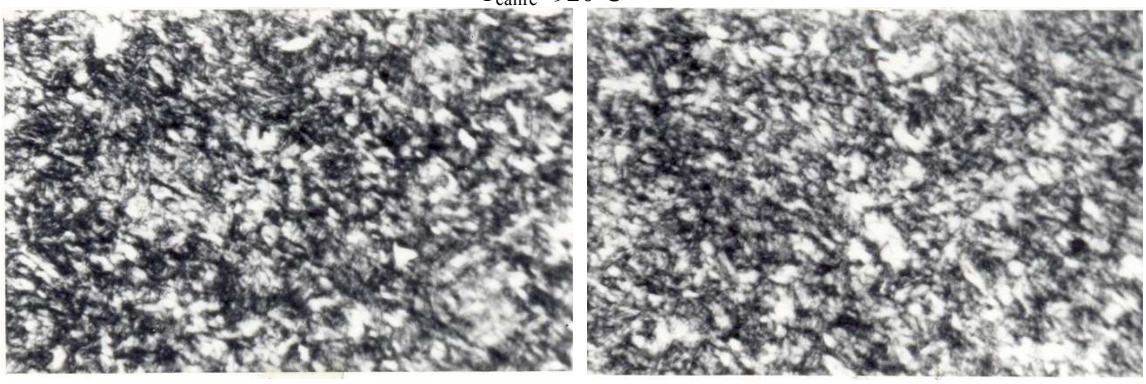

$T_{rev}=580^0C$ $T_{rev}=600^0C$

$T_{rev}=620^0C$

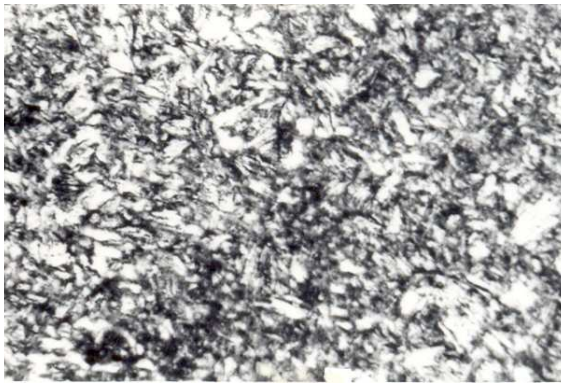

$T_{rev}=640^0C$

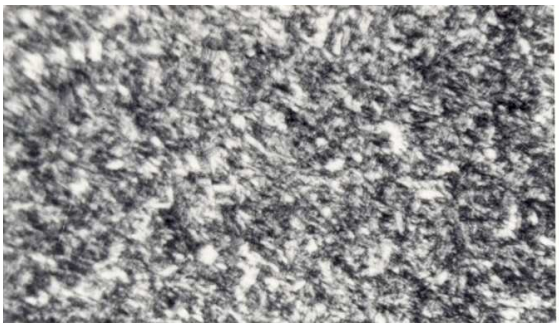

$T_{rev}=660^0C$

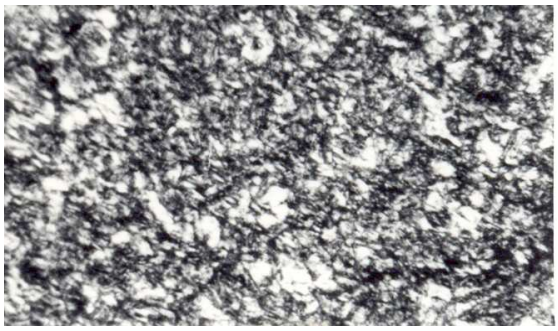

$T_{rev}=680^0C$

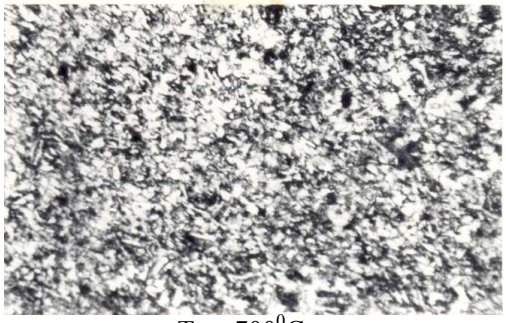

$T_{rev}=700^0C$

III . CONCLUSIONS

Based on the researches carried out a heat treatment technology can be determined which further lead to an optimum set of mechanical properties according to the technical conditions :

A . Annealing

- austenite at temperature 920^0C
- exposure , 2 minutes / mm ;
- water cooling

B. Tempering

- heating at temperature 680^0C
- exposure , 4 minutes / mm
- air cooling

The ultimate strength and the yielding poit decrease while the tempering temperature increases within 580 – 700^oC

Plasticity characteristic , A_5 % and tenacity KV_L increase when the tempering temperature increases within 580 – 700°C

An optimum assembly of strength and tenacity properties can be obtained for austenite temperatures when tempering takes placewithin the range 580 – 700°C .

The micro-structural analysis showed the structural modificationswhich takes place when tempering within 580 – 700°C .

Upon heating , the martensite out of balance structuraltend to get transformed . The process is based on diffusion whose amplitude is higher when the temperature is higher too .

With smaller tempering temperatures , 580 – 700°C , the martensite acs gets segmented . High temperature heating causes a more acute fracmentation process ,the fragments turns into globes and the globe carbons keep on increasing so that at tempering temperature 580 – 700°C , the structure is made up of a feritic matrix and globular perlite .

REFERENCES

[1] Mitoşeriu O. , Constantinescu S. , Radu T. ,ş.a. , *Modern methods to perform the properties of metal materials ,* University „ Dunărea de Jos „ of Galaţi , 1998 ;

[2] Drugescu E.: Thermiques *treatmant* , Didact. şi Pedag., Publishing House , Bucureşti, 1998

[3] Constantinescu S.: *Metals properties and physical control methods*, Didact şi Pedag. Publishing House , Bucureşti , 2004;

[4] Constantinescu S.: *Distructive and nondestructive tests of metals*, Evrika Publishing House , Galaţi, 2000 ;

[5] Walanbe T.: *Mechanical proprieties of Cr-Mo steels after eleveted temperature service,* Partea I: Document II S-IX-116-79; Partea II: Document II S-IX-1167- 1990 ;

[6] Constantinescu S., Drugescu E.,Radu T. : *Practical application of AE of the different grades of steel. "* Proceedings of the 25thEuropean Conference on Acoustion Emission Testing " EWGAE 2002 " Prague Czech Republic , 11 –13 september, 2002 , p. 135

[7] Constantinescu S. : *Influence of manufacturing process on chemical and structural homogeneity of welded pipe sheets for tanks and vessels working under pressure. "* Proceeding of the International Conference on Advances in Materials and Processing Technologies, september 18 – 21 , Leganes, Madrid, Spain, 2001 , p.57 ;

[8] Constantinescu S.., Drugescu E ,Radu T. : *The coating on the steel support ,* 2003European Congress and Exhibition on Advanced Materials and Processes, 1-5 sept., Lausanne, Switzerland, 2003 , p. 59, paper F4-456 . 2003

[9] Knauschner A. ,*Elektrochemische Metallabscheidung*, Oberflachenveredeln und Planttierent von Mettalen, Leipzig, 1988, pag.61-119;

[10] Taffner K.şi alţii : *Symposium low alloy high strenght steels* , Nurenberg 21 – 23 May 1990 .

[11] Morrison W. B.şi alţii : *Controlled processy of high strenght low alloy steels* , New York 1996

[12] Pickering F. B. , *Britisch, Steel corporation* , Conference Leeds , 1994 .

[13] Steven N., *Jise*, vol.193, pag.141, 1989 .

[14] Sugiyama T. , *Kobe Seel Engineering Reports*, vol.25, nr.4, 1995.

[15] Delman B. : *Introduction a la cinetique heterogene*, cap.V, VI, VII, VIII, IX, Paris, 1989.

Received April 2007

Conf.dr.ing. Stela CONSTANTINESCU *University „ Dunărea de Jos „ of Galaţi,*
Drd.ing. Lucica ORAC *Faculty of Metallurgy and Materials Science – România*

CARACTERIZAREA OTELURILOR DIN PUNCT DE VEDERE AL PROPRIETATILOR FIZICO MECANICE

REZUMAT: Pentru a putea caracteriza oţelurile marca ASTMS14 grad F din punct de vedere al caracteristicilor fizico-mecanice un rol deosebit îl au încercările la tracţiune.

Se determină următoarele caracteristici mecanice: Rezistenţa la rupere (R_m) , Limita de curgere ($Rp_{0,2}$) , Alungirea la rupere (A_5) , Incercarea de rezilienţă (KV_L) .

Pe baza cercetărilor efectuate se poate stabili tehnologia de tratament termic de călire şi revenire care conduce la obţinerea ansamblului optim de proprietăţi mecanice, în conformitate cu prescripţiile din condiţiile terhnice , respectiv: *A. Călire* (austenitizare la temperatura de 920^{o}C; menţinere, 2 min/mm; răcire apă.) şi *B. Revenire* (încălzire la temperatura de 680^{o}C; menţinere, 4 min/mm; răcire: aer)

Analiza microstructurală a evidenţiat transformări structurale care au loc la revenire în domeniul de temperaturi 580 – 700^{o}C.

La încălzire, martensita, structură în afară de echilibru, tinde să se transforme. Procesul are la bază fenomene de difuzie, a căror amplitudine de desfăşurare este cu atât mai mare cu cât temperatura este mai ridicată.

La temperaturi mici de revenire, 580 – 700^{o}C, acele de martensită se fragmentează.

BULETINUL INSTITUTULUI POLITEHNIC DIN IAŞI
Tomul LIII (LVII), Fasc. 3, 2007
Secția
ŞTIINȚA ŞI INGINERIA MATERIALELOR

ASPECTS CONCERNING THE CORROSION OF SOME HSLA STEELS IN NATURAL SEAWATER

BY
MARIA LUNGU, N. AELENEI, GINA UNGUREANU, D. MARECI, I.M.POPA

ABSTRACT. The corrosion behaviour of five high-strength low-alloyed (HSLA) steels in natural seawater was studied. The method of assessment corrosion was by the use of DC electrochemical monitoring as linear anodic polarization and cyclic polarization measurements. These measurements point out that the studied alloys have a pronounced tendency to corrosion in natural seawater and undergo a generalized type of corrosion even at reduced over-potentials. The corrosion rate increases linearly with the over-potential value beginning from potential electrode of approximately –400 mV (ESC). The sample with the lowest manganese content shows the higher corrosion in seawater.

KEYWORDS: *HSLA steel, corrosion rate, potentiometry*

1.Introduction

The corrosion means destruction of a metal or alloy by it reaction with the environment. This reaction is mainly an electrochemical oxidation process that usually produces soluble metal ions, rust or other metal oxides. Since corrosion is an electrochemical process it requires an electrolyte or current-carrying medium between different parts of the corrosion cell. In marine submerged areas, seawater is the electrolyte, whereas in marine atmospheric areas, salt spray provides the electrolyte
Seawater is an aggressive fluid that interacts with structural materials to varying degrees. There are two competing processes that operate simultaneously in seawater environments: the chloride ion activity - which tends to destroy the passive film, and the dissolved oxygen - which acts to promote and repair the passive film on metallic materials of construction. In addition, seawater is a living medium by which microbiological films can modify the material performances.

Corrosion research are focused on understanding and characterizing the specific nature of corrosion occurring on the materials used in desalination plants, different structural elements of the ships or other seaport equipments. The rate of corrosion is a crucial parameter necessary for making long-term predictions about the structural integrity of these. The most accurate measure of corrosion rate at our disposal is to compare current structural steel thickness with original thickness found on ship's plans, determine how much metal has been lost over a specific period of time and use the
Calculated corrosion rate for a linear extrapolation to determine overall corrosion rate for that particular location. Cumulative corrosion analyses may provide a more accurate variable rate.

Corrosion testing depends on the extent and type of information desired and the environmental conditions expected in service for a particular alloy. Corrosion in seawater environments is dependent on a number of factors such as alloy composition, water chemistry, pH, microbiological organisms, pollution and contamination, alloy surface films, geometry and surface roughness, galvanic interactions, fluid velocity characteristics and mode, oxygen content, heat transfer rate, and temperature. Understanding how these factors interact and affect materials performance is essential in order to design seawater corrosion tests that minimize experimental variations and best

simulate service conditions. Ideally, the mechanism of materials degradation during an accelerated test needs to duplicate the corrosion mechanism that is operative in a natural service environment. However, accelerated tests tend to breakdown materials by different, often unknown, pathways than those observed in natural environmental exposures. Using preliminary models and precise surface analytical techniques, research can evaluate materials breakdown leading to verification or modification of our understanding of mechanisms by which materials degrade and fail. Improved understanding of materials degradation modes can lead to more accurate physical models which can hopefully lead to accelerated corrosion tests that can mimic natural exposures and reliably predict materials performance.

This study deals with accelerated corrosion tests on some high-strength low- alloyed (HSLA) steels in natural seawater

2. Experimental

Five high-strength low-alloyed (HSLA) steels, utilizable in naval constructions for welded, bolted or riveted structures in which weight savings or added durability is important, were analyzed in respect with corrosion behavior in natural seawater. The compositions of these alloys are presented in Table 1.

Table 1. The compositions of the studied alloys

Alloy	Composition, %										
	C	Si	Mn	P	S	Al	Ti	Cu	Ni	Cr	Mo
A	0.170	0.220	0.750	0.025	0.011	0.005	-	0.020	0.020	0.050	-
A32[a]	0.160	0.210	1.340	0.018	0.008	0.027	0.013	0.032	0.018	0.014	0.002
D	0.120	0.320	1.100	0.021	0.010	0.048	0.004	0.030	0.220	0.040	0.004
D32[b]	0.170	0.310	1.380	0.021	0.024	0.060	0.006	0.019	0.110	0.024	0.003
E32[c]	0.170	0.360	1.470	0.020	0.011	0.080	0.007	0.032	0.016	0.013	0.004

(a)– Sample contain also: Nb-0.050% and V – 0.050%; (b)– Sample contain also: V-0.001% and Nb0.001; (c) – Sample contain also: V – 0.580% and Nb –0.047%.

The microstructures of the studied steels were analyzed with an optical microscope of OLIMPUS PME 3- ADL type, after a standard chemical attack with nital (2 % concentrated HNO_3 in ethyl alcohol [1]. All samples showed similar two-phase microstructures as that one illustrated in figure 1 for sample D32. This figure indicates a hypoeutectoide structure; the light colour parts represents the ferrite iron (alpha iron) while the dark portions represents the pearlite (88% ferrite, 12% cementite)– a lamellar structure of alpha ferrite and cementite.

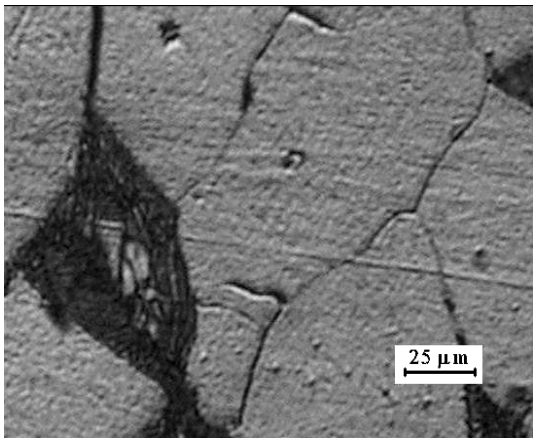

Fig. 1 Microstructure of D32 sample

The corrosion medium, natural seawater, was collected from Black Sea in Constanta coast and has the composition, expressed in g L^{-1}: Cl^- - 8.26: HCO^-_3 – 0,183; CO^{2-}_3 – 0.022; SO^{2-}_4 – 1.137; Na^+ - 4.47; K^+ - 0.158; Ca^{2+} - 0,203; Mg^{2+} - 0,557, corresponding to a salinity of 15.0 g L^{-1}.

Corrosion behavior was realized by rapid electrochemical tests, particularly by dynamic potentiometry. The measurements of open potential circuit and potentiodynamic polarization were performed on a VoltaLab 21 Electrochemical system (PGP201 economical potentiostat - Radiometer Copenhagen) equipped with the acquisition and processing data software VoltaMaster 4. The three-electrodes electrochemical cell used was equipped with a thermostatic system and a stirring. Mechanical lathing from commercial materials performed the working electrodes. These electrodes were performed in cylindrical form and mounted in a Teflon support to enable the connection to rotating electrode of the electrochemical system. A 0.07 – 0.08 cm^2 cross-area of working electrode was used. This area was precisely measured before embedding in Teflon support. All measurements were performed for freshly

polished surface. Each specimen was polished with SiC paper down up 2000 grit specification, degreased with acetone, washed in distilled water, and maintained in double-distilled water until the immersion within the electrochemical cell. A saturated calomel electrode (SCE) was used as a reference and platinum as auxiliary electrode. The electrolytes were maintained at 25 ^{o}C throughout the tests. The measurements were performed in natural aerated seawater.

The linear polarization curves were registered with the 1 mV/s potential scan rate, on ± 150 mV, against the open circuit potential. Cyclic polarization curves were registered on electrode potential range of (-1000…+1500 mV) with a 10 mV/s potential scan rate.

The surface appearance after such electrochemical treatment was analyzed with a research microscope of MC 1 type (IOR Romania) equipped with digital camera for micrographs acquisition.

The corrosion potential $E_{cor} \equiv E$ (I=0), Tafel slopes (b_a and b_c), polarization resistance (R_p), corrosion current densities (J_{cor}) and corresponding corrosion rates (v_{cor}) were evaluated using the facilities of the VoltaMaster 4 soft.

3. Results and Discussions

For sample "**A"** a symmetric linear polarization curve is obtained (Figure 2), that being so-called Tafel behavior, indicating that the controlled process is only the general corrosion. For this sample the Tafel slopes are practically equals as can be seen in Table 2.

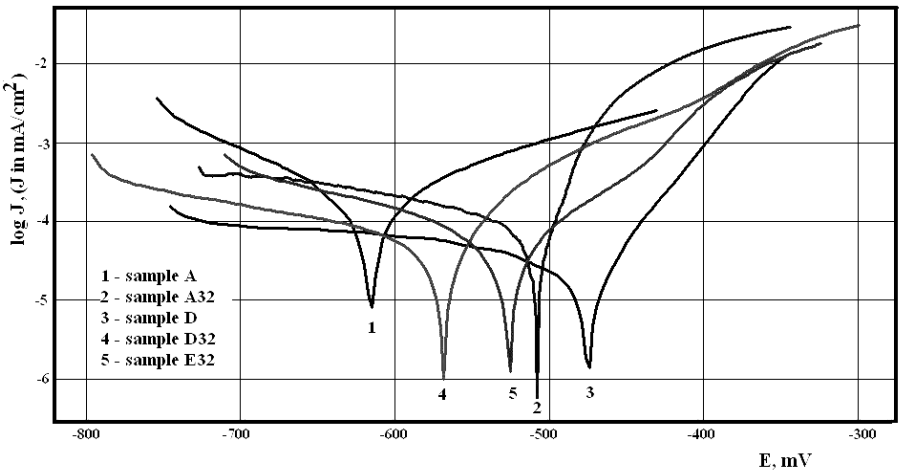

Figure 2 - Linear polarization curves for studied steels in natural seawater

For the other four samples the polarization curves in Evans diagram are asymmetrical, the cathode slope being of two to four time higher than the anodic slope. This can be an indication that the cathodic process is controlled of concentration or that general corrosion begins by appearance of some pits.

The thermodynamic tendency of corrosion, expressed by corrosion potential E (I=0), is higher for sample **A** and lower for sample **D. C**orresponding, sample **A** presents the highest instantaneous current density and corrosion rate, of 3… 11 time higher than the other samples, while the sample D shows the lowest corrosion rate. It seems that this increase of corrosion tendency of sample **A** is due to the reduced content of manganese, while the corrosion resistance of sample **D** is a consequence of increased content of nickel and reduced content of carbon.

Table 2 Electrochemical parameters for corrosion process of studied samples in marine natural water

		Sample / Parameter		A	A32	D	D32	E32
OCP , mV(SCE)				-560	-527	-497	-547	-562
Linear polarization, dE/dt = 0.5	Tafel method,	**E(I=0), mV(SCE)**		-617	-510	-474	-569	-528
		b_a (mV/decade)		119.1	96.1	40.6	74.3	78.3
		b_c (mV/decade)		-110.0	-206.6	-112.4	-319.4	-126.3
		R_p (ohm.cm²)		136.2	993.7	942.8	434.1	420.0
		J_{cor} (mA/cm²)		0.146	0.0231	0.0136	0.0613	0.0390
		v_{cor} (μm/year)		1843	270	159	717	456
Cyclic polarization curve dE/dt = 10 mV/s	Tafel method,	**E(I=0), mV(SCE)**		-695	-813	-810	-762	-713
		b_a (mV/decade)		188.3	130.3	140.9	192.9	153.3
		b_c (mV/decade)		-203.0	-129.3	-163.0	-157.4	-188.5
		R_p (ohm.cm²)		49.2	365.1	452.7	261.6	261.9
		J_{cor} (μA/cm²)		712	55.7	53.5	113.3	107.1
		v_{cor} (μm/year)		5501	651	625	1325	1252
		$E_{rp, mV(SCE)}$		-598	-700	-772	-646	-676
	For linear portion $J(mA/cm^2) = A.E(V) + B$		A	253.3	209.7	231.6	250.2	211.2
			B	102.7	80.9	90.6	86.5	79.4
	Consumed energy (mW/cm^2)		Q	436.18	374.4	416.1	429.1	373.9

The equilibrium parameters characterizing the corrosion processes at metal/solution interface were also determined from the anodic branch of the cyclic polarization curves which were registered at a ten time higher scan rate. These results are also presented in Table 2. In these conditions, all calculated parameters (E_{cor}, J_{cor} and v_{cor}) are higher than those evaluated at 1 mV/s scan rate. This is the expected result taking into account that Stern method used here [2,3] is based on extrapolation of the potential-current curve at I = 0 (at equilibrium) while the measured currents are in non-equilibrium state and depends on potential scan rate [4]. The potential scan rate influences the value of the polarization resistance and indirectly the value of the corrosion potential. Excepting the absolute values of the corrosion rates, which are of two-three time higher than those obtained at 1 mV/s scan rate, these data reflect the same behavior of the five studied samples: **A** is the most corrodible sample, while **D** is the most resistant to corrosion.

The Cyclic polarization curves obtained for the five samples in natural seawater are represented in Fig. 3 . All these curves are typical for general corrosion, the cathode branch overlap perfectly on the anodic branch and both are linear at potentials superior to –400 mV

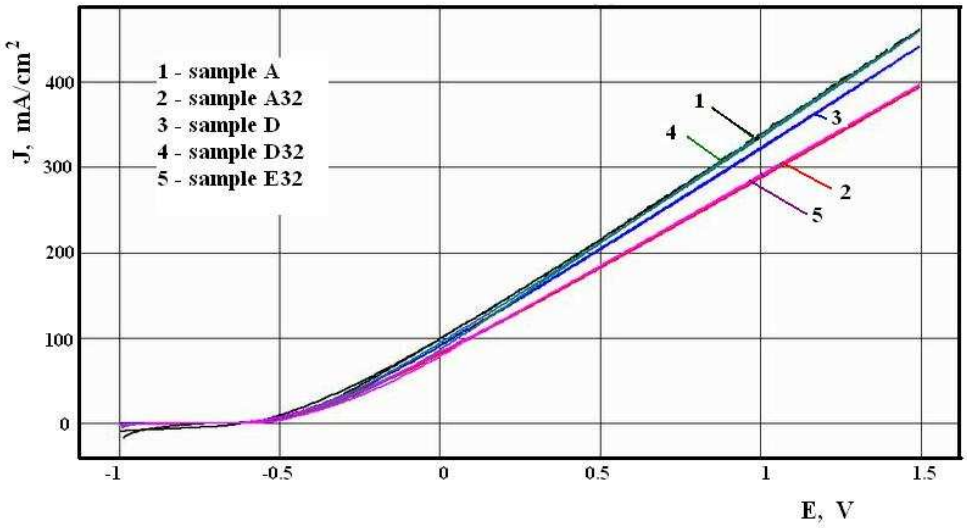

Figure 3 Cyclic polarization curves for the steel samples in natural seawater; dE/dt = 10 mV/s

Corrosion current density is proportional with applied owerpotential, the linear dependence being represented by equation: J = a.E + b. The "**a"** and "**b"** coefficients are also presented in Table 2. These data shows a very similar behavior of the five studied alloys to the over potential stimulated corrosion. Contrary to the results obtained for instantaneous current densities (J_{cor} at corrosion potential), at high over potentials samples **A** and **D32** behaves nearly identical, as well as the sample **A32** and **E32,** the potentiodynamic curves being superposed.

The current densities increases appreciable at higher potentials; thus for electrode potential of 1500 mV the current density is over 5 10^3 time higher than the instantaneous current density. This generates o very pronounced corrosion on alloy surface as can be seen in Figures 4 and 5.

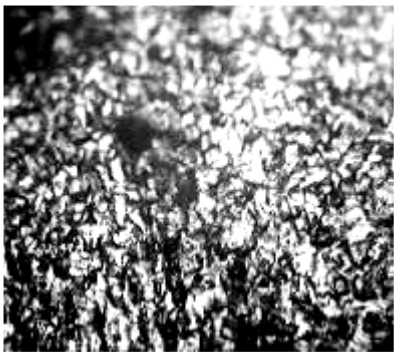

Figure 4
The micrograph of A sample after electrochemical treatment

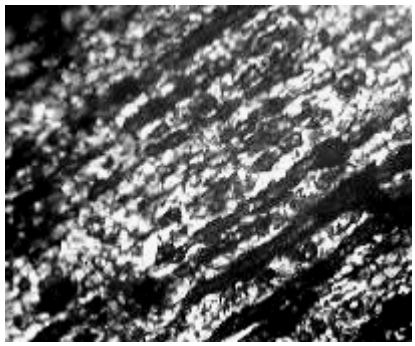

Fig.5
The micrograph of A32 sample after electrochemical treatment

In the case of cathodic polarization, the corrosion reduces completely at a potential, improper named re-passivation potential, very closed on the corrosion potential. The values of these potentials are also presented in Table 2 as (E_{rp}).

4. Conclusions

The five high-strength low-alloyed steels studied smple show a pronounced tendency of corrosion and a generalized corrosion under stimulated conditions, that is when the potential electrode is higher than a value of approximately –400 mV(ESC). The sample with the lowest manganese content shows the higher corrosion in seawater, while the sample which conain an increased quantity of nickel and a reduced quantity of carbon shows a reduced rate of corrosion

Received, March, 2007 *Technical University Iasi*

REFERENCES

1. Geru N., Bane M., Gurgu C., Cosmeleata G., Marin M., Analiza structurii materialelor metalice, , E.T. Bucuresti, 1991
2. M. Stern, A.L Geary., *J. Electrochem. Soc.*, **104,** 56 (1957).
3. M. Stern, A.L Geary., J. *Electrochem. Soc.*, **105,** 638 (1958).
4. R.G. Kelly, J.R. Scully, D.W. Shoesmith, R.G. Buchheit, *„Electrochemical Techniques in Corrosion Science and Engineering"*, Marcel Dekker Inc., New York, 2003.

„Gh. Asachi"Technical University of Iasi,
Faculty of Chemical Engineering,
Department of Chemical engineering
D. Mangeron 71, Iasi, Romania

ASPECTE PRIVIND COROZIUNEA UNOR OTELURI SLAB ALIATE IN APA DE MARE NATURALA

Rezumat: S-a studiat în laborator comportarea la coroziune în apă de mare a cinci probe de oţeluri aliate cu rezistenţă ridicată. Studiile s-au făcut prin măsurători de polarizare anodică liniară şi prin voltametrie ciclică. Măsurătorile au evidenţiat faptul că toate probele prezintă o tendinţă de coroziune ridicată, iar aceasta este de tip generalizat şi se manifestă încă de la supra-potenţiale relativ mici. Viteza de coroziune creşte liniar cu valoarea supra-potenţialului electrodului începând de la aproximativ -400 mV(ESC). Proba cu conţinut mai scăzut de mangan prezintă coroziunea cea mai pronunţată.

BULETINUL INSTITUTULUI POLITEHNIC DIN IAŞI
Tomul LIII (LVII), Fasc. 3, 2007
Secția
ŞTIINȚA ŞI INGINERIA MATERIALELOR

PECULIARITIES OF PLASTIC FLOW OF NEAR SURFACE LAYERS OF METALS IN EARLY STAGES OF DEFORMATION

BY

JONAS VILYS and VALDAS KVEDARAS

Abstract. *At present there is no clear understanding of the character of plastic deformation process in microareas of a polycrystalline alloy. The task of our work was to propose a quick-acting inductive measurement method for the testing of characteristics of the modified surface layer of ferromagnetic materials and analyze them by inductive method and by investigation of dislocation structure. The carried out experimental research confirms the potential of the application of the inductive method for the quick-acting and non-destructive control of surface layer characteristics of ferromagnetic materials. The analysis of the obtained experimental data shows the peculiarity of micro-plastic flow near a free surface of a solid body and its rather significant influence on the general character and kinetics of macroscopic deformation of metals.*
Key words: *micro-non-uniform deformation, dislocation structure, inductive measurement method, ferromagnetic materials, non-destructive control.*

1. INTRODUCTION

At present, in literature there is a great amount of experimental data on the influence of various factors on mechanical characteristics of materials. However, the existing physical theories of durability, explaining different phenomena and experimental facts, often can not be related to one another both qualitatively and quantitatively. It is determined by the fact that characteristics of mechanical properties of metal usually are no related to the state of stresses arising in local volumes of metal subjected to deformation. There is a close relationship among anisotropic properties, development of micro-non-uniform deformation of the polycrystalline conglomerate, and strength properties of real polycrystalline alloys [1].

However, there is no full and clear understanding of the character of plastic deformation process in microareas of a polycrystalline alloy, in particular, it concerns the distribution of deformations in the stage of micro-yield. There is a disputable question regarding the beginning of plastic deformation at a monotonic tension. Hence, regularities of distribution of non-uniform deformation in microvolumes of polycrystalline alloy have not been investigated thoroughly. Such investigations are very valuable because the studying of micro-non-uniform plastic deformation will help to understand a complex picture of strength and plastic properties of a material as a whole [2 - 4].

At present, investigating fracture processes of metals with body-centred cubic (BCC) lattice it is accepted to divide all process of strain accumulation and fracture into four stages [5] (Figure 1).

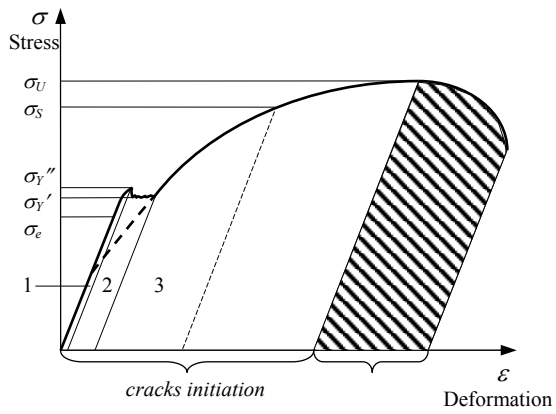

Figure 1. Failure process stages at static tension BCC lattice possessing metals

The first stage – stage of micro-yield, lasts from the beginning of the loading until the occurrence of the first lines of sliding (Lüders lines) on the yield plateau [6]. At this stage such characteristics as a limit of proportionality and a limit of elasticity are determined. The second stage - stage of yield, is characterized by non-homogeneous deformation in the form of front Lüders passing along all working length of a sample. The third stage – stage of strain hardening, at certain critical stresses submicrocracks with the size of approximately 1 - 3 μm occur on the surface layer of metal. This stage finishes at the moment, when maximal load is achieved and the neck formation begins. The fourth stage – stage of cracks propagation, starts from the beginning of neck formation until the final fracture of a specimen.

Investigation of the influence of the surface layer on the physical-mechanical properties and heterogeneity of plastic deformation of metals sometimes meets difficulties related to the determination of local character of stress distribution in that layer, especially in the range of small strains. Radiography, microhardness measurements, residual stress distribution curves, decoding of dislocations, metallographic methods, method of different etching rate of the stressed and not stressed areas of crystal and others are used at present for the determination of these characteristics [7, 8]. However, all these methods are long lasting, labour consuming and rather inexact. Taking the above into consideration, the problem of developing a simple, reliable and rapid method for determining local character of stress distribution in this layer without damaging a surface, remains.

The main objective of the work is to propose a quick acting measurement method for the testing of characteristics of the modified surface layer of ferromagnetic materials and analyze them by inductive method and by investigation dislocation structure.

Plastically deformed metal in the prestrained layer, differently from the strained main metal, is characterized by high concentration of microdefects, such us motionless dislocations, vacancies of atoms of interference and their interaction, which restrict their mobility, and results in metal strain hardening during prestrain. The above mentioned increases magnetic viscosity of steel [9,10]. As a result, the coercive force increases, and the residual inductance and magnetic penetration decrease [11]. Using the above described changes of properties of ferromagnetic materials, influenced by applied mechanical stresses, tests were carried out with the aim to check a possibility to use these properties for the determination of the locality of plastic deformation. The main point of the method is the following. If deformed ferromagnetic material is placed into magnetic field, the magnetic inductance will change, depending on the change of magnetic penetration. The same happens when ferromagnetic part touches the core of magnetic coil. Measuring the change of coil inductance, it is possible to check stress changes in ferromagnetic body. A schematic diagram of the inductive device is given in Figure 2.

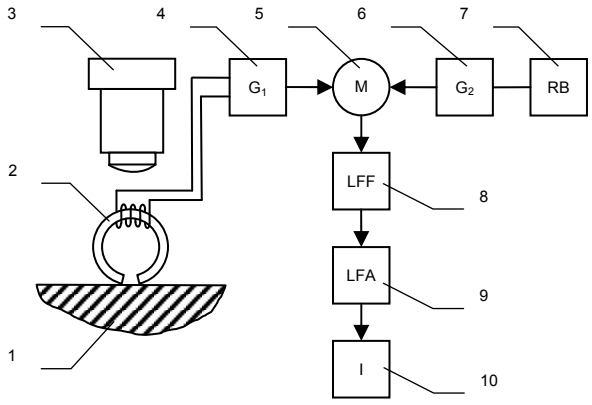

Figure 2. A schematic diagram of inductive measurement: 1 – sample, 2 – magnetic probe, 3 – objective, 4 – first high frequency generator, 5 – mixer, 6 – second high frequency generator, 7 – regulation block, 8 – low frequency filter, 9 – low frequency amplifier, 10 – indicator

The action of the device is based on the principle of a resonant method of measurements with an inductance of the moment of a resonance on zero beating. Two generators of high frequency, G_1 and G_2, are assembled in the inductive device according the same electric scheme. The magnetic probe is attached to the first generator G_1. Frequency of the second generator G_2 is changed by regulation block RB. Oscillation of high frequency from both generators goes to mixer, then through low frequency filter LFF and low frequency amplifier LFA goes to indicator I. When magnetic probe is attached to generator G_1, the frequency of second generator G_2 is changed by regulation block till the indicator shows the fluctuation of zero. The inductance is determined by indications of regulation block.

The magnetic probe, which was fastened directly to an objective of a microscope by the holder, was made of the magnetic head of the tape recorder. The working gap of the magnetic probe can be adjusted depending on the measurement base. Position of the working gap of the magnetic probe was established by the screws in such way that the sharp ends of the probe were in the focus of microscope. During measurements the electromagnetic probe with the micrometric screw of microscope is brought to the sample surface, up to the contact with it. Then inductance of the probe is measured. Since the gap of the probe is shunted by a site of sample between the ends of the probe, its inductance depends on the magnetic penetration of the given sample area and on the mechanical stress in the probe covered site of near surface layer of a sample.

The changes of dislocation structure of low-carbon steel in near surface layers at various static loading were studied by use the method of transmission electron microscopy [12].

2. EXPERIMENTAL

Investigating the development of micro-non-uniform deformation of a sample was carried out by the inductive method. Tests were carried out on flat samples of low-carbon steel with the dimensions of a deformable part $1.8 \times 12.0 \times 62.0$ mm. The chemical composition of this steel is specified in Table 1.

Table 1. Chemical composition of low-carbon steel specimens

C	Si	Mn	Cr	P	S	Ni
0.07	0.025	0.35	0.10	0.03	0.025	0.20

Mechanical properties of the steel subjected to recrystalizing annealing in vacuum of 2.10^{-4} mm Hg at 670 °C temperature for 2 hours are given in Table 2. The average size of grains after heat treatment was 30 μm. Before the test the near surface layer of

80 μm depth was removed from all samples by electropolishing. Strain rate at monotonic tension was $3.4 \cdot 10^{-4}$ s^{-1}.

Table 2. Mechanical properties of tested low-carbon steel specimens

Tensile strength R_m, MPa	Yield strength R_e, MPa	Elongation A, %	Contraction Z, %
360	270	35	60

The initial stage of plastic deformation was investigated most carefully. The local character of plastic deformation at a stage of micro-yield in superficial area of a sample was studied as follows. Using microhardness device *PMT-3*, marks were made every 200 μm along the length of the polished surface of a sample. Aiming to estimate the effect of anisotropy of material properties in microvolumes of a sample on magnetic penetration, at the beginning inductance measurements were carried out on the marked places of the annealed unloaded sample. The working gap of the magnetic probe was 30 μm. Further the sample was subjected to the certain loading and the inductance of a probe was repeatedly measured, shunting its working backlash by the marked places of the sample loaded by tensile stress. From the obtained data the curves of inductance of the probe versus applied load were constructed (Figure 3). In the figure the length of deformable part of the sample is 5 mm.

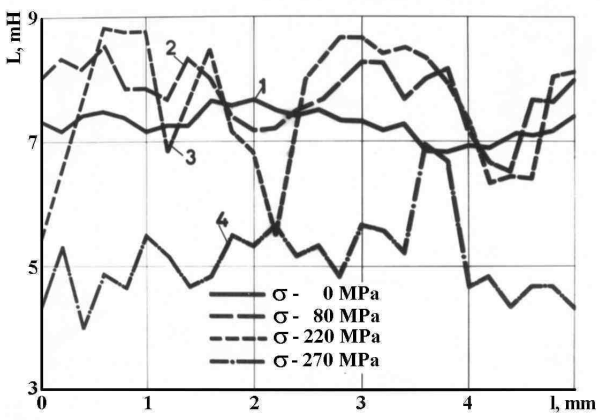

Figure 3. Change of inductance (L) of the probe on gage length (l) of a sample of low-carbon steel in stage of micro-yield depending on the magnitude of the applied stress

Curve 1 corresponds to the change of inductance of the annealed sample. Curve 2 presents change of inductance versus the length of working part of the sample after the removal of the stress of 80 MPa. It is obvious that on the basic part of a sample after unloading the inductance has increased in comparison with the initial condition. However, in two areas of the sample the inductance has decreased, which shows the presence of residual stress. Hence, in these zones the limit of elasticity is surpassed. So, after unloading of the sample from the stress not exceeding a limit of elasticity, the continuous growth of inductance in those areas of a sample, where local stress does not exceed the limit of elasticity, and the decrease of inductance in those microareas, where local pressure exceeds that limit, are observed. The increase of tensile loading results in further reduction of inductance in earlier deformed areas, which means that the residual

stress (curve 3) grows. Reduction of inductance is observed in other areas as well, i.e. plastic deformation occurs there as well. However, in some areas of the sample inductance is still increasing, i.e. the limit of elasticity here is not surpassed yet. The moment of achievement of the yield limit is preceded with the maximum increase of inductance in some areas of the sample. After unloading of the sample from the stress appropriate to the upper yield limit, in all superficial areas of the sample the noticeable recession of inductance (curve 4) is observed. However, this curve also shows that when the upper yield limit is achieved, a rather big inductance is still observed in one superficial area. It means that in this area residual stresses have not been formed yet. It is necessary to note that at the end of the first stage of deformation such areas were observed rather seldom.

The tensile loading of a sample at stresses higher than the yield limit, in all stages of yield, has resulted in sharp reduction of inductance along all length of a deformable part of the sample. Thus, on the basis of inductance change after load removal it is possible to notice local volumes of metal, in which the limit of elasticity is surpassed (the inductance in local volumes of metal is reduced), and to determine the moment when the yield limit is achieved (reduction of the inductance in all microvolumes of a sample).

In the initial condition the structure of annealed low carbon steel consists of the grains having small dislocation density with rare grid of suborders. At dislocation density of 10^7 cm^{-2} one dislocation falls to the area of 10 μm^2, and at magnification of 40 thousand field of vision of the microscope makes 3.5 μm^2. Therefore in some grains in all the field of vision of the microscope no dislocation was noticed.

After some insignificant tensile strain, i.e. at the stress about 40 MPa (the yield strength of annealed material was 270 MPa) in some single grains patterns of plastic deformation were found out (Figure 4a). The microphoto shows that in the grain body non-uniformly distributed dislocations have appeared; main part of them has accumulated at inclusion. The bent pieces of dislocations also are visible. Such configurations of dislocations are formed under action of the applied stress, because in annealed condition such areas of dislocations were not observed. In process of increase of a degree of plastic deformation, in more and more grains of plastic deformation are noticed, and in some grains (Figure 4b) considerably greater number of dislocations is observed. In grain A there are no dislocations, while in a grain B dislocations as enough long and direct lines could be observed. There is no interaction between them.

At the certain critical stress equal to the elastic limit σ_e, dislocations begin to occur almost in all near surface grains. The general structure becomes more complex. Interaction of dislocations is observed. On separate dislocations some steps are visible, and distribution of dislocations in structure of a grain is more uniform (Figure 4c). In the photo can be seen areas with long dislocations, as though cores on which other moving dislocations are arrested. At the same time these condensations of dislocations, apparently, are places of active work of several sources.

After deformation of a material up to the upper yield limit, the density of dislocations grows. More and more often there are thresholds on the dislocations; these thresholds are the consequence of dislocation crossings. The bent pieces of dislocations are observed also, and dislocations are distributed in all matrixes. In connection with development of processes of their complex crossing the local textures have appeared, and the tendency to formation of the local congestions, reminding the beginning of cellular structure formation (Figure 4d) is observed. In such a way formed dense condensations of

dislocations on the one hand may be active sources of dislocations, and on the other hand they may be an obstacle for other moving dislocations. Arrested in such obstacles dislocations, increase dislocation density of walls and their extent.

Hence, deformation of metal conducts not only to moving existing dislocations, but it results also in their multiplication. The increase of number of dislocations may disturb their further moving due to their interaction. The barriers, interfering moving of dislocations and, consequently, their sliding, arise. It explains the hardening, accompanying cold deformation: if the metal is more deformed, then it is more difficult to deform it further.

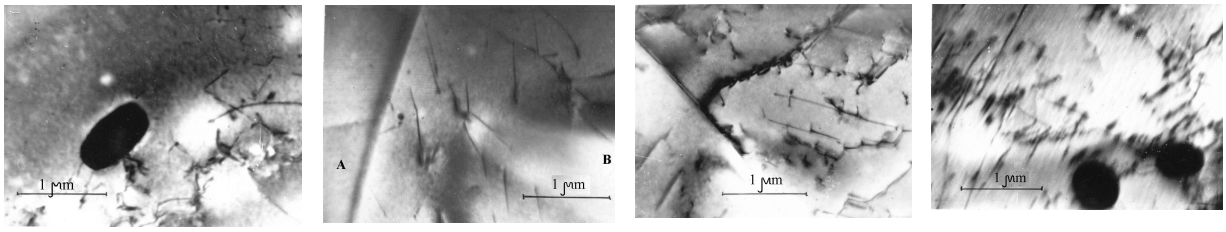

a b c d

Figure 4. Dislocation structure of low-carbon steel in near surface layer in stage of micro-yield at various loadings: a – σ = 40 MPa; b - σ = 80 MPa; c – σ = 110 MPa; d – σ = 270 MPa

On the yield plateau (Figure 5a) the separate generated cells, where sites with separate small density of dislocations are surrounded by sites with the raised density of dislocations are observed. Besides, it may be seen, that process of crushing of the big size cells and formation of the smaller size cells is possible. Thus, formation of cells may proceed in two ways: crushing of larger cells or formation at once small cells.

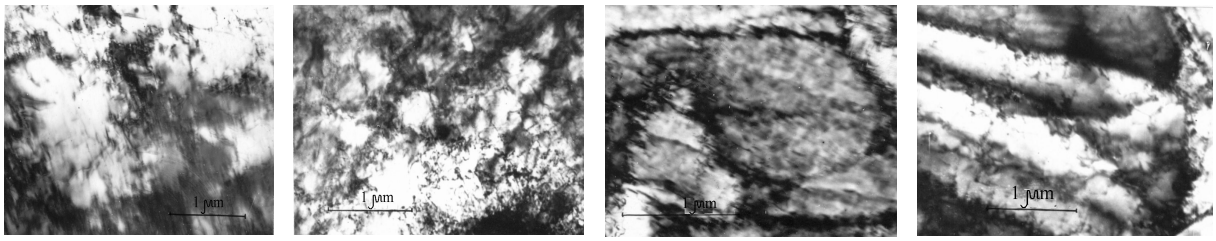

a b c d

Figure 5. Dislocation structure of low-carbon steel in near surface layer at various loadings higher than the micro-yield: a – the separate generated cells on the yield plateau ; b – cellular structure at the stage of deformation hardening; c - rectilinear congestions of dislocations at the stage of deformation hardening; d - dislocation structure at the stage of deformation hardening at the critical stress σ_s

At the stage of deformation hardening (Figure 5b) well advanced cellular dislocation structure is formed. The density of dislocations grows so rapidly, that often separate dislocations are not resolved any more. Besides dislocations inside the cells frequently settle down in such a manner that form bordering constructions and divide the cell into even smaller cells. The magnitude of cells at this stage equals to 0.5-0.9 μm.

Further increase of deformation degree up to σ_s (Fig. 1), in some grains is observed transformation of the cellular structure in to rectilinear congestions of dislocations (Figure 5c). Apparently, the number of active dislocation sources already decreases, and the further plastic deformation proceeds basically due to the moving of the previously formed dislocations. The cells of dislocations will be transformed in to band structure (Figure 5d). Bright subgrains, density of a dislocation in which is rather insignificant,

have undergone rather small deformation – they have only moved in relation each to other, whereas the basic part of deformation effect was concentrated in the areas dividing subgrains. These areas look like narrow strips which seem dark because of high density of dislocations in them.

The residual stresses discovered by the inductive method and investigation of dislocation structure shows that at the earliest stages of the monotonic tension of a sample attributes of plastic deformation are observed in the elastic region in separate grains of near surface layer of a metal. The plastic deformation does not occupy simultaneously all superficial volume of the metal when the stress increases. The consecutive deformation of separate macrovolumes of near surface layer is observed until all macrovolumes are covered by plastic deformation of critical volume. The most intensive spreading of plastic deformation to the majority of near surface grains begins when the elastic limit σ_e is achieved. Thus, local character of plastic deformation course in separate grains is especially strong at small deformations. Hence, local character of plastic deformation distribution is not steady and it depends on strain value. The localness decreases during the process of the increase of plastic deformation. Thus, in a real polycrystalline material, at linear tension, as a result of the interaction of differently oriented grains, each grain is in condition of complex state of stresses, and this state is different in every grain.

Local character of plastic deformation distribution in near surface layer in the micro-yield stage is noticed not only among separate grains, but also in a volume of one grain. Analysis of the presented data shows that at deformation of a polycrystalline material grain boundaries and neighbouring areas, where localization of plastic deformation is possible, play an important role and this should have a significant effect on the strength and plasticity of the material. From the considered data a conclusion may be drawn that in the micro-yield stage local plastic deformation in microareas passes rather actively, and this points out the inevitability of non-elastic processes in metals subject to loading. The first steps of plastic deformation are initiated in the surroundings of elastic non-uniform deformation of a material at grain boundaries. At monotonic tension of low-carbon steel in all other stages of deformation (yield and strain hardening) the inductive method and investigation dislocation structure also shows a micro-non-uniform plastic deformation.

On the basis of our test it may be concluded that when a polycrystalline sample is subject to tension, the non-uniform field of elastic micro-stresses occurs inevitably due to elastic anisotropy of metals on grain boundaries. The beginning of plastic deformation in separate microareas of a polycrystalline will be determined not only by the magnitude of elastic micro-stresses, but also by strength properties of the given microvolume, depending on its crystallographic orientation. It will predetermine a non-simultaneous start of plastic deformation not only inside of the grains, but also in their separate areas. These phenomena may be explained by the law of a minimum energy amount on deformation of all polycrystalline units.

Taking into account data of our investigations the inductive method may be recommended to be used for the evaluation of localness of residual stresses and small plastic strains in macro- and microvolumes of a sample, for the evaluation of change of electromagnetic parameters of metal in the cross-section, for the determination of true elastic limit, degree of strain hardening, revelation of changes taking place during artificial and natural ageing, initiation and propagation of micro-cracks, etc., in materials possessing ferromagnetic features. This method allows conducting a constant monitoring

of manufactured production without interrupting the production process.

3. CONCLUSIONS

1. A new inductive quick-acting measurement method for the testing of characteristics of the modified surface layer of ferromagnetic materials was proposed. The carried out experimental research confirms the potential of the application of the inductive method for the quick-acting and non-destructive control of surface layer characteristics of ferromagnetic materials. This method allows conducting a constant monitoring of manufactured production without interrupting the production process.
2. The inductive method may be recommended for the evaluation of localness of residual stresses, small plastic strains in macro- and microvolumes and other physical and mechanical characteristics of metal.
3. The development of micro-non-uniform deformation of low-carbon steel specimens at static tension in all stages of deformation was investigated by the inductive method and investigation of dislocation structure.
4. Analysis of the presented data shows that at deformation of a polycrystalline material grain boundaries and neighbouring areas, where localization of plastic deformation is possible, play an important role and this should have a significant effect on the strength and plasticity of the material.

REFERENCES

1. Fernandes, J.-V., Menezes, L.F., Rodrigues, D.M., Chaparro, B.M., Vieira, M.F. Non-uniform deformation after prestrain. *European Journal of Mechanics - A/Solids*, 2000, 19, p. 209–221.
2. Kramer, J.R., Pangborn, R., Weissmann, S. Dislocation distribution in plastically deformed metals. *Fatigue Environ. and Temp. Eff. Pɔoc. 27th Sagamore Army Mater. Res. Conf., Lake George, N.Y.,* 14-18 July, 1980, New York – London, 1983, p. 103–117.
3. Wu, C. H., Hsu, J., Chen, C. H. Effect of surface stress on the stability of surfaces of stressed solids. *Acta mater.* 1998, 46, p. 3755–3760.
4. Kolmakov, A.G., Vstovsky, G.V. Multifractal Analysis of Metallic Surface Structure Changes during Mechanical Treatment. *Materials Science and Technology,* 1999, 15, p. 705–710.
5. Terentjev, V. F. *Fatigue of Metallic Materials*. Nauka, Moscow, 2002, 248 p. (In Russian).
6. Suna, H.B., Yoshidaa, F., Ohmorib, M., Ma, X. Effect of strain rate on Lüders band propagating velocity and Lüders strain for annealed mild steel under uniaxial tension. *Materials Letters*, 2003, 57, p. 4535–4539.
7. Polyak, M. *Strengthening technology*. Vol. 1. Mashinostrojenie, Moscow, 1995, 832 p. (In Russian).
8. Polyak, M. *Strengthening technology*. Vol. 2. Mashinostrojenie, Moscow, 1995, 688 p. (In Russian).
9. O'Sullivan, D., Cotterell, M., Cassidy, S., Tanner, D.A., Meszaros, I. Magneto-acoustic emission for the characterisation of ferritic stainless steel microstructural state. *J. Magn. Magn. Mater,* 2004, 271, p. 381–389.
10. Augutis, V., Ramanauskas, R., Čiuplys, A., Vilys, J., Čiuplys, V. Determination of metal surface hardened layer depth using magnetic Barkhausen noise. *Materials science,* 2006, 12, p. 84–87.
11. Sinha, A.K. *Physical metallurgy handbook*. New York (etc.): McGraw-Hill, 2003, 1000 p.
12. Vilys, J., Čiuplys, V., Terentjev, V., Kolmakov, A., Kvedaras, V. *Particularies of plastic deformation of metals near surface layers*. Kaunas, Technologija, 2003, 208 p.

Jonas Steponas Vilys. Department of Manufacturing Technologies, Kaunas University of Technology, Kestucio St. 27, LT-44025 Kaunas, Lithuania; e-mail: jonas.vilys@ktu.lt

Valdas Kvedaras. Department of Technological Processing, Klaipeda University, Bijunu St. 17, LT-91225 Klaipeda, Lithuania; e-mail: valdas.kvedaras@ku.lt

PARTICULARITATI ALE CURGERII PLASTICE IN STRATURILE SUPERFICIALE ALE METALELOR IN STADIILE INCIPIENTE ALE DEFORMARII

Rezumat: In present nu exista o intelegere clara a caracterului procesului deformarii plastice in microzonele unui aliaj policristalin. Scopul lucrarii noastre este de a propune o metoda rapida inductive pentru testarea caracteristicilor straturilor superficiale ale materuialelor feromagnetice si analiza lorprin metoda inductive si prin investigarea structurii dislocatiilor. Cercetarile experimentale effectuate confirma potentiala aplicarea metodei inductivepentru controlul rapid nedestructiv a caracteristicilor straturilor superficiale ale materialelor feromagnetice. Analiza datelor experimentale obtinute arata particularitatea curgerii micro-plastice in vecinatatea suprafetei libere a corpului solid si influenta semnificativa a sa asupra caracterului general si cineticii deformarii macroscopice a deformarii metalelor.

BULETINUL INSTITUTULUI POLITEHNIC DIN IAŞI
Tomul LIII (LVII), Fasc. 3, 2007
Secția
ŞTIINȚA ŞI INGINERIA MATERIALELOR

DISLOCATION STRUCTURE CHANGES IN SURFACE METAL LAYER AT MONOTONIC AND CYCLIC LOADING

BY

ANTANAS CIUPLYS, VYTAUTAS CIUPLYS

Abstract: *In this article dislocation structure changes in surface metal layer at monotonic and cyclic loading of low-carbon steel were investigated. Formation of dislocation structure was investigated using new perspective multifractal parametrization.*

Multifractal analysis considers distribution of some values in the geometrical medium, therefore, distribution of metal dislocation structure unit elements in plane was investigated. Photos of dislocations were approximated by use of computer software. Main multifractal characteristics and strains (in case of monotonic tension) and number of cycles (in case of cyclic loading) dependencies were computed. Having these dependencies, it is possible to describe precisely regularities of dislocation structures evolution.

Quantitative evolution of low-carbon steel dislocation structures revealed that dislocation structure evolution on the surface is identical at monotonic and cyclic deformation of the metal.
Keywords: *dislocation structure, low-carbon steel, monotonic and cyclic loading, surface layer, multifractal parametrization.*

1. INTRODUCTION

The creation of new quantitative description (parameterization) methods of materials complex structures and substructures is one of the most important objectives in materials science [1-3]. Parameterization is one of the ways to describe different systems with some quantitative characteristics as size, dimension, measure, area, mass, temperature and etc. Chosen way of materials structures parameterization gives possibility to optimize properties by means of new parameters, which can describe materials unstable conditions behaviour.

Very often traditional quantitative characteristics of a material structure may not be related to the factors, which influence change of the material structure. But use of multifractal parametrization and introduction of such quantitative characteristics as uniformity f_q and texturity Δ_q, enables to analyse structure formation at conditions more precisely [4,5].

2. EXPERIMENTAL

Plate type low-carbon steel specimens were used for the tests. Chemical composition of steel is presented in Table 1.

Table 1 Chemical composition of steel

C	Si	Mn	Cr	P	S	As
0.18	0.2	0.45	0.15	0.035	0.040	0.08

The specimens were deformed at room temperature by universal tension machine *Instron TT-DM*. Monotonic tension tests carried out at 2.78×10^{-3} s^{-1} strain rate. Repeated tension fatigue tests were carried out by fatigue *Shenk* type pulsator at 2800 cycles/min loading frequency at constant $\sigma = 230$ MPa load. The dislocation structures were investigated by use of transmission electron microscope *IEM-7A*.

Formation of dislocation structures at monotonic and cyclic loading of low-carbon steel was investigated using multifractal parametrization. Quantitative characteristics were obtained by use of original multifractal parametrization method. Initial processing of the dislocation structure photos was performed approximation them by digital graphic images by use of computer software *Adobe Photoshop 6*. Approximated view is reflected on the pixels matrix, where every pixel has corresponding colour characteristic. In our case, for an elementary particle (pixel) reflecting dislocation structure (dark background on a photo) value "1" was ascribed, and for the background – value "0". Computerized calculations were carried out using software *MFRDrom*. Traditinional multifractal characteristics $f(\alpha)$ and $D(q)$ spectra, as generalized Reni dimensions, were calculated during selection q values from the interval
[–100; 100] and apportionment dials 2, 3, 4, 6, 8, 12, 16, 24, 32, 48, 64, 128, 192, 256, 384 by use of scale selection schemes.

Everyone view of investigated dislocation structure was obtained as a result of calculation from six – seven square (768×768 pixels size) parts "cut out" of the photo, in order to get mean values of multifractal characteristics for every structure under investigation. Such square part corresponded to approximately 1.5 μm^2 area of a real foil.

Based on our theoretical and experimental investigations [5,6] it is assumed that for quantitative parametrization the following characteristics should be used: generalized Reni dimension D_q at positive values of q = max (in our case $q_{max} = 100$), and effective quantitative characteristics of uniformity f_q and texture Δ_q, at positive values of q = max. Characteristic D_q supplies certain quantitative information related to thermodynamic formation conditions of the structure under investigation. In some cases it may be asserted that large D_q values (when $q > 1$) correspond to large entropy values. Value D_q may be used as an effective mean to recognize material structures, which very difficult or imposible to identify by traditional quantitative methods [7]. Thus, the possibility arise to recognize structures, obtained at the same conditions, and to define connections among structures formation conditions. Value Δ_q reflects texture and orderliness, and symmetry damage of all structure configurations subjected to investigation. Increase of Δ_q (according to module) shows that amount of periodical components of the structure is growing, the degree of symmetry damage is decreasing and structure becomes more textural (more ordered). Degree of structure uniformity f_q is considered not like traditional characteristic of the structure view, but like character index of unit elements distribution, containing all the structure, in the Euclidian space. Higher value of f_q corresponds to more uniform structure [8].

Because multifractal analysis considers distribution of some values in the geometrical medium, therefore, in our case, distribution of metal dislocation structure unit elements in plane was investigated. Photos of dislocations were approximated and by use of computer software main multifractal characteristics and strains (in case of monotonic tension) and number of cycles (in case of cyclic loading) dependencies were computed. Main multifractal characteristics are given in Table 2 and 3. Having these dependencies, it is possible to describe precisely regularities of dislocation structures evolution.

Table 2. Distribution of dislocation structures main multifractal characteristics at static loading

Multifractal characteristics	Strain ε, %				
	0	0.15	0.7	1.8	2.8
$D_0 = f_0$	1.75610	1.89970	1.84680	1.96760	1.99130
α_0	2.03800	2.30900	2.17180	2.15300	2.11430
$D_1 = f_1 = \alpha_1$	1.60980	1.47840	1.56080	1.79640	1.98530
D_2	1.53600	1.42890	1.50520	1.77200	1.95990
D_{100}	1.22110	1.09980	1.24600	1.47230	1.65690
α_{100}	1.20890	1.08880	1.23360	1.45760	1.64260
f_{100}	0.13370	0.18890	0.20310	0.12970	0.08850
$\Delta_{100} = D_1 - D_{100}$	0.38870	0.37860	0.31480	0.32410	0.32840

Table 3. Distribution of dislocation structures main multifractal characteristics at cyclic loading

Multifractal characteristics	Number of cycles N				
	0	460	1400	2800	4200
$D_0 = f_0$	1.75610	1.44070	1.75950	1.93220	1.98240
α_0	2.03800	1.48030	1.89460	2.06230	2.22390
$D_1 = f_1 = \alpha_1$	1.60980	1.41260	1.67020	1.84210	1.85240
D_2	1.53600	1.40230	1.62030	1.79380	1.79160
D_{100}	1.22110	1.32210	1.36850	1.47090	1.46490
α_{100}	1.20890	1.31080	1.35810	1.55540	1.45060
f_{100}	0.13370	0.19110	0.32740	0.02220	0.03430
$\Delta_{100} = D_1 - D_{100}$	0.38870	0.09050	0.30170	0.37120	0.38750

It was noted that there is no linear relationship between both uniformity characteristic f_{100} and strain (also number of cycles) as well as between texture characteristic Δ_{100} and strain (also number of cycles) (Fig. 1 and 2). But large correlation coefficients among D_{100} and strain ε (in case of monotonic tension $r = 0.97019$) as well as among D_{100} and the number of cycles N (in case of cyclic loading $r = 0.91567$) allow us to assume that quantitative structure characteristics obtained, precisely enough reflect formation of dislocation structure.

Small amount of dislocations was noticed in annealed specimens. At monotonic tension increase of a deformation results more uniform structure, but when the deformation reaches yield plateau and dislocation density clearly increases, this characteristic begin to decrease. The texturity of the structure, which decreases at the beginning, with increase of deformation stays stable.

Evolution of dislocation structure is going on in a similar manner at cyclic loading too. Growth of the number of loading cycles results more uniform structure, but when the certain number of cycles is achieved, this characteristics falls down. From this moment texturity of the structure starts to increase. The dislocation structure becomes more and more ordered.

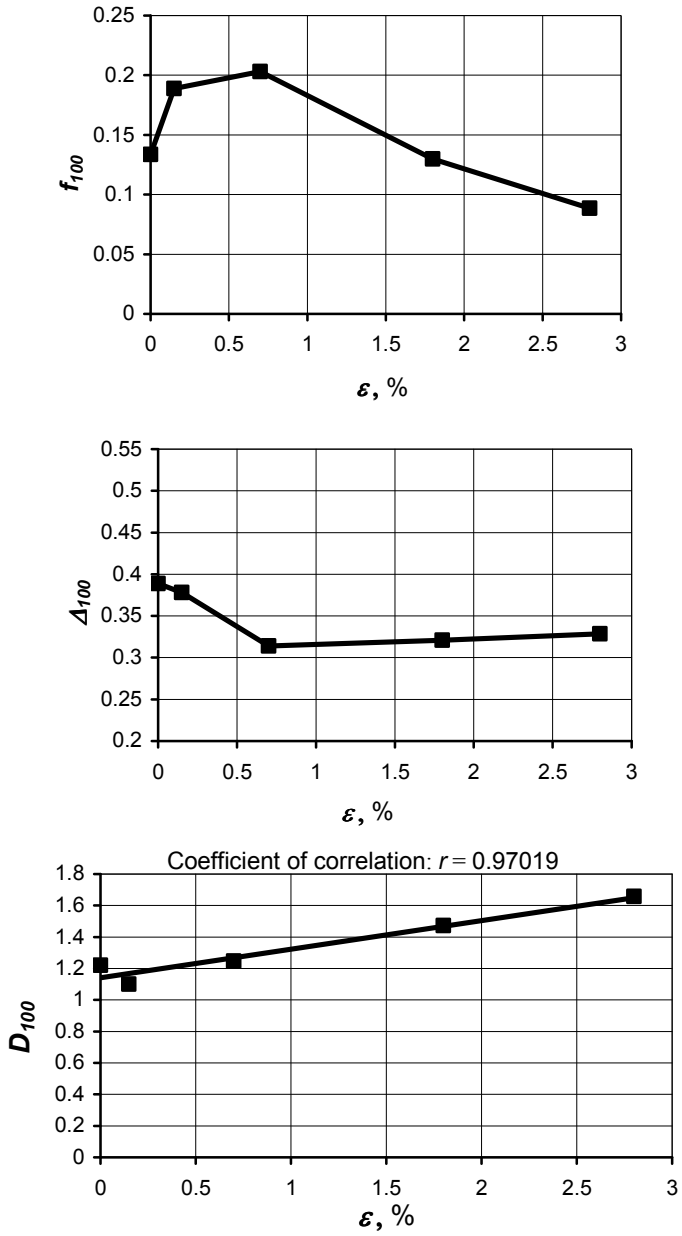

Figure 1. Dependance of low-carbon steel dislocation structures main multifractal characteristics on strain (in case of static loading)

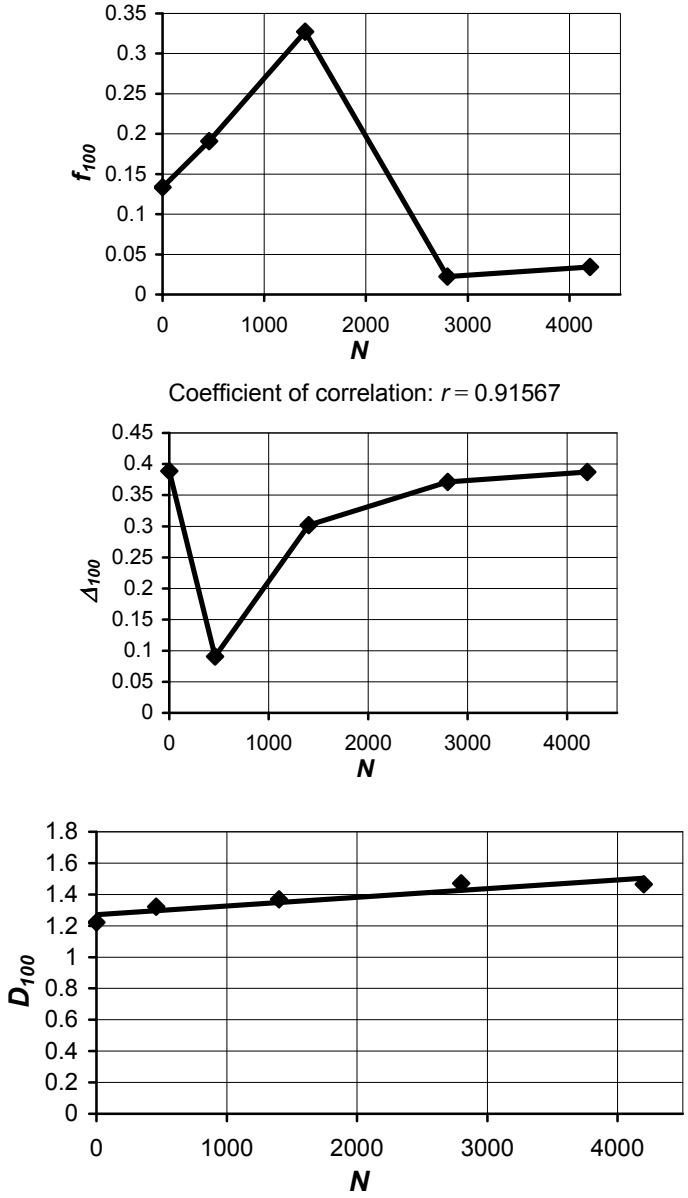

Figure 2. Dependance of low-carbon steel dislocation structures main multifractal characteristics on number of cycles (in case of cyclic loading)

Quantitative evolution of low-carbon steel dislocation structures, which were formed at monotonic and cyclic loading, revealed that dislocation structure evolution on the surface is identical at monotonic and cyclic deformation of the metal. Small differences, discovered as a result of this evolution by the multifractal parametrization method, may be explained by the different rate of deformation process.

3. CONCLUSIONS

1. New perspective methodology of fractal parametrization is applied to investigation of the relationship between material properties and their structure.
2. It is determined that evolution of dislocation structure in low-carbon steel specimens at both monotonic tension and cyclic deformation is similar, and

plastic deformation process at both loading modes in the metal surface layer is analogous.

REFERENCES

1. Mandelbrot, B.B. The Fractal Geometry of Nature. San Francisco, Freeman, 1983, 480 p.
2. Иванова В. С., Баланкин А. С., Бунин И. Ж., Оксогоев А. А. Синергетика и фракталы в материаловедении. Москва, Наука, 1994, 383 с.
3. Mecholsky J.J., Passoja D.E., Feinberg-Rigel K.S. Quantitative analysis of brittle fracture surfaces using fractal geometry. Journal of the American Ceramic Society, 1988, Vol.72, N.1, p. 60–65.
4. Stach S., Cybo J. Multifractal description of fracture morphology: theoretical basis. Materials Characterization. New York, Elsevier, 2003, Vol. 51, N. 1, p. 79–86.
5. Встовский Г. В., Колмаков А. Г., Бунин И. Ж. Введение в мультифрактальную параметризацию структур материалов. Москва, Научно-издательский центр «Регулярная и хаотическая динамика», 2001, 116 с.
6. Vstovsky G. V., Kolmakov A. G., Terentjev V. F. Using multifractal information for quantitative evaluation of broken symmetries of materials structures. Materials Science (Medžiagotyra). Kaunas, Technologija, 1999, Vol. 9, N. 2, p. 62–65.
7. Vstovsky G. V. Transform information: A symmetry breaking measure. Foundations of Physics. New York, Springer, 1997, Vol. 27, N. 10, p. 1413–1444.
8. Hirth J.P. Some current topics in dislocation theory. Acta Materialia. New York, Elsevier, 2000, Vol. 48, p. 93–104.

ANTANAS CIUPLYS, Department of Manufacturing Technologies, Kaunas University of Technology, Kestucio str. 27, LT-44312 Kaunas, Lithuania; e-mail: antanas.ciuplys@ktu.lt

VYTAUTAS CIUPLYS, Department of Manufacturing Technologies, Kaunas University of Technology, Kestucio str. 27, LT-44312 Kaunas, Lithuania; e-mail: vytautas.ciuplys@ktu.lt

MODIFICARI ALE STRUCTURII DISLOCATIILOR IN STARATURILE SUPERFICIALE ALE METALELOR LA INCARCARI CICLICE SI MONOTONE

Rezumat: In acest articol au for crcetate modificarile structurii dislocatiilor in stratul superficial al unui otel cu putin carbon. Formarea structurii dislocatiilora fost cercetatautilizand noua perspective a parametrizarii multifractalice. Analiza multifractala considera distributia unor valori in mediul geometric, de aceea, a fost investigate distributia structurii dislocatiilor metalului in plan.Fotografiile dislocatiilor au fost aproximateprin utilizarea unui software specific. Au fost calculate dependetele principalelor caracteristici multifractalice de tensiuni (in cazul tensiunilor monotone) si numarul de cicluri (in cazul incarcarilor ciclice). Avand aceste dependenteeste posibil sa se descrie precis regularitatea evolutiei structurilor de dislocati Evolutia cantitativa a dislocatiilor otelului cu putin carbon a relevant ca evolutia structuii dislocatiilor pe suprafata este identical la deformarea ciclica sau monotona a metalului.

BULETINUL INSTITUTULUI POLITEHNIC DIN IAŞI
Tomul LIII (LVII), Fasc. 3, 2007
Secția
ŞTIINȚA ŞI INGINERIA MATERIALELOR

EIS STUDY OF THE CORROSION BEHAVIOUR OF HSLA STEEL IN NATURAL SEAWATER

BY

D. MARECI[*], MARIA LUNGU[*], N. AELENEI[*], JULIA CLAUDIA MIRZA ROSCA[**]

ABSTRACT. The possibilities offered by Electrochemical Impedance Spectroscopy (EIS) technique for studying the progress of corrosion in high-strength low alloys (HSLA) was investigate. Corrosion test were performed in aerated natural seawater (Atlantic Ocean, Gran Canaria). Impedance diagrams provide the value of charge transfer resistance (R_{ct}). For the corrosion rate determination based on the Stern-Geary equation, the parameter B or the Tafel slopes were obtained using DC tests (polarization curves). The values of I_{corr} are converted into weight loss values by applying Faraday's law. The linear progress of the attack with immersion time suggests a slight barrier effect of the corrosion products layer.
KEYWORDS: EIS, *HSLA steel, corrosion progress*

1.INTRODUCTION

The electrochemical methods have been shown in numerous studies to be an efficient and convincing tool for analyzing the corrosion behavior of metals. The DC polarization curves can show the potential region in witch passivity is effectively maintained and the AC impedance method is particularly useful for monitoring certain electrochemical changes as function of time, as it is a non-destructive electrochemical technique. During the last three decades, the Electrochemical Impedance Spectroscopy (EIS) has proved to be advantageous for characterization of the various oxide films on the metal surface. This technique requires minimal invasive procedures; neither the oxidation nor the reduction was forced to take place in the open circuit mode. From the EIS data it can be obtained information about the passive film dissolution (rate, control factors) and the passive film characteristics (film thickness, dielectric constant, diffusion coefficient of the diffusing species etc.).

In the electrochemical estimation the polarization data are converted into instantaneous corrosion current (I_{corr}) by means of the well-known Stern-Geary equation [1, 2]:

$$I_{corr} = \frac{b_a b_c}{2{,}3R_p(b_a + b_c)} = \frac{B}{R_p} \qquad (1)$$

where R_p is the polarization resistance, which is defined by:

$$R_p = \left(\frac{\Delta E}{\Delta I}\right)_{\Delta E \to 0} \qquad (2)$$

b_a and b_c are the Tafel slopes for the partial anodic and cathodic processes, respectively, and B is a constant.

The values defined by equation (2) does not always coincide with the charge transfer resistance, R_{ct}, which is the parameter directly related with the corrosion rate and which needs to be inserted in equation (1) according to the theoretical basis of this equation. It should be noted that R_p is a measure of overall resistance, which, besides the effect of R_{ct} may also include other possible effects such as mass transport and ohmic resistances (e.g. due to the formation of solid phases barriers). For this reason R_{ct} refers more exactly to the kinetics of the corrosion reaction.

Impedance diagrams provide the value of R_{ct}. For the corrosion rate determination based on the Stern-Geary equation it is necessary to know the values for parameter B or the Tafel slopes. These values can be obtained using DC tests (polarization curves).

In the present work the corrosion behaviour of steel in natural seawater was investigated both by EIS and polarization curves. Maintaining the solution in repose serves to simulate the stagnant conditions of the corrosive medium, which are common in practice [3, 4].

The values of I_{corr} are converted into weight loss values by applying Faraday's law.

2. EXPERIMENTAL

As working electrode was used a low-alloyed steel with an area of 0.7 cm^2. The alloy composition is given in table 1.

Table 1. The composition of the used steel sample

Composition[a] (% wt)								
C	Si	Mn	P	S	Al	Cu	Ni	Cr
0.170	0.220	0.750	0.025	0.011	0.005	0.020	0.020	0.050

The corrosion medium was natural aerated seawater, collected from Atlantic Ocean in Las Palmas de Gran Canaria Coast containing in g/l: chloride 35.7; sulphate 2.55; sodium 10.6; sulphur 0.75 and other components in very low concentration. The pH was 7.8. The working electrodes processed in cylindrical shape and mounted in a tetrafluoroethylene support, presents a one-dimensional circular area surface exposed to corrosion. Before experimental measurements the samples have been mechanically polished with abrasive SiC paper up to a granulation number of 2500, cleaned in ethyl alcohol and preserved in distilled water.

Microstructural characterisation

In order to study the microstructure of the carbon steel its surface was chemically treated in agreement with standard procedures. In this case, the chemical attack was realized with a (HNO_3) solution [5]. The treated surfaces were examined by an optical microscope OLIMPUS PME 3- ADL.

Electrochemical measurements

Electrochemical measurements were carried out at 25^0C. All the electrochemical measurements were performed with a PAR 263 A potentiostat connected with a PAR 5210 lock-in amplifier. The acquisition and data analysis were realized with PowerCorr software for polarization curve measurements and ZSimWin software for impedance measurements. A saturated calomel electrode (SCE) was used as reference and platinum as auxiliary electrode.

The polarization resistance (R_p) was calculated from the linear polarisation curve, registered with 0.166 mV/s scanning rate in a potential domain of ± 10 mV around open circuit potential (E_{OC}). The Tafel slopes were evaluated from the polarization curves obtained with 0.5 mV/s potential scan rate on the potential interval of ± 150 mV vs. E_{OC}.

Electrochemical impedance spectroscopy (EIS) measurements were carried out at open circuit potential in aerated solutions. All spectra were recorded in the 10^{-1} Hz to 10^5 Hz frequency range. The applied alternating potential signal had 10 mV amplitude. The tests were normally repeated two or three times, checking that they presented reasonable reproducibility.

In the electrochemical estimations of corrosion the I_{corr} (□A/cm^2) values obtained from R_p and R_{ct} have been converted into corrosion rates (v_{corr}) by means Faraday's law and these corrosion rates have been converted into weight loss M by integration:

$$M = \int v_{corr}\, dt \qquad (3)$$

Taking into account equation (1) this results in

$$M = \frac{AB}{nF}\int \frac{dt}{R_{ct}} \qquad (4)$$

were A = atomic weight of the metal, n = number of electrons exchanged, F = Faraday's constant (96485 C). The integral in equation (4) was determined graphically.

3. Results and Discussions

The microstructure of the carbon steel after chemical attack is shown in Figure1.

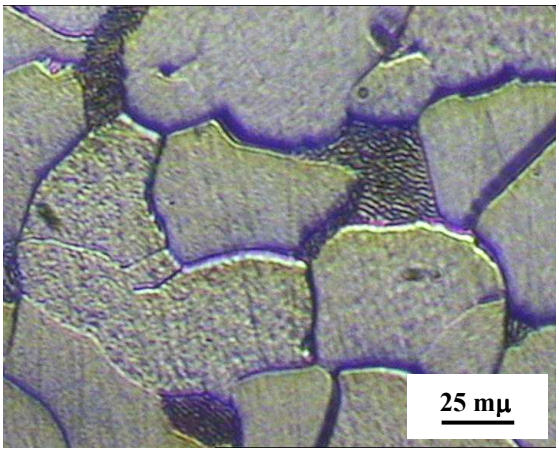

Figure 1. Microstructures of low-alloyed steel

This figure indicates a hypoeutectoide structure; the light colour parts represents the ferrite iron (alpha iron) while the dark portions represents the pearlite (88% ferrite, 12% cementite), a lamellar structure of alpha ferrite and cementite.

Figure 2 shows the polarization curves of used steel after 1 and 14 days of immersion in natural seawater.

The Tafel slopes (b_a and b_c) were calculated by fitting the theoretical polarization curve with the experimental polarization curve registered in the potential range of ± 150 mV vs. E_{OC} by the use of a PowerCorr software. Table 2 presents the average values of these parameters. This table shows that the Tafel slopes, b_a and b_c did not vary greatly with the exposure time to the aerated natural seawater. From the Tafel slopes, B values of close to 0.025 V have been obtained for this low-alloyed steel.

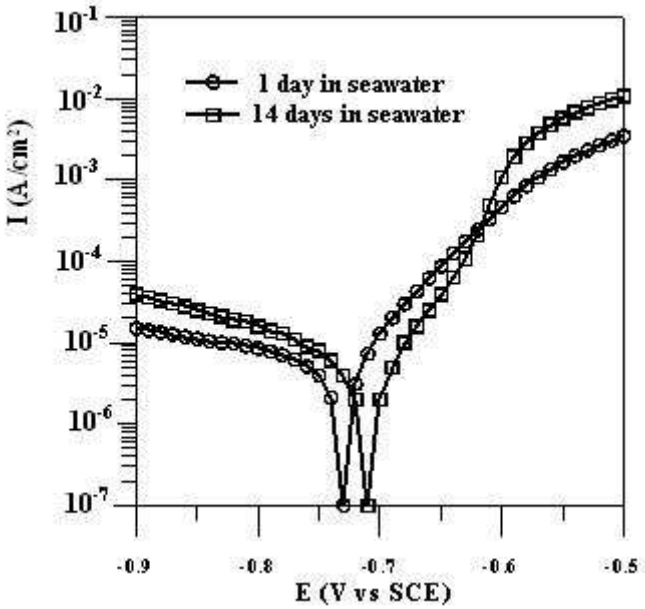

Figure 2. Polarization curves for low-alloyed steel after 1 and 14 days of immersion in natural seawater

Table 2. Values of Tafel parameters and B deduced from polarization measurements

b_a (mV/dec)	b_c (mV/dec)	B (mV)
After 1 day of exposure to natural seawater		
70	210	23
After 14 days of exposure to natural seawater		
80	190	24

The experimental impedance data obtained at E_{OC} with the samples at different intervals of immersion time in natural seawater are presented as Bode plots in Figures 3 and 4.

All spectra point out that in the higher frequency region, log Zmod are constant with a phase angle values near 0^0 at high frequency. This is a typical response for the resistive behaviour and corresponds to the solution resistance, $R_{sol.}$.

In the medium frequency range, a linear relationship between log Zmod and log frequency is observed for all the tests, but with different slopes (always less than –1) and maximum phase angle less than -90^0 which means that the film has not a fully

capacitive character. These features can be attributed to the charge transfer associated with the effect of ionic double layer capacitance. In the low frequency domain, the time constant is caused most probably by a mass transport process in the film.

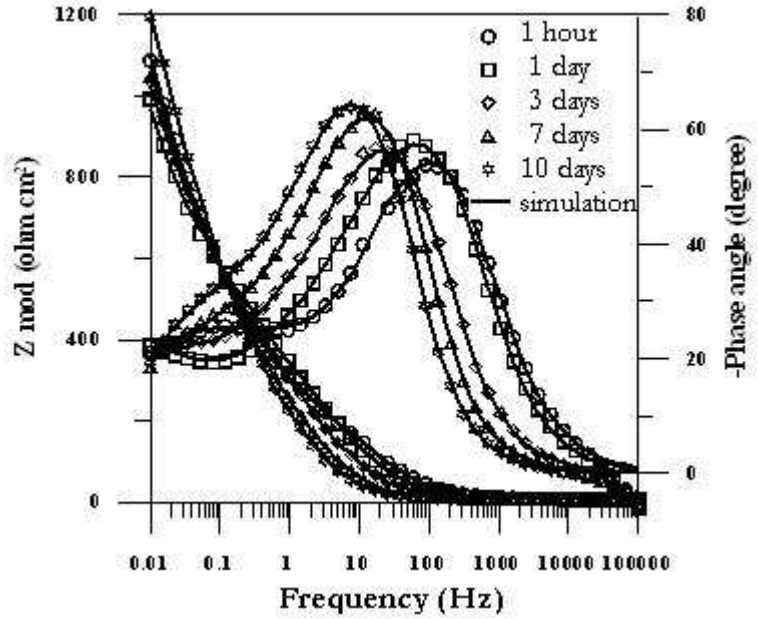

Figure 3. Bode plots for studied steel immersed for different time in natural seawater

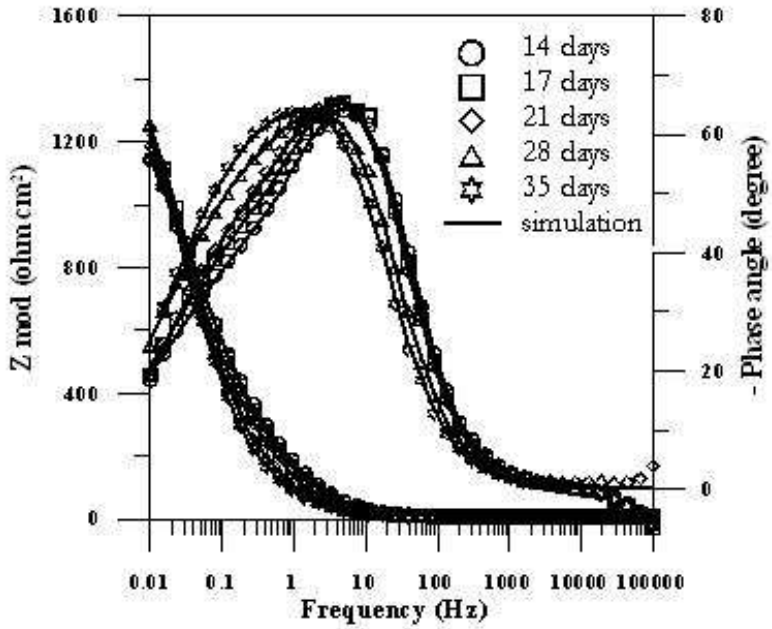

Figure 4. Bode plots for studied steel maintained different time periods in natural seawater

For the interpretation of the electrochemical behaviour of a system from EIS spectra, an appropriate physical model of the electrochemical reactions occurring on the electrodes is necessary. The data shows a good fitting to the transfer function of the equivalent circuit presented in Figure 5, the error being smaller than 5%.

Instead of pure capacitors, constant phase elements (CPE) were introduced in the fitting procedure to obtain good agreement between the simulated and

experimental data. The impedance of CPE is defined as $Z_{CPE} = \frac{1}{Q(j\omega)^n}$ where Q is a proper combination of elements of the circuit that cannot be separated in the electrochemical system, related mainly on surface inhomogenities and mass transport in solid phase; n is related to the slope of the lgZ vs lgf Bode–plots; ω is the angular frequency and j is imaginary number ($j^2 = -1$).¨n¨ ranges from –1 to +1.When the value of n is equal to -1, the CPE presents inductance characteristics; if n is equal to 0, CPE represents a resistance; for n equal to 0.5, CPE is associated to diffusion process and for n equal to 1, CPE represents a capacitor [6].

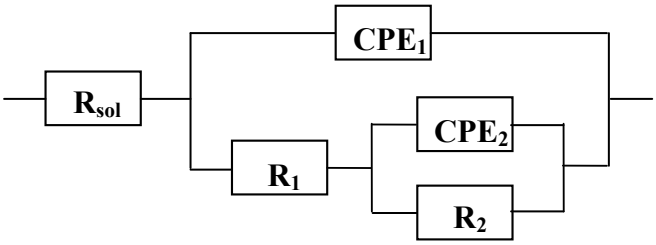

Figure 5. Equivalent circuit (EC) used in the generation of simulated data

The EC contain two R-CPE elements in parallel. Other combinations of resistances and capacitances were tried to model the corrosion of carbon steel to natural seawater but none of these were found to give a satisfactory fit. The impedance data for carbon steel after different exposure times (days) in the natural seawater were fitted with the EC presented in Fig. 5 and the resultant parameters are given in Table 3.

In the Fig. 3 and 4, the experimental data are shown as individual points, while the theoretical spectra resulting from the fits to a relevant EC model are shown as lines.

The physical meaning given to the circuit is the association of the film/electrolyte interface (R_1CPE_1) with the diffusion process (R_2CPE_2); R_2 is the diffusion resistance of current carries in the film. The time constant at high frequencies is originated from the R_1CPE_1 combination while the one at low frequencies initiated from the R_2CPE_2 combination. R_1 representing the charge transfer resistance and CPE_1 the double layer capacitance, as shown by the high value of the n_1 exponent [7-9].

Table 3. Impedance parameters of low-alloyed steel in aerated natural seawater at open circuit potential

	R_1 (Ω cm^2)	CPE_1 (S cm^{-2} s^n)	n_1	R_2 (Ω cm^2)	CPE_1 (S cm^{-2} s^n)	n_2	R_p (Ω cm^2)	
							EIS	Linear polarization
After 1 hour	176	$1.2\ 10^{-4}$	0.82	2246	$2.3\ 10^{-3}$	0.44	2422	-
After 1 day	112	$1.5\ 10^{-4}$	0.84	2107	$2.2\ 10^{-3}$	0.44	2219	2150
After 3 days	93	$2.2\ 10^{-4}$	0.88	2060	$2.1\ 10^{-3}$	0.44	2153	-
After 7 days	160	$3.4\ 10^{-4}$	0.93	1893	$2.3\ 10^{-3}$	0.43	2053	-

	R_1 (Ω cm^2)	CPE_1 (S cm^{-2} s^n)	n_1	R_2 (Ω cm^2)	CPE_1 (S cm^{-2} s^n)	n_2	R_p (Ω cm^2)	
							EIS	Linear polarization
After 10 days	235	$5\ 10^{-4}$	0.93	1729	$2.2\ 10^{-3}$	0.53	1964	-
After 14 days	233	$7.1\ 10^{-4}$	0.93	1482	$2.1\ 10^{-3}$	0.56	1715	1780
After 17 deys	226	$8.3\ 10^{-4}$	0.93	1570	$2.1\ 10^{-3}$	0.58	1796	-
After 21 days	222	$1\ 10^{-3}$	0.92	1451	$2.1\ 10^{-3}$	0.58	1673	-
After 28 days	230	$1.5\ 10^{-3}$	0.90	1440	$1.9\ 10^{-3}$	0.58	1670	-
After 35 days	220	$2\ 10^{-3}$	0.88	1510	$1.8\ 10^{-3}$	0.58	1730	-

The R_{sol} equal to 10 ± 3 Ω, practically does not vary with immersion time and was not inserted in Table 3.

The natural seawater favours the formation of the corrosion product layer. A mass transport mechanism intervenes in the system formed by the corrosive medium/corrosion products/metal [10]. In this case the corrosion process can depend totally or partially on diffusion through this layer.

The polarization resistance, R_p, is equal to the sum of R_{ct} (R_1) and the diffusion resistance, R_2 [11]. The polarization resistances obtained from the polarization curves are in agreement with the polarization resistance obtained from EIS.

The serie of R_{ct} values has been used to calculate the data that has served to construct the corrosion progress curves in Figure 6.

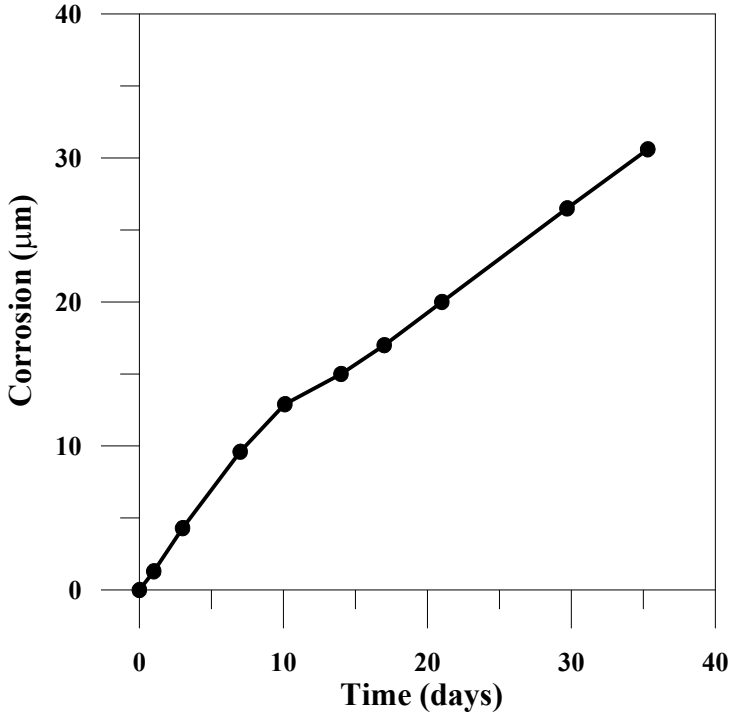

Figure 6. Electrochemically estimated curve of progress of attack as a function of exposure time to the aerated natural seawater for low-alloyed steel

The progress of the attack, (see Fig. 6), obtained from the electrochemical estimations, facilitate the quantitative analysis of the effect of time on the deterioration of the studied steel. During the first 10 days of immersion the corrosion rate is practically constant. This suggests a slight barrier effect of the corrosion products layer. Up to 10 days the attack continued to progress almost linearly but the slope of the curve of progress corrosion decreases possibly due to the decrease in the porosity of the corrosion products layer.

4. Conclusions

EIS measurements are use for studying the progress of corrosion of high-strength low alloys (HSLA) in aerated natural seawater. The application of this technique has revealed that the corrosion of the HSLA progresses is almost uniform during 35 days of exposure to the aerated natural seawater, despite the growth of corrosion products layer on the metallic surface. The linear progress of the attack with immersion time suggests a slight barrier effect of the corrosion products layer.

Received, March, 2007

**„Gh. Asachi"Technical University of Iasi,*
*** Las Palmas de Gran CanariaUniversity,*
Chemical Engineering Departament,
35017, Las Palmas de Gran Canaria, Spain

REFERENCES

1. M. Stern, A.L Geary., *J. Electrochem. Soc.*, **104,** 56 (1957).
2. M. Stern, A.L Geary., J. *Electrochem. Soc.*, **105,** 638 (1958).
3. E. Almeida, M. Morcillo, *Surf. Coat. Technol*., **124**, 169 (2000).
4. V. Barranco, S. Feliu Jr., S. Feliu, *Corros. Sci*. **46**, 2203 (2004).
5. Geru N., Bane M., Gurgu C., Cosmeleata G., Marin M., Analiza structurii materialelor metalice, , E.T. Bucuresti, 1991.
6. J.Pan, C.Leygraf, D.Thierry,M.Ektessabi, *J.Biom.Mater.Res*., **35**, 309 (1997).
7. T.P. Moffat, R.M. Latanision, *J. Electrochem. Soc*. **139**, 1869 (1992).
8. S. Haupt, H.H. Strehblow, *Corros. Sci*., **29**, 163 (1989).
9. E.B. Castro, J.R. Vilche, *Electrochim. Acta,* **38**, 1567 (1993).
10. K. Jutter, W.J. Lorenz, M.W. Kendig, F. Mansfeld*, J. Electrochem. Soc.*, **135**, 332 (1988).
11. J.R. Scully, *Corrosio*n, 56, 199 (2000).

UTILIZAREA SPECTROSCOPIEI ELECTROCHIMICE DE IMPEDANTA (EIS) IN COMPORTAMENTUL LA COROZIUNE A UNUI OTEL SLAB ALIAT IN APA DE MARE

Rezumat: Spectroscopia Electrochimica de Impedanta ofera posibilitatea studierii evolutiei coroziunii in timp pentru otelurile slab aliate. Testele de coroziune au fost realizate in apa de mare aerata (Oceanul Atlantic, Gran Canaria). Din diagramele de impedanta se obtin valorile pentru rezistenta la transferul de sarcina (R_{ct}). La stabilirea vitezei de coroziune utilizand ecuatia Stern-Geary, parametrul B sau pantele Tafel au fost obtinute folosind teste in curent continuu (DC), adica curbe de polarizare. Valoarea curentului de coroziune I_{corr}, a fost transformata in pierdere de masa aplicand legea lui Faraday. Variatia liniara a coroziunii in timp sugereaza o bariera slaba a produsilor de coroziune formati pe suprafata materialului metalic.

BULETINUL INSTITUTULUI POLITEHNIC DIN IAŞI
Tomul LIII (LVII), Fasc. 3, 2007
Secţia
ŞTIINŢA ŞI INGINERIA MATERIALELOR

THE COMPARATIVE STUDY OF THE DIFFUSION LAYERS TO THE SILICONIZED STEELS

BY

ZOLTAN MARKOS

Abstract: *At the siliconizing thermochemical treatments for steels, the treatment method has big influence on layers morphology and quality. After a long period of theoretical and experimental research, we can present some considerate concerning to the diffusion layer structure and properties. The paper presented some advantages and disadvantages of siliconizing technologies in powder and gas mediums.*
Keywords: *thermochemical treatment, siliconizing in gas and powder medium, steels*

1. Theoretical aspects

The siliconizing thermochemical treatment is a very complex process. The main factors which affect the compactness and the hardness in the diffusion layer could be, on the on hand, the technological factors (silicon potential, temperature, work conditions etc.), and on the other hand the percentage of carbon of the treated steel.

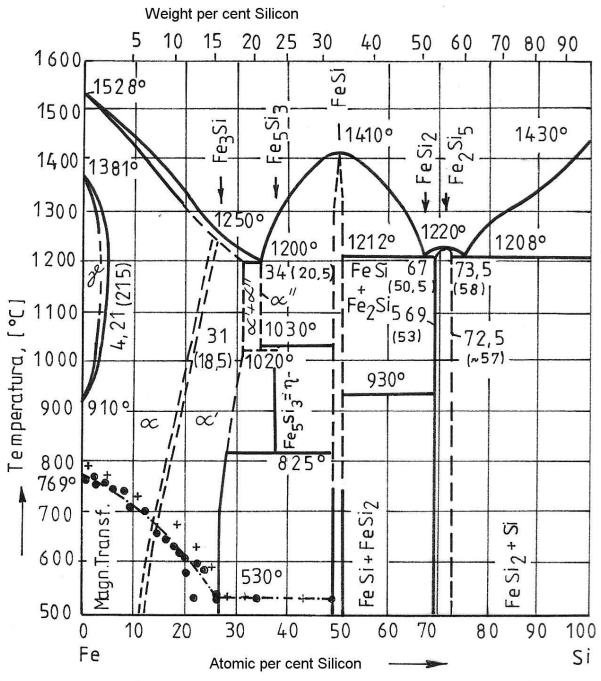

Fig.1. *The Fe-Si phase diagram*

The siliconizing can be made in different mediums, such as liquid, solid or gas. Because of the high working temperatures (between 950…1150^{o}C), the experiments in liquid medium (melted salts) didn't had the adequate results and have been stopped. This way, the experiments have been made in gas and powder mediums.

The siliconizing aiming the obtaining of a diffusion layer enriched with 6….14% Si at the surfaces of the samples. The siliconized layer gives an important resistance at oxidation and in acid mediums, both at normal and high

temperatures. The siliconized pieses could the way to substitute the high silicon alloyed casting pieces, which have a high brittleness and poor workability.

The siliconized layer structure contains silicon alloyed ferrite. Studied the Fe-Si phase diagram (Fig.1.), it can be observed that the Ferrite solves a quantity of about 11…12 at.% Si (up to this concentration, the silicon atoms presents a disorder statistical repartition). At higher silicon rates, the atoms have regular positions in the net and this way a similar chemical compounds structure is formed. The iron silicate (Fe_3Si, Fe_5Si_8, FeSi, Fe_2Si,…) are very high hardness constituents.

Because of carbon presents, the silicon alloyed cementite with chemical formula $Fe_{5,55}CSi_{1,12}$ or Fe_4CSi and Fe_6CSi appears in the structure. In conclusion, the siliconized layer hardness varies between very large limits (217….700μHV) and depends on both steel carbon rates and treatment medium silicon potential.

2. The siliconizing in gas medium

The siliconizing in gas medium assure an saturation in Si with high speed, uniform and compact diffusion layer and the sample surface remain clean and without adherences.

At the siliconizing at low pressures, the active gas was $SiCl_4$. The pressure were 10^{-2} torr and for the delusion of $SiCl_4$ an active (H_2) or an inert gas (Ar) is used. In the Fig.2. is presented the microstructure of a siliconized steel (OLC45 STAS 880-80) at 1100°C, for 50 minutes on a mixture of $SiCl_4$ and H_2.

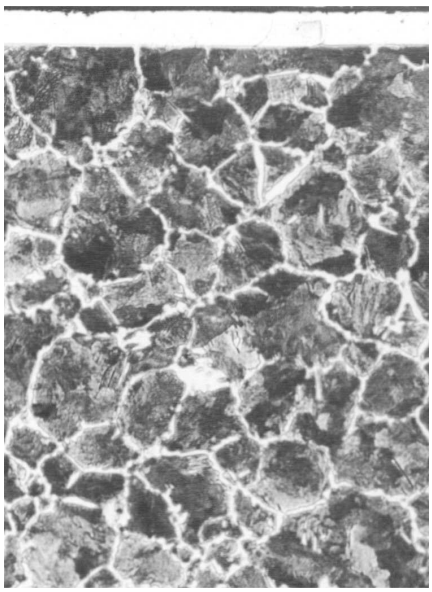

Fig.2. *The microstructure of the siliconized steel al low pressure in gas medium*

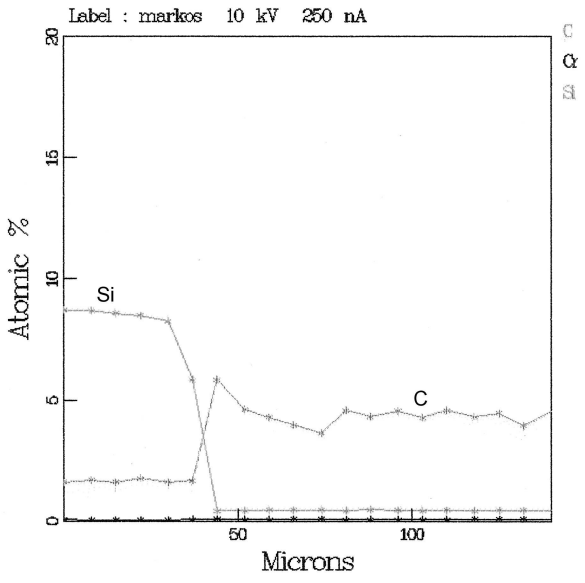

Fig.3. *The Si and C distribution after the electron probe microanalysis*

An increased saturation speed was obtained (the thickness of layer is 40μm) and the layer is compact and adherent. At treatments made in gas at low pressures, the sample's surface remains clean even for treatments made at high

temperatures. After the electron probe microanalysis an uniform distribution of the Si on the diffusion layer can be observed.

3. The siliconizing in powder medium

The siliconizing in powder mediums technologies, in closed boxes, represent simple methods, easy to apply in any treatment workshops. By choosing adequate parameters, the diffusion layer is compact and adherent.

Having in view the obtaining of treatment medium the ferro-silicon (containing 50….70% Si) with a granulation of about 0,06….0,3 mm is used. The most adequate complementary material is alumina (Al_2O_3), which assure the adherence decrease and its rate is about 25…30%. The activator used substance is NH_4Cl, and its rate must be of about 2…3% in the siliconizing mixture. A very high importance belongs to the siliconizing box tightening. For the lead tightening paste based on soda waterglass can be used, but the most utilized method is the welding of the lead.

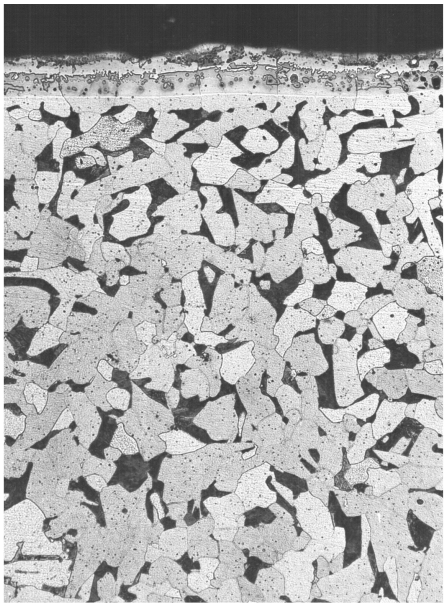

Fig.4. *The microstructure of the siliconized steel in powder medium whit paste*

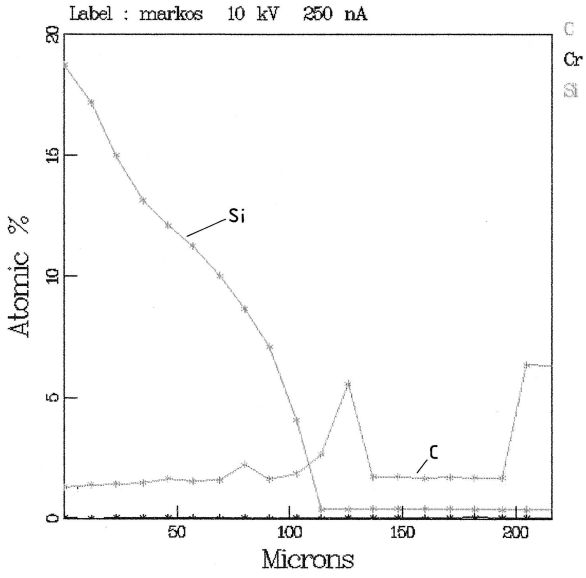

Fig.5. *The Si and C distribution after the electron probe microanalysis*

The process temperature has an important influence on the diffusion speed and on the diffusion layer compactness. In the case of the treatment made at 1050….1100^{o}C, the diffusion velocity is high (approx. 0,1 mm/hour), but the diffusion layer presents porosity and at the sample surface the adherences appear. At lower temperatures the diffusion speed is smaller, but the surface is cleaner. For obtaining of an uniform thickness layer, a siliconizing in paste can be used.

Fig.4. shows the microstructure of an improving steel which contain 0,15% C (OLC 15 – STAS 880-80) after a treatment at 950^{o}C for 6 hours and Fig.5. shows the results of the electron probe microanalysis. The diffusion layer presents porosity and adherences.

4. Conclusions

For choosing the adequate siliconizing technology, the technical conditions in the treatment department have been taken into consideration.

The siliconizing in gas mediums at low pressures assure the obtaining of very good results and a very easy control of work parameters. The diffusion speed is high and the layer is compact and adherent. In the same time, the method reclaim very expensive and complex equipment.

The siliconizing in paste presents a simple method which can be made in any treatment department. The obtained results depend on the siliconizing box tightening. The treatment made at low temperatures (950…1000^{o}C) assures a compact diffusion layer, the samples surfaces are relative clean, but the diffusion speed is bit low. At higher temperatures (1050…1100^{o}C), the siliconizing speed increase, but the layer porosity is higher and the surface present adherences.

REFERENCES

1. Bradley, B., Jellinek, M.: Production of silicon metal from dichlorsilane – Patent no.3824121/16.08.174. USA
2. Markos, Z., Florea, R.: Influence du procédé de chauffage sur les résultats du traitment d'enrichisse-ment de silicium - Bulletin of the University of Braşov, Vol. XXXI. Part.II. 1989.
3. Markos, Z., Banciu, R.: Research regarding the treatment temperature for steel siliconizing - Romanian Journal of Engineering, University "Ovidius" of Constanta, 1999.

Zoltan MARKOS - ***TRANSILVANIA*** University of Braşov
Department of Materials Engineering and Welding – Bul. Eroilor nr.29. – 500036 Brasov
e-mail: z.markos@unitbv.ro

STUDIU COMPARATIV AL STRATURILOR DE DIFUZIE LA OȚELURILE SILICIZATE

Rezumat: La tratamentul termochimic de silicizare a oțelurilor, tehnologia utilizată are o influență hotărâtoare asupra morfologiei şi calității stratului de difuzie. In urma unor studii teoretice şi practice îndelungate, autorul prezintă unele considerații cu privire la structura şi proprietățile straturilor de difuzie obținute la silicizarea în medii gazoase şi pulverulente.

BULETINUL INSTITUTULUI POLITEHNIC DIN IAŞI
Tomul LIII (LVII), Fasc. 3, 2007
Secția
ŞTIINȚA ŞI INGINERIA MATERIALELOR

RESEARCH CONCERNING THE INFLUENCE OF STRUCTURE ON THE EROSION OF IRON GRAY

BY

LARISA ISTRATE, DAN GELU GALUŞCĂ, BOGDAN CIOBANU

Abstract : *This paper presents some theoretical and experimental aspects concerning the influence of iron gray structure on complex erosion phenomenon. Great attention must be paid to the copy method of the erosion phenomenon, which should be similar to what is encountered in practice of using hydraulic machines and installations.*

In this direction, the erosion process of the adjustment parts is very similar to the one made by modelling installations with rotary disc and liquid jet.

Keywords: *erosion, cavitation, iron gray*

1. Introduction

The "erosion" phenomenon is known in the modern engineering as the "Cancer of hydraulic machines and adjustment parts"[1]. In the case of complex erosion, the systematic analysis of the response of materials to the cavity attack is possible only in conditions found in research labs, with the help of devices and installations which permit the generation and production of an erosion phenomenon with desired intensity and which can be controlled and maintained at the same parameters for a long time.

Conventionally, the working liquid is water at a different temperature and pressure from atmospheric values. Other liquids can be utilized as well, with variable temperatures and pressures [4].Choosing the experimental method based upon rotary disc and liquid jet is justified by a number of economic advantages, such as: relative short period of test, easy adjustment of hidro-dynamic parameters, low cost

2. Material and methods

The lab tests were made on a sequence of specimens, tested as to their response to the impact with hydraulic jet (with or without emery material). The specimens were made of Fc 250 and Fgn 500-7, through frontal smoothing, processed as sector-like form of circular crown with internal diameter congruous with the circle from the sample disc and with a central hole which allowed the fastening with a screw to the rotary disc.

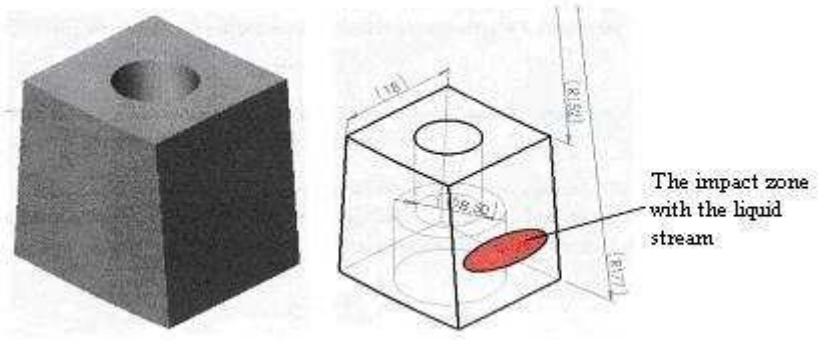

Fig.1. The form of the specimens distinguishing the surface on which places the impact.

The erosion tests were made in water with temperature of 20±°C. All four specimens, with different grades of roughness Ra (6,3 şi 12,5 μm) were tested for 32 hours, after which they were submitted to a precise process of cleaning and weighing on an analytical balance with a precision of ±0,0001 mg. The pressure in the working chamber, measured at the mounting level of samples on the immersed disc, was kept constant during the experiment, and was recorded during the testing on a tape recording device.

Table1. Chemical composition and main mechanical properties of utilized iron casts

Material	Stas	şarja	CHEMICAL ANALYSIS										
			C	Si	Mn	P	S	Cr	Mg	Ni	Sc	Ce	C+Si
Fc250	SREN 1561/99	30/1/F	3,35	1,99	0,80	0,250	0,095	0,072	-	0,048	0,942	4,070	5,330
Fgn 500 - 7	SR EN 1563/99	33/1/F	3,87	2,47	0,36	0,057	0,011	-	0,076		1,112	4,703	

Material	Stas	şarja	MECHANICAL TESTS			
			Rm	HB	A_5	R_{po2}
Fc250	SREN1563/99	30/1/F	271	226	-	-
Fgn 500 - 7	SR EN1563/99	33/1/F	561	226	12,4	376

The samples were examined with the NEOPHOT optical microscope, which is in the possession of "Robinete Industriale " factory from Bacau. They were prepared through smoothing and attacked with Nital 5%. The installation designed for studying the influence of structure on complex erosion phenomenon (impact, cavity, cavity-abrasive, and through hydro-abrasive effect) and carried out in the "Fluid Mechanics, Machines and hydraulic and pneumatic drives" lab from the Technical University „Ghe. Asachi" Iaşi is of rotary disc installation and sunk fluid jet type (the capacity provided by the injector is smaller than peak capacity which can be drained by the installation) [3].

3. Results and discussions

To mark out the influence of quality parameters of structure on the cavity-abrasive wear and tear process for chosen materials were utilized the following characteristic measures [2]:

- weight loss ΔG of specimens, through cavity-abrasive wear and tear for a t time imposed for testing. The value of weight loss was determined through weighing on an analytical balance before and after the cavity-abrasive wear and tear process, for preset periods of time.
- volume loss ΔV of specimens, congruous to a imposed testing time t and to a given roughness. R_{ai} was determined taking into consideration the specific weight of material from which the specimen is built and which is a constant:

$$\gamma = 7.2 \text{ g/cm}^3 \quad (1)$$

- average depth penetration MDPR, determined by the rapport between total volume loss ΔV_t (congruous to total testing time) and surface A of the specimen :

$$MDPR = \Delta V_t / A \quad (2)$$

The foundation of determining average depth penetration is the hypothesis that the material lost through cavity-abrasive wear and tear is quasi-uniform distributed.

- speed of erosion ν, representing the decreasing speed of specimen`s volume in a supposed period of time and defined as a tangent of the angle between direction of tangent to the dependence curve $\Delta V = f(t)$, in the point congruous to supposed testing time t, and abscissa:

$$\nu = d(\Delta V)/dt \quad (3)$$

The experimental results concerning weight loss, average depth penetration, values of roughness between and after wear and tear test, as well as erosion speed, are given in the following tables [5].

Table2. Weight loss for 1= 40 mm

Epruveta	Condiții de testare l[mm]	m_i [g]	m_f [g]	Δ_G [mg]	R_{ai} [μm]	R_{af} [μm]	Fig.
$E_{1\ (Fgn\ 500-7)}$	40	46.47019	46.21014	260.05	6.3	14.7	g
$E_{2(Fgn\ 500\ -7)}$	40	46.51000	46.06037	449.63	12.5	15.9	h
$E_{3\ (Fc250)}$	40	45.53023	44.73058	799.65	6.3	-	-
$E_{4\ (Fc250)}$	40	46.94032	46.50053	439.79	12.5	18.7	d

Table3. Weight loss for 1= 60 mm

Epruveta	Testing conditions l[mm]	m_i [g]	m_f [g]	Δ_G [mg]	R_{ai} [μm]	R_{af} [μm]	Fig.
$E_{1\ (Fgn\ 500-7)}$	60	47.17056	47.03033	140.23	6.3	14.4	a
$E_{2(Fgn\ 500\ -7)}$	60	46.88031	46.75037	129.94	12.5	19	b
$E_{3\ (Fc250)}$	60	47.53022	47.39051	139.71	6.3	15.1	c
$E_{4\ (Fc250)}$	60	46.49079	46.34021	150.58	12.5	17.3	i

Table4. Weight loss for 1= 80 mm

Epruveta	Testing conditions l[mm]	m_i [g]	m_f [g]	Δ_G [mg]	R_{ai} [μm]	R_{af} [μm]	Fig.
$E_{1(Fgn\ 500-7)}$	80	46.46012	46.39025	69.87	6.3	27.6	j
$E_{2(Fgn\ 500\ 7)}$	80	46.73042	46.63064	99.78	12.5	25.3	k
$E_{3\ (Fc250)}$	80	47.96020	47.87034	89.86	6.3	20.8	l
$E_{4\ (Fc250)}$	80	48.22032	48.08058	139.75	12.5	19.9	f

Analyzing the values of top wear and tear speeds and MDPR in accordance with tables 5 and 6, one observes that they increase at the same time with roughness increase.

Table 5. Average depth of penetration MDPR

Epruveta	Testing conditions l[mm]	MDPR [mm]
$E_{1\ (Fgn\ 500-7)}$	40	0.08026
$E_{2\ (Fgn\ 500-7)}$		0.13877
$E_{3\ (Fc250)}$		0.24680
$E_{4\ (Fc250)}$		0.13573
$E_{1\ (Fgn\ 500-7)}$	60	0.04328
$E_{2\ (Fgn\ 500\ -7)}$		0.04010
$E_{3\ (Fc250)}$		0.04312
$E_{4\ (Fc250)}$		0.04647
$E_{1\ (Fgn\ 500-7)}$	80	0.02156
$E_{2\ (Fgn\ 500\ -7)}$		0.03079
$E_{3\ (Fc250)}$		0.02773
$E_{4\ (Fc250)}$		0.04312

Tabel 6.Erosion speed ν [5].

Epruveta	Testing conditions l[mm]	ν [mm³/h]	Testing conditions l[mm]	ν [mm³/h]	Testing conditions l[mm]	ν [mm³/h]
E_1 (Fgn 500-7)	40	1.12868	60	0.60863	80	0.30325
E_2 (Fgn 500 -7)		1.95151		0.56397		0.43307
E_3 (Fc250)		3.47070		0.60637		0.39001
E_4 (Fc250)		1.90880		0.65355		0.60650

Through analysis of obtained experimental data, it was observed that cavity-roughness depends not only on mechanical properties of erosion of the material but also on the status of superficial layer. The final status of superficial layer in relationship with roughness parameter, structure and even nature and depth of internal stress can have a critical role on cavity-roughness [3].

This kind of response from material can be in conjunction with the type of liquid washing of the specimens, produced in the presence of surface micro-irregularities. In the sector with small roughness, the wear and tear develops slower and with their growth, increases fast both the wear and tear and resistance to motion.

Looking at the aspect of wear and tear, it presents itself as craters at the level of active surface of the sample with a closed and irregular profile. The cavity-wear and tear develops in size and depth with the increased time of exposure to erosion.

In case of smaller testing times, cavity-wear and tear presents itself as pinches spreaded on a small depth which doesn`t exceed 1mm. At the same time is pointed out the existence of more than one front of advancing wear and tear. In case of small roughness, Ra = 6,3 one observes an intergranular penetration of cavity-wear and tear and which is more developed in areas with intercrystalline deficiencies.

The wear and tear, penetrating in this way the material, produces the dislocation of metallic granules. From a quantitative viewpoint, the cavity-wear and tear depends on the time of exposure to the cavity.

Concerning the effect of the distance between injector nozzle and the surface of specimen on which the impact takes place, one observes an acceleration of the material discarding phenomenon at the same time with a decrease of distance 1 from 80 to 60 mm[2].

With a further decrease of distance up to 40 mm, although we recorded an increase of the wear and tear process, it wasn’t so obvious as in the precedent case.

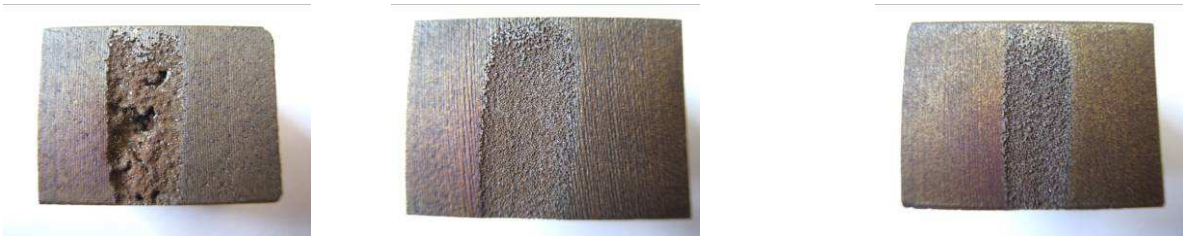

a b c

Fig2. Aspect of specimen wear and tear from Fgn 500-7 in a) l = 40mm; b) l = 60 mm; l = 80 mm; Ra_i = 6,3 mm; testing time t = 32 ore

a b c

Fig3. Aspect of specimen wear and tear from Fgn 500-7 in: a) l = 40mm; b) l = 60 mm; l = 80 mm; Ra_i = 12,5 mm; testing time t = 32 ore

a b c

Fig.4. Aspect of specimen wear and tear from Fc 250 in: a) l = 40mm; b) l = 60 mm; l = 80 mm; Ra_i = 6,3 mm; testing time t = 32 ore

a b c

Fig5. Aspect of specimen wear and tear from Fc 250 in: a) l = 40mm; b) l = 60 mm; l = 80 mm; Ra_i = 12,5 mm; testing time t = 32 hours

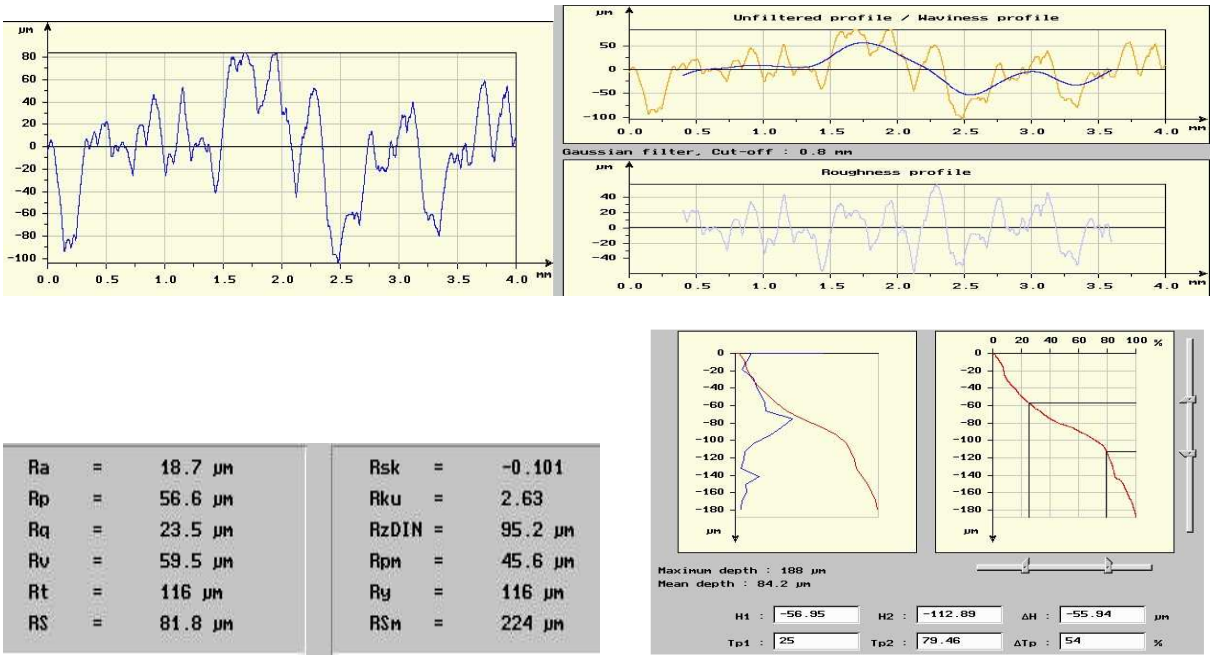

E_4 (l 40) a)

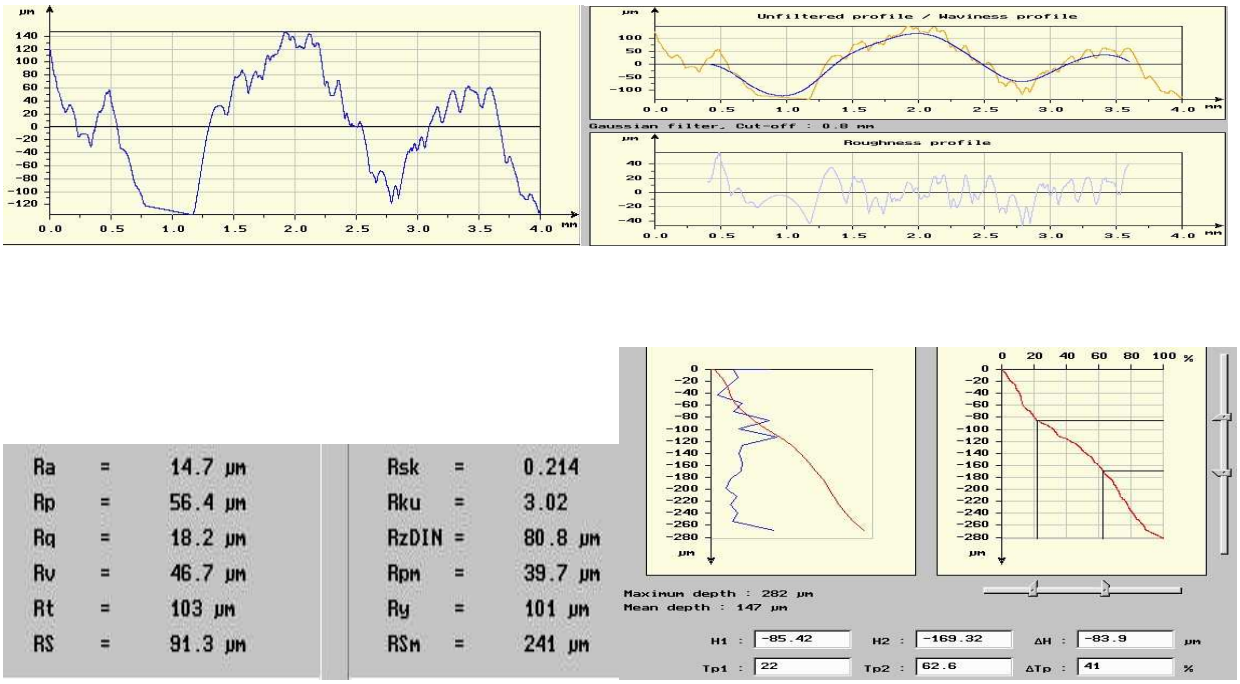

E_1 (l 40) b)

Fig6. Roughness of metallic surfaces subjected to wear and tear tests

Roughness influence is marked out through an increase in weight loss due to cavity-wear and tear with the increase of roughness Ra of active surfaces of specimens exposed to tests. Roughness of metallic surfaces subjected to wear and tear tests influences in a clear manner the process of material discarding; wear and tear gets faster and more pronounced at the same time with an increased roughness of the

loaded surface. This is explained by the dynamic of the wear and tear process observed while sampling the experimental data.

4. Conclusions

- The intensity of the wear and tear through cavity-erosion phenomenon increases at the same time with the increase of surface roughness; this is more obvious in a small roughness sector
- A decrease in distance between injector nozzle and specimen`s surface intensifies the wear and tear process
- Cavity-wear and tear develops in size and depth as the time of exposure to erosion increases.

References

[1]**ANTON, I.**, "The cavitation", *Vol. I., II*., Editura Academiei R. S. România, 1984.
[2]**CIOBANU, B**, "Research concerning the influence of microgeometry of active surfaces parameters on the performance of hydraulic machines", Doctorate thesis, Iasi 2003
[3]**CIOCAN, L "**Contributions concerning the surface roughness on cavity erosion through hydro-dynamic jet", Doctorate thesis Iasi 1985
[4]**ISTRATE, L**., The protocol of research. Materials and devices used, Paper 2
[5]**ISTRATE, L**., Research concerning the influence of structure on the erosion of iron gray, Paper 3.

CERCETĂRI PRIVIND INFLUENAŢA STRUCTURII ASUPRA EROZIUNII FONTELOR CENUŞII

REZUMAT: Lucrarea reprezintă câteva aspecte teoretice şi experimentale privind influenţa structurii fontelor cenuşii asupra fenomenului de eroziune complexă. O atenţie deosebită trebuie acordată metodei de reproducere a fenomenului de uzură care să se asemene cât mai mult cu cele întâlnite în practica exploatării maşinilor şi instalaţiilor hidraulice. În aceste sens, foarte asemănător procesului de uzură de la organele de reglaj este cel reprodus de instalaţiile de modelare cu disc rotativ şi jet de lichid.

BULETINUL INSTITUTULUI POLITEHNIC DIN IAŞI
Tomul LIII (LVII), Fasc. 3, 2007
Secția
ŞTIINȚA ŞI INGINERIA MATERIALELOR

THE EFFECT OF REACTION PARAMETERS ON POLYANILINE POWDERS CRYSTALLINITY

BY

IULIA MIHAI[1], MARIA IVANOIU[1], CLAUDIA GORDIN[1], SAMUEL DOREY[2], DENIS ANOKHIN[2], DIMITRI IVANOV[2], NATALIA GOSPODINOVA[2]

ABSTRAC*T - Polyaniline (PANI) is one of the most intensively investigated conducting polymers during the last time. The establishment of the favorable reaction parameters allowing the design of its properties, determining the potential application areas (alternative energy sources and transformers, media for erasable optical information storage, non-linear optics, membranes, etc.) is an important scientific problem. This polymer was prepared by oxidative polymerization with ammonium persulfate in aqueous acidic solution at 0ºC and at negative temperatures in presence of different salts. The structural ordering within crystalline polyaniline* powders *has been studied using X-ray diffraction. PANI powders, obtained immediately after synthesis, have significant crystalline fractions which nominally approximate the proposed pseudo-orthorhombic type I (emeraldine salt-I, ES-I) salt structure (Pouget, J. P.; et all. Macromolecules 1991, 24, 779). An enhanced crystallinity in terms of structural perfection is observed by beans of X-ray diffraction spectra. The reaction parameters effect on the structure and X-ray diffraction of the polymer are discussed further on.*
KEYWORDS*: emeraldine salt; oxidative polymerization; acid; powder; cristallinity*

INTRODUCTION

Polyaniline and some of its derivatives have been extensively studied because of their ease of preparation by chemical and electrochemical methods, good environmental stability, and also because their electrical properties can be modified by both the oxidation state of the main chain and by protonation [1-4]. These materials are found to be useful for a wide range of applications ranging from lightweight batteries to corrosion inhibitors [5-7]. Continuous efforts have led to some novel applications and to their commercialization [8-10]. Developments are directed to the numerous unsolved problems that remain, such as poor mechanical properties, processability at high temperature, and solubility in common organic solvents [11-13]. The preparation methods of polyaniline involve two main techniques (chemical and electrochemical) using suitable protonation media [14]. We hereby report the influence of different synthesis parameters on the PANI structure using X-ray diffraction method. PANI was synthesized by oxidative polymerization.

EXPERIMENTAL

Materials

Reagent-grade aniline, ammonium persulfate were purchased from Aldrich and used as received. Potassium chloride (KCl) was purchased from Carlo Erba; sodium chloride analytical grade (NaCl) was purchased from Prolabo; anhydrous lithium

chloride (LiCl), calcium chloride ($CaCl_2$), anhydrous sodium sulfate (Na_2SO_4), sodium formate (NaCOOH), and ammonium hydrogen sulfate (NH_4HSO_4) were purchased from Fluka; formic acid was purchased from Sigma Aldrich.

Polymer synthesis

The polyaniline was obtained by the oxidation of aniline in acidic aqueous medium. The oxidation was done by the means of an oxidant commonly used, the ammonium persulfate. The acid used is the formic acid. Two solutions were prepared in the first stage: 1) aqueous solution of aniline and 2) aqueous solution of the oxidant. The two vessels were placed in an ice bath and then in a refrigerator. After 30 min. a temperature of 0-0,5°C was reached. For negative temperatures (of -10°C to -35°C) the flasks were cooled in a freezer. After that, the reacting substances were mixed and stirred. The polymerisation products resulted like a light/dark green suspension depending on initial aniline concentration. At a given time one may notice that PANI was deposed as precipitate on the bottom flask. The obtained polymers are separated by filtration through paper filters and washed for several times with aqueous acidified solutions using the synthesis acids. The suspension of PANI in aqueous acidic solution is allowed to stand at room temperature without stirring and then the liquid is decanted from the precipitate. The wet powder of PANI was dried onto a glass support at room temperature. Finally the dried product remains like a powder.

Characterization methods

Structure of PANI was investigated by X-ray diffraction (XRD) using a Philips X'Pert apparatus. PANI powder have been analysed without further preparation after synthesis excepting some samples, which have been pressed as pellets to perform some conductivity measurements.

RESULTS AND DISCUSSION

Polyaniline was synthesized with formic acid with an increasing concentration of NaCl. The diffractograms of polyaniline obtained in presence of formic acid show only a halo, meaning that material is amorphous. The precision of such reflections in highly amorphous materials is poor since signal-noise ratio is weak. Increasing the amount of salt determines the increase of crystalline ordering of PANI products in the presence of formic acid. PANI diffractograms presents four major reflections at 9.2, 15.2, 21.4, 25.7°, respectively corresponding to d-spacings = 9.5, 5.8, 4.2, and 3.4 Å.
The 25.7° reflection is the most intensive reflection. These four reflections are accompanied by other small ones at especially 27.2° (3.3 Å) and two weak broad reflections at 29.7 and 35.5° (d-spacings = 3.0 and 2.5 Å respectively). The last one is rather insignificant compared to the four major reflections, which are well marked.

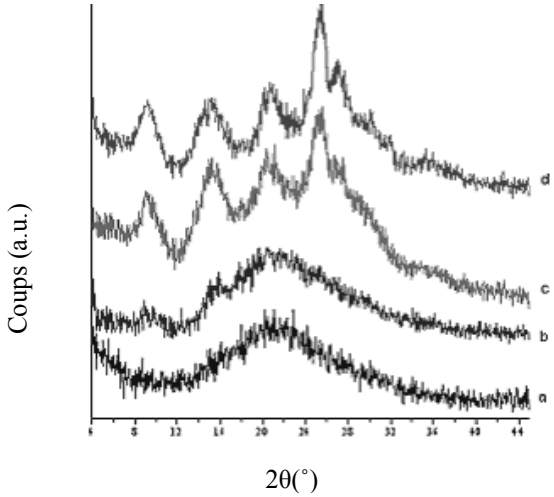

Figure 1: XRD patterns obtained from PANI powders synthesized with formic acid in presence of an increasing concentration of NaCl: a) 0 M, b) 0.5 M, c) 2 M, and d) 4.2 M. Aniline concentration = 0.01. The synthesis was performed at 0°C and powders are dried at T_{room} on glass support.

That resolution means that the intensity ratios between the 25.7° reflection and the other three reflections at 9.2, 15.2, and 21.4 are really different when PANI is synthesized with formic acid. This aspect tends to indicate a higher crystallinity when the intensity difference between the 25.7° reflection and other ones is weaker. A final reflection could be distinguishable at high salt content of 5.8° (d = 15.1 Å) with formic acid. This distance may correspond to a high ordering creation in PANI materials and is representative for the high crystallinity fraction.
All these results are perfectly in accordance with those from Pouget *et al.* [24] works. They performed $(NH_4)_2S_2O_8$-oxidative synthesis of polyaniline in HCl 1M at –13°C with subsequent HCl treatment to reach 50% doping degree. They have made their own classification distinguishing two form of emeraldine salt: ES-I and ES-II. In view to our results, our polyaniline can be classified into the ES-I category. All the main reflections observed (d-spacings = 9.6, 5.9, 4.26, and 3.51 Å) in the "low temperature" ES-I have been indexed according to them in a pseudo-orthorhombic cell with lattice parameters a = 4.3 Å, b = 5.9 Å, c = 9.6 Å. They have attributed the largest d-spacing to c because it is close to a polymer repeat distance. Furthermore, because of the presumed chain tilting, other three distances may be assigned to interchain distances.
In conclusion, the rise of salt concentration increases the polyaniline crystallinity fraction in presence of formic acid. The high content of salt gives rise to ordering creation at larger scale.

Since anions are bigger than cations, we suppose that their influence on water structure is greater. However we wanted to investigate the effect that cations may have on chain organization. We have chosen alkali chloride salts since Cl^- is chaotropic (weakly hydrated) and favors solute hydration. Cations having very different hydration ability have been chosen. Syntheses were performed in formic acid either in presence of NaCl, LiCl and $CaCl_2$ salts with a concentration of 4.2M, or in presence of KCl with a concentration of 2.3M in order to investigate the influence of different cations on crystallinity. KCl was employed with a lower concentration, because its

solubility is lower than other salt solubility. Addition of all salts mentioned above leads to the formation of PANI semi-crystalline.

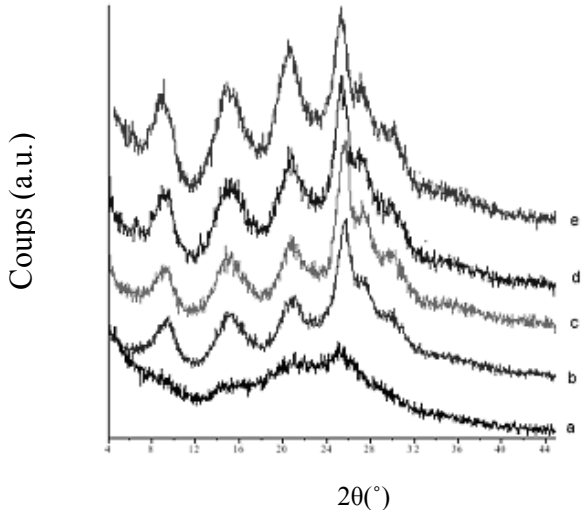

Figure 2: XRD patterns obtained from PANI products synthesized with formic acid in presence of alkali chloride salts: a) without salt, b) LiCl 4.2M, c) $CaCl_2$ 4.2M, d) KCl 2.3M, and e) NaCl 4.2M. Aniline concentration = 0.04. The synthesis was performed at 0°C and powders were dried at T_{room} on glass support.

Ca^{2+} and Li^+ that are strongly hydrated leading to polyaniline highly crystalline but presenting the 25.7° reflection very intensive compared to other reflections at 9.2, 15.2, and 21.4°. This fact indicate a lower crystallinity fraction.

On the other hand, diffractograms of PANI synthesized in presence of NaCl or KCl present the peak at 5.8° (1,5 nm) characteristic of large scale order. We may thus resume the ability of alkali chloride salts to increase the crystallinity in the following order : $Ca^{2+} < Li^+ < Na^+ < K^+$. This sequence is perfectly in agreement to the increasing chaotropic feature from Ca^{2+} to K^+.

According to the impossibility to increase acid concentration because of the PANI chain hydrolysis, we have used sodium salts to investigate the influence of different anions : HSO_4^-, Cl^-, and $HCOO^-$. On one hand, increasing the aniline concentration in presence of formic acid weakly increases the crystallinity fraction. On the other hand, synthesis in presence of HCOONa leads to polyaniline wholly amorphous.

Furthermore, the halo maximum is shifted to a higher d-spacing if compared to it obtained with formic acid only. The syntheses in presence of anions such as Cl^- and HSO_4^- lead to PANI semi-crystalline. It is important to notice that the Na_2SO_4 concentration was weak because we did not succeed in working with upper Na_2SO_4 concentration because of its lack of solubility at that temperature. In both HSO_4^- and Cl^- diffractograms, four main reflections in both cases are observed at 9.1, 14.6, 20.6, 25.7° (d-spacing = 9.6, 6.0, 4.3, 3.4 Å). The very weak reflection at 5.8° is also observed with both anions. The intensity ratio between the 25.7° reflection and the three reflections at 9.1, 14.6, and 20.6° is lower when the polyaniline is synthesized with Cl^- anions.

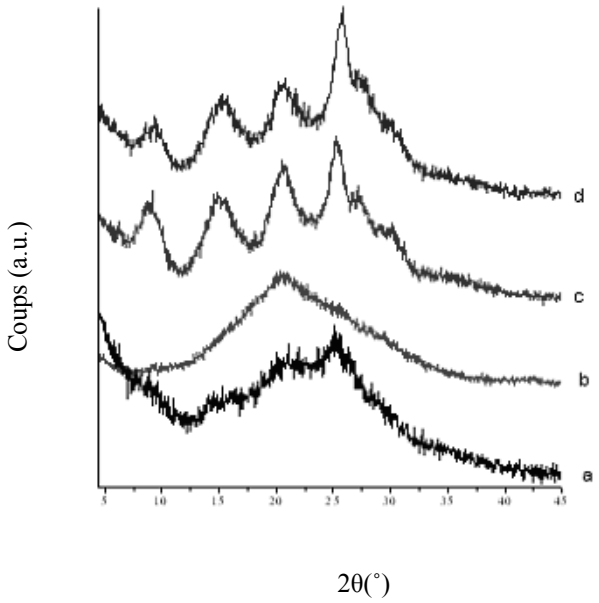

Figure 3: XRD patterns obtained from PANI products synthesized with formic acid in presence of different salts: a) without salt, b) NaCOOH M, c) NaCl 4.2 M, d) Na_2SO_4 M. Aniline concentration = 0.04. The synthesis was performed at 0°C and powders were dried at T_{room} on glass support.

One may summarize the ordering creation ability of that anions according to their chaotropic ability in the following series: $HCOO^- < HSO_4^- < Cl^-$; this sequence inversely corresponds to the hydration ability of the anions ($HCOO^-$ is more hydrated than Cl^-).

Some of these salts were used to perform polymerization at low temperatures and at concentrations, which allow keeping the medium liquid during polymerization without ice formation. In that conditions, we have retained NaCl and $CaCl_2$, which are, salts considerably allowing decreasing freezing temperature. $CaCl_2$ salt with a higher concentration than previously allowed us to work at a temperature of –35°C whereas with NaCl, the working temperature was –27°C. Syntheses of PANI in presence of both $CaCl_2$ and NaCl salts lead to polyaniline powders well crystallized (Figure 4a and Figure 4b respectively).

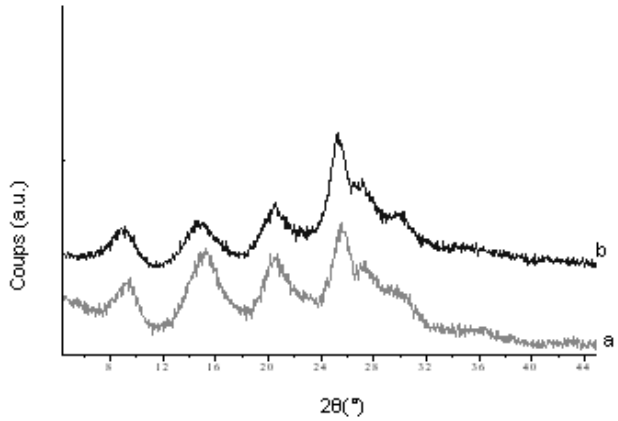

Figure 4: XRD patterns obtained from PANI products synthesized with formic acid in presence of different salts: a) with $CaCl_2$ 3.5M at –35°C, b) with NaCl 4.2M at -27°C. XRD patterns were obtained in reflexion mode for a), b). Aniline concentration = 0.04. The PANI products were dried at T_{room} on glass support.

The ordering ability of cations at low temperature respects the following sequence: $Ca^{2+} > Na^{+}$. In respect to chaotropic feature, crystallinity of PANI synthesized with Na^{+} should be higher than Ca^{2+} but NaCl does not allow working at a so low temperature. Therefore, the temperature plays an important role for the chain organization.

CONCLUSIONS

PANI has been synthesized with formic acid, in presence of different salts, and at different temperatures. It points out that formic acid mixed with different salts leads to a better crystallized polyaniline. Crystallinity fraction of PANI powders increases with the chaotropic characteristics of ions. Some of these ions allow working at low temperatures, which has been demonstrated as an important factor to promote chain organization. In consequence, we could promote or hinder the ordering creation by adding salts differing in nature and in concentration.

REFERENCES

[1] MacDiarmid AG, Chiang JC, Halpern M, Huang WS, Mu SI, Somasiri NLD, Wu W and Yaniger SI, Mol Cryst Liq Cryst 121:173 (1985).
[2] Huang WS, Humphery BD and MacDiarmid AG, J Chem Soc Faraday Trans 1 82:2385 (1986).
[3] Paul EM, Rico AJ and Wrighton MS, J Phys Chem 89:1441 (1985).
[4] (a) Bedekar AG, Patil SF, Patil RC and Vijayamohanan K, J Mater Chem 5(7):963(1995). (b) Bedekar AG, Patil SF, Patil RC and Deore B, Matter Lett 25:48 (1995).
[5] Arbizzani C, Mastragostino M and Crosati BS, Handbook of Organic Conductive Molecules and Polymers, Vol 4, Ed by Nalwa HS, John Wiley & Sons, Chichester 595 (1997).
[6] Olcani A, Abe M, Ezoe M, Doi T, Miyata T and Miyake A, Synth Met 57:3696 (1993).
[7] McAndrew TP, Trip 5 (1):7(1997).
[8] Matsunaga T, Daifuku H, Nakajima T and Kwagoe T, Polym Adv Tech. 1:33 (1990).
[9] Gregory RV, Kimbrell WC and Kuhn H, J Coated Fabrics 20:1 (1991).
[10] Takashima T, Kaneto M, Kaneto K and MacDiarmid AG, Synth Met 71:2265 (1995).
[11] Yang J, Zhao C, Cui D, Hou J, Wan M and Xu M, J Appl Polym Sci 56:831 (1995).
[12] Laska J, Pron A and Lefrant S, J Polym Sci Part A Polym Chem 33:1437 (1995).
[13] Cao Y, Smith P and Heeger AJ, Synth Met 48:91 (1992).
[14] Patil RC, Patil SF, Mulla IS and Vijayamohanan K, Polym Int 49:189 (2000).

IULIA MIHAI[1], MARIA IVANOIU[1], CLAUDIA GORDIN[1], SAMUEL DOREY[2], DENIS ANOKHIN[2], DIMITRI IVANOV[2], NATALIA GOSPODINOVA[2]

[1]"GH. ASACHI" TECHNICAL UNIVERSITY,
[2]UNIVERSITÉ DE HAUTE ALSACE
INSTITUT DE CHIMIE DES SURFACES ET INTERFACES, 15, RUE, JEAN STARCKY, BP2488, 68057 MULHOUSE CEDEX, FRANCE

EFECTUL PARAMETRILOR DE REACTIE ASUPRA CRISTALINITATII PUDRELOR DE POLIANILINA

Rezumat: Polianilina (PANI) este unul dintre cei mai intens studiaţi polimeri conductori din ultimul timp. Stabilirea parametrilor de reacţie favorabili ce permit designul proprietăţilor sale constituie o problema ştiinţifica importanta deoarece condiţionează potenţiale aplicaţii (surse alternative de energie, dispozitive pentru stocarea energiei, optica neliniara, membrane etc.). Acest polimer a fost preparat prin polimerizare oxidativa cu persulfat de amoniu in soluţie apoasa acida la 0˚C si la temperaturi negative in prezenta a diferite săruri. Ordonarea structurala a pudrelor cristaline de polianilina s-a studiat folosind difracţia de raze X. Pudrele de PANI obţinute imediat după sinteza prezintă fracţii cristaline semnificative cu o structura apropiata de cea propusa pentru polianilina-sare de tip I (ES-I) (Pouget, J. P.; et al. Macromolecules 1991, 24, 779). Din spectrele de raze X rezulta o îmbunătăţire a ordonării structurale prin creşterea cristalinităţii. In continuare se discuta efectul parametrilor reacţiei de sinteza asupra structurii polianilinei corelat cu rezultatele obţinute prin studiul cu raze X.

BULETINUL INSTITUTULUI POLITEHNIC DIN IAŞI
Tomul LIII (LVII), Fasc. 3, 2007
Secția
ŞTIINȚA ŞI INGINERIA MATERIALELOR

A STUDY REGARDING THE INFLUENCE OF COPPER AMONT ON THE MECHANICAL PROPERTIES OF THE SINTERED MATERIALS MADE FROM POWDERS BASED IRON

BY

C. PAVEL, V. CÂNDEA, C. POPA, C.V. PRICĂ[1]

Abstract*: It is already known that the metallic powder sintered materials have in their structure a certain porosity, which can not be removed. Next to this porosity, the impurities and some structural defects affect all the material's mechanical properties. The aim of this paper was to determine how the copper added to the iron powder influences the material's mechanical properties and also what is the optimum amount of copper which has to be used. The paper presents the results obtained by testing the samples obtained by sintering iron powder (DWP 200.28) mixed with different quantities of copper. The determined material's mechanical properties were the tensile strength, the hardness and their fatigue strength.*

Keywords: *iron powder, copper, sintered material, mechanical properties.*

INTRODUCTION

The P/M parts are used more and more frequently, but, by analogy with wrought materials, their mechanical properties are weaker then those for compact materials because of their specific and complex structure. The structure of the metallic sintered powder materials is made from a powder particle mass, a pores ensemble and unfortunately, impurities. The pores, which may have variant forms, sizes and specific areas, have, usually, an entirely unfavorable orientation, so, they can be considered stress points and they represent the base of the origin and propagation of the fissures into the material. The impurities, especially those from slag, could appear anywhere in the material structure; they are of dark color and as a shape, they are, especially round. As the pores, they may be considered stress points, with the same effects. If we can act rather easily upon the pores by the surface, we have to use special methods upon those inside the material. Concerning the impurities, because they appear during the powder elaboration, the possibilities to act for their elimination are limited.

To improve the mechanical properties of the sintered materials there has to reduce their porosity and this can be done either by mechanical and thermo-chemical treatments, by raising the compacting pressure and sintering temperature, or by adding different elements such as copper, boron or phosphorus in the powder's mixture, to favor the apparition of liquid phase during the sintering process. For this work, to

improve the material's mechanical strength and also its workability, it was added powder of Cu.

EXPERIMENTAL CONDITIONS

For this study there was chosen iron powder type DP because it has a high level of chemical purity and a very good compressibility. Made by S.C.DUCTIL S.A.Buzău, this powder is recommended for the sintered parts which have a density over 7.1 - 7.2 g/cm^3 after a single pressing. For the experiments there was used iron powder DWP 200.28, which characteristics from the producer are given in Table 1 [1]. For the used copper powder – PA Cu 99.1S.F. - the characteristics are given by its producer TEHNOMAG Cluj-Napoca and they are specified in Table 2 [1].

Table 1. The Fe powder characteristics [1].

Properties	**Amount [%]**
Granulometric distribution [%] SR EN 24497	
> 160 μm	max.15
160 - 100 μm	20 – 40
100 - 63 μm	20 – 40
< 63 μm	10 – 45
Apparent density [g/cm^3] SR EN 23923-1	2,7– 2,9
Fluidity [sec/50 g] ISO 4490	≤ 33 [sec/50 g]
Chemical composition [%]	
C STAS 1457	≤ 0,02
Si SR EN 24829-2	≤ 0,05
Mn SR EN ISO 10700	≤ 0,20
P SR EN 10184	≤ 0,015
S SR EN 24935	≤ 0,015
O_2 (loss in H_2) SR EN 24491-2	≤ 0,20
The properties of the samples compressed with 600 MPa without lubricant	
Density ISO 3995	6,95 g/cm^3
Strength	24,5 MPa
Compressibility SR EN 23927	≥ 6,98 g/cm^3

Table 2. The Cu powder characteristics [1].

Properties	**Amount [%]**
Granulometric distribution [%] SR EN 24497	
> 150 μm	1
150 - 63 μm	39.66
63 - 38 μm	42.84
< 38 μm	16.5
Apparent density [g/cm^3] SR EN 23923-1	4.16
Fluidity [sec/50 g] ISO 4490	15
Chemical composition [%]	
O_2 (loss in H_2) SR EN 24491-2	0.18
Cu	99.71
Impurities	0.11

Note: The total oxygen content, max 0.22 %.

The samples for the study were obtained from iron powder type DWP 200.28 mixed with 2,4, 5, 10 and 15 % Cu, and 0.8 % Zn stearate. Each mixture of powders was homogenized in a laboratory homogenizer type Turbula, for 30 minutes. After homogenization there were determined the fluidity and the apparent density for every mixtures and the results are given in Table 3.

Table 3. Fluidity and aparent density for each mixture.

Material	Fluidity [sec/50g]	Aparent density [g/cm^3]
Fe	max.33	2,7-2,9
Fe + 2,4 %Cu	42	2,96
Fe + 5 %Cu	42	2,96
Fe + 10 %Cu	43	2,92
Fe + 15 %Cu	42	2,92

Table 4.
Density of compacts.

Material	Density of green [g/cm^3]
Fe	6,95
Fe + 2,4 %Cu	7,01
Fe + 5 %Cu	7,08
Fe + 10 Cu	7,14
Fe + 15 %Cu	7,21

So, there were obtained 5 different mixtures, which represent 5 different materials.
All the mixtures of powders were bilateral compressed with 600 MPa. The densities of the compressed samples (10 samples from each mixture, so the given values represent the average for each material) are given in Table 4.
The sintering was done in a Tunnel furnace, in hydrogen atmosphere, at 1150°C for 30 minutes. The sintering process of the Fe-Cu mixtures is accompanied by some phenomenon, as: formation of the Fe-Fe bundle in solid state, formation of the Fe-Cu bundle in solid state, Cu melting, Cu diffusion, solubilization and precipitation of Fe in melted Cu.
On the Fe-Cu diagram it can be seen that the Cu solubility in Fe grows up with temperature rising until approximately 8.5 % at 1100 ^{0}C, which is the system sintering temperature. At this temperature Fe is soluble in Cu approximately 4 %. During the cooling the system there can be obtained structures as [2]: alloyed Fe with Cu (α), non-alloyed Fe, Fe alloyed with phase ε of Cu alloyed with Fe, phase ε of Cu alloyed with Fe, non-alloyed Cu.
For each material it was determined its density, and there were done tests for tensile strength, hardness and number of cycles supported by the samples until their fracture. For fatigue the tests were done under bending loads of constant amplitude through symmetrical alternate plane bending. There was determined the number of cycles supported by the material until its fracture (total or partial).

RESULTS AND DISCUSSIONS

While in the conventional metallurgy the copper it is considered an impurity, in powder metallurgy it is considered like a principal alloying element due to its hardening effect (solid solution of substitution and hardening through precipitation) and also to the apparition of liquid phase which activates the sintering. Copper like alloying element is used frequently because it improves the material's homogeneity and the dimensional stability of the parts made from that material. As a result there will be improved the sintered material's mechanical properties. The results of the tests are given like diagrams in figures 1, 2, 3 and 4 [3]. From the figure 1 it can be seen that the material density has best values for a quantity of 5 %Cu. As it can be seen in figure 2 for the hardness there was observed the same comportment of the material like for the density: the best values were for 5 %Cu. The results were verified for the others tests too: for the tensile strength (figure 3) and for the number of the cycles supported by the material (figure 4) were obtained the greatest values. Verifying the

lowest values on the graphics it can be said that it correspond to the maximum concentration of Cu, 15 %, like a consequence of the rising of the free Cu amount [1].

CONCLUSIONS

The optimum quantity of copper which has to be added depends also of the type of the used iron powder. So, for the atomized iron powder, which is the case of powder used for this experiment, it can be said that when the copper content grows up, the material density, its hardness and mechanical strength and also the number of cycles supported by the material were improved. This conclusion is valid only for a Cu amount between 2 and 7.5 %, due to the apparition of the martensitic structure. Over this value it appears a diminishing of the material mechanical properties and even a drastically one at more then 10 %, like a consequence of the rising of the free Cu amount.

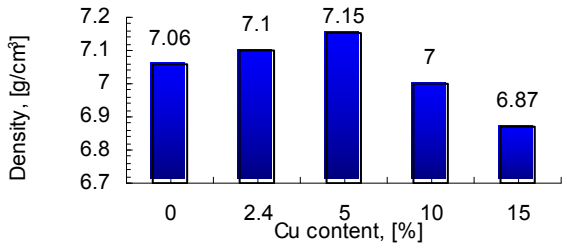

Fig.1 The influence of Cu amount on the material density.

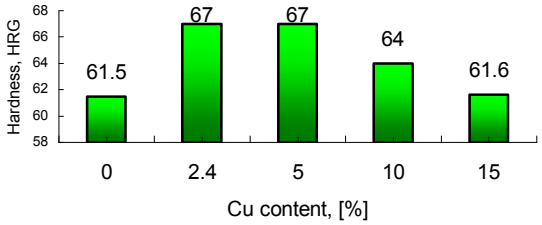

Fig.2 The influence of Cu amount on the material hardness

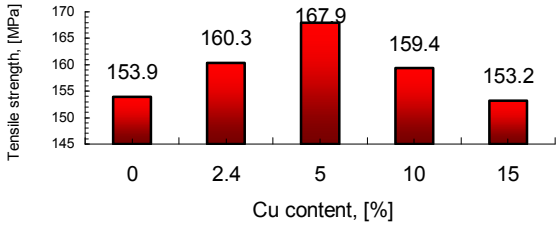

Fig.3 The influence of Cu amount on the material tensile strength.

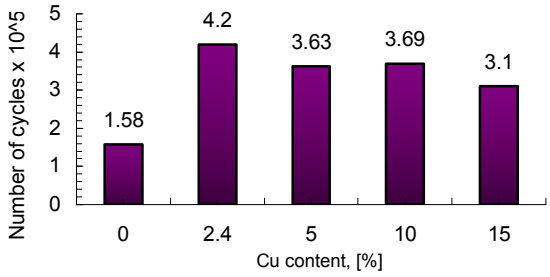

Fig.4 The influence of Cu amount on the material fatigue strength.

REFERENCES

1. Prospectus S.C.DUCTIL S.A.Buzău and TEHNOMAG Cluj-Napoca.
2. Copper Base Powder Metallurgy, vol.7, Ed.Pierre W.Taubenplant, AMAX Cu Inc.,1980.
3. Pavel, C. - *Thesis,* Technical University of Cluj-Napoca, (2004).

[1]Technical University of Cluj-Napoca, Faculty of Materials Science and Engineering, Muncii Av., No.103 -105, Cluj - Napoca, Romania

STUDIU CU PRIVIRE LA INFLUENȚA CANTITĂȚII DE CU ASUPRA PROPRIETĂȚILOR MECANICE ALE MATERIALELOR SINERIZATE DIN PULBERI CU BAZA Fe

Rezumat: Este bine cunoscut faptul că materialele sinterizate din pulberi metalice au în structura lor o anumită porozitate ce nu poate fi eliminată. Pe lângă această porozitate, impuritățile şi unele defecte din structură afectează proprietățile mecanice ale acestor materiale. Scopul acestei lucrări a fost determinarea influenței adaosului de Cu în pulberea de Fe asupra proprietăților mecanice ale materialelor sinterizate şi de asemenea, determinarea cantității optime de Cu din amestec pentru care se obțin valorile cele mai ridicate ale acestora. Lucrarea prezintă rezultatele testelor făcute pe probe obținute prin sinterizarea unor amestecuri din pulbere de Fe (DWP 200.28) cu diferite cantități de Cu. Proprietățile mecanice determinate au fost: rezistența mecanică, duritatea şi rezistența la oboseală.

BULETINUL INSTITUTULUI POLITEHNIC DIN IAŞI
Tomul LIII (LVII), Fasc. 3, 2007
Secția
ŞTIINȚA ŞI INGINERIA MATERIALELOR

RESEARCH ABOUT Fe30Cu70 (wt. %) STRUCTURES OBTAINED BY MECHANICAL ALLOYING

BY

C. V. PRICA[1], V. CANDEA[1], C. PAVEL[1], G. ARGHIR[1]

Abstract*: This paper presented the milling time influence on ball-milled Fe30Cu70 alloy structures. An unstable, f.c.c. Fe30Cu70 solid solution was prepared using high-energy ball milling of an elemental powder mixture. Alloy evolution was analyzed by X-ray diffraction and optical microscopy. After 16 hour of milling it has been concluded that true alloying at atomic level occurs during milling. The average grain size depend by milling time. It was found that the grain sizes varying in nanoscale order, between 23 and 8 nm. The milling duration have a strongly influence on powder morphology, solid solubility and phases form in Fe-Cu system. The mixing enthalpy (positive in this system) also depend on alloy composition.*

Keywords: *mechanical alloying, Fe-Cu system, suprasaturated solid solution, nanostructure*

INTRODUCTION

The mechanical alloying (MA) has been used extensively in recent years to synthesize nonequilibrium phases such as amorphous, nanocrystalline and quasicrystalline materials. Also, the formation of metastable phases by MA of elemental powder blends has been presented in a vary of alloy system in last few years [1,2]. The Fe-Cu system is an example of system with a positive enthalpy of mixing, under equilibrium condition Fe and Cu are completely immiscible. The phase formation in alloy systems with positive heath of mixing is far from understood from thermodynamic and kinetic viewpoint. In Fe-Cu alloys system it's found that the solid solubility are largely extended by MA technique. The single fcc and bcc Fe_xCu_{100-x} phase region was obtained from $x < 60$ %at. and $x > 80$ %at. during ball milling. The mechanism responsible for this enhanced solubility is still a subject of debate.

EXPERIMENTAL RESULTS

An Fe30Cu70 mixture from Fe and Cu elemental powders was subjected to mechanical milling in an planetary ball mill to 16 h. The mill characteristic was: plate diameter, D = 500 mm, vial diameter, d = 80 mm, plate rotation, n_p = 1200 rpm, vial rotation, n_v = -800 rpm. In the intermediate stage of milling, to 1, 2, 4, 8 and 16 h the Fe_xCu_{100-x} samples was investigated by XRD and optical microscopy.
The $Fe_{30}Cu_{70}$ samples with different milling times have been investigated by XRD. Figure 1shows X-ray diffraction pattern for Fe30Cu70 after different milling times.

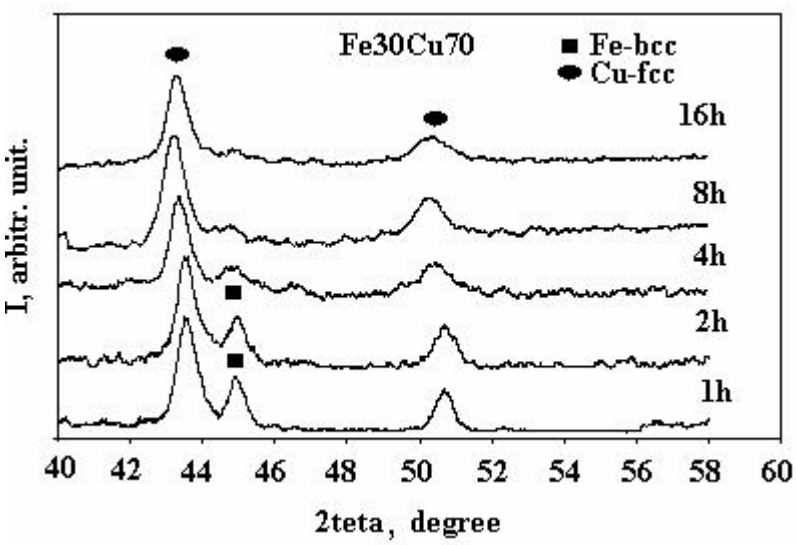

Fig. 1. X-ray diffraction pattern for Fe30Cu70 after different milling times.

The elemental lines of Cu and Fe in the diffraction pattern broaden significantly during milling and are reduced in intensity. After 8 h the Fe peaks have completely disappeared and only fcc peaks remain. This indicated that true alloying takes place during milling. The broadening of x-ray diffraction lines is due to a refinement of the crystal sizes. This is illustrated in figure 2, showing the average grain size obtained for Fe30Cu70 after 16 h of milling.

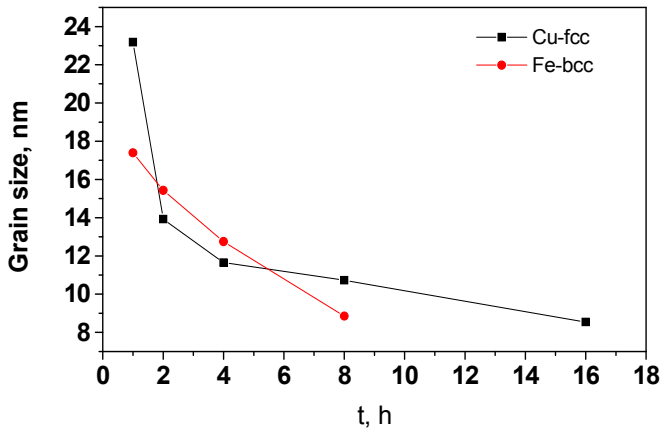

Fig. 2. Grain sizes vs. milling times for fcc (■) and bcc (•) phases.

The average grain size was calculated with Scherrer formula. After 1 h of milling the fcc grain size is 23,5 nm and for bcc is 17,5 nm. Further milling, the grain size is reduced to 8.85 nm for bcc phase and to 8.50 nm at 16 h of milling (fig. 2.). It was observed the increasing of crystal parameters for both fcc and bcc networks in first 8 hours. Between 8 to 16 h of milling, for fcc phase the crystal parameter decreasing with milling time. This indicated that the steady state was attained. The microstructures for Fe30Cu70 at different milling times is shown in figure 3.

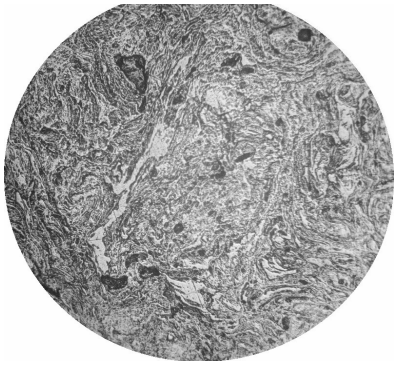

Fig. 3. a) Microstructure of Fe30Cu70 after 1 h of milling (x 200).

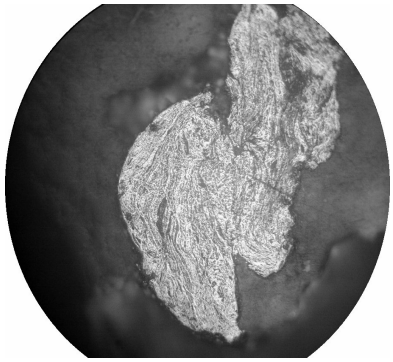

Fig. 3. b) Microstructure of Fe30Cu70 after 2 h of milling (x 100).

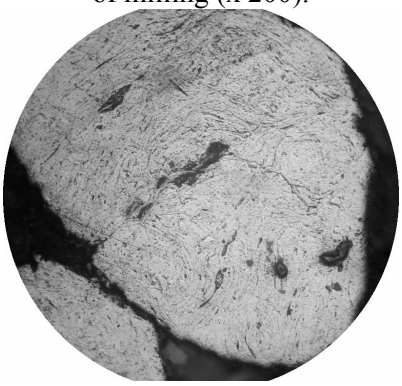

Fig. 3. c) Microstructure of Fe30Cu70 after 4 h of milling (x 200).

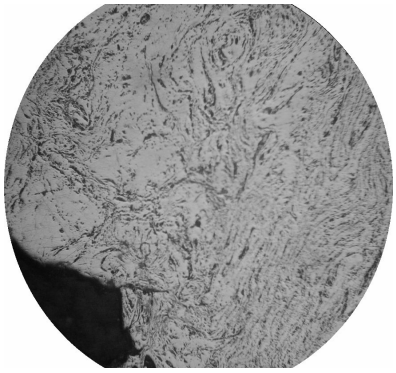

Fig. 3. d) Microstructure of Fe30Cu70 after 8 h of milling (x 250).

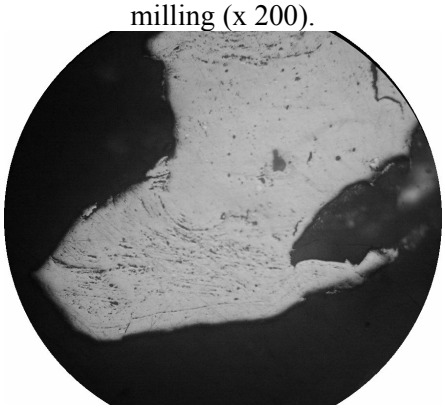

Fig. 3. e) Microstructure of Fe30Cu70 after 16 h of milling (x 200).

It was observed the lamellar structure develops after 1 h of milling as a results of severe plastic deformation of Fe and Cu elemental powders (fig. 5.a). The mixing and plastic deformation of particles followed by their fracture and welding which result in the formation of composite particles with a layer microstructure (fig. 5.b, c, d). In this case of Fe30Cu70 welding predominance, the random welding orientation and equiaxed particle formation. With increasing the milling times layer get thinner and thinner and convoluted. In this stage of MA thermal diffusion occurs. After 16 h of milling the alloy structure presents homogeneity – fig. 5. e, a steady state processing is characterized by an equilibrium between fracture and welding of particles leads to a stable average particle size.

CONCLUSION

After 16 h of milling of Fe30Cu70 powders mixture result an homogen solid solution. The bcc peaks from diffraction pattern is complete disappeared after 8 h of milling. The particle sizes is influenced by both milling times and composition of alloy. The lamellar structure develops during ball-milling of Fe30Cu70 powder mixture. This is rafinated with increasing the milling times and after 16 h of milling the alloy structure presents homogeneity.

REFERENCES

[1] W. Kapell, M. M. Codescu, I. Pasuk, E. Patroi, V. Kuncser, M. Valeanu, D. Predoi, G. Filoti, J. of Optoel. And Adv. Mater., Vol. 6, No. 3, p. 973-978 (2004).
[2] C.V. Prica, G. Arghir, Matematiceskih modeli fiziceskih proyeccov, Vol. I, Taganrog, Russia, p. 11-14 (2005).

[1]103-105, Muncii Avenue, 400641 Cluj-Napoca, Tehnical University, Science and Engineering of Materials Faculty, Romania

CERCETĂRI ASUPRA STRUCTURII Fe30Cu70 (% MASICE) OBȚINUT PRIN ALIERE MECANICĂ

Rezumat: Această lucrare prezintă influența duratei de măcinare asupra structurii aliajului Fe30Cu70 obținut prin aliere mecanică. A fost realizată o soluție solidă suprasaturată Fe30Cu70, metastabilă, prin măcinarea amestecului de pulberi elementale într-o moară planetară de înaltă energie. Evoluția structurii aliajului a fost investigată prin difracție cu raze X şi microscopie optică. După 16 ore de măcinare se poate concluziona că s+a realizat alierea Fe30Cu70 la nivel atomic. Dimensiunea medie a cristalitelor este puternic influențată de durata măcinării, aceasta fiind de aproximativ 23 nm după o oră de măcinare şi ajungând la 8 nm după 16 ore. Durata măcinarii influențează de asemenea şi morfologia, solubilitatea în stare solidă şi formarea fazelor în sistemul Fe – Cu. Entalpia de formare, pozitivă în acest caz este de asemenea influențată de compoziția amestecului.

BULETINUL INSTITUTULUI POLITEHNIC DIN IAŞI
Tomul LIII (LVII), Fasc. 3, 2007
Secția
ŞTIINȚA ŞI INGINERIA MATERIALELOR

^{1}H NMR STUDIES FOR TWO COPOLYMER SYSTEMS

BY

IONUT CAMELIU ICHIM, MARIUS CIPRIAN RUSU AND MIHAI RUSU

Abstract: *This paper deals with the synthesis, characterization and estimation of the reactivity of bromine containing methacrylic monomers. 2-(2-bromopropionyloxy) propyl methacrylate (BPPM) and 2-(2-bromoisobutyryloxy) propyl methacrylate (BIPM) were synthesized and characterized by ^{1}H NMR and ^{13}C NMR spectroscopy. The free radical initiated copolymerization of BPPM and BIPM with methyl methacrylate (MMA) were performed inside NMR equipment at 60°C. The total monomer concentration was 1M in all cases, using 1 ml as the volume size of the polymerization batches. Were used deuterated benzene (C_6D_6) as solvent, 2,2'-azobisisobutyronitrile (AIBN), as radical initiator in concentration 1.5 wt % with respect to the mixture of monomers and p-xylene as an internal reference component 0.1 M.*

The copolymer compositions obtained from ^{1}H NMR spectra led to the determination of the reactivity ratios employing Finemann-Ross and Kelen-Tüdös linearization methods. Both estimations have led to similar results suggesting that the length of the bromine containing monomers side chain does not affect the reactivity of the methacrylic double bond.

Keywords: *radiopaque agent, bromine containing methacrylates, copolymerization, reactivity ratio*

1. INTRODUCTION

Radiopacity is generally proportional to the effective atomic number of the material. The elements hydrogen, carbon, nitrogen, oxygen are commonly found in the body and the polymers, so elements with higher atomic numbers than these should be enhance the radiopacity of a polymer implant. Candidate materials for enhancing the radiopacity of medical implants would have higher atomic numbers than the elements present in the body and would have to be biocompatible. The atomic number must be sufficiently high so that relatively small thickness of absorber material can be used in the body. The preferred organic elements for biocompatibility and radiopacity are bromine, iodine, barium and bismuth (Table 1) [1].

Table 1. Atomic number and certain linear attenuation coefficients for some elements and materials

Element or material	**Atomic number or effective atomic number**	**Linear attenuation coefficient at 50 KeV, cm^{-1}**
Hydrogen	1	0,000028
Carbon	6	0.417
Fat	6.46	0.193
Muscle	7.64	0.233
Oxygen	8	0.00028
Bone	12.31	0.573
Bromine	35	13.29
Zirconium	40	40.04
Iodine	53	60.76
Barium	56	49.68
Bismuth	83	82.12

According to these studies about enhancing the radiopacity, the purpose of our work was the synthesis and characterization of bromine containing methacrylates. 2-(2-bromopropionyloxy) propyl methacrylate (BPPM) and 2-(2-bromoisobutyryloxy) propyl methacrylate (BIPM) (Scheme 1) were synthesized with the aim of using them in the preparation of radiopaque polymeric matrix based on PMMA.

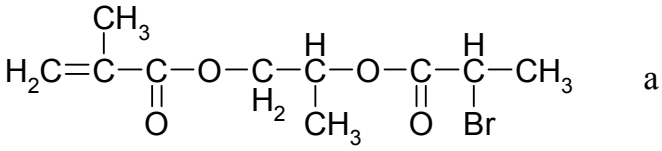
a

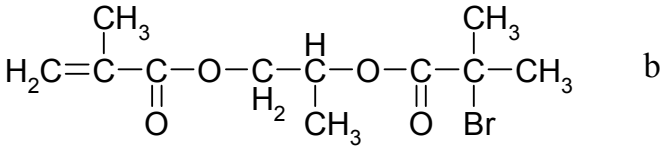
b

Scheme 1. Chemical structures of BPPM (a) and BIPM (b)

2. EXPERIMENTAL

2.1. Synthesis of 2-(2-bromopropionyloxy) propyl methacrylate (BPPM)

The synthesis, transposed from that of Klumperman et al [2], comprises of two steps (Scheme 2). First, 2-bromopropionyl chloride was synthesized by the reaction between 2-bromopropionic acid and thionyl chloride.

For this, a dry 250 ml two-neck round-bottom flask was used. Thionyl chloride was added drop-wise over a period of 2 hours. The reaction was carried out under stirring at 0°C. The unreacted thionyl chloride was removed by distillation under vacuum.

Second, 2-(2-bromoisobutyryloxy) ethyl methacrylate (BIEM) was synthesized by the reaction between 2-hydroxypropyl methacrylate (HPMA) and 2-bromopropionyl chloride using tetrahydrofuran (THF) as solvent and pyridine (Py) as HCl acceptor. This synthesis was carried out in a 500 ml three-neck round-bottom flask. 2-bromopropionyl chloride was added drop-wise through a dropping funnel over a period of 3 hours and the reaction was carried at 0°C.

For the purification of BPPM, the reaction solution was introduced into a separation funnel with a mixture of 300 ml water and 300 ml ethylic ether and stirred for 40 minutes. The water mixture was extracted. Then, the resulting organic layer was washed two times sequentially with 150 ml of 1M hydrochloric acid and 100 ml of a saturated sodium bicarbonate aqueous solution 10 %.

After this, the organic phase was washed with 200 ml distilled water. The organic layer was dried on magnesium sulfate and then filtered.

The solvent was evaporated off under reduced pressure. The product structure was identified by ^{1}H NMR and ^{13}C NMR (Figures 1-2):

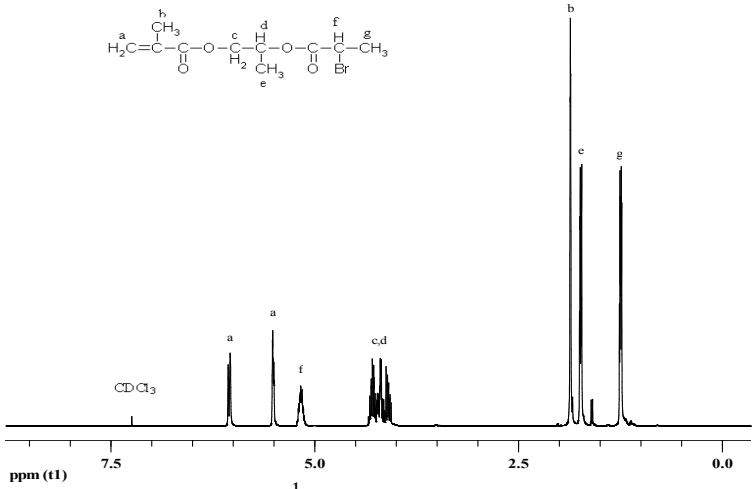

Figure 1. The ^{1}H NMR spectra of BPPM

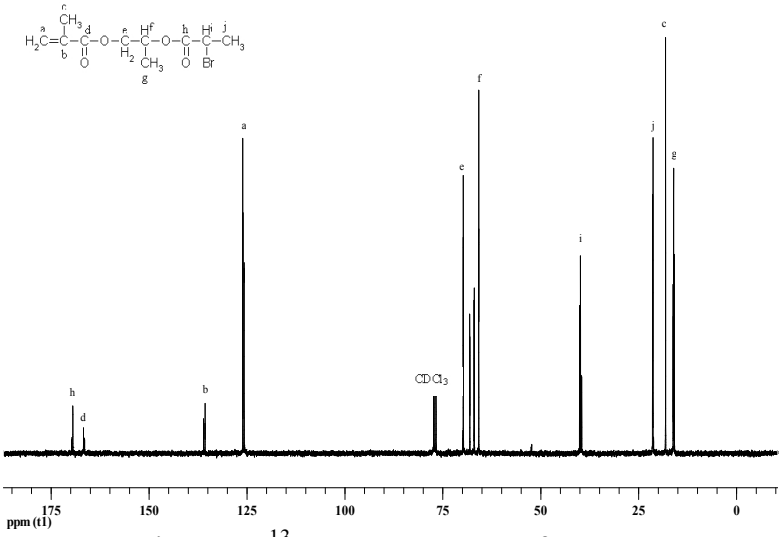

Figure 2. ^{13}C NMR spectra of BPPM

2.2. Synthesis of 2-(2-bromoisobutyryloxy) propyl methacrylate (BIPM)

BIPM was synthesized by estherification of hydroxypropyl methacrylate with 2-bromoisobutyryl bromide, method used by Zhongyu Li et al [3] (Scheme 3). 2-Hydroxypropyl methacrylate (HPMA), triethylene amine (TEA) and tetrahydrofuran (THF) as solvent was added into a dry 250 ml three-neck round-bottom flask. This mixture was stirred at room temperature under nitrogen flow. 2-bromoisobutyryl bromide was added drop-wise through a dropping funnel over a period of 15 minutes. The reaction was carried out for 48 hours at room temperature and under continuing stirring.

The resulting solid phase was separated by filtration and then the solvent (THF) from the liquid phase was evaporated. In the next step, the product was washed sequentially with diethyl ether and a 10% solution of potassium carbonate in a separation funnel. The organic layer was dried on magnesium sulfate and then filtered.

The solvent was evaporated off under reduced pressure. The product structure was identified by ^{1}H NMR and ^{13}C NMR (Figures 3-4).

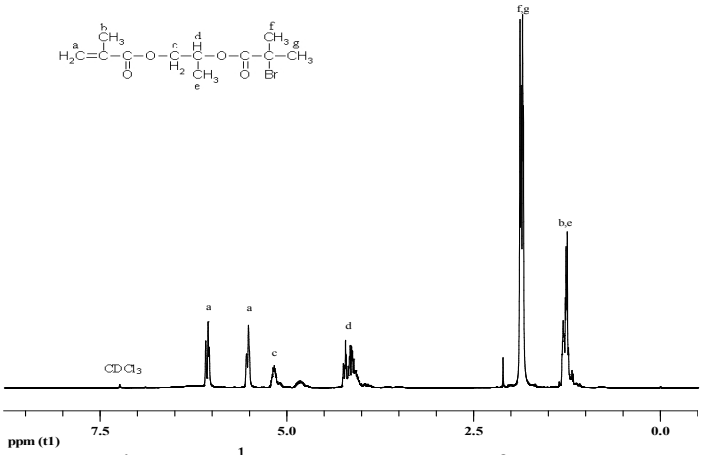

Figure 3. ^{1}H NMR spectra of BIPM

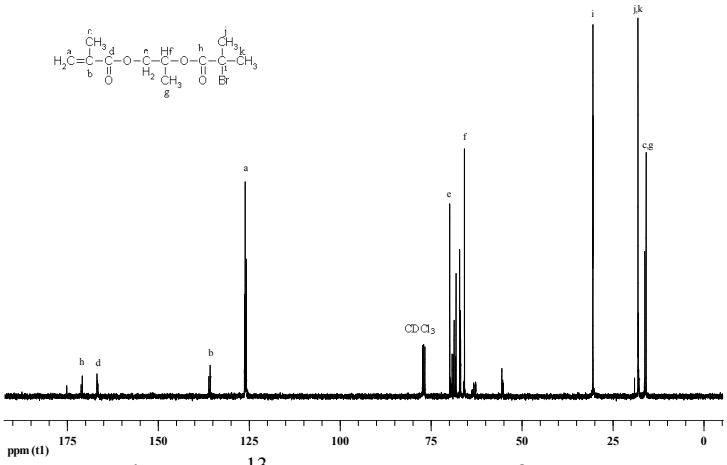

Figure 4. ^{13}C NMR spectra of BIPM

2.3. Copolymerization

Copolymerization reactions of the prepared monomers with MMA were carried out directly in the thermostatic cell of a NMR spectrometer at 60°C. The total monomer concentration was 1M in all cases, using 1 ml as the volume size of the polymerization batches. Were used deuterated benzene (C_6D_6) as solvent, 2,2'-azobisisobutyronitrile (AIBN), as radical initiator in concentration 1.5 wt % with respect to the mixture of monomers and p-xylene as an internal reference component 0.1 M. The feed molar composition of monomer and comonomer is given in Table 2.

Table 2. Molar concentrations of the monomers involved in copolymerization

Copolymers	BPPM – MMA		Copolymers	BPPM – MMA	
	[BPPM], mol/l	[MMA], mol/l		[BPPM], mol/l	[MMA], mol/l
COP 1	0.102	0.901	COP 6	0.105	0.905
COP 2	0.301	0.700	COP 7	0.297	0.700
COP 3	0.500	0.499	COP 8	0.500	0.500
COP 4	0.701	0.302	COP 9	0.700	0.300
COP 5	0.898	0.104	COP 10	0,900	0.110

3. RESULTS AND DISCUSSION

3.1. Copolymerization data acquisition

In order to know the bromine containing monomers behavior in radical copolymerization processes with MMA, the reactivity ratios of BPPM and BIPM were determined using ^{1}H RMN spectra.

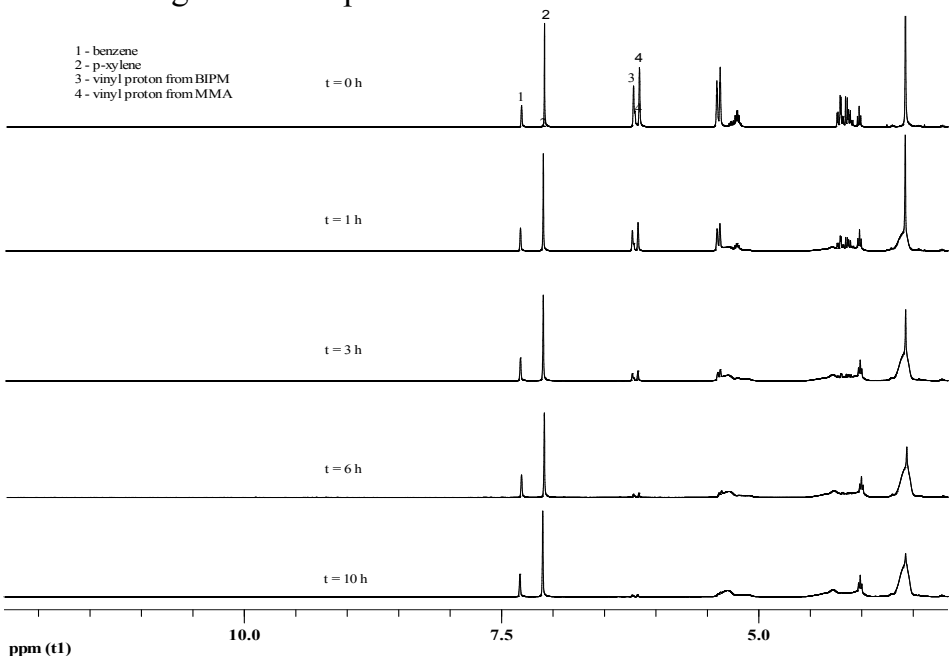

Figure 5. Some representative ^{1}H NMR spectra of the BIPM-MMA system (COP 8) at different times of reaction

Figure 5 shows some spectra of the BIPM-MMA system at different reaction times together with the assignments of the peaks employed in the determination of the monomer concentration. P-xylene was used as reference for the quantitative analysis of the monomer peaks.

3.2. Determination of monomer reactivity ratios

The monomer reactivity ratios for the copolymerization of MMA with BPPM and BIPM were determined for the monomer feed ratios and the copolymer composition. The Finemann-Ross (FR) [4] and Kelen-Tüdös (KT) [5] methods were used to determine the monomer reactivity ratios. The values of reactivity ratios obtained from KT and FR methods are summarized in Table 3.

Table 3. Comparison of reactivity ratios by various methods

System	Method	r_1	r_2	$r_1.r_2$
Poly(BPPM-co-MMA)	FR	1.01 ± 0.42	1.08 ± 0.62	1.09
	KT	1.01 ± 0.50	1.08 ± 0.68	1.09
	Average	1.01 ± 0.46	1.08 ± 0.65	1.09
Poly(BIPM-co-MMA)	FR	0.94 ± 0.60	0.94 ± 0.58	0.88
	KT	0.96 ± 0.58	0.96 ± 0.54	0.92
	Average	0.95 ± 0.59	0.95 ± 0.56	0.90

Taking into account the errors, the reactivity ratios for the system BPPM-MMA, and by this the behavior of the monomers, is similar to the case of the system BIPM-MMA when the composition of the copolymer, the same during the reaction, is equal at any time with the feed compositions.

It is obvious that in this case is favored the tending to form short homogeneous sequences.

4. CONCLUSIONS

2-(2-bromopropionyloxy) propyl methacrylate (BPPM) and 2-(2-bromoisobutyryloxy) propyl methacrylate (BIPM) were synthesized and characterized by ^{1}H NMR and ^{13}C NMR spectroscopic techniques. Copolymers of BPPM and BIPM with MMA having various compositions were prepared in solution by free radical polymerization at 60 ˚C. The reactivity ratios of the comonomers were estimated using Finemann-Ross and Kelen-Tüdös methods. Both estimations have led to similar results suggesting that the length of the bromine containing monomers side chain does not affect to the reactivity of the methacrylic double bond.

REFERENCES

[1] Jonathan S. Stinson, 2003, U.S. Patent 6626936
[2] Venkatesh R., Yajjou L., Koning C.E., Klumperman B., Macromol. Chem. Phys., 2004, 20:2161
[3] Zhongyu Li, Pengpeng Li, Junlian Huang, Polymer, 2006, 47(16), 5791
[4] Finemann M., Ross S., J. Polym. Sci. A., 1964, 2:1687
[5] Kelen T., Tüdös F., J. Macromol. Sci. Chem., 1975, A9:1

ICHIM IONUT CAMELIU, RUSU MARIUS CIPRIAN, RUSU MIHAI

Department of Natural and Synthetic Polymers, Faculty of Chemical Engineering, "Gh. Asachi" Technical University of Iasi, Romania

STUDII ^{1}H RMN PENTRU DOUA SISTEME DE COPOLIMERI

Rezumat: In aceasta lucrare se trateaza sinteza, caracterizarea si determinarea reactivitatii unor monomeri metacrilici care contin brom. 2-(2-bromopropioniloxi) propil methacrilat (BPPM) si 2-(2-bromoisobutiriloxi) propil methacrilat (BIPM) au fost sintetizati si caracterizati prin spectroscopie ^{1}H RMN si ^{13}C RMN. Copolimerizarea radicalica a BPPM si BIPM cu metil metacrilat (MMA) a fost facuta in interiorul echipamentului de RMN, la 60^{o}C. Concentratia totala de monomer a fost 1M in toate cazurile, folosind flacoane de polimerizare de 1 ml. S-au folosit benzen deuterat (C_6D_6) ca solvent, 2,2'-azobisisobutironitril (AIBN) ca initiator in concentratie de 1.5% masa in raport cu amestecul de monomeri si p-xilen ca referinta interna 0.1M.

Compozitiile de copolimer obtinute din spectrele ^{1}H RMN au dus la determinarea constantelor de reactivitate folosind metodele de liniarizare Finemann-Ross si Kelen-Tüdös. Amandoua estimari au dus la rezultate similare, sugerand faptul ca lungimea lantului monomerilor care contin brom nu influenteaza reactivitatea dublei legaturi metacrilice.

BULETINUL INSTITUTULUI POLITEHNIC DIN IAŞI
Tomul LIII (LVII), Fasc. 3, 2007
Secția
ŞTIINȚA ŞI INGINERIA MATERIALELOR

THE COMPARATIVE STUDY ABOUT THE WEAR RESISTANCE OF SUPERFICIAL LAYERS DERIVED FROM ELECTRIC SCINTILLATION WITH HARD CARBIDE ELECTRODES

BY

DANIELA CIOBANU GHERCĂ*, VASILE NECULAIASA*, IOAN ȚENU*, IONEL GHERCA*

Abstract : *The problem of mathematical valuation and resistance wear prognostication of high wear machinery parts belonging to farm equipments and food industry has a peculiar technical and economic importance. The resistance of wear can act as an indicator in choosing materials for the construction of these triboelements. Some mathematical formulae have been used for the wear resistance study, formulae infered from the formula wich describes analytically the massic wear.*

Key words*: electric scintillation, volume temper+annealing, abrasive wear .*

1. THEORETICAL CONSIDERATIONS

The problem of mathematical valuation and wear resistance prognostication of high wear machinery parts belonging to farm equipments and food industry has a peculiar technical and economic importance because it can contribute to the judicious supply of the companies, to the solution choice for increasing durability, to the assurance of high quality works, to the judicious renewals planning etc. At the same time,the resistance of wear can act as an indicator in choosing materials for the construction of these triboelements.

The researches highlight the fact that the main factors that influence upon the wear of these work components exercise implicitly a direct influence upon durability [1], [2], [3].

Some mathematical formulae have been used for the wear resistence study, formulae infered from the formula wich describes analytically the massic wear,that is [2]:

$$U_m = K \cdot \frac{Q \cdot L_f}{3H}, \qquad (1)$$

Where: $-U_m$ represents the massic wear of the triboelement; K– a constant depending on the material; Q–the pressing force; L_f–the length of the friction way; H–the material durity of the triboelement.

If in the formula (1) we replace the pressure force by the p.S product, the formula (1) becomes:

$$U_m = K \cdot \frac{p \cdot v \cdot S}{3H} \cdot t \tag{2}$$

From the formula (1), the material constant can be computed by the formula:

$$K_m = \frac{3U_m \cdot H}{L_f \cdot S \cdot p} \tag{3}$$

In our case, at 60 min of wear test, L_f is 5429m,and the samples had a 8mm diameter, resulting a surface S=50,24mm^2. So the (3) formula becomes:

$$K_m = 1{,}099 \cdot 10^{-5} \frac{U_m \cdot H}{p}. \tag{4}$$

The trust interval of wear resistance variation has been computed using the formulas /2/:

$$\bar{x} - u_\alpha \sqrt{\frac{\sigma^2}{n}} \le x \le \bar{x} + u_\alpha \sqrt{\frac{\sigma^2}{n}} \tag{5}$$

and

$$\sigma^2 = \frac{\sum_{i=1}^{n} (x_i - \bar{x})^2}{n}. \tag{6}$$

For α =0,05 a tust interval with bilateral risk is settled, P=1 –α/2=0,975, where u_α =1,96 [2].

2. THE COMPARATIVE STEADY OF WEAR RESISTANCE

The comparative study about the wear resistance of superficial layers derived from DASE with hard carbide electrodes and the work regime 2 of ELITRON22 and MAX101 apparatus has been accomplished using the formula:

$$\frac{U_{ma}}{U_{mb}} = \frac{H_{ma}}{H_{mb}} \cdot \frac{K_{mb}}{K_{ma}}, \tag{7}$$

Where: H_{ma} represents the durity of the subsided layer and H_{mb} represenrs the basic material durity.

The values of the material constants, both for basic materials(K_{mb}) treated in variant A(volume temper+annealing) and for the subsided layers in variant B(K_{ma1})(WCo8 electrode scintillation),respectively variant C(K_{ma2})(Ti15Co6 electrode scintillation) are shown in tables 1, 2, 3 and the value of the relation between the subsided layers and basic materials of wear resistance, as well as the average values of their ($\bar{X}$) are shown in table 4.

Using the formulas the above mentioned and the values of the wear resistance ratios depending on pressure, shown in table 4, wase calculated the trust intervals of the ewar resistance variation (x) resulting :

1,932 ≤ x ≤ 1,991, for RUL2 steel scintillated with a WCo8 electrode;

1,913 ≤ x ≤ 1,972 , for RUL2 steel scintillated with a Ti15Co6 electrode;

2,896≤ x ≤ 2,9 , for OSC8M steel scintillated with WCo8 electrode;

2,8 ≤ x ≤ 2,891, for OSC8M steel scintillated with Ti15Co6 electrode;

$1,92 \leq x \leq 1,993$, for unalloyed white cast iron scintillated with WCo8 electrode;

$1,888 \leq x \leq 1,953$, for unalloyed white cast iron scintillated with Ti15Co6 electrode.

Table 1.The values of material constant, for basic materials

Basic Material	**Microdurity of the basic material, $HV0_{.005}$ daN/mm^2**	**Pressure, MPa/K_{mb}**					
		0,5	1	1,5	2	2,5	3
RUL2	770	0.328	0,165	0,111	0.081	0,066	0,054
OSC8M	595	0,392	0,197	0,131	0,099	0,079	0,067
Fa	420	0,180	0,090	0,o60	0,,45	0,036	0,030

Table 2. The values of material constants for WCo8 scintillated samples

Basic material	**Microdurity of the subsided layer, $HV_{0,05}$ daN/mm^2**	**Pressure, MPa/K_{ma1}**					
		0,5	1	1,5	2	2,5	3
RUL2	1835	0,394	0,197	0,132	0,099	0,080	0,068
OSC8M	1474	0,320	0,162	0,110	0,086	0,069	0,058
Fa	1342	0,291	0,144	0,096	0,072	0,060	0,051

Table 3. The values of material constants for Ti5Co6 scintillated samples

Basic material	**Microdurity of the subsided layer, $HV_{0,05}$ daN/mm^2**	**Pressure, MPa/K_{ma2}**					
		0,5	1	1,5	2	2,5	3
RUL2	1435	0,308	0,155	0,104	0,079	0,064	0,053
OSC8M	1211	0,283	0,142	0,095	0,070	0,057	0,048
Fa	1074	0,233	0,117	0,079	0,060	0,049	0,041

Table 4. The wear resistance ratios depending on pressure

Basic material	**Electrode**	**Pressure, MPa/U_{ma}/U_{mb}**						$\overline{X}$
		0,5	1	1,5	2	2,5	3	
RUL2	WCo8	1.975	1,993	2,001	1,947	1,963	1,890	1,962
OSC8M		3,026	2,896	2,942	2,843	2,827	2,853	2,898
Fa		1,973	1,993	1,993	1,993	1,914	1,876	1,957
RUL2	Ti15Co8	1,974	1,980	1,985	1,907	1,918	1,895	1,943
OSC8M		2,812	2,816	2,930	2,871	2,814	2,834	2,834
Fa		1,969	1,961	1,973	1,920	1,873	1,865	1,921

Using the wear resistance ratios depending on pressure shown in table 4 , the diagrams of corresponding fig.1 and fig.2 have been drawn.

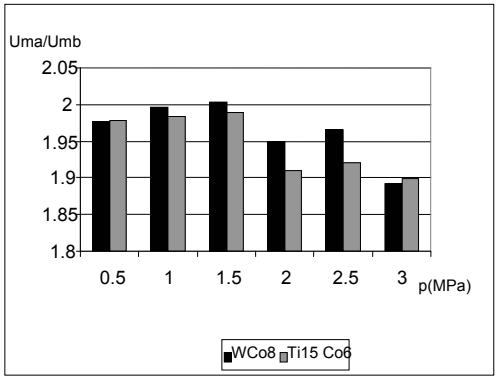

a)

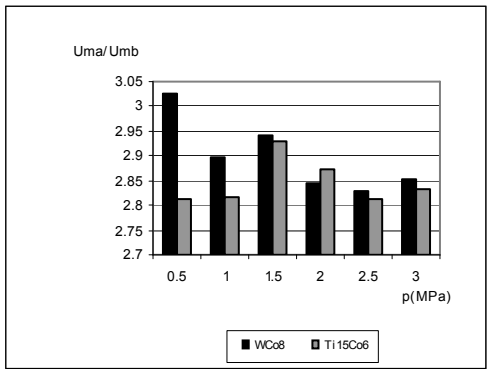

b)

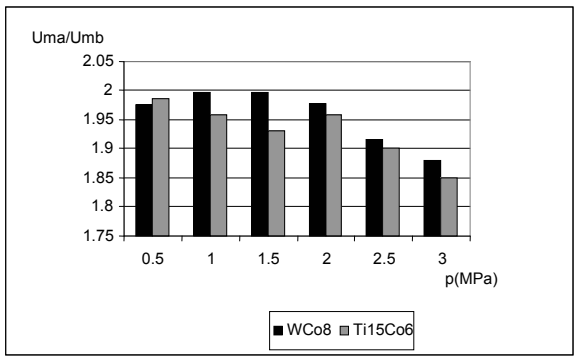

c)

Fig. 1.The variation of the wear resistance depending on contact pressure , of deposit layers on: a) RUL2 steel; b) OSC8M steeel; c) unalloyed white cast iron

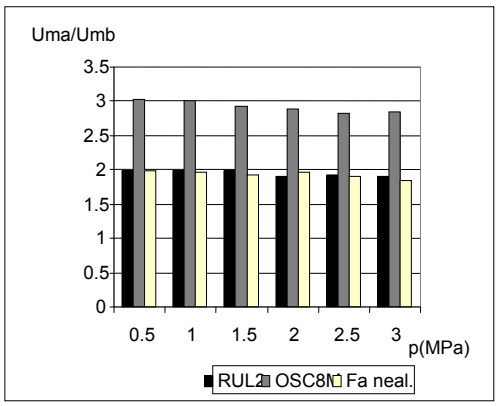

a)

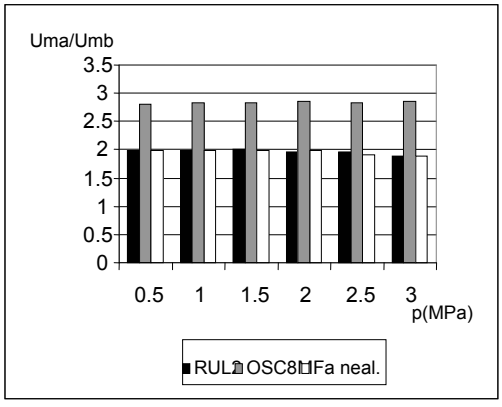

b)

Fig.2.The variation of the wear resistance depending on contact pressure , of deposit layers derived from electric scintillation with: a) WCo8 electrodel; b) Ti15Co6 electrode

3. CONCLUSIONS

After analyzing the trust intervals of the wear resistance variation (x), and the aspect of diagrams, can be made the following conclusions:

1. The trust intervals of the wear resistance shown the scintillated RUL2 steel and unalloyed white cast iron samples show a gross of the wear resistance of about tow, and the scintillated OSC8M samples shown a gross of this indicator of about three, compared to the unscintillated samples;
2. For all the experimented materials the wear resistance of the superficial layers derived from electric scintillation with WCo8 is higher than superficial layers derived from electric scintillation with Ti15Co6, the biggest diference are met at deposed layers on OSC8M steel;
3. For all the experimented materials the wear resistance diminisht as the contact pressure grows.

REFERENCES

[1]. Abramciuc Alex., (1996) – Caracteristicile tribologice ale straturilor obținute la durificrea prin scânteie electrică a aliajelor de aluminiu, Tehnologii moderne în construcţia de maşini, vol. 3, Iaşi, p. 73-80.
[2]. Grămăticu M. – Contribuţii privind influenţa compoziţiei chimice, structurii şi tratamentului termic a unor oţeluri folosite în construcţia sculelor de lucrat solul, Teză de doctorat, I. P. Iaşi.
[3]. Neculăiasa V., Ţenu I., (1996) – Bazele cercetării experimentale a maşinilor şi instalaţiilor din agricultură şi industria alimentară, Cercetări tribologice, U.T. Iaşi, Facultatea de Mecanica.

STUDIUL COMPARATIV AL DURABILITAŢII STRATURILOR SUPERFICIALE OBŢINUTE PRIN SCÂNTEIERE ELECTRICĂ CU ELECTROZI DIN CARBURI DURE

(Rezumat)

Problema aprecierii matematice şi prognosticării rezistenţei la uzare a organelor de mare uzură de la maşinile agricole şi din industria alimentară are o importanţă tehnico-economică deosebită. Rezistenţa la uzare poate servi ca indicator în alegerea materialelor pentru construcţia acestor triboelemente. Pentru studiul rezistenţei la uzare s-au utilizat câteva relaţii matematice deduse din relaţia ce descrie analitic uzura masică.

BULETINUL INSTITUTULUI POLITEHNIC DIN IAŞI
Tomul LIII (LVII), Fasc. 3, 2007
Secția
ŞTIINȚA ŞI INGINERIA MATERIALELOR

THE INFLUENCE ANALYZE OF THE STEELS SINTERED STRUCTURES ON THE DYNAMIC AND STATIC PROPERTIES

BY

LIVIU BRÂNDUŞAN, CHERTES VIORICA

Abstract: *The mechanical properties of the sintered steels are very influenced by their macro and microstructures. For dignifying the structure influence on some mechanical properties, it was elaborated sintered materials using iron powder of different granulations or different powder mixtures which lead to a certain structure. It was shown that a material obtained from a powder with delicate granulation behaves, at mechanical requests, almost in the same way as a material obtained from a large fraction. This is because by using these different fractions there are obtained materials of whose structures present small and uniform distributes pores. Using the different powders mixtures permit the obtaining of some microstructures with better mechanical properties at the intergranulars decks. During the request, in these areas there are maximum tensions which cause the material's break. Using the cooper powder or the iron powder low or high alloyed determines an improvement of the mechanical properties by changing the material's microstructure. The iron powder add high alloyed has the most powerful effect on the fatigue resistence. The cooper presence in the mixture determines not only the changing in the pores configuration but also the changing of the material's microstructure at the intergranular decks level. The pores' spheroidization is due to forming the liquid phase at sintering begetting by the cooper presence.*
Keywords: *sintered materials, material's properties, material's breaking*

1. INTRODUCTION

Because at the obtaining a large scale of sintered pieces it is used iron powder, it is justified to establish its characteristics' influence on the mechanical properties of the elaborated materials. Some authors present the porosity influence or the density of these materials on the mechanical characteristics [1, 2, and 5]. This is because the pores presence n the sintered macrostructure determines not only the properties level but also the specific of their breaking. The macrostructure is related with powder's characteristics, with some element's presence which lead to a liquid phase sintering, and also with the parameters of the forming and sintering process. The powder's characteristics, influences the sintering process by granulation, granule's shape and the aspect of their surfaces. Using a delicate powder or a large granulation one leads to forming small and uniform pores, as long as a liquid phase sintering determines forming spherical pores which has a lower effect of tension concentration.

Material's structure has a big influence on the mechanical properties of the sintered materials at the intergranular decks level. This is because the breaking process happens by deforming and successive section of the decks until the crack covers the entire material. The presence of some alloying elements in this section can lead to

form some structures with mechanical properties better than the ones of the base material.

2. ELABORATION OF MATERIALS

The researches were realized on two material categories, both having iron powder at the base DWP 200.28 elaborated by atomization at S. C. DUCTIL S. A. Buzău and whose granulometric characteristics are presented in table 1.

Table 1. Characteristics of the DP 400 iron powder

Grain size distribution	**%**
>160μm	≤10
160-100μm	20-40
100-63μm	20-40
<63	10-45
Apparent density g/cm^3**:**	2,7-2,9
Timp de curgere, Sec/50g**:**	≤33

For obtaining the first category it were made 3 powder batches which differ one to another by granulometrical distribution like this:

- batch A is formed by powder of which grain size distribution is identical to that of the initial powder;
- batch B contains grains with their grain size over 125 μm, of the initial powder;
- batch C contains grains with their grain size under 125 μm, of the initial powder.

It was added to every batch of the basic powder 0, 1, or 2 mass % copper powder.

The second category of materials was obtained from the main powder which was added, in different proportions, iron powder low alloyed Distaloy SA (Fe + 1,75% Ni + 1,5% Cu + 0,5% Mo) or iron powder high alloyed Distaloy AE (Fe + 4% Ni + 1,5% Cu + 0,5% Mo).

Every composition obtained in this manner, was homogenized in a spatial homogenizer for 15 minutes. There were done specimens of these compositions, for tension test, by bilateral pressing at 600 MPa and sintering at 1150 ^oC for 30 minutes in endogas. The density of the sintered tests was around 7,3 g/cm^3. All tests were tension tested to determine the breaking resistence, the elongation one and the elasticity and it was determined for some of them the cycle number supported until breaking by a solicitation at flat inflection alternate symmetrical.

3. RESULTS OBTAINED

The influence of the powder's characteristics and of the cooper add on the mechanical properties of the sintered materials is presented in figures 1, 2 and 3.

As it can be seen in figure 1, once the cooper add increases, the breaking resistence at tension also increases. Firstly, this increase this increase is determined by alloyed ferrite forming, which is characterized for better mechanical properties than the ones that iron has.

The most important increasing is registered by the materials obtained from more delicate powder or from powder which contains all the granulometric fractions. This is due to the pores' presence, which is small and uniform distributed in the material and to the high number of intergranular decks.

These decks, which have a smaller section befriended the forming process of the alloyed ferrite with cooper in all their section and determined an improvement of the properties in the area where the breaking happens.

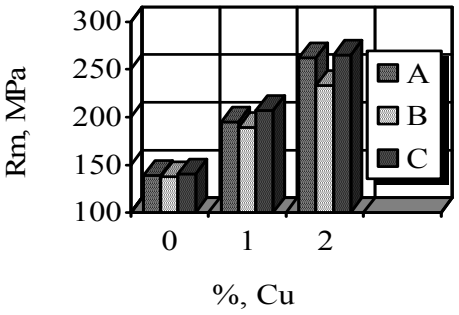

Fig.1. The influence of copper contain and grain size distribution on ultimate tensile strength

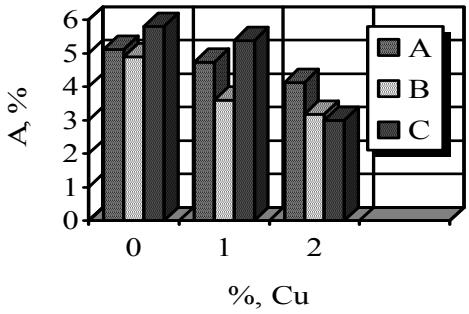

Fig. 2. The influence of copper addition and of grain size distribution on elongation

The increasing of the tension breaking resistence of the materials obtained from gross powder is lower. This is because in their structure appear big pores, and the intergranular decks section is bigger make difficult the diffusion process of the cooper in the entire volume. In the same time, the macropores section situated at the intergranular decks level constitutes tension concentrators which befriends cracks detonator and breaking [1, 2, and 3]. So, the cooper difussion in powder materials with small granulation is more intense.

From figure 2 it can be seen that, once the cooper contain increases, the meterials' elongation decreases. This decrease is duet o the fact that the alloyed ferrite, which is present at the decks level between the particles, presents a lower plasticity. The materials obtained from the main powder have a constantly decrease of the elongation.

The materials from group „C" present the biggest elongation in situation that they contain almost 1% cooper. This is duet o the fact that their pores, which are spherical and small, have the tension concentration factor smaller. At a 2% cooper contain they have the smallest elongation because the cooper broke into the intergranular spaces formes the alloyed ferrite and make the material fragile. The cooper influence in the material's elongation obtained from gross is more pronounced in the first interval and less pronounced in the second one. This is because just a part of cooper contributes to ferrite alloyed forming and the other one contributes to pore's spheroidization. [3, 5].

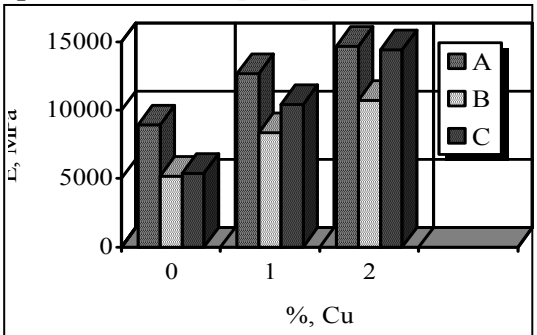

Fig. 3. The influence of copper addition and of grain size distribution on modulus of elasticity

The influence of the size of powder grains and of the cooper add on the elasticity way is presented in figure 3. It is shown that once the cooper contain increases, the elasticity way increases also. The mot important increasing is registered by the materials from group „C", obtained from a delicate powder fraction. At a high contain of cooper (2%) their elasticity module is comparable with the module of elasticity of the elaborated materials from the main powder, otherwise it is under their level. This is because at the lower contain of cooper the materials from group „C" present the biggest elongation. The materials from group „B" have the lower elasticity module. It is in some part in concordance with the other properties.

It can be said that the breaking resistence at tension, the elongation and the elasticity module are related of the cooper in iron. The mechanical properties of the

material obtained in group „A" and „C" can be compared. This is because their structure is almost the same.

The influence of the alloying materials on mechanical properties is presented in the images from figures 4, 5, and 6.

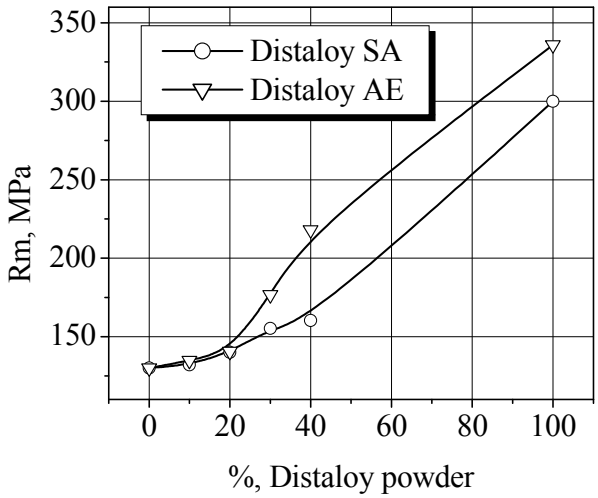

Fig. 4. The resistence variation of breaking at traction related to the alloyed powder contain

The analyze of graphic from figure 4 shows that once the powder add, which can be low alloyed Distaloy SA or high alloyed Distaloy AE in iron powder, increases, the tension test resistence increases too. This increasing is determined by the presence of the alloying elements (Ni, Cu, Mo) in the material's structure of the intergranular decks formed at the contact between the iron grains and the alloyed ones. These elements lead to obtaining some specific microstructures with better resistence properties [3, 4].

Even the nickel diffuses slowly to the iron granules interior it diffuses faster at the contact limit between these granules and along the crystal grains surface. That's why the nickel diffusion is incomplete and leads to forming some areas richer or poorer in nickel. At cooling, in these areas, it can appear untransformed austenite with superior mechanical properties. The nickel presence in iron leads to increasing the resistence at tension breaking, of the flowing limit and of elongation.

The molybdenum and cooper in iron diffusion is faster. Molybdenum leads to forming some delicate structures while the cooper, by forming some solid solutions determines the ferrite toughness. So, all alloying elements lead to improving some mechanical properties.

The most considerable improving of the tension breaking resistence is take by the powder add Distaloy AE, especially at the higher contains over 20%. This fact shows the important role of nickel in the materials obtained and which in the powder reminded, represents 4%. More than that, this powder obtained by atomization has grains with sleek surface and are compacted. Duet o the sleek surface the contact between grains is better and facilitates the diffusion process. In the same time, these materials are characterized by a small number of pores and big dimensions reported to the materials obtained from spongy powder, which is characterized by a big number of small pores [4, 5]. For the high density materials, the tension break is controlled by the size of the small pores, and the crack propagates from a pore to another niting them until the material's breaking. So, the breaking resistence of the materials obtained from mixture of iron powder and Distaloy SA, which is smaller.

At contains until 20% abundant or weak alloyed powder, the tension breaking resistence is reported to the one of the materials obtained from iron powder. This means that breaking section contains un insignificant number of intergranular decks which contain alloyed elements. While the weak or abundant powder contains increases, the number of the decks is in a continual increasing and so, the tension resistence is improving.

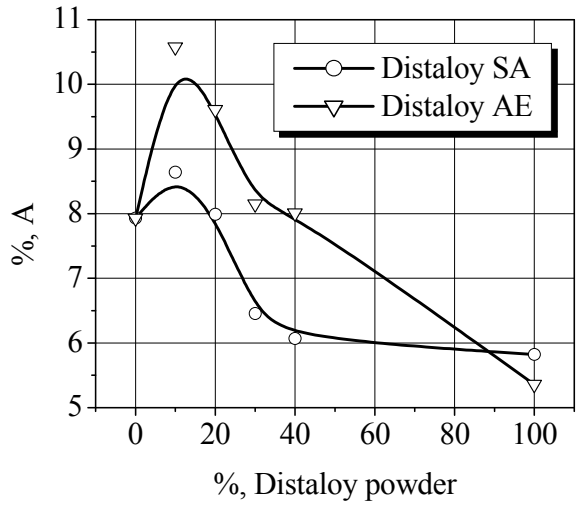

Fig. 5. The influence of the alloyed powder add on material's elongation

Figure 5 illustrates the variation curves of material's elongation obtained from mixtures of iron powder alloyed and non alloyed. It is shown that once the alloyed powder contains increases, the material's elongation decreases. This decrease of the elongation is determined by the cooper molybdenum presence which hardens the material and leads to forming some delicate structures. Generally, materials which contain Distaloy SA powder have a lower elongation than the materials which contain Distaloy AE. This is because material's elongation is reported to their section. For materials from spongy powders characterized by small pores, intergranular decks section is lower. In the same time, duet o the rough grains' surface, these materials present secondary pores too, situated right in the intergranular decks , which reduce their deformation capability [5, 7]. It can be seen a maximum elongation situated approximately at 10-20% alloyed powder add. This maximum is bigger for materials which contain Distaloy AE, probably duet o an optimum report of alloying element sat the intergranular decks level. After this maximum, the elongation is continual decreasing.

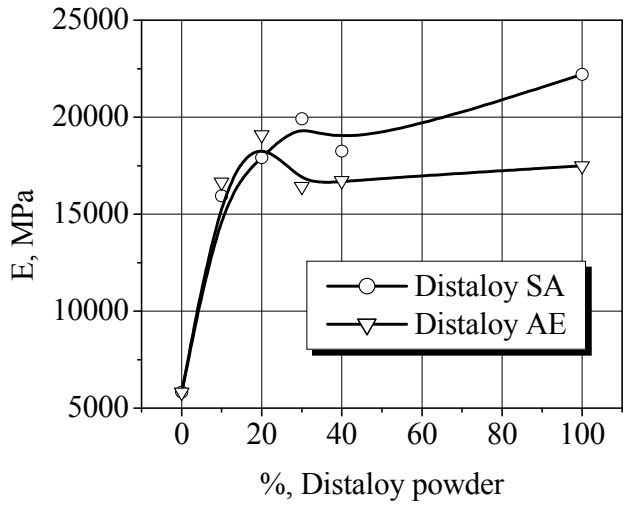

Fig. 6. The influence of the alloyed powder add on the elasticity module

The elasticity module depends in big measure for the material's structure. At the materials obtained from mixtures of iron powder alloyed and unalloyed it is shown a pronounced increasing of the elasticity module in the interval 5-20% powder add Distaloy (fig. 6). Over this value the elasticity module is maintaining approximately constant, at the elasticity module level of the alloyed powder.

In the first interval the elasticity module is approximately the same for the two categories of materials. This means that, for this area, the alloyed powder type used in this mixture doesn't influence significant the elasticity module. In the second interval the elasticity module of the materials which contain Distaloy AE is smaller that for the ones which contain Distaloy SA because their deformation capacity is bigger. The nickel's presence in bigger quantities at the intergranular decks level, duet o the high alloyed powder add, make that iron present cubic systems with centered faces characterized by an elasticity module smaller than for the cubic systems with centered volume. It is shown that between elasticity module variation and

elongation is a certain bond. Both of them change in the same way related to the alloyed powder quantity placed in mixture with iron powder.

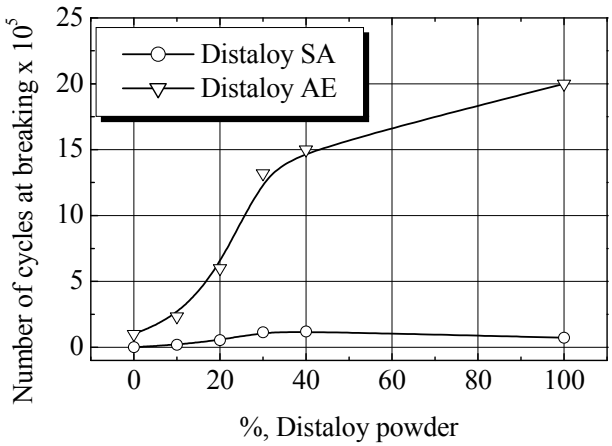

Fig. 7. The influence of the alloyed powder add on the cycle number supported by the material until braking

After fatigue test by plan inflection symmetrical alternant, it was observed an increase of the cycle's number supported until breaking (fig. 7). The biggest increase was registered by the materials obtained as a result of the add of iron powder high alloyed. The biggest increase of the cycle's number until breaking happens in the interval 10-30% alloyed powder, in the area where it was registered the biggest deformation capacity of the materials and the higher elasticity module. This means that for these materials the energy need for propagation and detonation the crack is bigger.

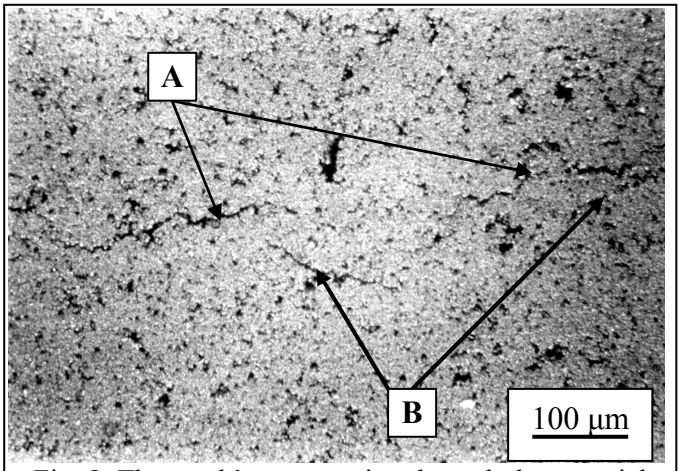

Fig. 8. The crack's propagation through the material solicited at fatigue

In figure 8 it can be observed the principal cracks A developed from the material's border to the central area and secondary cracks B situated near the principal cracks. It was shown that crack's development happens from a pore to another through intergranular decks no matter the material structure. Round pores with sleek surface improve the resistence at propagation of the crack. This is because cracks at fatigue are initiated at the pore's surface or at the material's edges level where the density is smaller and the pores are bigger. Duet to the sharp edges and to asperities from the surface of the pores, they constitute powerful concentrates of tension and detonating source of the cracks. It was shown that pores don't change the breaking mechanism at fatigue of the intergranular decks. They constitute the bond places where these cracks can propagate.

4. CONCLUSIONS

Mechanical properties of materials of iron powder are established by utilized powder characteristics. Obtained materials of fine powder fraction or with a large grain size distribution have a modulus of elasticity, tensile strength, and elongation bigger than those obtained materials of raw powder. Addition of copper leads to an increase of ultimate tensile strength, modulus of elasticity, and reducing the elongation. Changing these properties is in correlation to the intensity of diffusion phenomena, which takes place in these materials during sintering.

After the researches made on the sintered materials from iron powder and iron powder low or high alloyed it is shown a change of the mechanical properties related to the type and the powder quantity added. If the traction resistence increases linear with the increasing of the alloyed powder add, not the same thing happens with the elongation, elasticity module and cycles number supported by the material until breaking. In their case, it is registered an unlinear variation, some of them present a maximum. It could be seen that the powder add high alloyed leads to a bigger improving of all the mechanical properties studied.

REFERENCES

[1] H. Danninger, G. Jangg, B. Weiss, R. Stickler, The Influence of Porosity on Static and Dynamic Properties of PM Iron., World Conference on Powder Metallurgy, 2-6 july, (1990), Vol. 1, p. 433-439.

[2] H. Danninger, G. Jangg, B. Weiss, R. Stickler, Microstructure and Mechanical Properties of Sintered Iron. Part I: Basic Consideration and Review of Literature, PMI, Vol. 25, No. 3, 919930, p. 111-116.

[3] L. Brandusan, G. Arghir, R. Orban, S. Domşa, Properties of Sintered Steels from Mixture of Alloyed and Non-Alloyed Iron Powders, Powder Metallurgy World Congress & Exhibition, Vienna, (2004), Vol. 3, p. 81-86.

[4] L. Brandusan, E. Pica, A. Ilişiu, Studies on Static and Dynamic Breaking Process of Sintered Materials from Iron Powder, 4th International Powder Metallurgy Conference, Sakarya, TURKEY, (2005), p. 343-349.

[5] L. Ledux, C. Prioul, The Influence of Pore Morphology on the Monotonic and Cyclic Properties of Sintered Iron., Modern Developments in Powder Metallurgy, (1989), Vol. 21, p. 41-53

[6] Surdeanu T., Maria Perneş, Piese sinterizate din pulberi metalice, Editura Tehnica, Bucuresti, 1984.

[7] Firstof, S., Podrezov, Yu., Optimization of Mechanical Properties of Porous Materials., Powder Metallurgy Progress, (2001), Vol.1, No. 1, p. 5-18.

LIVIU BRÂNDUŞAN, CHERTES VIORICA, Technical University of Cluj-Napoca, 103-105 Blv. 400641 Cluj Napoca

ANALIZA INFLUENȚEI STRUCTURII OȚELURILOR SINTERIZATE ASUPRA PROPRIETĂȚILOR STATICE ŞI DINAMICE

Rezumat: Proprietățile mecanice ale oțelurilor sinterizate sunt puternic influențate de macro şi micro-structura acestora. Pentru punerea în evidență a influenței structurii asupra unor proprietăți mecanice, s-au elaborat materiale sinterizate utilizând pulberi de fier de granulații diferite sau amestecuri de diferite pulberi ce conduc la o anumită structură. S-a constatat că un material obținut dintr-o pulbere de granulație fină se comportă, la solicitări mecanice, aproape în acelaşi mod ca şi un material obținut dintr-o fracție largă. Aceasta deoarece prin utilizarea acestor fracții se obțin materiale a căror structură prezintă pori mici şi uniform distribuiți. Utilizarea amestecurilor de diferite pulberi permite obținerea unor micro-structuri cu proprietăți mecanice mai bune la nivelul punților intergranulare. În timpul solicitării, în aceste zone se înregistrează tensiunile maxime ce cauzează ruperea materialului. Utilizarea pulberii de cupru sau a pulberii de fier slab sau bogat aliată în amestec cu pulberea de fier determină o îmbunătățire a proprietăților mecanice prin modificcarea microstructurii materialului. Cel mai puternic efect asupra rezistenței la oboseală îl are adaosul de pulbere de fier bogat aliată. Prezența cuprului în amestec determină atât modificarea configurației porilor, cât şi a microstructurii materialului la nivelul punților intergranulare. Sferoidizarea porilor se datorează formării fazei lichide la sinterizare generate de prezența cuprului.

BULETINUL INSTITUTULUI POLITEHNIC DIN IAŞI
Tomul LIII (LVII), Fasc. 3, 2007
Secția
ŞTIINȚA ŞI INGINERIA MATERIALELOR

A SEM STUDY OF THE TEXTURAL PROPERTIES OF THE HYBRID MATERIALS: HYDROTALCITE LIKE ANIONIC CLAYS – GENTAMICIN

BY

GABRIELA CARJA*, SIMONA RATOI, GABRIELA CIOBANU and ION BALASANIAN

Abstract: New organic – inorganic hybrid nanostructures based on gentamicin – iron substituted hydrotalcite were synthesized by using two different synthesis methods: direct coprecipitation and reconstruction. The textural characteristics of the obtained hybrids were followed by using scanning electron microscopy (SEM) technique. The plate-let morphology defines the texture of the iron containing clay but these features changed to nonporous solid structures for the drug-clay hybrid materials.

Keywords: hydrotalcites, hybrid – nanostructures, SEM, textural properties

1. INTRODUCTION

Hydrotalcite (HT) is a class belonging to the naturally occurring anionic clay with the formula $Mg_6Al_2(OH)_{16}CO_3{\cdot}4H_2O$. It presents a positively charged brucite-like layers ($Mg(OH)_2$) in which some of Mg^{2+} are replaced by Al^{3+} in the octahedral sites of the hydroxide sheets. Interstitial layers formed by CO_3^{2-} anions and water molecules compensate the excess of the positive charge resulting from this substitution. The layers are stacked one on top of the other and are held together by weak interactions of hydrogen bonds [1]. Both magnesium and aluminium can be isomorphously substituted by other divalent or trivalent cations so a wide range of compositions containing various combinations of M(II), M(III) and different anions A^{n-} can be synthesized. The large variety of anions that can be incorporated in the brucite-like layer and the high anionic exchange capacity of these materials allow using them as matrices for tailoring specific organic – clay hybrid nanostructures with new potential applications [2]. Previous studies also suggest that the hybrids based on drugs – LDHs could form the basis for a controlled drug – release system [1, 3]. Moreover it is possible to control the point of drug release and the pharmokinetic profile by selection of the metals ions in the host layers of the drug – LDH hybrid while the confinement of the drugs between the metalhydroxide layers can also isolates the molecules from the environment thereby can improve drugs long-term stability and storage. Gentamicin belongs to the class of aminoglycoside antibiotics and is widely used for the treatment of serious infections caused mainly by Gram – negative bacteria.

Successful treatment of the infections (e.g. osteomyelitis) is achieved only by delivering a sufficient high antibiotic concentration at the site of infection. On the other hand gentamicin has toxic side effects on the kidney and the inner ear and systemic administration of high antibiotic concentration is not desirable. The use of hydrotalcite – like anionic clay as biocompatible inorganic matrices to incorporate gentamicin has been already reported in our previous published work [2].

The present paper aims to report new results about the textural properties of the composites based on gentamicin-anionic clays, type LDH. Scanning electron microscopy (SEM) is used as an advanced technique to obtain information about the texture of these materials at micro-nanoscale.

2. EXPERIMENTAL PROCEDURE

2.1. Samples synthesis

All chemicals were commercially purchased and used without further purification. Gentamicin – anionic clays hybrids were obtained as following:

Preparation of the reference sampletype iron substituted clay - FeHT
The precipitants NaOH / Na_2CO_3, the metal salts used as precursors, Mg $(NO_3)_2 \cdot 6H_2O$ / $FeSO_4 \cdot 7H_2O$ (molar ratio 2 / 1) were added dropwise together in such a way that the pH remained at a constant value of 9.5. The resulting white precipitate was aged at 338 K for 24 h under stirring. After an aging step, the obtained precipitates were separated by centrifugation, washed extensively with warm deionized water until sodium free and dried under vacuum at 40°C.

Preparation of the gentamicin containing samples
Gentamicin – FeHT hybrids were prepared by using direct synthesis by the coprecipitation method or the reconstruction method; the amount of gentamicin was optimized to overcome 2 times the anionic exchange capacity of the clay.

(a) Direct synthesis by the coprecipitation method:
100 ml of an aqueous solution of Mg $(NO_3)_2 \cdot 6H_2O$ / $FeSO_4 \cdot 7H_2O$ and an aqueous solution of gentamicin 0.3 M were slowly added dropwise together; pH=10 was maintained by the continuous addition of 0.1 M NaOH. The obtained white precipitate was separated by centrifugation, washed extensively with warm deionized water until sodium free and dried under vacuum at 30°C.This sample is denoted as GELDH1.

(b) Synthesis by the reconstruction method:
0.5 g FeHT anionic clay was calcined at 550°C for 5 h, under continuous air flow. 1 g of freshly calcined hydrotalcite – like sample was added in an aqueous solution containing 0.05 mol of gentamicin, under bobbling N_2 in the medium; the obtained precipitate was aged for 12 h at 45°C, separated by centrifugation, washed with warm deionized water until sodium free and dried under vacuum at 30°C. This sample is denoted as GELDH2.

2.2. General procedures

Powder X - ray diffraction (XRD) patterns were recorded using a Philips PW 1840 diffractometer under the following conditions: 40 kV, 30 mA, monochromatic CuKα radiation (λ = 0.15418 nm) over a 2θ range from 4 to 70º.

A Hitachi S-800 scanning electron microscope was used for scanning electron microscopy (SEM).

3. RESULTS AND DISCUSSION

The XRD patterns of GELDH1 and GELDH2 hybrids, not shown, are characteristic to organic / LDH hybrid structures [1]. Strong diffraction peaks appear at lower 2θ angles though the typical features of hydrotalcite - like materials, described in *R*-3*m* rhombohedral symmetry, are also observed. The basal reflection of FeLDH is equal to 0. 72 nm (see Table 1) though the corresponded values increases to 0.83 and 0.87 nm for GELDH2 and GELDH1respectively. The lattice parameters *a* and *c* are shown in Table 1; the parameter *a* corresponds to the metal - metal distance within the layer pointing out the cations stacking in the 003 plane while the *c* parameter is related to the distance between layers.

Table 1. Chemical composition and the lattice parameters of the synthesized samples.

Sample	Mg : Fe (by ICP)	d_{003} (nm)	Lattice parameters (nm)		IFS*
			a	*c*	
FeHT	2. 0 / 1.1	0.720	0.3049	2.43	0.28
GeLDH1	1.9 / 1.0	0.87	0.317	3.51	0.69
GeLDH2	2.1 / 1.1	0.83	0.314	3.75	0.77

The almost constant values of the *a* parameter show an unaltered metal – metal distance in the brucite like layer while the modified values of the *c* parameter and the increase of the interlayer free space (IFS) values, from 0.28 nm for FeLDH to 0.77 nm and 0.69 nm for GELDH2 and GELDH1 respectively; this result reveals that the interlayer structural characteristics altered for the gentamicin – clay composite materials.

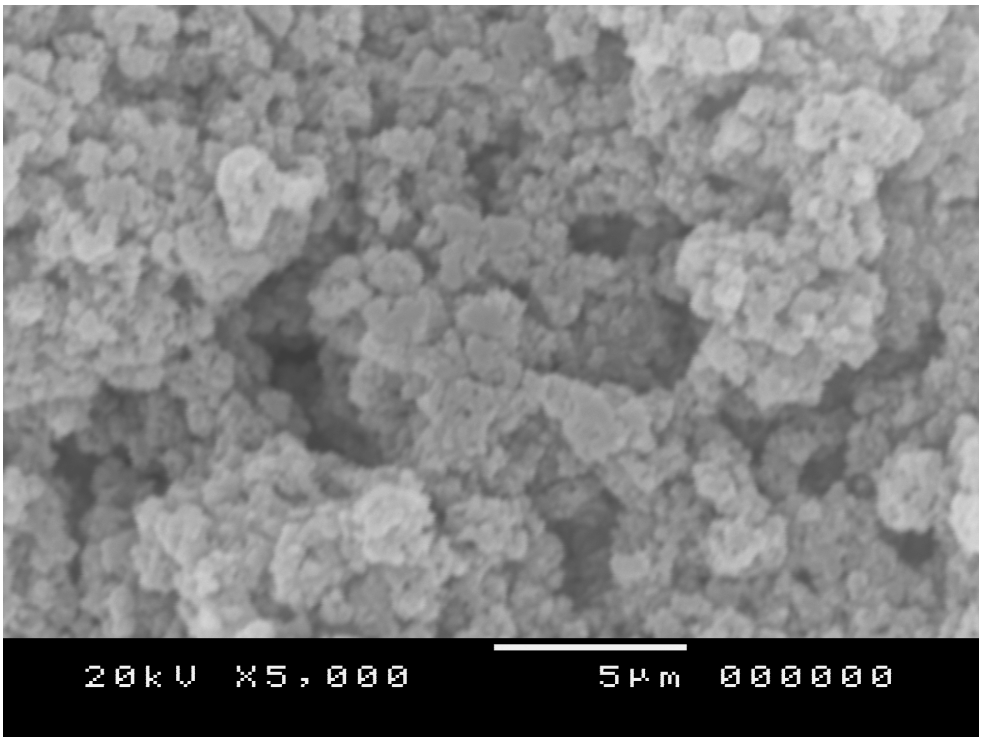

Figure 1. The SEM image of FeHT.

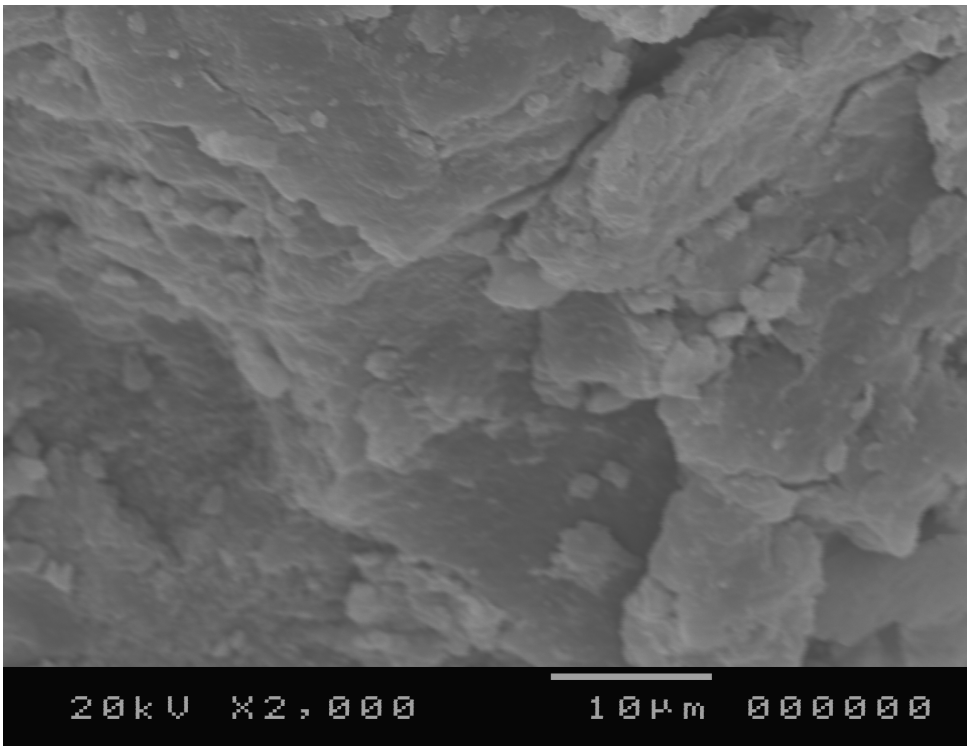

Figure 2. The SEM image of GeLDH1.

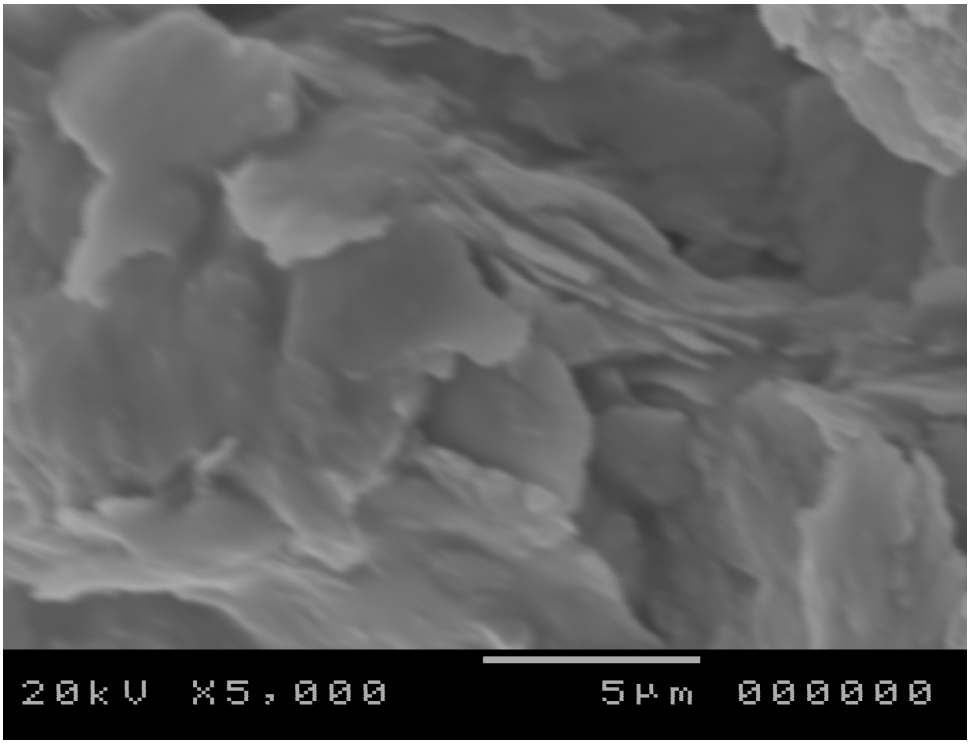

Figure 3. The SEM image of GeLDH2.

The SEM image of FeHT is presented in Figure 1; the typical thin platelet morphology of LDHs particles, highly interconnected can be observed in this case.
The SEM analysis points out the alteration of the textural characteristics of the samples containing gentamicin. When the drug is introduced in the porous matrix of the iron substituted clay the SEM images of GELDH1 and GeLDH2 (shown in Figure 2 and Figure 3) indicate that the incorporation of acetamiprid in the inorganic clay matrixes gives rise to an intricate morphology defined by a compact, nonporous solid structure that is different from the "sandrose" morphology of LDHs; however this morphology is typical for intercalated LDHs nanocomposites [4].

4. CONCLUSIONS

Hybrid materials based on gentamicin – iron substituted hydrotalcites were synthesised by using the direct coprecipitation method and the reconstruction method. X-ray analysis results point out to the modification of the clay lattice parameters when the drug is introduced in the clay matrix. The scanning electron microscopy results show that the typical thin platelet morphology of LDHs is characteristic for the parent clay while a compact, nonporous solid structure is formed in the case of the obtained hybrids. As a consequence both the structural and textural properties of the clay alter for the new composites.

Received March, 27, 2007 *The "Gh. Asachi" Technical University Iaşi*

REFERENCES

1. F. Cavani, F. Trifiro, A. Vaccari, **Catal. Today 11** (1991) 173 and references therein.
2. W. Jones, M. Chibwe, in: I.V. Mitchel (Ed.), **Pillared Layer Structures Current Trends and Applications, Elsevier, London, 1991, p. 67.**
3. G. Carja, R. Nakamura, H. Niiyama, **Appl. Catal**. A 236 (2002) **91**.
4. G. Carja, R. Nakamura, T. Aida, H. Niiyama, **J. Catal.** 218 (2003) **104**.

GABRIELA CARJA "Gh. Asachi" Technical University of Iasi, Faculty of Chemical Engineering, Bvd. D. Mangeron 71, 700050, Iasi, Romania, email: carja@uaic.ro, tel/fax 0040232 201231
SIMONA RATOI "Gh. Asachi" Technical University of Iasi, Faculty of Chemical Engineering, Bvd. D. Mangeron 71, 700050, Iasi, Romania
GABRIELA CIOBANU"Gh. Asachi" Technical University of Iasi, Faculty of Chemical Engineering, Bvd. D. Mangeron 71, 700050, Iasi, Romania
ION BALASANIAN"Gh. Asachi" Technical University of Iasi, Faculty of Chemical Engineering, Bvd. D. Mangeron 71, 700050, Iasi, Romania

STUDIUL PROPRIETATILOR DE TEXTURA ALE COMPOZITELOR : ARGILA ANIONICA DE TIP HIDROTALCIT – GENTAMICINA FOLOSIND MICROSCOPIA ELECTRONICA DE BALEIAJ

Rezumat: Lucrarea prezinta informaţii noi despre proprietatile texturale ale unor materiale de tip compozite de tipul argila anionică substituita cu fier– gentamicin. Analiza de raze X arata modificarea proprietatilor structurale ale argilei atunci când medicamentul este incorporat in matricea anorganica stratificata. Microscopia electronica de baleiaj de dovedeşte un instrument util in observarea caracteristicilor texturale ale materialelor hibride preparate si urmărirea modificării caracteristicilor de textura la nivel micro-nano in cazul noilor hibrizi sintetizaţi.

BULETINUL INSTITUTULUI POLITEHNIC DIN IAŞI
Tomul LIII (LVII), Fasc. 3, 2007
Secţia
ŞTIINŢA ŞI INGINERIA MATERIALELOR

STUDIES OF CRYSTALLINITY OF DI- AND TRIBLOCK COPOLYMERS BASED ON POLY(ε-CAPROLACTONE) AND POLY(DIMETHYLSILOXANE)

BY

CLAUDIA GORDIN[1], SLIM SALHI[2], IULIA MIHAI[1], CHRISTELLE DELAITE[1], MIHAI RUSU[1], TAMARA ELZEIN[3], MAURICE BROGLY[3]

ABSTRACT:*Well defined diblock and triblock copolymers based on poly(dimethylsiloxane) and poly(ε-caprolactone) were prepared by ring opening polymerization of ε-caprolactone using hydroxyalkyl terminated siloxane oligomers initiators. Their chemical structures and molecular weights were determined using ^{1}H-NMR, FTIR and SEC techniques, and thermal properties were determined by DSC. The DSC analyses were also conducted in order to estimate the crystallinity degrees of the PCL and PDMS blocks. The values of crystallinity degrees obtained through DSC were also confirmed by FTIR, a very good correlation between FTIR and DSC results being observed. We noticed that crystallinity degree of PCL blocks is strongly affected by the PDMS content and by increasing the content of PDMS in block copolymers the crystallinity of PCL blocks increases. This fact is also supported by the AFM results that suggest that PDMS chains play a major role in the crystallization of PCL blocks, a change of the crystalline morphology being observed.*

KEYWORDS: *Block copolymer; coordinated anionic ring-opening polymerization; poly(dimethylsiloxane); poly(ε-caprolactone); crystallization.*

INTRODUCTION

Block copolymers based on PDMS and PCL are very interesting materials because they combine the properties of polymers of each block. PDMS is a biocompatible polymer witch presents a low glass transition temperature (-123°C), high chain flexibility, good thermal, oxidative and UV stability. Their low surface energy makes them excellent candidates as surface modifying additives. Because of their mechanical weakness, low solubility parameters and immiscibility with most organic polymers it is necessary to form copolymers with other polymers [1-10].

PCL is miscible with a large variety of polymers, biocompatible and biodegradable, good reasons for choosing him as a partner in copolymerisation with PDMS [11-13].

Considering that both blocks are biocompatible and biodegradable we assumed that block copolymers based on PDMS and PCL have applications in biomaterials field [1-6].

In this paper we present a study of cristallinity of di- and triblock copolymers based on poly(ε-caprolactone) and poly(dimethylsiloxane) and the effect of PDMS on cristallinity of PCL blocks.

MATERIALS AND TECHNIQUES

Materials

Diblock copolymers poly(ε-caprolactone)-poly(dimethylsiloxane) (PCL-PDMS) were prepared by ring-opening polymerization of ε-caprolactone using hydroxyalkyl terminated siloxane oligomers and aluminum alkoxides as initiators.

Triblock copolymers poly(ε-caprolactone)-poly(dimethylsiloxane)- poly(ε-caprolactone) (PCL-PDMS-PCL) were obtained by Yilgor and colab.[1] from dihydroxyl terminated PDMS using tin octoate as catalyst.

The synthesis of well-defined copolymers was confirmed by ^{1}H-NMR spectroscopy, FTIR and SEC analyses, a monomadal chromatogram and weak values of polydispersity indices being obtained.

The characteristics of the diblock and triblock copolymers synthesized are presented in table 1.

Table 1. The characteristics of the copolymers

Block copolymer	Theoretical block length, M_n, g/mol	M_n PCL theoretic	M_n PCL ^{1}H NMR[1]	M_n copolymers (SEC)[2]	Pdi[3]
Diblock copolymers PCL-PDMS					
D_1	3,000-4,900	3,000	3,080	13,000	1.17
D_2	4,900-4,900	4,900	5,150	10,100	1.16
D_3	10,000-4,900	10,000	10,500	15,600	1.14
Triblock copolymers PCL-PDMS-PCL					
T_1	2,000-3,000-2,000	4,000	4,200	7,900	1.81
T_2	3,000-5,000-3,000	6,000	5,900	6,600	1.95
T_3	10,000-5,000-10,000	20,000	17,920	14,700	1.76
T_4	10,000-10,000-10,000	20,000	20,400	16,200	1.91

[1] Determined by ^{1}H NMR by comparing the PCL and PDMS characteristics resonance signals
[2] Determined by SEC using a PS calibration curve
[3] Polydispersity indices

Techniques

Nuclear Magnetic Resonance (^{1}H NMR) spectra were recorded on a 400 MHz spectrometer (Brucker AC 400) using deuterated chloroform as a solvent.

Size exclusion chromatography (SEC) was carried out using a Waters 2690 liquid chromatograph equipped with three columns, Waters Styragel 5 μm, 10^4, 500 and 100 Å columns; injection and refractometer temperature, 35°C; injection volume, 100 μL; solvent, THF at 1mL/min, a refractive index detector (Waters 410). Size exclusion chromatography was calibrated with PS standards.

Differential Scanning Calorimetry (DSC). Thermal analyses were performed with a Mettler TA 4000 differential scanning calorimeter and thermograms were recorded between –150°C and +150°C with a heating rate of 10°C/min.

Transmission Infrared Spectroscopy (FTIR). Diblocks and triblocks copolymers powders in KBr pellets were analyzed by infrared spectroscopy in the simple transmission device. Measurements were performed with an IFS48 Bruker spectrometer and the number of scans was fixed to 100 with a resolution of 4 cm^{-1}.

Atomic Force Microscopy (AFM). Measurements were performed with a Nanoscope IIIa/Dimension 3000 (Digital Instruments) in the tapping mode and under ambient conditions.

RESULTS

DSC analyses

DSC analyses were conducted in order to estimate the thermal properties and the crystallinity degree of the PCL and PDMS blocks. A representative thermogram is given in figure 1.

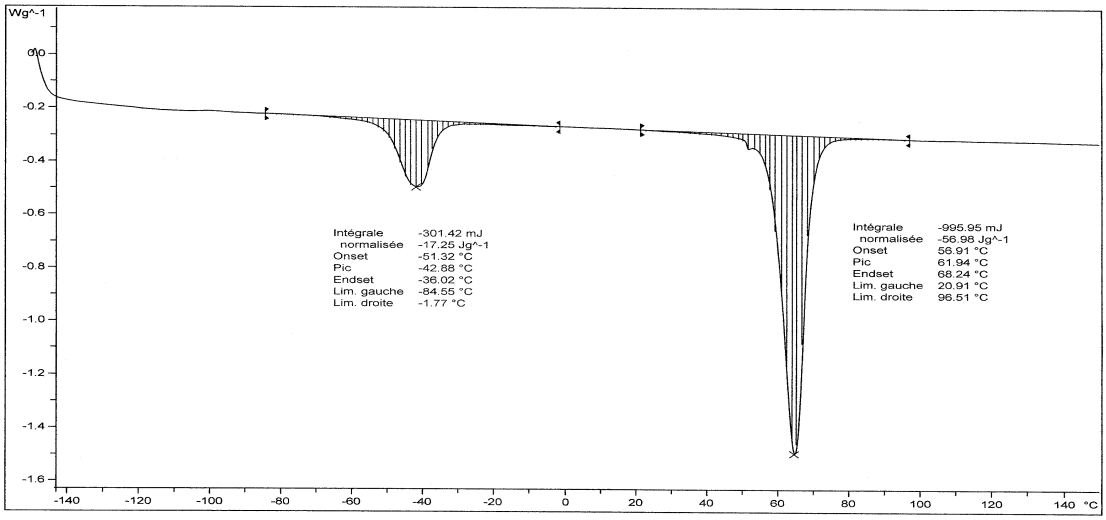

Figure 1. Characteristic thermogram of D_2 diblock copolymer

Characteristic endotherms are observed, corresponding to the melting temperature of PDMS blocks (low temperature peak) and PCL blocks (high temperature peak) in the copolymers. The melting temperature of PDMS is lowered in copolymers compared to the pure homopolymer due to the fact that PDMS is a very flexible polymer with high chain mobility.

Based on DSC thermograms we estimated the melting enthalpy (ΔH_m) of PCL blocks and dividing by the reference enthalpy of a totally crystalline PCL (ΔH_m=142 J/g) [10] we access the degree of crystallinity (X_c) (Table 2). By increasing the PCL block length the melting point of these blocks show a sensitive modification but it was observed a decreasing of cristallinity degree. Observing the evolution of the crystallinity content of the PCL as a function of the weight percent of PDMS we observe that the crystallinity content of PCL increases as PDMS content increases as shown in figure 2.

Table 2. Results of DSC analyses

Block copolymer	Tm PDMS (°C)	Tm PCL (°C)	ΔHm PDMS	ΔHm PCL	Xc PDMS (%)	Xc PCL (%)
PDMS	-124.5	-	15,2	-	24.0	-
PCL	-	60	-	109.8	-	77.3
D_1	- 48.5	58.3	33.3	116.5	52.5	82.02
D_2	- 42.9	61.9	35.4	111.2	55.8	78.3
D_3	- 48.8	62.8	7.3	113.0	11.5	79.57
T_1	- 46.6	63.7	5.8	121.1	9.1	85.3
T_2	- 43.5	64.6	14.9	130.8	23.5	92.1
T_3	- 40.1	59.0	24.3	113.9	38.4	80.2
T_4	- 40.7	64.3	30.0	118.6	47.3	83.6

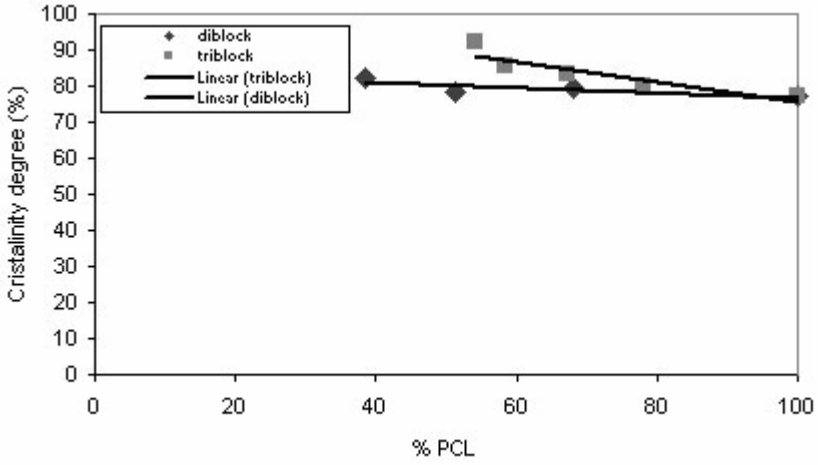

Figure 2. Cristallinity of PCL blocks

Infrared analyses

FTIR studies were conducted to verify the attributions of spectral bands (table 3) for confirming the synthesis of block copolymers and also to estimate the crystallinity degree of the PCL blocks. For all block copolymers the same global shape was obtained, with different bands intensities due to the composition as well as to the crystallinity degree.

Infrared spectra in the transmission mode of the D_2 PCL-PDMS diblock copolymer is showed in figure 3

Tabel 3. Attributions of spectral bands

Position (cm^{-1})	Vibration
2962	*v*as(CH)
2865	*vs (*CH2*)*
1727	*v*(C=O)
1420	δas (CH) et δs (CH)
1399	C-O et C-C stretching in the crystalline phase for PCL
1262	δs (CH)
1247	*v*as(COC)
1193	*v*(OC–O)
1021	*v*as(Si-O-Si)

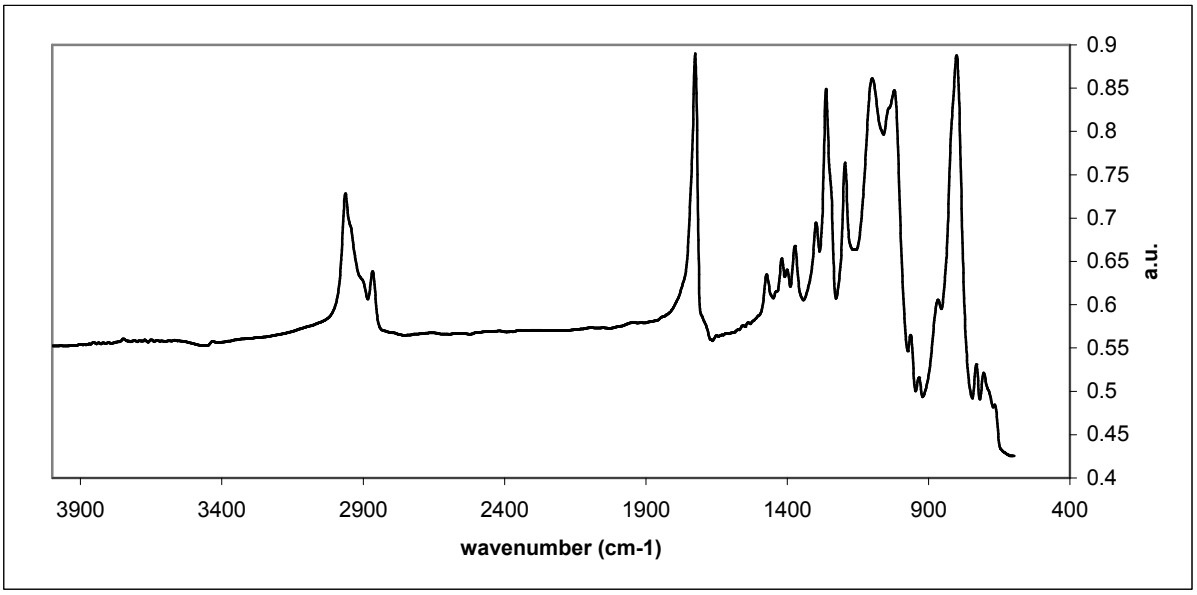

Figure 3. Infrared spectrum in the transmission mode of D_2 diblock copolymer

For obtaining the crystallinity of PCL blocks we considered the areas of characteristic peaks for the crystalline phase ($1295cm^{-1}$) as well as for the amorphous phase ($1157cm^{-1}$) [14-17]. The study of crystallinity for diblock copolymers wasn't possible because the peak at $1157cm^{-1}$ wasn't isolable.

We calculated the crystallinity using the Beer-Lambert law (equation 1).

$$A = \varepsilon \times l \times C \quad (1)$$

A-absorbance; ε- absorption coefficient ; l -path length of the sample; C-concentration

This equation can be used for the crystalline phase (equation2) as well as for the amorphous phase (equation3).

$$C_{crist} = \frac{A_{crist}}{\varepsilon_{crist} x\, l} \quad (2)$$

$$C_{am} = \frac{A_{am}}{\varepsilon_{am} x\, l} \quad (3)$$

The crystallinity is defined by the equation (4) and (5).

$$\chi_c = \frac{C_{crist}}{C_{crist} + C_{am}} \quad (4)$$

$$\chi_c = \frac{A_{crist}}{A_{crist} + \left(\frac{\varepsilon_{crist}}{\varepsilon_{am}}\right) x\, A_{am}} \quad (5)$$

By increasing the PCL block length it was observed a decreasing of cristalinity degree as we observed in DSC. We obtained a very good correlation between the DSC results and the ones obtained on FTIR (Table 4).

Table 4. Crystallinity obtained for triblock copolymers

Triblock copolymers	Area pic 1295 cm^{-1}	Area pic 1157 cm^{-1}	Crystallinity PCL (%)-FTIR	Crystallinity PCL-(%)DSC
T_1	2,0348	0,3594	85,6	85,3
T_2	1,5970	0,0943	94,7	92,1
T_3	4,4909	1,2956	78,5	80,2
T_4	0,1208	0,0230	84,6	83,5

AFM analyses

On AFM the PCL sample appears like spherules with a characteristic diameter of ≈ 10 μm but AFM images for block copolymers show a lamellar, plane superposition with a characteristic thickness of ≈ 25 nm (figure 4 and 5). This type of crystallization is specific to nanostructurated block copolymer systems. This means that organization of PCL chains is favored, PDMS chains acting as a co-crystallizing agent for PCL chains.

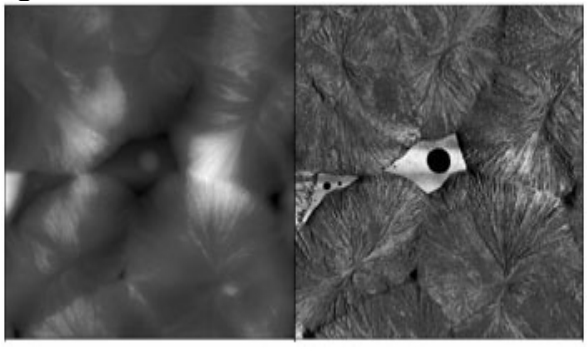

Figure 4. AFM image for PCL sample

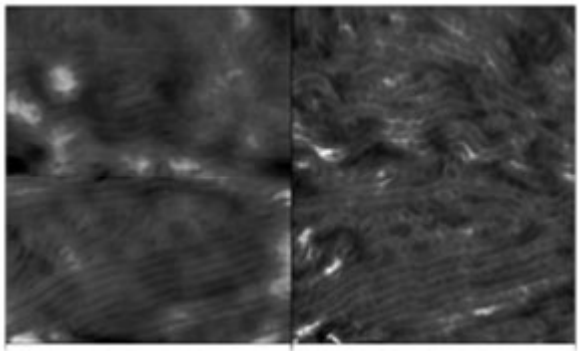

Figure 5. AFM image for D_1 block copolymer

CONCLUSIONS

Well defined diblock and triblock copolymers based on poly(dimethylsiloxane) and poly (ε-caprolactone) were prepared by the ring opening polymerization of caprolactone using hydroxyalkyl terminated siloxane oligomers as the initiator and macromonomer and aluminum alkoxides as initiators. Their chemical structures and molecular weights were characterized using ^{1}H-NMR, FTIR and SEC, and thermal properties were determined by DSC. The DSC and FTIR analyses were also conducted in order to estimate the crystallinity degree of the PCL blocks. We noticed that by increasing the content of poly(dimethylsiloxane) in block copolymers the crystallinity of poly (ε-caprolactone) block increase and the organization of PCL chains is favored, PDMS chains acting as a co-crystallizing agent for PCL chains.

REFERENCES

1. I. Ylgor and J.E. McGrath, *Adv. Polym. Sci.*, **86** (1988), p. 1
2. T. Nagamune, A. Ueda and S. Nagai, *J. Appl. Polym. Sci.*, **62** (1996), p. 359
3. D.K. Kim, S.B. Lee, K.S. Doh andY.W. Nan, *J. Appl. Polym. Sci.*, **74** (1999), p. 1917
4. R.R.Li, P.D. Dapkus, M.E. Thomson, W.C. Jeong, C. Harrison, P.M. Chaikin, R.A. Register and D.H. Adamson, *Appl. Phys. Lett.*, **76** (2000), p. 1989
5. J.Y. Chang, C.A. Ross, V.Z.H. Chan, E.I. Thomas, R.G.H. Lammertik and G.J. Vasco, *Adv. Mater.*, **13** (2001), p. 1174
6. K. W. Guarini, C.T. Black, K.R. Milkova and R.L. Sandstrom, *J.Vas. Sci. Technol.*, **19** (2001), p. 2784
7. R. A. Segalman, A. Hexemer, R. C. Hayward and E. Kramer, *Macromol.*, **36** (2003), p. 3272
8. R. Chandra and R. Rustigi, *Prog. Polym. Sci.*, **23** (1998), p. 1273
9. J. Wang, M.K. Cheng and Y. Mi, *Polym.*, **43** (2002), p. 1357
10. A.P.D.Elfick, *Biomaterials*, **23** (2002), p. 4463
11. T. Elzein, M. Nasser-Eddine, C. Delaite, S. Bistac and P. Dumas, *J. Colloid Interf. Sci.*, **273** (2004), p. 381
12. H.Y. Kweon, M.K. Yoo, I.K. Park, T.H. Kim, H.C. Lee, J.S. Oh, T. Akaide and C.S. Cho, *Biomaterials*, **24** (2003), p. 801
13. S. Li, H. Garreau, B. Pauvert, J. McGrath, A. Toniolo and M. Vert, *Biomacromol.*, **3** (2002), p. 525
14. Coleman, M.M., Zarian, J. J. Polym. Sci. B. 1979, **17**, 837.
15. Schrader B., "Infrared and Raman Spectroscopy, Methods and Applications", VCH, 1995.
16. Hummel, D.O. "Infra Red Spectra of Polymers", Wiley & sons, N.Y, 1966.
17. Socrates, G. "Infra Red Characteristic group frequencies", Wiley & sons, N.Y. 1980.

[1] "Gh. Asachi" Technical University, Faculty of Chemical Engineering, Department of Naturals and Synthetic Polymers, 71A, Bd. D. Mangeron, Iasi, Romania

[1] Université de Haute Alsace, Ecole Nationale Supérieure de Chimie de Mulhouse (ENSCMu), Laboratoire de Chimie Macromoléculaire, 3, rue Alfred Werner, 68093 Mulhouse Cedex, France

[3] Institut de Chimie des Surfaces et Interfaces (UPR 9069), 15 Rue Jean Starcky, BP 2488 68057 Mulhouse cedex, France

STUDIUL CRISTALINITATII DI- SI TRIBLOCCOPOLIMERILOR PE BAZA DE POLI(CAPROLACTONA) SI POLI(DIMETILSILOXAN)

Rezumat: Copolimeri dibloc si tribloc, cu o structura bine definita, pe baza de poli(caprolactona) (PCL) si poli(dimetilsiloxan) (PDMS), au fost sintetizati prin polimerizarea cu deschidere de ciclu a ε-caprolactonei, utilizand oligomeri siloxanici hidroxi functionalizati ca initiatori. Structura chimica si masa moleculara a acestor bloccopolimeri au fost determinate utilizand ca tehnici :
^{1}H-NMR, FTIR si SEC iar proprietatile termice au fost determinate prin DSC. Analizele DSC au fost utilizate, de asemenea , si pentru estimarea gradului de cristalinitate a blocurilor de PCL, respectiv PDMS . Gradul de cristalinitate a acestor blocuri a fost determinat si prin analize FTIR, o buna corelatie intre rezultatele obtinute folosind cele doua tehnici fiind observata. Pe seama acestor rezultate putem spune ca gradul de cristalinitate al blocurilor de PCL este influentat de procentul de PDMS din bloccopolimeri, mai exact la cresterea procentului de PDMS din bloccopolimeri gradul de cristalinitate al blocurilor de PCL creste. Aceste concluzii sunt confirmate si de rezultatele AFM ce sugereaza faptul ca lanturile de PDMS joaca un rol important in cristalizarea blocurilor de PCL, o modificare a morfologiei cristaline fiind observata.

BULETINUL INSTITUTULUI POLITEHNIC DIN IAŞI
Tomul LIII (LVII), Fasc. 3, 2007
Secția
ŞTIINȚA ŞI INGINERIA MATERIALELOR

SYNTHESIS AND CHARACTERISATION OF La-Fe-O PEROVSKITE-TYPE OXIDES FOR REMOVAL OF NO_x FROM EXHAUST GASES

BY

NICOLAE APOSTOLESCU, MIRCEA TEODOR NECHITA, GABRIELA ANTOANETA APOSTOLESCU

Abstract: *The large amounts of NO_x from exhaust gases are one of the greenhouse effect. Selective catalysts are under research for reducing the NO_x from different sources. Mixed oxides showed a good catalytic properties but their major disadvantage is the low surface area. Synthesis of La-Fe-O perovskite-type oxide was investigated by TG, XRD and BET methods to obtain the higher specific surface area.*
Keywords: *$LaFeO_3$, perovskite-type oxide, ciano*

1. INTRODUCTION

In the last years, a worldwide effort to discover improved solutions for the removal of NO_x emissions is continuous lead by scientific community [1]. The major pollutant responsible for photochemical smog formations and acid rain is nitrogen oxides, NO_x. Because the great amount of various nitrogen oxides into our atmosphere (more than 30 million tons of NO_x are vented each year) a rigorous control is required.

The most important sources of NO_x emission is represented by fuel combustion in automobile engines. Some solutions for decreasing NO_x amount produced by fuel combustion can be the reduction of exhaust emissions using the alternative energy sources or other catalytic methods. Therefore, $DeNO_x$ catalysts or new after treatment systems for the removal of NO_x gases which function also in an oxidizing atmosphere, have to be developed. Using specific catalysts, the reduction of NO_x with hydrocarbons present in the feed stream can be solutions for removal NO_x in the exhaust gas of automobile engines. Studies on a large area of materials that can be used as catalyst betray that the metal oxide catalyst shows high thermal stability but poor activity of NO_x reduction.

The perovskite oxides are one of important category of materials used and studied as catalyst, because of technologically important physical characteristics. So in 1971, cobalt perovskites were suggested as substitutes for noble metals in automotive exhaust catalysts [2]. In the last time, studies regarding simultaneous removal of NO and diesel soot over perovskite oxides was done by Teraoka et al. [3, 4]. Perovskite $LaFeO_3$ and similar compounds have attracted considerable attention because of their widespread uses in fuel cells [5], catalysts [6] and environmental monitoring applications [7]. This perovskite catalyst can be easy prepared by different methods, like sol-gel [8, 9], combustion synthesis [10, 11] and hydrothermal synthesis [12], freeze-dry-ing [13], but all these wet chemical methods, request calcinations at

relative high temperature and long soaking to produce powders with good crystal structure.

In this paper we study the preparation of La-Fe-O perovskite-type oxide with high surface area using the thermal low temperature decomposition of the heteronuclear complex $La[Fe(CN)_6]\cdot nH_2O$.

2. EXPERIMENTAL

Synthesis. $LaFeO_3$ polycrystalline powder is prepared by thermal low temperature decomposition of heteronuclear complex $La[Fe(CN)_6]\cdot nH_2O$. The complex is prepared by mixing the lanthanum nitrate solution with potassium ferricyanide solution in molar ration 1:1 [14 - 16]. After vacuum filtration and quick washing of the precipitate with water and ethylic alcohol, it is dried first at 60°C. The dry solid is heated in oven at desired temperature with a ramp of 1°C/min and then maintained at final temperature in air, for 120 minutes.

Characterization. X ray diffraction patterns were performed on a Siemens D 501 powder diffractometer (30 mA, 40 kV) using CuKα radiation. The sample was rotated with 120 min^{-1} and the 2θ angle was in steps of 0.02°. The specific surface area was calculated from the nitrogen adsorption/desorption isotherms at -196°C carried out on a Sorptomatic 1990 type instrument. For thermal analysis the Netzsch STA 409C equipment was used with a synthetic air atmosphere. The desorption test were conducted in an tubular reactor connected at a gas mixture line with flow meters controllers that can synthesize different experimental conditions. The analysis of the resulted gases was made on a Chemical Ionization Mass Spectrometer AIRSENSE 500 (V&F Absam, Austria).

3. RESULTS AND DISCUSSION

Probes synthesized at different temperatures were used for determination of the crystalline structure by X-ray measurements. The results presented in Fig 1., shows that the perovskyte-type oxide is synthesized after 500°C, with a high purity of the crystalline orthorhombic phase according to the JCPDS 37-1493 [17].

At temperatures below the self ignition point (328°C, Fig. 2.) the phase is crystalline, the main component is a mixture of the heteronuclear complex $La[Fe(CN)_6]\cdot nH_2O$ JCPDS 36-0675 and 25-1198 [17]. After that point the concentration of the crystalline structure of the perovskite-type oxide grows with temperature.

To understand the processes that took place in solid, a sample was tested for thermal analysis (Fig. 2.). From the results can be seen the main process at 328°C, when the weight loss is big, corresponding to the self ignition of the gel. The first endothermic process at about 185°C is due to the lost of the crystallization water, the dry complex has about 4.24 molecules of water (18% lost in the TG measuring).

$$La[Fe(CN)_6]\cdot nH_2O \rightarrow La[Fe(CN)_6] + n\ H_2O$$

The main reaction from the decomposition of the $La[Fe(CN)_6]$ is with oxygen from air at about 328°C, and it has an extremely exothermic effect:

$$La[Fe(CN)_6] + O_2 \rightarrow LaFeO_3 + \text{burning products}$$

A third process from 417°C, also an exothermic reaction, probably the burning of the remaining organic components. With this, the preparation of $LaFeO_3$ is ended; the mass loss is 25.5% from the anhydrous complex.

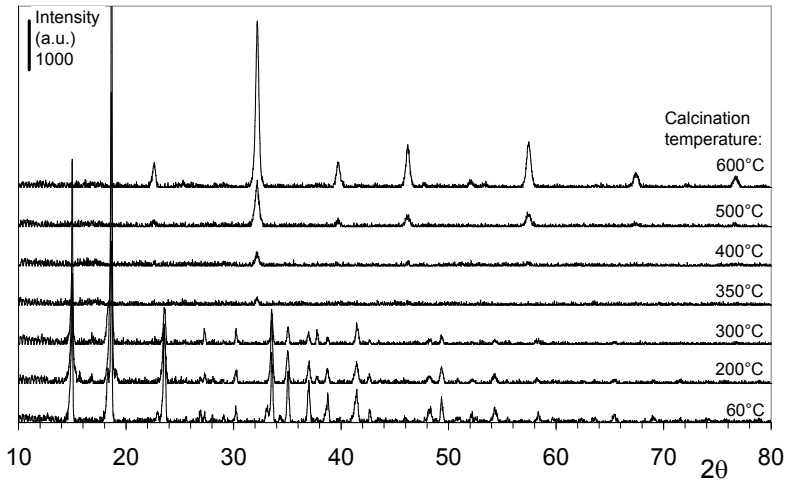

Fig. 1. The X-ray diffraction spectra of $LaFeO_3$ synthesized at different temperatures.

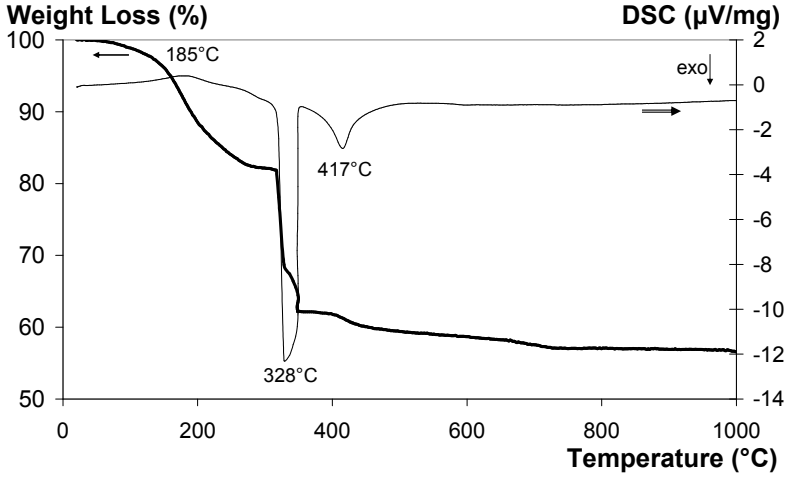

Fig. 2. The thermal analysis of $LaFeO_3$ synthesized from $La[Fe(CN)_6]$

Table 1. Specific surface area measured after calcination at different temperatures

Calcinations temperature, °C	500	600	700	1000
Specific surface area, (BET), m^2/g	23	16	12	4

The specific surface area (BET) of the $LaFeO_3$ perovskite-type oxide powder synthesized at different temperatures is presented in the Table 1. The high surface area obtained at low calcinations temperature is due to the amorphous phase from the prepared oxide. After 600°C, the surface area is low, but the crystalline phase is high. The processes of sinterisation took place at high temperatures and reduce the specific surface area. If we compare with the surfaces obtained by ceramic method (0.3 - 0.5 m^2/g [16]) this results are good.

4. CONCLUSIONS

The results presented show that the thermal decomposition of the heteronuclear complex lanthanum and iron nitrates leads to the formation of pure, nanosized

orthorhombic $LaFeO_3$ perovskite-type oxide at temperatures around 600°C. The surface area is high comparing with the ceramic method of preparing the perovskite.

REFERENCES

1. Armor, J.N., *Catalytic Removal of Nitrogen Oxides: Where are the Opportunities?* In: Catal. Today, vol. 26, 1995, p. 99-105.
2. Nam, I.S., *A Catalytic Process for the Reduction of NOx from Stationary Sources*, In: Catalysis, vol. 7 (3), 1996, p. 554.
3. Teraoka, Y., Kanada, K., Kagawa, S., *Synthesis of La-K-Mn-O perovskite-type oxides and their catalytic property for simultaneous removal of NOx and diesel soot particulates*, In: Appl. Cat. B: Env., vol. 34, 2001, p. 73-78.
4. Hong S.S., Lee, G.D., Park, J.W., et al., *Catalytic Reduction of NO over Perovskite-type catalysts*, In: Korean Journal of Chemical Engineering, vol. 14(6), 1997, p. 491-497.
5. Mih, N.Q., *Ceramic fuels cells*, In: J. Am. Ceram. Soc, vol. 76 (4), 1993, p. 563-588.
6. Delmastro, A., Mazza, D., Ronchetti, S. et al., *Synthesis and characterization of non-stoechiometric $LaFeO_3$ perovskite*, In: Mater. Sci. Eng. B. - Solid, vol. 79 (2), 2001, p. 140-145.
7. Martinelli G., Carotta, M.C., Ferroni, M., *Screen-printed perovskite-type thick film as gas sensors for environmental monitoring*, In: Sensors Actuators B - Chem., vol. 55 (2-3), 1999, p. 99 - 110.
8. Vasquez-Vasquey, C., Kogerler, P., Lopez-Quintela, M.A. et al., *Preparation of $LaFeO_3$ particles by sol-gel technology*, In: J. Mater. Res., vol. 113 (1), 1998, p. 451-456.
9. Xiao, J., Hong,G.Y., Yu, D.C. et al., *Synthesis and properties of $LaFeO_3$ ultrafine powders*, In: Acta. Chim. Sinica, vol. 52 (8), 1994, p. 784-788.
10. Manoharam, S.S., Patil, K.C., *Combustion route to fine particle perovskite oxides*, In: J. Solid State Chem., vol. 102 (3), 1993, p. 267-276.
11. Apostolescu, N., Nechita, M.T., Apostolescu, G.A. - *Synthesis Of La-Fe-O Perovskite-Type Oxides For Removal Of NOx From Exhaust Gases*, Bulletin of the Transilvania University of Braşov, Supplement: BRAMAT 2007, vol. IV, 2007, ISSN 1223-9631, p.633-636.
12. Zheng, W.J., Liu, R.H., Peng, D.K., et al., *Hydrothermal synthesis of $LaFeO_3$ under carbonate-containing medium*, In: Mater. Letter, vol. 43 (1 - 2), 2000, p. 19-22.
13. Flavala,D., Kirchnerova, J., Tofan,C., *Catalytic Decomposition of Nitric Oxide by Perovskites*, In: Korean J. Chem. Eng., 16 (4), 1999, p. 470-477.
14. Yoon, J.W., Grilli, M.L., Di Bartolomeo, E., Polini, R., Traversa, E. - *The NO_2 response of solid electrolyte sensors made using nano-sized $LaFeO_3$ electrodes* Sensors and Actuators B, 76, 2001, p. 483-488.
15. Traversa, E., Sakamoto, M., Sadaoka Y. - *A chemical route for the preparation of nanosized rare earth perovskite-type oxides for electrochemical applications*, Partic. Sci. and Tech., 16, 1998, p. 185-214.
16. Nakayama S. - *$LaFeO_3$ perovskite-type oxide prepared by oxide-mixing, co-precipitation and complex synthesis methods*, J. Mat. Sci., 36, 2001, p. 5643.
17. * * * - *Powder Diffraction File*, JCPDS - Int. Center for Diff. Data, Swartmore, Pa., 1987.

NICOLAE APOSTOLESCU, MIRCEA TEODOR NECHITA, GABRIELA ANTONETA APOSTOLESCU - "Gh. Asachi" Technical University, Faculty of Chemical Engineering, 71A D.Mangeron B-dul., Iaşi, 700050, Romania. E-mail: napostol@ch.tuiasi.ro

SINTEZA SI CARACTERIZAREA OXIZILOR La-Fe-O TIP PEROVSKITE PENTRU INDEPARTAREA NO_X DIN GAZELE EVACUATE

Rezumat: Cantităţile mari de oxizi de azot din gazele de eşapament sunt una din cauzele producerii efectului de seră. Catalizatorii selectivi sunt studiaţi pentru micşorarea cantităţii de oxizi de azot produsă de diferite surse. Oxizi micşti au arătat proprietăţi catalitice bune, dar principalul lor dezavantaj îl constituie suprafaţa specifică redusă a acestora. Sinteza oxizilor de tip perovskitic cu La-Fe-O a fost investigată prin tehnici de spectroscopie cu raze X, termogravimetrie şi prin determinarea suprafeţei specifice BET pentru obţinerea unui material cu suprafaţă specifică sporită.

BULETINUL INSTITUTULUI POLITEHNIC DIN IAŞI
Tomul LIII (LVII), Fasc. 3, 2007
Secția
ŞTIINȚA ŞI INGINERIA MATERIALELOR

THE ALGORITHM USED IN DESIGNING THE HEAT EXCHANGER

BY

CONSTANTIN BORIS

Abstract: The heat transfer in the heat exchanger can be described by mean of two equations with partial derivatives. To solve them we need an initial condition and two boundary conditions for each equation. For solving the differential equations it has been created a programme for a set of equations with partial derivatives that use the Runge-Kutta method.

Keywords: transfer equation, Runge-Kutta method, shell, partial derivatives, space-grid, enthalpy

In the present paper we are trying to present the basic mathematical aspects that underlie our designing of the heat exchangers with fins, like: the mean logarithmic temperature, efficiency, effectiveness, the designing of the very long fins, the numerical resolution of the equation of the heat transfer with initial condition and boundary condition. Also we have tried to create a software composed from a few subroutines available on the market, which describe the configurations included in TEMA standard and subroutines which we have elaborated in order to solve the heat transfer equation and the development in Bessel functions necessary for designing the fins.

For the beginning we take into consideration the simple case of a shell and one tube heat exchanger. We presume that: the fluid flow from the shell and tube are in counter current, the outside surface of the shell and of tube is perfectly isolated, the water that flows through the shell and the tube is absolutely incompressible, we don't have phase transformers, the water has constant density in all the U system- the total heat transfer coefficient is constant, the caloric efficiency doesn't depend upon the temperature. Using the equation with partial derivatives, the system is modulated and there calculated the enter temperature and the exit temperature of the heat exchanger. Additionally it is calculated heat transfer using the energy balance. Hereinafter, the system is analyzed also from a classical point, using the logarithmic mean temperature, and afterward making a comparation of the two methods. The parameters for the heat exchanger are listed in the following table:

Parameter	Tube	Shell
T_{in}	498,15 K	298,15 K
ρ	1001 kg/m^3	1001 kg/m^3
C_p	4184 J/kgK	4184 J/kgK
V	0,01 m/s	0,01 m/s
D	1 m	2 m

The L length of the device is of 4 m, and the total heat transfer coefficient U is of 1700 W/m^2 K.Traditionally, in order to determine the heat transfer in the tube, we use the relation:

$$\mathbf{q} = \mathbf{U} \cdot \mathbf{A} \cdot \Delta \mathbf{T}_{\mathbf{lm}} \tag{1}$$

where:

$$\Delta \mathbf{T}_{\mathbf{lm}} = \frac{\Delta \mathbf{T}_2 - \Delta \mathbf{T}_1}{\ln\left(\frac{\Delta \mathbf{T}_2}{\Delta \mathbf{T}_1}\right)} \tag{2}$$

represents the logarithmic mean temperature. Secondly, in the analyze of a heat exchanger, as in any problem of heat transfer, we must start from an energy balance. In the majority of the cases, an energy balance has the form:

Acumulation = input – output + generation

In the case of our system, we have to write an energy balance taking into consideration that we have also a balance of the enthalpy. The initial equation from where we begin is:

$$\rho V \frac{\partial H}{\partial T} = H \cdot \dot{m}\Big|_x - H\dot{m}\Big|_{x+\Delta x} - U \cdot A \cdot (T_{in} - T_{out}) \tag{3}$$

In order to continue the derivation, the size V, m and A will be replaced with specific terms for this physical system, resulting:

$$\rho\pi r^2 \Delta x \frac{\partial H}{\partial T} = H\rho\nu\pi r^2\Big|_x - H\rho\nu\pi r^2\Big|_{x+\Delta x} - U2\pi r\Delta x(T_{in} - T_{out}) \tag{4}$$

Dividing the equation (4) by $\rho\pi r^2\Delta x$ results:

$$\frac{\partial H}{\partial T} = \frac{H\nu}{\Delta x}\Big|_x - \frac{H\nu}{\Delta x}\Big|_{x+\Delta x} - \frac{U2(T_{in} - T_{out})}{\rho r} \tag{5}$$

Simplifying:

$$\frac{\partial H}{\partial T} = \nu\left(\frac{H_x - H_{x+\Delta x}}{\Delta x}\right) - \frac{U2(T_{in} - T_{out})}{\rho r} \tag{6}$$

where $-\left(\frac{H_x - H_{x+\Delta x}}{\Delta x}\right)$ is the definition for the derivative of H. The equation (6) can be rewritten:

$$\frac{\partial H}{\partial T} = -\nu\frac{\partial H}{\partial x} - \frac{U2(T_{in} - T_{out})}{\rho r} \tag{7}$$

If we work with a real system, the enthalpy doesn't constitute a property with which one can work easy. Much more easily is to work with the temperature measure.

The thermodynamics determines a connexion between the enthalpy and temperature through the relation:

$$\hat{H}(T) = \overset{)}{C}_p \cdot T$$

Substituting this equation in (7), results:

$$\overset{)}{C}_p \frac{\partial T}{\partial T} = \nu \overset{)}{C}_p \frac{\partial T}{\partial x} - \frac{U2(T_{in} - T_{out})}{\rho r} \qquad (8)$$

Dividing by Cp, results:

$$\frac{\partial T}{\partial T} = -\nu \frac{\partial T}{\partial x} - \frac{U2\pi(T_{in} - T_{out})}{\rho \overset{)}{C}_p r} \qquad (9)$$

The equation for the shell differs very little from the equation for the tube. The main differences are: the V term is different; the generation term will be positive because the shell gains heat:

$$\rho\pi(r_{manta}^2 - r_{tub}^2)\Delta x \frac{\partial H}{\partial T} = H\rho\nu\pi(r_{manta}^2 - r_{tub}^2)\Big|_x + H\rho\nu\pi(r_{manta}^2 - r_{tub}^2)\Big|_{x+\Delta x} +$$
$$+ U2\pi r_{tub}\Delta x(T_{in} - T_{out})$$

The derivation is realized following the above mentioned steps, resulting:

$$\frac{\partial T}{\partial T} = -\nu \frac{\partial T}{\partial x} + \frac{U2\pi r_{tub}(T_{in} - T_{out})}{\overset{)}{C}_p \rho(r_{manta}^2 - r_{tub}^2)} \qquad (10)$$

The heat transfer in the heat exchanger can be described by mean of two equations with partial derivatives, (9) and (10). To solve them we need an initial condition and two boundary conditions for each equation.

For the tube the conditions are:

The initial conditions: `T(z = 0 la z = 4) = 298,15 K`

The boundary conditions: `T(x = 0,t) = 473,15 K` ; `T(x = 4,t) =` $dT/dt = 0$

For the shell the conditions are:

The initial conditions: `T(x = 0 la x = 4) = 298,15 K`

The boundary conditions: `T(x = 0,t) =` $dT/dt = 0$; `T(x = 4,t) = 298,15 K`

For solving the differential equations it has been created a programme for a set of equations with partial derivatives that use the Runge-Kutta method, program that is presented hereinafter:

```
function syspde_para
clear all;
close all;
n_eq = 2;  % INPUT
m_int = 50; %INPUT
xo = 0.0;
```

```
xf = 4.0;
n_int = 1000;
to = 0.0;
tf = 1450;
% 0 = Dirichlet
% 1 = Neumann
Bc = [0 1; 1 0; 0 1; 1 0]; % INPUT
mx = m_int + 3;
dx = (xf – xo)/m_int;
dxi = 1/dx;
xgrid = [(xo-dx : dx : (xf+dx)]';
nt = n_int +1
dt = (tf-to)/n_int;
tgrid = [(to):dt:(tf)]';
y = zeros(n_eq,nt,mx);
for k_eq = 1:1:n_eq
for i_BC = 1:1:2
        if (i_BC = = 1)
                if (BC(k_eq, i_BC) = =0)
                        i_x_v(k_eq, i_BC) = 3;
                else
                        i_x_v(k_eq, i_BC) = 2;
                end
        else
                if (BC(k_eq, i_BC) = =0)
                        i_x_v(k_eq, i_BC) = mx-2;
                else
                        i_x_v(k_eq, i_BC) = mx-1;
                end
        end
end
% i_x_v
% i_x_d
j_t = 1;
for k_eq = 1:1:n_eq
        for i_x = 2:1:mx-1
                x = xgrid(i_x);
                y(k_eq,j_t,i_x) = syspde(k_eq, x);
        end
end
y1 = zeros(n_eq, mx);
for k_eq = 1:1:n_eq
        for k_bc = 1;1:2
                if (BC(k_eq, k_bc) = =0)
                        if (k_bc == 1)
                                i_x = 2;
```

```
                                else
                                        i_x = mx – 1;
                                end
                                x = xgrid(i_x);
                                for j_t = 1:1:nt
                                        T = tgrid(j_t);
                                        for m_eq = 1:1:n_eq
                                                Y1(m_eq, : ) = y(m_eq, j_t, : );
                                        end
fprintf(1,'D: k_eq= %i kbc= %i i_x = %i x = %f t = %f  \n',k_eq, k_bc, i_x, x, t)
          y(k_eq, j_t, i_x) = syspde (k_eq, k_bc, x, t, y1, i_x, dx);
                                end
                        end
                end
        end
        j_t = 1;
        t = tgrid(j_t);
        for k_eq = 1:1:n_eq
                y1(k_eq, : ) = y(k_eq, j_t, : );
        end
        for k_eq = 1:1:n_eq
                for k_bc = 1:1:2
                        if BC(k_eq, k_bc) = = 1)
                                if k_bc == 1)
                                        i_x = 1;
                                        i_x2 = 2;
                                        i_x3 = 3;
                                else
                                        i_x = mx;
                                        i_x2 = mx-1;
                                        i_x3 = mx-2;
                                end
                                x = xgrid(i_x);
fprintf(1,'N: k_eq= %i kbc= %i i_x= %i x = %f t = %f \n',k_eq, k_bc, i_x, x, t)
          y(k_eq, j_t, i_x) = syspde (k_eq, k_bc, x, t, y1, I_x, dx);
                        end
                end
        end
        dydt_1 = zeros(n_eq,mx);
        dydt_2 = zeros(n_eq,mx);
        for j_t = 2:1:nt
                t = tgrid(j_t-1);
                for k_eq = 1:1:n_eq
                        y1(k_eq, : ) = y(k_eq, j_t-1, : );
                end
                dydt_1 = syspde_para_input(n_eq, i_x_v, y1, t, dxi, mx);
```

```
        t = t + dt;
        for k_eq = 1:1:n_eq
                for i_x = i_x_v(k_eq,1) :1: i_x_v(k_eq,2)
                        y1(k_eq, i_x) = y1(k_eq, i_x) + dt*dydt_1(k_eq, i_x);
                end
        end
        for k_eq = 1:1:n_eq
                for k_bc = 1:1:2
                        if (BC(k_eq, k_bc) = =0)
                                if (k_bc = = 1)
                                        i_x = 2;
                                else
                                x = xgrid(i_x);
                                y1(k_eq, i_x) = y(k_eq, j_t, i, x);
                                end
                        end
                end
                t = tgrid(j_t);
                for k_eq = 1:1:n_eq
                        for k_bc = 1:1:2
                                if (BC(k_eq, k_bc) = = 1)
                                        if (k_bc = = 1)
                                                i_x = 1;
                                        else
                                                i_x = mx;
                                        end
                                        x = xgrid(I_x);
 y1(k_eq, i_x) = Syspde_boudary_conditions(k_eq, k_bc, x, t, y1, i_x, dx);
                                end
                        end
                end
                dydt_2 = syspde_para_input(n_eq, i_x_v, y1, t, dxi, mx);
                for k_eq = 1:1:n_eq
                        for i_x = 1:1:mx
        y(k_eq,j_t-1,i_x) + 0.5*dt*(dydt_1(k_eq,i_x) + dydt_2(k_eq, i_x) );
                        end
                end
                t = tgrid(j_t);
for k_eq = 1:1:n_eq
                        for k_bc = 1:1:2
                                if (BC(k_eq, k_bc) = = 1)
                                        if (k_bc = = 1)
                                                i_x = 1;
                                        else
                                                i_x = mx;
                                        end
```

```
                                        x= xgrid(i_x);
                                        for m_eq = 1:1:n_eq
                                                y1(m_eq, : ) = y(m_eq, j_t,: );
                                        end
y(k_eq, j_t, i_x) = Syspde_boundary_conditions(k_eq,k_bc,x,t,y1,i_x,dx);
                                end
                        end
                end
end
t = y;
nframe = 40;
if (n_int > nframe)
        nskip = round(n_int/nframe);
else
        nskip = 1;
end
lplot = 1;
fps = 3;
plc{1} = 'k-';
plc{2} = 'r-';
plc{3} = 'b-';
plc{4} = 'g-';
plc{5} = 'm-';
plc{6} = 'k:';
plc{7} = 'r:';
plc{8} = 'b:';
plc{9} = 'g:';
plc{10} = 'm:';
if (lplot = = 1)
        fpsinv = 1.0/fps;
        newplot;
        Tmax = max(max(max(T)));
        Tmin  = min(min(min(T)));
        Xtext = xo + 0.1*(xf – xo);
        Ytext = Tmin + 0.9*(Tmax – Tmin);
        for j_t = 1:nskip:nt
                for k_eq = 1:1:n_eq
                        for i_x = 2:1:mx-1
                                vector_plot(i_x) = T(k_eq,j_t,i_x);
                        end
                        plot(xgrid(2:mx-1) , vector_plot(2:mx-1),plc{k_eq} );
                        hold on
                end
                axis([xo xf Tmin Tmax]);
                XLABEL('Position(m)')
                YLABEL('Temperature (K) ')
```

```
                temps = char(strcat('time =', num2str(tgrid(j_t)), 'sec'));
                text(xtext, ytext, temps)
                hold off
                pause(fpsinv);
        end
    end
    for ii = 1:n_eq
     fprintf('input temperatures %2.0f are %6.2f and %6.2f \ n',ii, y1(ii,2),
y1(ii,mx-1));
    end
    qdiff = 0;
    rho_tube = 1000.1;
    v_tube = 1e-2;
    Cp_tube = 1000.0*4.184;
    h_tran_coeff = 1700;
    r_tube = 0.5;
    Asurf = 2.0*pi*r_tube*dx;
    for ii = 2:mx-1
        qdiff = h_tran_coeff*Asurf*(y1(1,ii)-y1(2,ii) + qdiff;
    end
    Asurf = 2.0*pi*r_tube*4;
    DelT1 = y1(1,2) – y1(2,2);
    DelT2 = y1(1,mx-1) – y1(2,mx-1);
    Tlogmean = (delT1 – delT2)/ (log(delT1/delT2));
    Qlogmean = h_tran_coeff*Asurf*Tlogmean;
    fprintf(' %12.2f  \n',qdiff);
    fprintf(' %12.2f  \n', qlogmean);
    function y_out = syspde_boundary_conditions(k)eq,k_bc,x,t,y1,i_x,dx);
    if (k_bc = =1)
        if (k_eq = = 1)
            y_out = 473.15;
        elseif (k_eq = = 2)
            y_out = y1(k)eq, i_x+2) – 2*dx*(0.0);
        elseif (k_eq = = 3)
            y_out = 2;
        else
            y_out = y1(k_eq, i_x+2) – 2*dx*(-1.0);
        end
    else
        if (k_eq = = 1)
            y_out = y1(k_eq, i_x-2) – 2*dx*(0.0);
        elseif (k_eq = = 2)
            y_out = 298;
        elseif ( k_eq = = 3)
            y_out = y1(k_eq, i_x-2) –2*dx*(0.0);
        else
```

```
                    y_out = 3;
            end
    end
    function y_out = syspde_initial_conditions(k_eq,x);
    if (k_eq = = 1)
            y_out = 298;
    elseif (k_eq = = 2)
            y_out = 298;
    elseif (k_eq = =3)
            y_out = 300;
    else
            y_out = 100 + 100*(2-x)/(2);
    end
    function dydt = syspde_para_input(n_eq,i_x_v,y1,t,dxi.mx)
    for k_eq = 1:1:n_eq
            for i_x = i_x_v(k_eq,1) : 1 : i_x_v(k_eq,2)
    dydx_matrix(k_eq, i_x) = 0.5*(y1(k_eq, i_x+1) – y1(k_eq, i_x-1))*dxi;
    d2ydx2_matrix(k_eq, i_x) = (y1(k_eq, i_x+1) – 2.0* y1(k_eq, i_x)  + y1(k_eq,
i_x-1))*dxi^2;
            end
    end
    dydt = zeros(n_eq,mx);
            L = 4.0
            rho_tub = 1000.1;
            rho manta = 1000.1;
            Cp_tub = 1000.0*4.184;
            Cp_manta = 1000.0*4.184;
            k_tub = 1000;
            k_manta = k_tub;
            alpha_tub = k_tub/rho_tub/Cp_tub;
            alpha_manta = k_manta/rho_manta/Cp_manta;
            h_tran_coff = 1700;
            r_tub = 0.5;
            r_manta = 1;
            d_tub = 2.0*r_tub;
            d_manta = 2.0*r_manta;
            A_tub = pi*(r_tub^2);
            A_manta = pi*(r_manta^2 – R-tub^2);
            V_tub = A_tub*L;
            V_manta = A_manta*L;
            Asurf = 2.0*pi*r_tub*L;
            Tsurround = 200.0;
            afac_tub = h_tran_coff*Asurf/(rho_tub*Cp_tub*V_tub);
            afac_manta=h_tran_coff*Asurf/(rho_manta*Cp_manta*V_manta);
            ffac_tub = afac_tub*Tsurround;
            ffac_manta = afac_manta*Tsurround;
```

```
            v_tub = 1.0e-2;
            v_manta = -v_tub;
        k_eq = 1;
            for_x = i_x_v(k_eq,1) : 1 : i_x_v(k_eq,2)
dydt(k_eq, i_x) = -v_tub*dydx_matrix(k_eq, i_x) + alpha_tub*d2ydx2_matrix(k_eq,
i_x) – afac_tub*(y1(1, i_x) – y1(2,i_x));
            end
        k_eq = 2;
            for i_x = i_x_v(k_eq, 1) : 1 : i_x_v(k_eq,2)
dydt(k_eq,i_x)=-v_manta*dydx_matrix(k_eq,i_x)+alpha_manta*d2ydx2_matrix(k_eq,
i_x) + afac_manta*(y1(1, i_x) – y1(2, i_x));
            end
```

After reaching steady state, the outlet temperatures of each of the streams were determined as: $T_{Tube\ Out}$ = 394,07 K and $T_{Schell\ Out}$ = 324,61 K. The total amount of heat transfer was calculated as: q_{Total} = 2636 kW, very close to value q_{Total} = 2572 which was calculated using the classical relationship:

$$\mathbf{q_{total}} = \mathbf{U}\, 2\pi\, r \Delta x \left(T_{tube} - \mathbf{T_{shell}} \right)$$

REFERENCES

1. Bowman R.A., Muller A.C., Nagle W.M.**, Mean temperature difference in design**, Trans. ASME, 62: 283-294, 1990.

2. Constantin Boris, **Schimbătoare de căldură**, Tehnopress, Iaşi ISBN 973-702-110-X, 2005.

3. Curievici I. , Simionescu A. , Dinulescu H**. Experimental study of a wire heat exchanger**, Preprints of papers presented at the "First Heat Transfer Conference", Iaşi, 1973, vol. II, p.581-593.

4. Eckert E.R.G. **Introduction to heat and mass transfer,** McGraw Hill Book Company, inc., New York, 1963.

5. Fraas A.P**. Heat Exchangers Design**, John Wiley Inc., New York, ediția a-II-a, 1989.

6. Gardner K., Taborek J**., Mean temperature difference**: A reappraisal, AIChE Journal., 23(6):770-786, 1977.

7. Hewitt G.F. **Heat Exchanger Design Handbook**, Begell House, New York, 1998.

8. Hennecke D.K. , Sparrow E.M. **Local heat sink on a convectively cooled surface – application to temperature measurement error.** Int.J.Heat Mass Transfer, 13:287-304, 1970.

9. Incropera F.P. , DeWitt D.P. **Fundamentals of Heat and Mass Transfer**, 4th Edition Wiley, USA, 1996.

10. Larry Wall, Tom Christiansen, Randal Schwartz **Programming Perl**, O'REILLY U.S.A.,1996.

11. Mukherjee R. **Effectively Design Shell and Tube Heat Exchangers**, Chemical Eng. Progress, Febr.1998, pp.112-123.

12. Tinker T**. Shellside Characteristics of Shell-and-tube Heat Exchangers: A Simplified Rating System for Commercial Heat Exchangers**, Trans. ASME, 80, pp.36-52, 1958.

13. Tubular Exchanger Manufacturers Association, "Standards of the Tubular Exchanger Manifacturers Association", 7th ed., TEMA, New York, 1988.

ALGORITM UTILIZAT PENTRU PROIECTAREA UNUI SCHIMBĂTOR DE CĂLDURĂ

Rezumat: Lucrarea de fata face parte dintr-un şir de lucrări in care incercam sa prezentam aspectele matematice de baza care stau la baza proiectarii unui schimbator de caldura cu aripioare, cum ar fi : temperatura medie logaritmica, eficienta, efectivitatea, proiectarea aripioarelor foarte lungi, rezolvarea numerica a ecuatiilor transferului termic cu conditii initiale si la granita. Deasemenea s-a incercat punerea la punct a unui program de calculator construit din citeva subrutine disponibile pe piata, care descriu configura]iile cuprinse in standardul TEMA si subrutine elaborate de noi pentru rezolvarea ecuatiei de transfer termic si dezvoltare in functii Bessel necesare proiectarii aripioarelor.

BULETINUL INSTITUTULUI POLITEHNIC DIN IAŞI
Tomul LIII (LVII), Fasc. 3, 2007
Secția
ŞTIINȚA ŞI INGINERIA MATERIALELOR

MULTITUBE HEAT EXCHANGERS

BY

CONSTANTIN BORIS

Abstract: In order to emphasize the performances of the heat exchanger it has been built for every variant of heat exchanger a classical heat exchanger having the same dimensions as the ones studied, but without wires in the interior of the tubes and they have been submitted to the same experiments as the heat exchangers with wires. Both, for the heat exchangers with wires and for exploratory heat exchangers it has been calculated the heat transmission factor k.

Keywords: multitube heat exchanger, deflector, shell, pitch , thermic efficiency, Reynolds number

The multitube heat exchanger with wires is composed from 19 conducting tubes, through which the air or hot gases circulate and a shell through which it flows the water or the liquid. The heat exchange tube is diametrically circulated by wires with both ends welded to the wall of the tube, disposed in such a way that the contact points between the wires and the wall form an helicoidal line on the surface of the tube. There have been analyzed three variants of heat exchangers.

The first variant of heat exchanger has the wires disposed in the transfer tubes on four directions. In the case of the second variant of heat exchanger with wires, a deflector was introduced in the air circuit, the rest of the heat exchanger remaining the same, as the first variant. In the case of the third variant of heat exchanger the wires form an helicoidal line on the surface of the transfer pipes.(fig. nr.1)

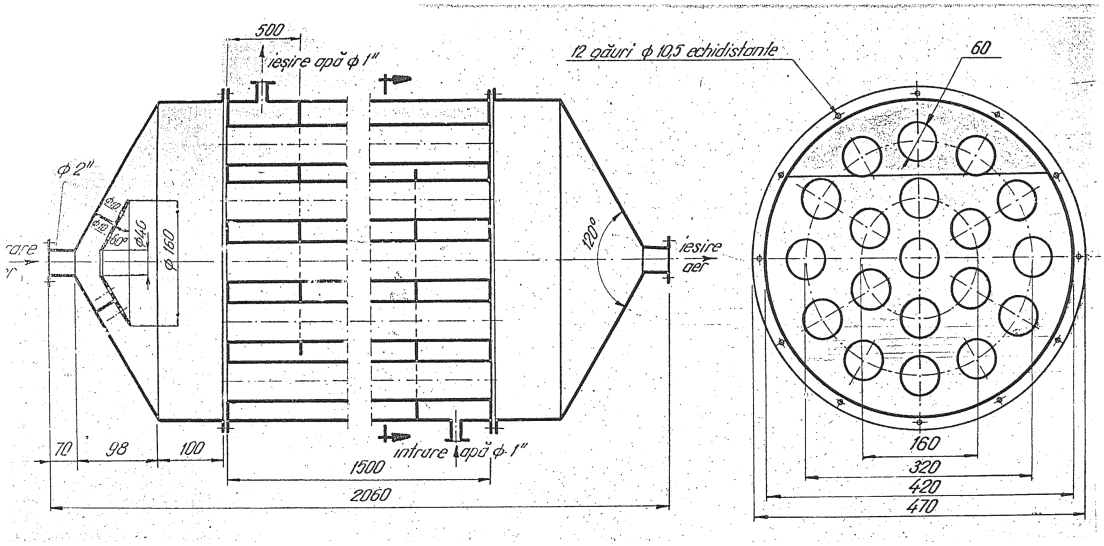

Figure nr.1

The dimensions of the three variants of heat exchangers are:

Transfer pipe		Variant	
	I	II	III
Inside diameter, mm	52	52	52
Outside diameter, mm	60	60	60
Length, mm	1480	1480	1480
Wire's diameter, mm	2	2	2
The length of the wire, mm	52	52	52
Longitudinal pitch of the wires, mm	4,6	4,6	5
Longitudinal pitch of the wire spiral, mm	18,4	18,4	288
Total number of the wires	6113	6113	6650
Total number of pipes	19	19	19
Inside lateral surface of the tubes, mp	4,591	4,591	4,467
Outside lateral surface of the tubes, mp	5,297	5,297	5,154
Lateral surface of the wires, mp	1,996	1,996	2,168
Total surface of heat exchange, mp	6,587	6,587	6,635
Flow section of the air, mp	0,036	0,036	0,036
The diameter of the shell, mm	420	420	420

With the help of the experimental data, there have been determined heat transmission factors and also the pressure drop, in the case of the analyzed heat exchanger, for a Reynolds numbers domain ranging between 2757 and 5661 and the air entry temperature in the heat exchanger between 80 and 180 celsius degrees.

In order to emphasize the performances of the heat exchanger it has been built for every variant of heat exchanger a classical heat exchanger having the same dimensions as the ones studied, but without wires in the interior of the tubes and they have been submitted to the same experiments as the heat exchangers with wires. Both for the heat exchangers with wires and for exploratory heat exchangers it has been calculated the heat transmission factor k, using formula (1).

In the case of many heat transfer tubes, the Reynolds number, for a given debit of air, was calculated using the following formula:

$$\mathrm{Re} = \frac{\mathbf{W} \cdot \mathbf{d}_{\mathbf{ech}}}{\boldsymbol{\upsilon}} \tag{1}$$

where:

d_{ech} = equivalent diameter of the transfer tube, m;

W = air velocity, in m/s;

υ = coefficient of kinematic viscosity, in m^2/s.

The equivalent diameter was calculated with the relation:

$$\mathbf{d}_{\mathbf{ech}} = \frac{3{,}14 \frac{\mathbf{d}^2}{4} - \mathbf{a} \cdot \mathbf{b}}{3{,}14 \cdot \mathbf{d} + \mathbf{d} \cdot \mathbf{a}} \ (\mathrm{m}) \tag{2}$$

in which:

d - transfer tube diameter, in m;

a - the length of the wire, in m;

b - the diameter of the wire, in m.

The velocity of the air was determined with the formula:

$$\mathbf{W} = \frac{\mathbf{D}_{air}}{3600\,\mathbf{n}\cdot\mathbf{S}_i\cdot\rho_{med}} \quad (m/s) \qquad (3)$$

in which:

S_i - the section of the transfer tube, in mp;

n - the number of pipes;

ρ_{med} - density of the air, in kg/m^3, at mean temperature.

In the figure nr.2 there are presented the values of the heat transfer coefficient according to the Reynolds number, obtained for the heat exchanger with fins who was developed.

On the same graph, there have been presented, in order to be compared, the data obtained from the trial heat exchanger. It can be noticed the accentuated growth of the heat transfer coefficient in the case of heat exchanger with fins, especially in the superior part of the Reynolds investigate domain.

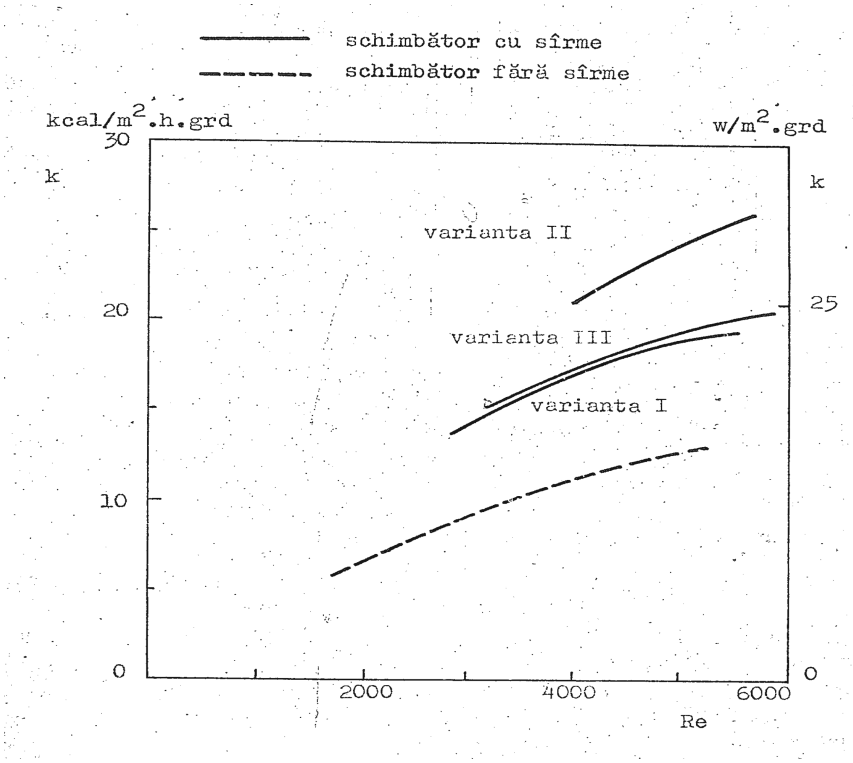

Figure nr.2

In the case of the first variant of heat exchanger it was noticed a growth of the heat transfer coefficient with about 70% in comparison with the the heat transfer coefficients obtained in the case of the classical heat exchanger.

This growth of the heat transfer coefficients cannot be explained by an extension/expansion with 30% of the heat exchange surface, due to the presence of the fins and so, it is confirmed the idea that the intensification of the heat transfer in the case of the heat exchanger, is determined by the modification of the growth of the turbulences of the gas stream/flow of gas.

The second variant of the heat exchanger has the same wires disposal as the first one, but it posses a deflector which distributes uniformly the air supply for the 19 pipes. For this variant the heat exchange coefficient are doubles in comparison to the classical one.

In the case of the third heat exchanger the wire disposal is according to an helicoidal line on the surface of the transfer tubes, and the uniform distribution of the air supply it is effectuated also by a deflector.

The heat transfer coefficient is bigger than the one for the first variant , but smaller than for the second variant.

The data of the analyzed heat exchanger have been introduced in the BRC 001 program, results being compatible with the ones obtained experimentally. The heat transfer coefficients are smaller, due to the fact that the programme introduces rezistences determined by the deposits (the real case).

In the figure nr.3 it is presented the pressure drop for the three variants of heat exchanger , according to the Reynolds number. The greatest pressure decline, can be seen in the case of the first variant, followed by the second variant of heat exchanger. The third variant of heat exchanger has the advantage that it has the same pressure drop on the air circuit as a classical heat exchanger.

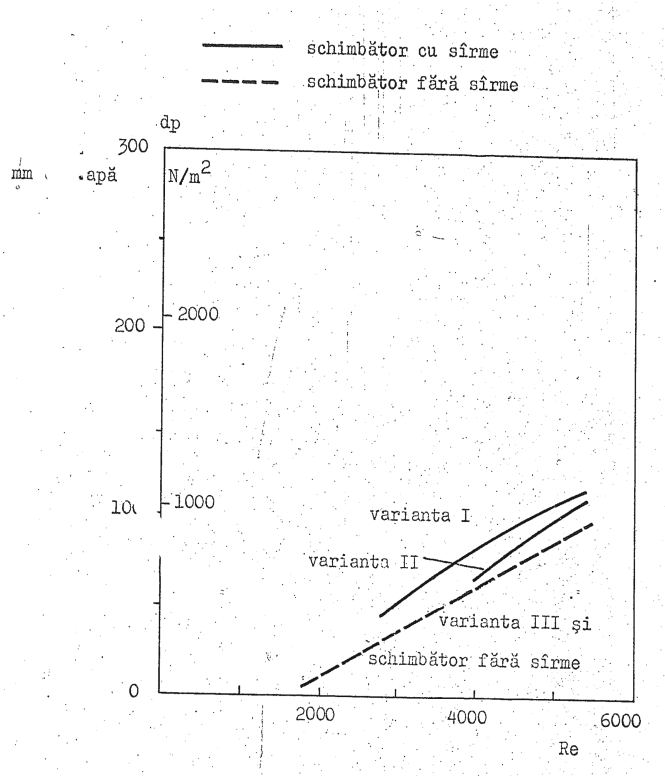

Figure nr.3

Calculating thermic efficiency and the number of transfer units for the same pumping energy (seen as the product between the pressure decline and the debit) it can be noticed that the heat exchanger with wires has got superior values to the heat exchanger without wires. Concerning the heat exchangers with wires, the second variant has got the greatest thermic efficiency, followed by the third variant and the first variant.

	Var.1	Var.2	Var.3	Whithout wires
air output debit, m^3/h	247,4	245,53	251,86	276,6
entry temperature, Celsius degrees	100	100	100	100
pressure drop, dp, mm col water	95	90	90	80
heat transfer coefficient k, kcal/m^2h grd	18,8	23,6	19,5	12,7
Reynolds number	4916	5073	5233	5193
debit x, dp	23503	22097	22667	22133
thermic efficiency	0,81	0,87	0,84	0,65
number of transfer units	1,74	2,13	2,11	0,86

These data confirm the idea that the intensification of the heat transfer is obtained especially due to the modification of the thermical field, in the sense of the growth of the temperature gradients in all the sections.

REFERENCES

1. Bowman R.A., Muller A.C., Nagle W.M.**, Mean temperature difference in design**, Trans. ASME, 62: 283-294, 1990.
2. Constantin Boris, **Schimbătoare de căldură**, Tehnopress, Iaşi ISBN 973-702-110-X, 2005.
3. Curievici I. , Simionescu A. , Dinulescu H**. Experimental study of a wire heat exchanger**, Preprints of papers presented at the "First Heat Transfer Conference", Iaşi, 1973, vol. II, p.581-593.
4. Eckert E.R.G. **Introduction to heat and mass transfer,** McGraw Hill Book Company, inc., New York, 1963.
5. Fraas A.P**. Heat Exchangers Design**, John Wiley Inc., New York, ediția a-II-a, 1989.
6. Gardner K., Taborek J**., Mean temperature difference**: A reappraisal, AIChE Journal., 23(6):770-786, 1977.
7. Hewitt G.F. **Heat Exchanger Design Handbook**, Begell House, New York, 1998.
8. Hennecke D.K. , Sparrow E.M. **Local heat sink on a convectively cooled surface – application to temperature measurement error.** Int.J.Heat Mass Transfer, 13:287-304, 1970.
9. Incropera F.P. , DeWitt D.P. **Fundamentals of Heat and Mass Transfer**, 4th Edition Wiley, USA, 1996.
10. Larry Wall, Tom Christiansen, Randal Schwartz **Programming Perl**, O'REILLY U.S.A.,1996.
11. Mukherjee R. **Effectively Design Shell and Tube Heat Exchangers**, Chemical Eng. Progress, Febr.1998, pp.112-123.
12. Tinker T**. Shellside Characteristics of Shell-and-tube Heat Exchangers: A Simplified Rating System for Commercial Heat Exchangers**, Trans. ASME, 80, pp.36-52, 1958.
13. Tubular Exchanger Manufacturers Association, "Standards of the Tubular Exchanger Manifacturers Association", 7th ed., TEMA, New York, 1988.

Received April 2007 Technical University Iasi

SCHIMBĂTOARE DE CĂLDURĂ MULTITUBULARE

Rezumat: Pentru a se putea pune in evidenta performantele schimbatoarelor de caldura cu sarme, s-a construit pentru fiecare varianta de schimbator de caldura cate un schimbator de tip clasic avand aceleasi

dimensiuni ca cel studiat, însa fara sarme in interiorul tevilor si au fost supuse acelorasi experimentari ca si schimbatoarele de caldura cu sarme. Atat pentru schimbatoarele cu sarme cat si pentru cele de proba s-au calculat coeficientii de transmisie a caldurii k, pentru comparatie.

BULETINUL INSTITUTULUI POLITEHNIC DIN IAŞI
Tomul LIII (LVII), Fasc. 3, 2007
Secția
ŞTIINȚA ŞI INGINERIA MATERIALELOR

HEATING BEHAVIOUR STUDY *IN VITRO* OF MAGNETIC PARTICLES USED IN HYPERTHERMIA WITH MAGNETIC FLUIDS FOR TREATMENT OF CANCER

BY

GIGEL NEDELCU

Abstract: Magnetic microparticles and nanoparticles have a large variety of applications in biomedicine such as hyperthermic treatment of tumors, magnetically targeted drug delivery by magnetic carriers. Also, non-targeted magnetic microparticles and nanoparticles biomedical are available for use as contrast agents (MRI) and as drug reservoirs that can be activated by a magnet applied outside the body. In this work, the heating influence of two magnetic colloids for applications in hyperthermia treatment of tumors is discussed. One colloid with magnetite in poly(ethylene glycol) and sodium dodecylsulphate, and another one with magnetite in mono(ethylene glycol) were heated inside an induction coil with a power of P = 0.5 kW and P = 0.4 kW, respectively. Frequence used was ν = 315 kHz. The temperature of the two colloids.was measured with a thermometer as time function.

Keywords: Magnetic particle, Magnetic suspension, Heating, Hyperthermia.

1. INTRODUCTION

In the last years nanomaterials are frequently used in biomedical applications. In this study we will focus on the magnetic particles, rather on application in hyperthermia with magnetic particles knowed as the *magnetic hyperthermia*. In the first place, these particles can be manipulate using a external magnetic field. They can generate heat in this AC magnetic field and can be used as the agents for malignant cell destruction and implicit the tissue from do they belongs.

Although it is possible to determine the manner in which behave magnetic particles finded out in suspension in vitro under the act of an external AC magnetic field [1], it is not clear yet their behaviour in physiological systems because they are submissive influences of physiological supplementary factors such as *the haematic flow*, *reticuloendothelial system* and high dynamic *tissue microenvironment* where can operate cellular receptors and cellular absorbtion.

Physical factors which must control are *heat generation* [2] and *temperature distribution*. A special importance must give to relations among the heat response at nanoscale level and the heat disengagement at macroscopic level. It is very important to understand the heating mechanism at microscopic level to prevent the heating and destruction of adjacently healthy cells.

In this work, are studied the heating processes of magnetic particles in biocompatible environments, aquous suspensions of a biocompatible polymers.

2. EXPERIMENTAL PROCEDURE

2.1. Magnetic colloid (ferrofluid)

Colloid I (Magnetite in PEG + SDS): used materials are $FeSO_4$ 2M in HCl 2M (x), $FeCl_3$ 1M in HCl 2M (y), 1.0M NH_3 in water as a precipitation agent, polyethylene glycol (PEG) 25% and sodium dodecyl sulphate (SDS) as an anionic surfactant.

Preparation method: in a 100 ml vessel were added x and y solutions, they were titrate under magnetic stirring with 40 ml NH_3 until mixture arrive to a black precipitate (magnetite). Then magnetic precipitate is separated, is washing with water until pH = 5.5 (neuter). 2 ml PEG 25% is added to precipitate and after that mixture is immersed in SDS.

Colloid II (Magnetite + MEG): $FeSO_4$ 2M in HCl 2M, $FeCl_3$ 1M in HCl 2M, 1.0M NH_3 and monoethylene glycol (MEG). It is used same method as to the colloid I with the difference that after washing the precipitate is immersed in 30 ml MEG.

2.2. Description of experimental instalation

Figure 1 describes the sketch of experimental device [1]. The colloid is entered into the eprubete which is in a magnetic field created by an inductor of 70 mm diameter, to a frequency of 315 KHz. He utilize a power of 0.5 KW for the colloid I and 0.4 KW for the colloid II. The probes temperature was measured with an alcohol thermometer in order to don't influence the heating degree of particles. All heating studies of particles were repeated three times for each probe.

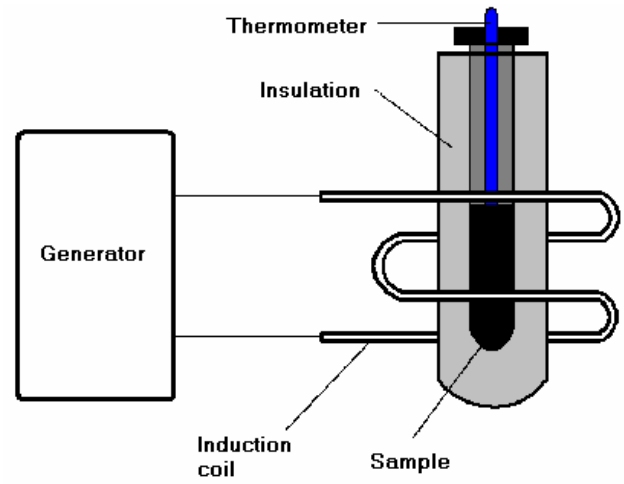

Figure 1. The sketch of experimental device. The sample was fixed in an field created by an induction coil conected to a AC power source. Temperature was measured with an alcohol thermometer through direct reading.

3. RESULTS AND DISCUTIONS

In this work was studied the heating behaviour in vitro of two magnetic colloids. Figure 2 and 3 presents the temperature variations depending on time of the colloids concentrations. In both colloids, the magnetic particles are in homogeneous suspension. The temperature period whereat the samples were analysed was 36°C (minimum temperature of human organism) and 46°C (maximum temperature of the

tumoral cells necrosis). This period was preferred to contain all the transformation that suffers the ferrofluid in organism under the action of the AC magnetic field.

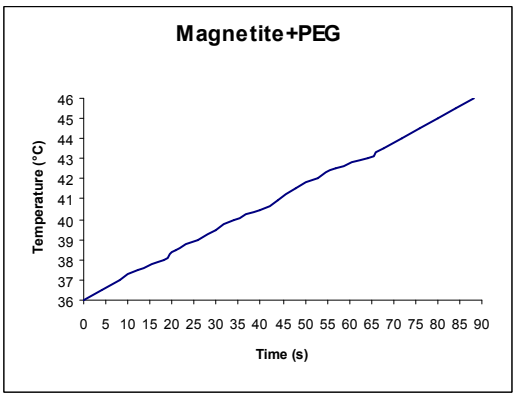

Figure 2. Temperature evolution (°C) depending on time (s) in colloid I.

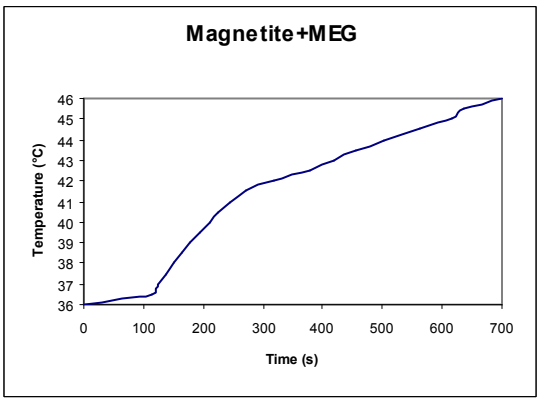

Figure 3. Temperature evolution (°C) depending on time (s) in colloid II.

For each sample were used 2 ml from each colloid.

The first colloid (figure 2) has a heating behaviour depending on time almost linear at a power P = 0.5 kW, the temperature having a quick growth in 36°C - 46°C interval for 90s. This quick breeding is explained through the fact that the brownian agitation of the particles into the colloid it is accelerated by the presences of surfactant SDS (sodium dodecyl sulphate) at the surfaces of magnetite particles.

The second colloid has a heating behaviour much slower at a power P = 0.4 kW. The abrupt variations occurs after nearly 100 s from the begining of experiment at 36.5°C (temperature which corresponds with normal temperature of human body) and after 300 s from the begining of experiment at 42°C (temperature which coincides with necrosis temperature of tumoral cells).

The heating time it is longer because the surfactant is missing from the surface of the magnetite particles and by reason of fact that used power has a lower value.

The heating behaviour of magnetite particles depends on frequency, application time but particles sizes and suspension medium, too.

In the case of colloid I, the endurance developed by viscosity against brownian relaxation it is smaller by reason of the presence of surfactant, whiles at colloid II, because of lake of surfactant, the suspension medium is much viscous whence results that the phenomenon of brownian relaxation is make heavier, therefore the heating time will be much longer [3-6].

The phenomenon of brownian relaxation which generates the heat is characterize by the brownian constant of time:

$$\tau_B = {3\eta V_B}/{k_B T}$$

where V_B is the hydrodynamic volume, that is the total volume of a particle coated with surfactant and/or polymer, η - viscosity of the suspension medium, $k_B T$ - thermal energy.

The particles heating occurs by Néel mecanism, too [3-6]. This phenomenon is explained through the motion of magnetic moments inside the particle in the magnetic field of the coil. This mechanism is characterized by the Néel time constant:

$$\tau_N = \tau_0 \exp\left(\Delta E \big/ k_B T\right)$$

where $\Delta E = KV$ - activation energy, $\tau_0 = 10^{-9} s$.

4. CONCLUSIONS

In this work were studied the heating beaviour *in vitro* of two types of magnetic colloids for their utilization *in vivo*. I tis observed that the particles beaviour through induction strongly depends on quantity of magnetic colloid, size of the particles, but mostly depends on content of suspension medium (viscosity, thermal conductivity).

There is some problems that must be put on record. Because the particles are polydispersed in te ferrofluid, the power generated is not uniform for all the particles depends on their sizes. Another problem is temperature measured at macroscopic level that is not the same with temperature measured at nano level. Therefore must developed models to correlate the two temperatures for feature utilization of particles in suspension mediums *in vitro*, as *in vivo* in organic environments as they are the sanguin tissue another types of tissues, chiefly one tumoral.

REFERENCES

1. Venkatasubramaniam S. Kalambur, Bumsoo Han, Bruce E. Hammer, Thomas W. Shield and John C. Bischof, **Nanotechnology, 16,** 2005, 1221
2. Andra W., **Magnetism in Medicine,** 1998, (Berlin: Wiley–VCH)
3. Rosensweig R. E., **J. Magn. Magn. Mater**., **252,** 2002, **370**
4. Jordan A., Wust P., Fahling H., John W., Hinz A. and Felix R., **Int. J. Hyperth., 9,** 1993, **51**
5. Hergt R., Andra W., d'Ambly C. G., Hilger I., Kaiser W., Richter U. and Schmidt H., **IEEE Trans. Magn., 34,** 1998, **3745**
6. Fannin P. C. and Charles S. W., **J. Phys. D: Appl. Phys., 22,** 1989, **87**

Received Mar. 31nd , 2007 *"Al.I.Cuza" University, Faculty of Physics,Iaşi*

STUDIUL COMPORTAMENTULUI LA ÎNCĂLZIRE *IN VITRO* A PARTICULELOR MAGNETICE UTILIZATE ÎN HIPERTERMIA CU FLUIDE MAGNETICE PENTRU TRATAMENTUL TUMORAL

Rezumat: Particulele magnetice au o mare varietate de aplicaţii în biomedicină cum sunt: tratamentul prin hipertermie al tumorilor maligne, purtători magnetici ai medicamentelor cu eliberare controlată, separarea magnetică a biomoleculelor şi ca agenţi de contrast în rezonanţa magnetică. Lucrarea de faţă se vrea a fi prima dintr-un set de lucrări despre tratamentul prin hipertermie al tumorilor maligne. În acest sens ne vom ocupa în această primă lucrare de hipertermia cu fluide magnetice în tratamentul cancerului. Pentru aceasta se vor analiza comportarile la încălzire a două tipuri de coloizi magnetici: primul tip de coloid ce conţine magnetită în polietilenglicol şi dodecil sulfat de sodiu, iar al doilea tip de coloid ce conţine magnetită în monoetilenglicol, ca precursori pentru magnetită s-au utilizat două săruri: $FeSO_4$ şi $FeCl_3$ care au fost precipitate cu NH_3. Coloizii magnetici vor fi introduşi fiecare într-o eprubetă şi testaţi la încălzire în interiorul unei bobine de inducţie la o putere P = 0.5 kW pentru primul coloid şi P = 0.4 kW pentru al doilea coloid. Cu ajutorul unui termometru cu alcool se vor măsura variaţiile de temperatură în funcţie de timp ale celor doi coloizi magnetici.

BULETINUL INSTITUTULUI POLITEHNIC DIN IAŞI
Tomul LIII (LVII), Fasc. 3, 2007
Secția
ŞTIINȚA ŞI INGINERIA MATERIALELOR

INTERCALATION OF PHARMACOLOGICAL AGENTS INTO LAYERED DOUBLE HYDROXIDES BY COPRECIPITATION METHOD

BY

MIHAELA FRUNZA[1], I.M.POPA[1] and V. MELNIG[2]

ABSTRACT. Some pharmacological agents (Chloramphenicol – Ch, Salicylic acid – SAL and Nicotinic acid – NIC) were intercalated into layered double hydroxides (LDH) lamella used as an inorganic host for the coprecipitation method. The intercalation compounds were examined by X-ray diffraction (XRD), FTIR spectroscopy, differential thermal analysis and thermo gravimetric analysis. The XRD patterns of the samples with the diffraction peaks are typical to those of well crystallized solids with the layered double hydroxides structure. The FTIR spectroscopy and thermogravimetric (DTG) analysis point out the presence of the organic compound in the network structure of the synthesized LDHs.

KEYWORDS: Layered double hydroxides, drugs, intercalation, coprecipitation method

1.INTRODUCTION

The class of materials known as layered double hydroxides (LDHs) or hydrotalcite-like materials have the general formula: $\left[M^{2+}_{1-x}M^{3+}_{x}(OH)_2\right]^{x+}A^{m-}_{x/m}\cdot zH_2O$, where M^{2+}= Mg, Zn, Ca, Co, Fe, Ni, Cu, etc., M^{3+}= Al, Fe, Cr, Ga, etc., A^{m-}= Cl^-, CO_3^{2-}, NO_3^-, etc., m is the formal charge of anion and x is the stoichiometric coefficient that can be widely varied. As it can be seen from the formula, the formal positive charge of the layer depends on the M^{2+}/M^{3+} ratio. These materials have many applications as catalysts, optical and electrical functional materials. LDHs- based controlled release systems have also been studied [1-6]. In this work we have investigated the intercalation behavior of chloramphenicol (Ch), salicylic acid (SAL), and nicotinic acid (NIC) into ZnAl-LDHs by coprecipitation method. Chloramphenicol is a synthetic antibiotic with a large spectrum containing both gram positive and gram negative germs. A great disadvantage of this antibiotic is represented by its high toxicity. The main toxic effect of Ch is its attack on the bone marrow, which can take two forms.

Salicylic acid is used in rheumatism treatment, but its adverse secondary effects, such a gastric and duodenal ulcer formation are quite common. The effect of LDHs in preventing taurcholate induced gastric injury in rat was demonstrated in the literature [7].

The incorporation of the pharmacological agents in the structure of layered double hydroxides (LDHs) can offer premises for controlling the release of the pharmacological agents from the layered structure and reducing the toxicity.

2. EXPERIMENTAL

2.1. General procedures

All chemicals were commercially purchased and used without further purification. X-ray powder diffraction (XRD) patterns were recorded on a Bruker AXS D8 diffractometer using monochromatic CuK α radiation (λ =0.154 nm), operating at 40 kV and 50 mA over a 2θ range from 4 to 70 degree. Thermal analyses (TG and DTG) were carried out in air on a Netzsch TG 209C thermal analyzer, from 298 to 1123 K, at a heating rate of 5 K /min. FTIR spectra were recorded on a FT-IR BOMEM MB 104 spectrometer under the following experimental conditions: 200 scans in the mid-IR range (400-4000 cm^{-1}) using KBr (ratio 5 / 95 wt %) pellets, and a resolution of 4.0 cm^{-1}.

2.2 Preparation of the samples

2.2.1. Preparation of reference *MgAlLDH*

100 ml of an aqueous solution of $Mg(NO_3)_2 \cdot 6H_2O$ (0.2mol) / $Al(NO_3)_3 \cdot 9H_2O$ (0.1mol) and an aqueous solution of NaOH / Na_2CO_3, were added drop wise together, in such a way that the pH remained at a constant value of 9.5. The resulting white precipitate was treated at 338 K for 24 h under continuous stirring. After the treatment, the obtained precipitates were separated by centrifugation, washed extensively with warm deionized water until it becomes sodium free and dried under vacuum at 40°C.

2.2.2. Preparation of reference *ZnAlLDH*

100 ml of an aqueous solution of $Zn(NO_3)_2 \cdot 6H_2O$ (0.2mol)/$Al(NO_3)_3 \cdot 9H_2O$ (0.1mol) and an aqueous solution of NaOH 1M, were mixed together by drop wise addition. During the whole process the flow was controlled in such way that the pH was kept at a constant value of 8.0. The resulting white precipitate was treated at 40°C for 24 h under continuous stirring. After the treatment, the precipitate was separated by centrifugation, washed extensively with warm deionized water until it becomes sodium free and dried under vacuum at 45°C.

2.2.3. Preparation of Ch-LDH nanocomposite (*MgAlLDH_Ch)*: by coprecipitation method was performed by using diluted solutions of of $Mg(NO_3)_2 \cdot 6H_2O$ (0.2mol) / $Al(NO_3)_3 \cdot 9H_2O$ (0.1mol), an aqueous solution of NaOH / Na_2CO_3 and Ch at a constant pH value of 9.5.

2.2.4. Preparation of SAL-LDH nanocomposite (*ZnAILDH_SAL):* by the coprecipitation method was done by using low diluted solutions of of $Zn(NO_3)_2 \cdot 6H_2O$ (0.2mol) / $Al(NO_3)_3 \cdot 9H_2O$ (0.1mol), an aqueous solution of NaOH and salicylic acid at a constant pH value equal to 7.5.

2.2.5 Preparation of NIC-LDH nanocomposite (*ZnAILDH_NIC):* by the coprecipitation method was done by using low diluted solutions of of $Zn(NO_3)_2 \cdot 6H_2O$ (0.2mol) / $Al(NO_3)_3 \cdot 9H_2O$ (0.1mol), an aqueous solution of NaOH and nicotinic acid at a constant pH value equal to 7.5.

3. RESULTS AND DISCUSSIONS

3.1. Powder X-ray diffraction (XRD)

The XRD patterns of the samples are shown in Figures 1 and 2; for both samples the diffraction peaks are typical to those of well crystallized solids with the layered double hydroxides structure. The powder XRD patterns of the precursor NO_3^- ZnAlLDH and the sample produced by reaction of SAL with LDH are shown in Fig. 1. The ZnAl-LDH precursor has an XRD pattern similar to those previously reported [8], with a basal spacing (d_{003}) of 8.7 Å (Fig. la). After reaction with SAL, the powder XRD pattern of the product maintains the characteristic features of ZnAl-LDH (Fig.1b). The XRD patterns for ZnAILDH_NIC are shown in Fig. 1c with a basal spacing of 15.23 Å. The expansion of basal spacing from ZnAlLDH to ZnAILDH_NIC is due to the inclusion of NIC into the LDH lamella. The intensity of reflections was strong indicating that the precursor and product samples obtained had good crystallinity.

The broadness of the basal spacing of the first peak is increased for Ch containing sample (Fig. 2b) indicating the enlargement of the interlayer space (IFS) when Ch was introduced in the synthesis medium.

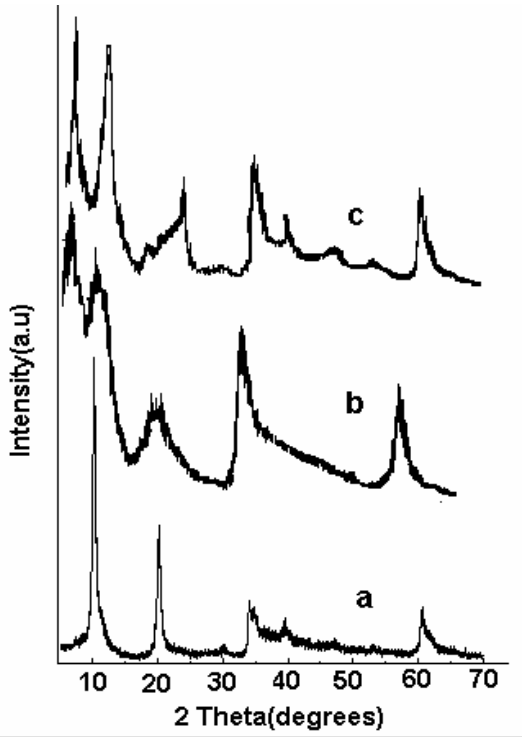

Figure 1 - XRD spectra (a) ZnAlLDH, (b) ZnAILDH_SAL, (c)ZnAlLDH_NIC

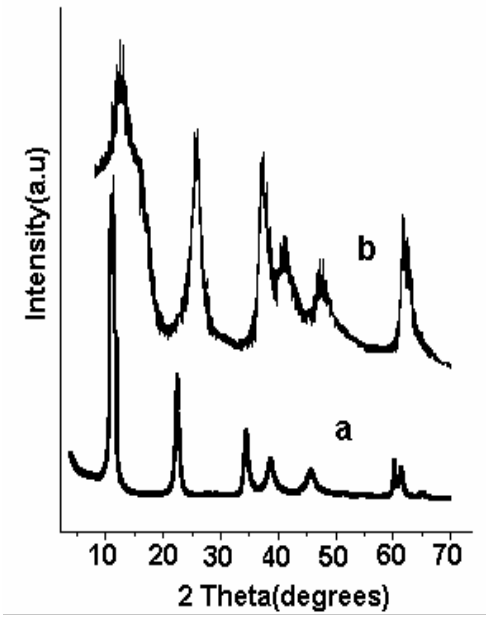

Figure 2 - XRD spectra (a) MgAlLDH, (b) MgAILDH_Ch

3.2. FTIR spectroscopy

The insertion of pharmacological agents in the lamella of MgAlLDH and ZnAlLDH is also confirmed by FTIR spectroscopy (Fig 3). All the vibration bands of the organic anion are observed together with the absorption bands of MgAlLDH and ZnAl LDH. The absorption band at around 3431cm^{-1} is attributed to the OH stretching due to the presence of hydroxyl group of LDH and/or physically adsorbed water molecule. The appearance of a strong band at 1381 cm^{-1} can be assigned to the $\square_3$ nitrate group, the counter anion in the ZnAl LDH. The band at 1626 cm^{-1} is due to $\square$(H-O-H) band vibration. The FTIR spectrum of the MgAlLDH and ZnAlLDH are shown in Fig 3a, 3b. The spectrum recorded after incorporation of the SAL is presented in Fig.3c. Due to the ionization of the acid group, the band previously detected for free SAL at 1651 cm^{-1} disappears, while a new band is recorded at 1570 cm^{-1}. The appearance of this band is caused by the $\square_{as}(COO^-)$ mode. Another band recorded at 1364 cm^{-1} is due to the symmetric vibration. $\square_s(COO^-)$. The band originated from the $\square(CH_3)$ mode is recorded at 1386 cm^{-1}. The band assigned to the nitrate group (1381 cm^{-1}) had lower intensity after the ion-exchange reaction; supporting the assumption that NO_3^- anion was replaced by SAL. The other bands are recorded in positions very close to those previously shown for free SAL. In addition, bands due to Zn/Al- OH translational modes are recorded.

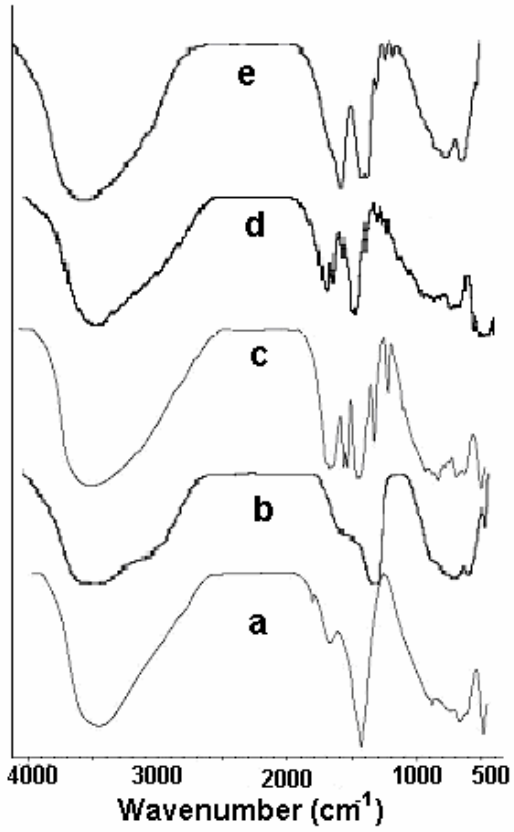

Figure 3 - FTIR spectra (a) ZnAlLDH, (b)MgAlLDH, (c)ZnAILDH_SAL, (d)ZnAlLDH_NIC, (e)MgAlLDH_Ch

Fig. 3d is the spectra of ZnAILDH_NIC. The FTIR spectrum contains both the characteristic peaks of pure NIC and typical peak of LDH. This indicates that both functional groups of NIC and ZnAl are present in ZnAILDH_NIC. In addition, the H-O-H bending vibration ($\nu_{H\text{-}O\text{-}Hbent}$) and O-H symmetric stretching vibration ($\nu_{H\text{-}O\text{-}Hsym}$) in these nanohybrid composites appear in the range 1603-1614 and 3400-3431 cm^{-1}, respectively. The carboxylate anion gave rise to two bands, a strong asymmetrical band near 1600 cm^{-1} and a weaker asymmetrical stretching band near 1400 cm^{-1}. The presence of strong, sharp band at about 1560 cm^{-1} in the FTIR spectrum of ZnAILDH_NIC is due to the formation of carboxylate anions. This indicated the intercalation of anionic organic moiety into lamella of the inorganic LDH.

For Ch containing samples(Fig. 3e) the characteristic peaks of aliphatic C-H stretch can be also identified at 2858 and 2927 cm^{-1} though the broad adsorption band of the hydroxyl stretching mode partially overlap the ν_{CH3} vibrations.

3.3. Thermal stability

The DTG curves of the LDHs and pharmacological agents - LDHs are depicted in Fig. 4.The steps up to 200^{o}C are due to the removal of the interlayer water molecules. They are quite strongly attached to the hydroxide layer and/or interlayer anion via hydrogen bonds and the interlayer balancing anion NO_3^-. The observed mass loss in the higher temperature range from 220 to 450^{o}C is attributed to the dehydroxylation of the ZnAl LDH basal layer.

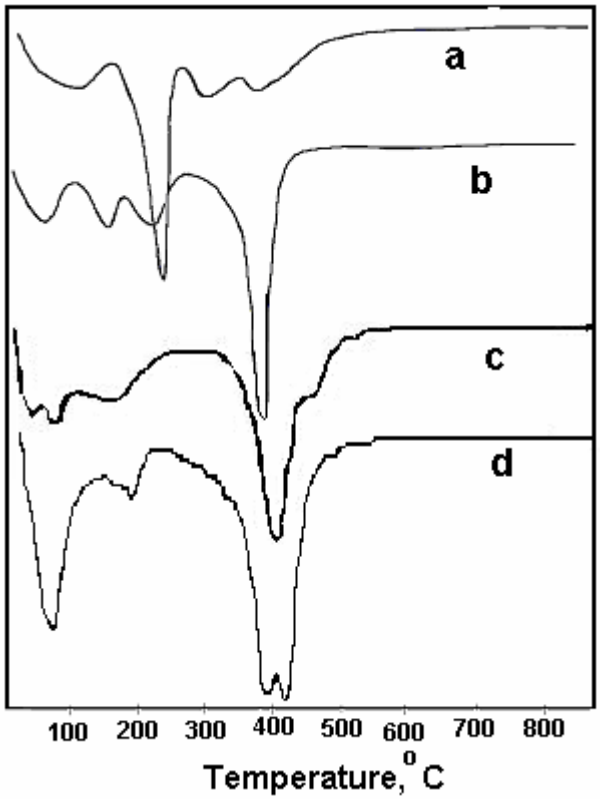

Figure 4 - DTG analysis (a) ZnAlLDH, (b) ZnAILDH_SAL, (c) ZnAlLDH_NIC, (d)MgAlLDH_Ch

The presence of microspores is confirmed on DTG plots. Indeed the desorption of the adsorbed water molecules from the intercalates appears as two separate events (as a two step process) for ZnAlLDH_SAL. ZnAlLDH_NIC and MgAlLDH_Ch (Fig.4b, c and d,) and as a continuous step for ZnAl-LDH.

4. CONCLUSIONS

The XRD patterns of the samples with the diffraction peaks are typical to those of well crystallized solids with the layered double hydroxides structure. The intercalation of the Ch, SAL and NIC in the lamella of LDHs is confirmed by FTIR spectroscopy. All the vibration bands of the anion drug are observed together with the absorption bands of LDHs.

Received, March, 2007

[1]Faculty of Chemistry, "Gh. Asachi" University, D. Mangeron, Nr. 71 A, 700050, Iasi, Romania
[2]Faculty of Physics, "Al. I. Cuza" University, Carol I, Nr. 11A, 700506, Iasi, Romania

REFERENCES

1. Wang Z., Wang E., Gao L. and Xu L., J. *Solid State Chem*. **178**, 736-741,2005
2. Li B., He J.,. Evans D. G and. Duan X, *Appl. Clay Sci*., **27**, 3-4, 199-207, 2004
3. Del Arco M., Cebadera E., Gutirrez S., Martin C., Montero M. J., Rives V., Rocha J. and Sevilla M. A., *J. Pharm. Sci*., **93**, 6, 1649-1658, 2004
4. Ambrogi V., Fardella G., Grandolini G. and Perioli L., *Int. J. Phar*. **220**, 23-32, 2001
5. Khan A. I., Lei L., Norquist A. J. and O'Hare D., *Chem. Commun*. 2342-2343, 2001
6. Frunza M., Carja G., Popa M. I., *Scientific Study & Research*, **VI** (2), 173-180, 2005
7. Yu B. P., Sun J., Li M. Q,. Luo H. S and. Yu J. P, *World J. Gastroenterol*. **9**(7), 1427-1430, 2003
8. . Xu Z. P and Zeng H. C., J. Phys. Chem. B, **105**, 1743-1749, 2001.

INTERCALAREA AGENTILOR FARMACOLOGICI IN HYDROXIZI DUBLI LAMELARI PRIN METODA COPRECIPITARII

REZUMAT: O serie de agenți farmacologici (Chloramphenicol – Ch, Salicylic acid – SAL and Nicotinic acid – NIC) au fost intercalați intre straturile hidroxizilor dubli lamelari folosiți ca gazda anorganica prin metoda coprecipitarii. Compuşii intercalați au fost examinați prin difracția cu raze X (DRX), spectroscopia FTIR si analiza termogravimetrica. Analiza DRX confirma că după fiecare sinteza s-au obținut picuri de difracție specifice solidelor bine cristalizate cu structura hidroxizilor dubli lamelari. Analiza prin spectroscopie FTIR cat si analiza TG-DTG arata prezenta compusului organic in matricea structurii LDHs sintetizate.

BULETINUL INSTITUTULUI POLITEHNIC DIN IAŞI
Tomul LIII (LVII), Fasc. 3, 2007
Secţia
ŞTIINŢA ŞI INGINERIA MATERIALELOR

DES RECHERCHES CONCERNANT L'INFLUENCE DE LA ROTATION DE LA COQUILLE SUR LA MICROSTRUCTURE DES PIÈCES COULÉES PAR CENTRIFUGATION EN BRONZE Cu-Pb-Sn

BY

FLORIN DIACONESCU

Résumé: Les conditions de solidification dans le champ centrifuge sont différentes que celles de la gravitation et elles contribuent à la formation d'une microstructure plus fine. Dans l'ouvrage on étudie les modifications microstructurales produites par les différentes rotations de la coquille, en tenant compte de leur effet sur le nombre des germes de cristallisation et sur l'échange de chaleur par convection. Dans les zones moyennes et intérieures des pièces couéles par centrifugation, la microstructure est plus fine avec la croissance de la rotation.

Mots clef: rotation, coquille, germe de cristallisation, modifications microstructurales

1. Introduction

La coulée centrifuge permet l'obtention des pièces coulées compactes, sans soufflures et inclusions nonmétalliques, mais leur séparation vers la surépaiseur intérieure d'usinage dépend de la force centrifuge, c'est-à-dire de la densité des inclusions ρ_i, de la vitesse angulaire ω et du rayon de giration r [2]. On resulte que la rotation de la coquille est un important paramètre de coulée centrifuge qui peut produire non seulement la séparation des inclusions nonmétalliques et gazeuses, mais la croissance du nombre des germes de cristallisation et le finissage de la microstructure. Voilà pourquoi nous sommes intéressés a déterminer la rotation optimale pour obtenir une fine microstructure, en évitant dans le même temps la tendance de ségrégation du plomb vers l'extérieur des pièces coulées par centrifugation en bronze CuPb10Sn10.

2. La méthodologie de la recherche

Pour étudier l'influence de la rotation de la coquille sur la microstructure des pièces coulées par centrifugation en bronze CuPb10Sn10, ont coulé des manchons avec les dimensions Ø120/ Ø30/120 mm sur une machine centrifuge avec axe verticale de rotation et rotation variable, en employant rotations de 700 rot/min, 800 rot/min, 880 rot/min et 900 rot/min. La gamme restrainte de rotations a été imposée d'un part de la réalisation de la géométrie intérieure des pièces et d'autre part de la limitation de ségrégation du Pb, qui apparaît à rotations plus grands que 1000 rot/min. La température de la coquille et d'alliage coulé ont été maintenues constantes à valeurs

de 160°C, respectivement 1180°C afin d'éliminer l'influence de ces paramètres sur la microstructure [1].

En pièces coulées par centrifugation ont prélevé des échantillons en trois places différentes en sectionnant longitudinalement les pièces et puis ont coupé les échantillons à 1/3 et 2/3 de l'hauteur en résultant les zones : supérieure (I), moyenne (II) et inférieure (III). Ont été étudiées les sections I-II et II-III pour éviter l'influence du couvercle et de la partie inférieure de la coquille sur la microstructure. Pour l'étude microscopique on employé une installation d'analyse de l'image, assistée par ordinateur, à l'Université Polytechnique de Bucarest.

3. Discussions

Dans les zones extérieures les microstructures ont présenté des dendrites de solution solide α, sur un fond obscur d'eutectoïd ($\alpha + \delta$). Plus a crû la rotation de la coquille, plus ont baissé les dimensions des dendrites de solution solide α, à la suite de la croissance du nombre des germes de cristallisation. L'explication consiste dans la croissance de l'intensité de l'échange de chaleur par convection et surtout par la vitesse de refroidissement plus grande à la surface alliage liquid-moule métallique [2]. Cependant, dans les zones extérieures-inférieures (III e) la microstructure a été plus grossière, parce-que les conditions de refroidissement ont été différentes vis-à-vis d'autres zones, c'est-à-dire les premières quantités coulées de métal s'ont refroidi, puis ils ont ateint la partie supérieure, pendant qu'à la partie inférieure les dernières quantités d'alliage liquid sont en contact avec la coquille chauffée et se solidifient lentement.

À la rotation de 800 rot/min dans les zones extérieure-supérieure (I e) et extérieure-inférieure (III e), les dendrites de solution solide α ont été plus longues et moins ramifiées, en ayant les axes premières orientées dans la direction du rayon, parce-que la rotation plus grande a déterminé une ségrégation plus prononcée du plomb et une plus forte infiltration du liquid qui n'a pas permis le développement des axes secondaires.

Aux rotations plus grandes (800 et 900 rot/min) l'aspect des microstructures est aproximativement le même, mais elles sont plus fines que celles des échantillons précédents, grace d'une plus intense homogénéisation du liquid et d'un plus intense échange de chaleur.

On resulte que pour les zones extérieures la microstructure plus fine que des autres zones est produite par le contact entre l'alliage et la coquille ou le couvercle de la moule métallique, qui ont déterminé l'intensification de l'échange de chaleur par convection et la croissance de la vitesse de solidification.

Dans la partie intérieure des pièces coulées, où se forme la surface libre à configuration cilindrique, l'échange de chaleur a lieu essentielement par radiation et convection, en etant plus lent. En conséquence, la microstructure des pièces coulées est plus grossière que dans les zones extérieures, en présentant des grandes dendrites de solution solide α et grandes zones d'eutectoïd ($\alpha + \delta$). De même, les séparations de plomb ont des grandes dimensions parce-qu'elles ont eu l'espace nécessaire pour se développer dans les zones interdendritiques. Cependant dans la zone supérieure (I i) et inférieure (III i) où les pièces coulées ont eu un contact avec le couvercle de la

coquille, respectivement avec la partie inférieure de la moule, la structure a été plus fine parce-qu'est intervenu l'apport d'échange de chaleur par convection.

Les plus défavorables conditions de refroidissement a eu la zone II –eme située entre 1/3 et 2/3 d'hauteur des pièces, c'est-à-dire la zone qui n'est pas venue en contact avec la partie inférieure de la moule ou avec le couvercle de la coquille. En conséquence, il s'ensuite que nous analyssons détaillé cette zone.

Les microstructures de l'échantillon coulée à 700 rot/min (figure 1) montrent qu'à l'extérieur (la zone II e) apparaît une structure dendritique fine, parce-que la vitesse de refroidissement d'alliage est plus grande que celle de la zone moyenne (II m) et dans le même temps les zones d'eutectoïd ($\alpha + \delta$) sont nombreuses, de petites dimensions et situées dans les espaces interdendritiques ou entre les branches des dendrites.

Analysse d'image, effectuée à l'installation assistée par ordinateur, a montré l'aire individuellement occupée par les séparations de plomb (tableau 1).

Tableau 1. La surface occupée individuellement par les séparations de Pb dans les pièces coulées par centrifugation à différentes rotations de la coquille (n)

L'échantillon	La zone II e		La zone II m		La zone II i	
	La surface μm^2	% du nombre total des séparations	La surface μm^2	% du nombre total des séparations	La surface μm^2	% du nombre total des séparations
mS n 1 (n_1=700 rot/min)	<250 250…400 400…600 820..1120	93 5 1 1	<250 250…500 500…1000 1225…1475	95 3 1 1	<500 500..1000	99 1
mS n 2 (n_2=800 rot/min)	<120 120…200 200…400 >400	70 20 7 rest	<175 175…350 350…500	88 10 2	<250 250..900	98 2
mS n 3 (n_3=880 rot/min)	<100 100…200 200…500	90 5 5	<100 100…400	95 5	<200 200…400 400…800 800…1400	88 8 2,3 1,7
mS n 4 (n_4=900 rot/min)	<90 90…150 150…230 230…300	85,4 11,45 2,1 rest	<100 100…200 200…300 300…500	86,5 10,1 2 rest	<200 200…400 400…800	91,8 5 3,2

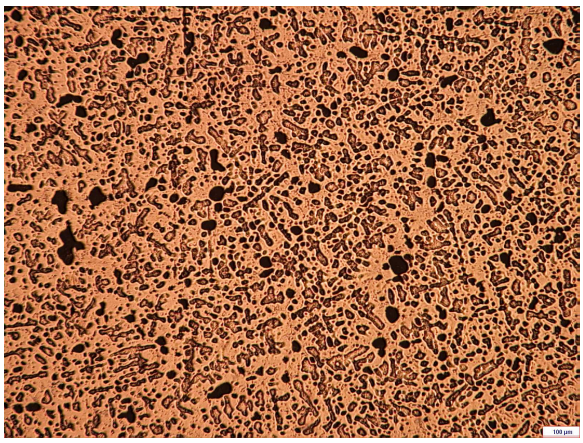

II. e – la zone extérieure

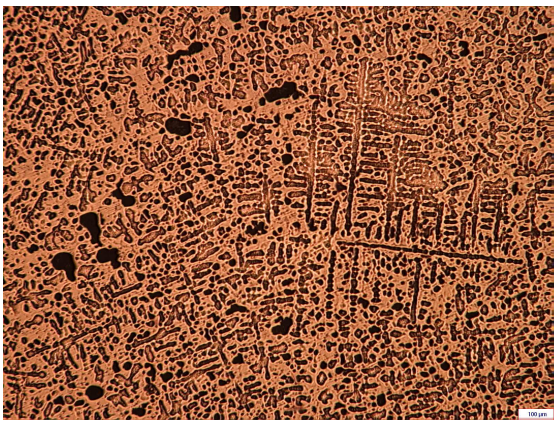

II. m – la zone moyenne

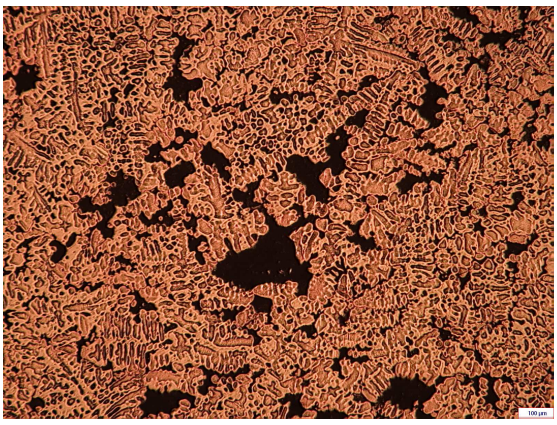

II. i – la zone intérieure

Figure 1. Les microstructures de l'échantillon mS n1, coulé par centrifugation à la rotation n = 700 rot/min. (×50)

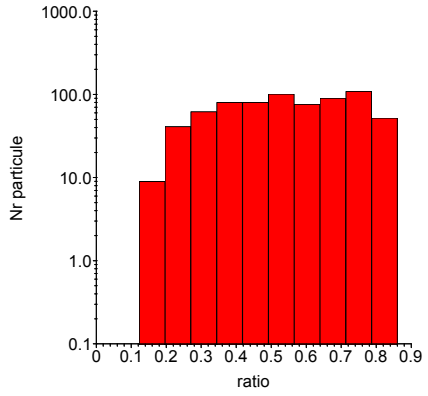

II. e – la zone extérieure

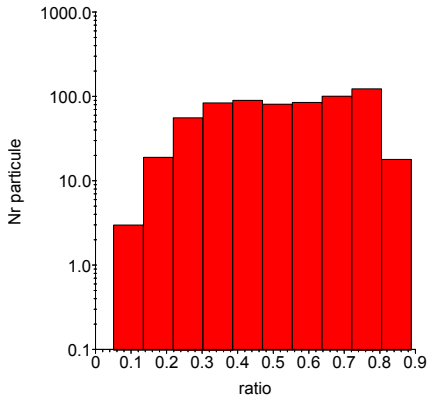

II. m – la zone moyenne

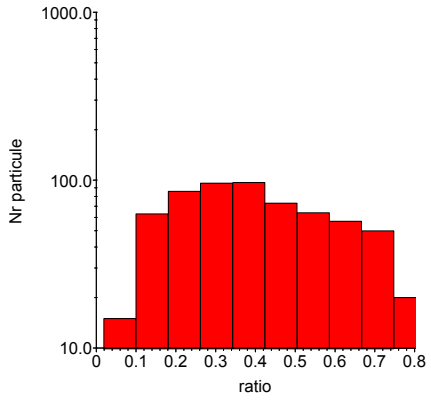

II. i – la zone intérieure

Figure 2. Le degré de sphéroïdisation (DS) des séparations de Pb dans l'échantillon mS n1, coulé par centrifugation à la rotation n = 700 rot/min.

Les séparations de plomb ont eu différentes degrés de sphéroïdisation (DS est le

rapport entre la largeur et la longueur de la séparation) comme on voit en figure 2, mais prédomine DS = 0,35…0,75 (59,9% du nombre total de séparations dans la zone extérieure, 66,65% dans la zone moyenne et 71,63% dans la zone intérieure). L'explication consiste dans la formation des dendrites nonramifiées qui permettent le développement des séparations de plomb sur les directions convenables.

Comparativement avec l'échantillon coulé à 700 rot/min, dans le cas de la pièce coulée à 800 rot/min (figure 3) apparaît une structure plus fine.

Dans la zone extérieure (II e) la microstructure a un aspect dendritique plus estompé, expliqué par la superposition de deux phénomènes: la croissance d'intensité de l'échange de chaleur par convection d'une part, qui n'a pas permis le développement des grandes et résistantes dendrites et d'autre part la fragmentation des dendrite minces à la suite de la rotation plus grande.

Dans la zone moyenne (II m) la microstructure a présenté un aspect dendritique plus évident. À cauze de la vitesse de refroidissement plus réduite, les unes des dendrites ont des axes premières à longueurs de 300…400 μm et des axes secondaires de 50…100 μm. De même, à la suite de la croissance de la vitesse de rotation, la microstructure a présenté encore et des fragmentes de dendrites qui, s'en unifiant avec celles intactes, ont fermé des volumes plus grandes de liquide où s'ont formé des séparations plus grandes de plomb, les unes ayant la forme ovale.

Dans la zone intérieure (II i) la microstructure a présenté des dendrites de solution solide α avec les axes premières plus courtes (200…300 μm) et les axes secondaires moins développées, parce-que la vitesse de refroidissement du côté de la surface libre a été plus grande. Dans la même zone apparaissent des fragmentes dendritiques parmi lesquels existentes, des grandes séparations de plomb et inclusions oxydiques.

Le degré de sphéroïdisation des séparations de plomb sont différentes (figure 4), mais prédominent les séparations avec DS = 0,3…0,7 c'est-à-dire 51,69% du nombre total à l'extérieur, 61% dans la zone moyenne et 66,34% à l'intérieur. Dans les petits espaces interdendritiques de l'extérieur on peut développer uniformement, sur toutes les directions, seulement des petites séparations de plomb avec une forme approchée de la forme sphérique, mais à l'intérieur, dans les microvolumes plus grands, leur développement peut avoir lieu sur certaines directions préférables en diminuant ainsi le degré de sphéroïdisation

Dans le cas d'échantillon mS n 3 coulé par centrifugation à 880 rot/min, la microstructure de la zone extérieure (II e) a un aspect dendritique très estompé à la suite de la rotation élevée et de la vitesse de refroidissement prononcée, produite par l'intensification de l'échange de chaleur par convection dans l'intérieur du liquide (voir la figure 5). Dans la zone moyenne (II m) la microstructure a présenté des fines dendrites de solution solide α avec des axes premières ayant la longueur environ 200 μm et des axes secondaires avec des longueurs de 50…150 μm. De même, on observé un grand nombre de dendrites désorientées, qui relevent une fragmentation plus prononcée des grandes dendrites, à la suite de l'action dynamique du liquide.

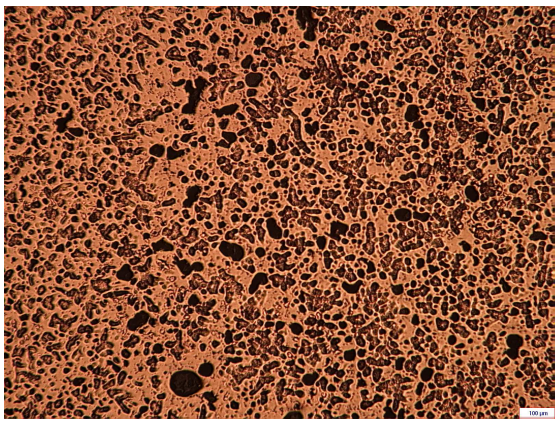

II. e – la zone extérieure

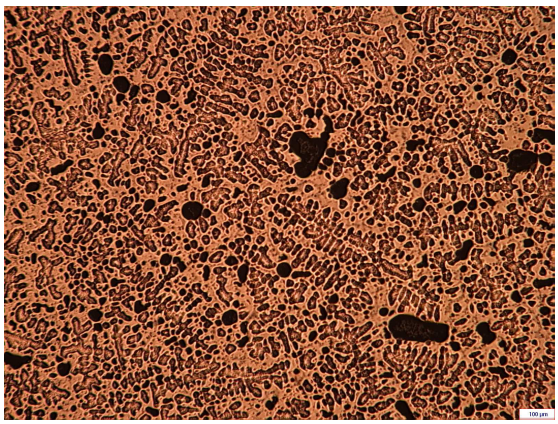

II. m – la zone moyenne

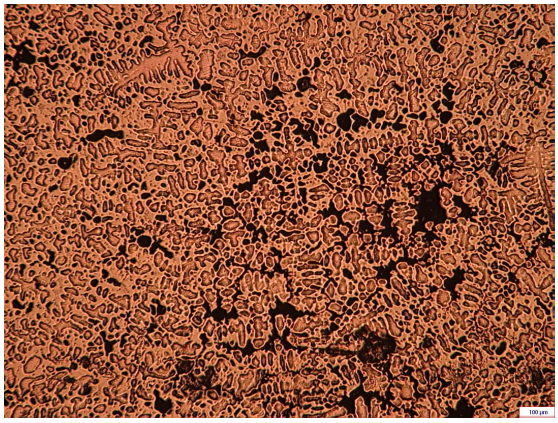

II. i – la zone intérieure

Figure 3. Les microstructures de l'échantillon mS n 2 coulé par centrifugation à la rotation n = 800 rot/min (× 50).

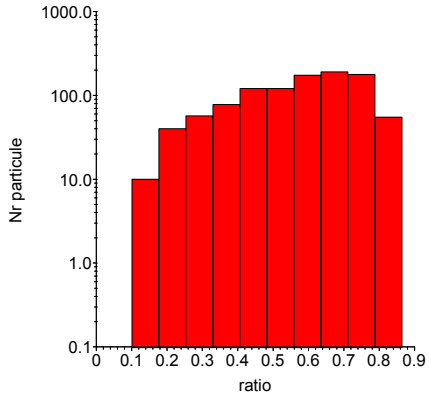

II. e – la zone extérieure

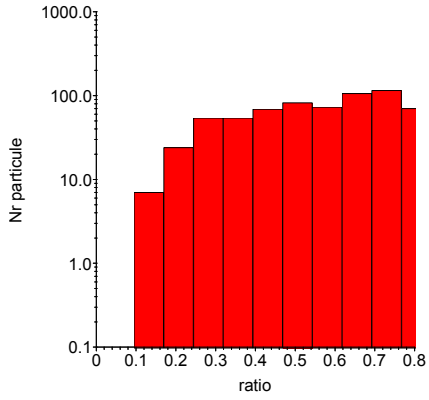

II. m – la zone moyenne

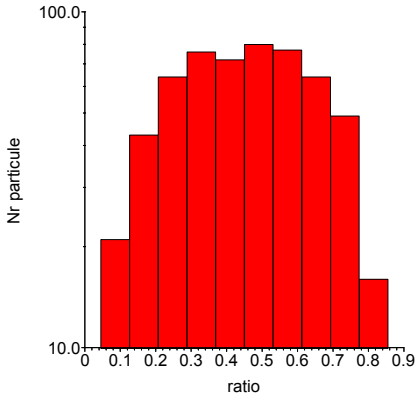

II. i – la zone intérieure

Figure 4. Le degré de sphéroïdisation (DS) des séparations de Pb dans l'échantillon mS n2, coulé par centrifugation à la rotation n = 800 rot/min.

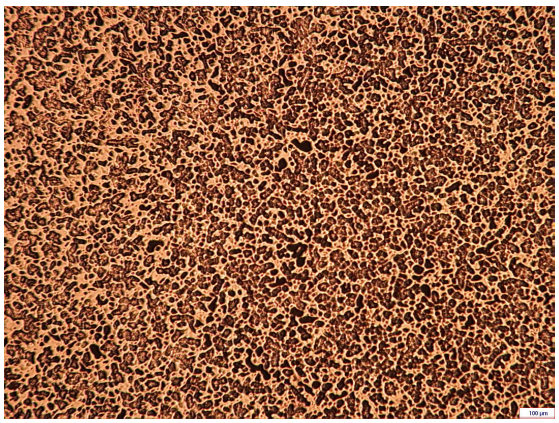

II. e – la zone extérieure

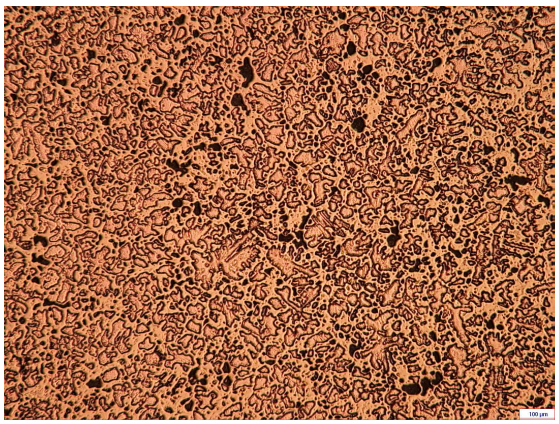

II. m – la zone moyenne

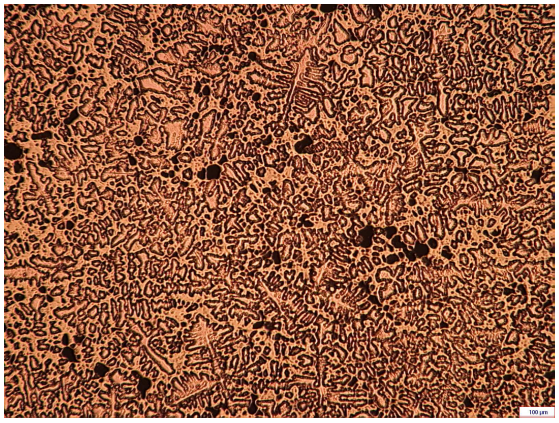

II. i – la zone intérieure

Figure 5. Les microstructures de l'échantillon mS n 3 coulé par centrifugation à la rotation n = 880 rot/min (× 50).

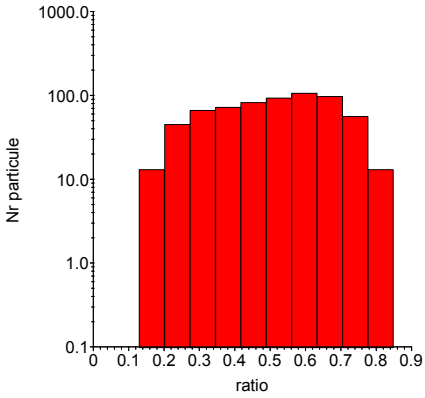

II. e – la zone extérieure

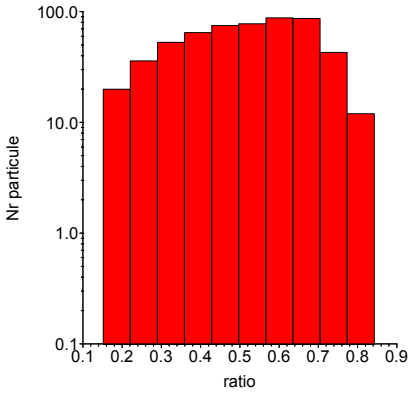

II. m – la zone moyenne

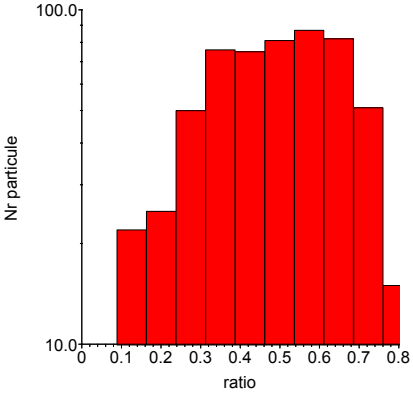

II. i – la zone intérieure

Figure 6. Le degré de sphéroïdisation (DS) des séparations de Pb dans l'échantillon mS n3, coulé par centrifugation à la rotation n = 880 rot/min.

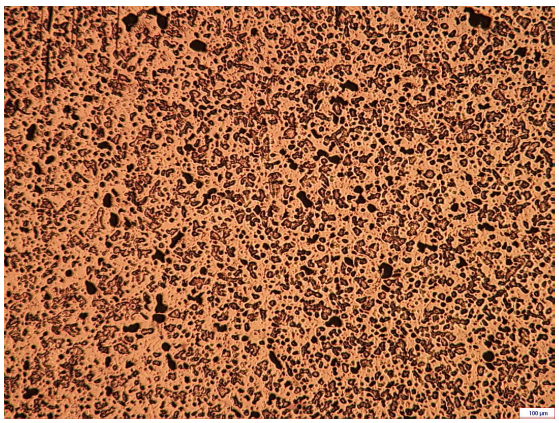

II. e – la zone extérieure

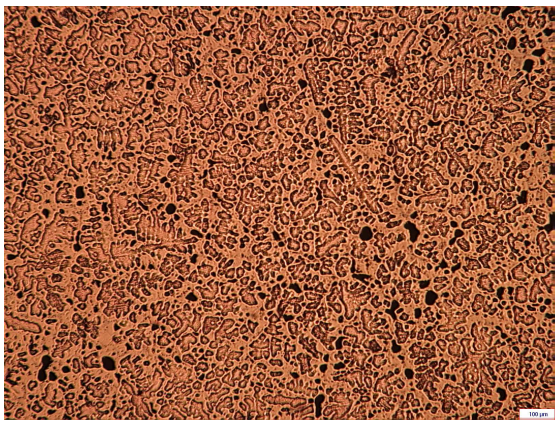

II. m – la zone moyenne

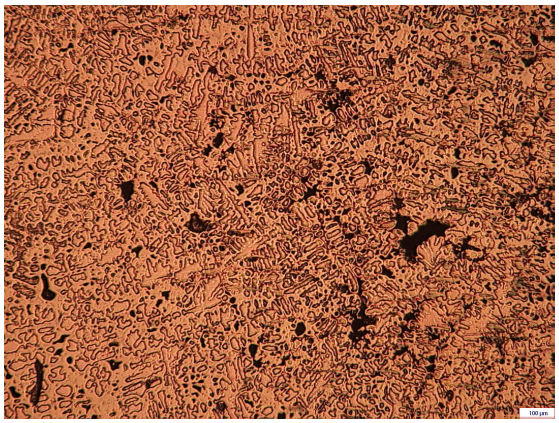

II. i – la zone intérieure

Figure 7. Les microstructures de l'échantillon mS n 4 coulé par centrifugation à la rotation n = 900 rot/min (× 50).

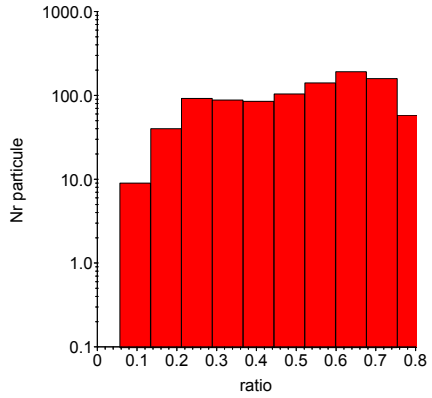

II. e – la zone extérieure

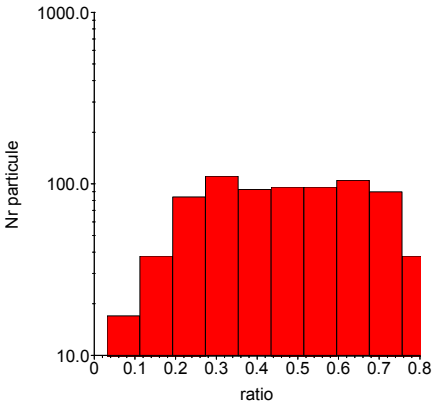

II. m – la zone moyenne

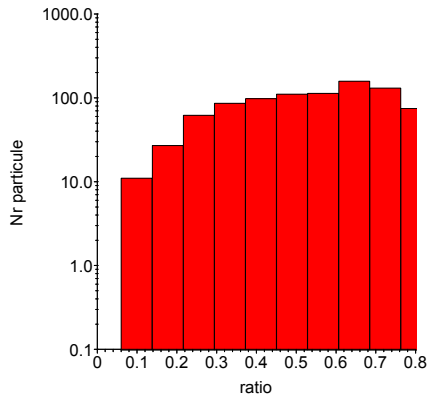

II. i – la zone intérieure

Figure 8. Le degré de sphéroïdisation (DS) des séparations de Pb dans l'échantillon mS n4, coulé par centrifugation à la rotation n = 900 rot/min.

Les dendrites n'ont pas eu la possibilité de se ramifier et de grossir ses axes à cause de la pression élevée du métall liquide, de sort que leur résistance a été diminuée et elles s'ont fragmenté facilement, en resultant une structure plus fine que dans les cas précédents. Dans la zone intérieure (II i) la microstructure a présenté des dendrites plus longues et plus ramifiées que dans les autres zones, mais elles sont plus fines que celles des échantillons coulés à rotations de 700 et 800 rot/min.

Le degré de sphéroïdisation (figure 6), mis en évidence par l'analyse d'image sur l'installation assistée par ordinateur, a montré que la majorité des séparations de plomb ont DS = 0,3…0,7 (67,73% à l'extérieur, 71,78% dans la
zone moyenne et 71,42% à l'intérieur), mais apparaissent encore des séparations avec DS = 0,8…0,9 à l'extérieur (10,88%) et à l'intérieur (12,4%).

Enfin, dans le cas d'échantillon mS n4 coulé par centrifugation à 900 rot/min, la microstructure, généralement, n'est pas très différente que celle d'échantillon mS n 3 coulé à 880 rot/min.

Dans la zone II – eme située dans la tiers moyenne d'hauteur de la pièce, on constaté cependant une différence de la microstructure sur la direction du rayon. Ainsi, dans la zone extérieure (II e) l'aspect dendritique est disparu, mais la microstructure est plus fine que celle du cas précédent (figure 7).

Dans la zone moyenne (II m) la microstructure a présenté des dendrites de solution solide α avec les dimensions de maximum 150 μm, donc un peu petites que dans le cas de la pièce coulée à rotation de 880 rot/min et dendrites fragmentées. La finition de la microstructure c'est produite à la suite du développement insuffisant des dendrites trouvées en contact avec le liquide pressé par la force centrifuge. Celles-ci, en etant minces, s'ont fragmenté facilement , en isolant des microvolumes de liquide dans lequel c'est formé l'eutectoïd (α + δ), qui finalement a englobé les séparations du Pb.

Dans la zone intérieure (II i) l'aspect dendritique se maintien, avec l'explication que les dendrites sont plus fines que dans le cas de la pièce coulée à 880 rot/min, mais les séparations du plomb se sont localisés dans les zones interdendritiques plus larges, qu'ont permis un développement plus accentué que dans la zone moyenne (II m).

Le degré de sphéroïdisation (figure 8) a été DS = 0,3…0,7 pour 68,58% des séparations de plomb de l'extérieur, pour 64,96% des séparations de la zone moyenne et 63,44% pour les séparations de l'intérieur. De même, à l'extérieur 23,75% des séparations ont eu DS = 0,7…0,9 , à l'intérieur 25,22% et dans la zone moyenne 17% ont eu DS = 0,8.

3. Conclusions

La rotation de la coquille a une importante influence sur la microstructure des pièces coulées par centrifugation en bronze CuPb10Sn10, c'est-à-dire à rotations plus grandes on obtient des structures plus fines.

Les causes directes qui déterminent l'obtention d'une structure plus fine sont:

- l'agrandissement de la rotation détermine une intensification de l'échange de chaleur par convection dans l'alliage liquide en II- eme étape de solidification, c'est-à-dire croît la vitesse de refroidissement et le nombre de germes de cristallisation, donc baissent les dimensions des dendrites;

• l'agrandissement de la rotation de la coquille détermine la croissance de la pression du métal liquide sur les dendrites qui se forment, en reduissant la croissance de la longueur des axes prèmieres en réalisant une ramification freinée, mais elle détermine l'augmentation du degré de fragmentation des dendrites, la finition de la microstructure et même la disparition d'aspect dendritique, comme on observé dans les zones extérieures des pièces coulées;

• la diminution des dimensions des dendrites de solution solide α, ainsi que leur fragmentation conduissent au finissage de la microstructure des pièces, parce-que les fragmentes dendritiques sont expulseés par la force centrifuge vers le front de solidification et là forment une réseau en éspace, qui délimite des microvolumes de liquide dans lesquelles accoucheraient des petites zones d'eutectoïd (α + δ), sous la température de 798°C et plus tard des fines séparations du plomb sous la température de 327°C.

Bibliographie

1. Diaconescu, F. – Cercetări şi contribuţii privind influenţa parametrilor tehnologici de turnare centrifugă asupra calităţii pieselor turnate din unele aliaje neferoase, Teză de doctorat, Universitatea Tehnică „Gh. Asachi" Iaşi, 2006.
2. Iudin, S.B, Levin, M.M.,Rozenfeld, S.E – *Turnarea centrifugă*, Editura tehnică, Bucureşti, 1973

FLORIN DIACONESCU
UNIVERSITÉ TECHNIQUE „GH. ASACHI" JASSY,
FACULTÉ DE SCIENCE ET GÉNIE DE MATÉRIAUX

CERCETĂRI PRIVIND INFLUENŢA TURAŢIEI COCHILEI ASUPRA MICROSTRUCTURII PIESELOR TURNATE CENTRIFUGAL DIN BRONZ CuPb10Sn10

Rezumat: Condiţiile de solidificare în câmp centrifug sunt diferite faţă de cele în câmp gravitaţional şi acestea contribuie la formarea unei microstructuri mai fine. În lucrare se studiază modificările microstructurale produse la diferite turaţii ale cochilei, ţinând seama de efectul lor asupra numărului de germeni de cristalizare şi asupra schimbului convectiv de căldură. În zonele mijlocii şi interioare ale pieselor turnate centrifugal, microstructura este mai fină odată cu creşterea turaţiei cochilei.

BULETINUL INSTITUTULUI POLITEHNIC DIN IAŞI
Tomul LIII (LVII), Fasc. 3, 2007
Secția
ŞTIINȚA ŞI INGINERIA MATERIALELOR

DES RECHERCHES CONCERNANT L'INFLUENCE DE LA TEMPÉRATURE DE PRÉCHAUFFAGE DE LA COQUILLE SUR LA MICROSTRUCTURE DES PIÈCES COULÈES PAR CENTRIFUGATION EN BRONZE Cu-Pb-Sn

BY

FLORIN DIACONESCU

Résumé: Dans l'ouvrage on étudie les modifications microstructurales produites par des différentes températures de préchauffage de la coquille, en tenant compte de leur effet sur l'échange de chaleur par convection et sur le nombre des germes de cristallisation. Aux températures elévées de préchauffage, à cause d'échange de chaleur lent baisse le nombre de germes de cristallisation, croissent les dimensions des dendrites de solution solide α et la microstructure devient plus grossière. La plus fine microstructure est obtenue à températures de préchauffage de 60…80°C.

Mots clef: température de prechauffage, échange de chaleur, germe de cristallisation, modifications microstructurales

1. INTRODUCTION

La température de préchauffage de la coquille est un très important paramètre de coulée centrifuge qui peut produire non seulement la séparation des inclusions nonmétalliques et gazeuses, mais elle peut influencer le nombre des germes de cristallisation et le finissage de la microstructure. L'obtention des pièces coulées compactes, sans soufflures et inclusions nonmétalliques et leur séparation vers la surépaiseur intérieure d'usinage dépend de la force centrifuge, c'est-à-dire de la densité des inclusions ρ_i, de la vitesse angulaire ω et du rayon de giration *r,* et dans le même temps d'échange de chaleur entre l'alliage liquide et la coquille [2]. Dans le même temps la fluidité d'alliage, qui croît avec l'augmentation de la température, assure la séparation facile des inclusions oxydiques et gazeuses vers la surface intérieure des pièces coulées par centrifugation .Voilà pourquoi nous sommes intéressés a déterminer la température de préchauffage optimale pour obtenir une fine microstructure, une bonne séparation des inclusions en évitant dans le même temps la tendance de ségrégation du plomb vers l'extérieur des pièces coulées par centrifugation en bronze CuPb10Sn10.

2. LA MÉTHODOLOGIE DE LA RECHERCHE

Pour étudier l'influence de la température de préchauffage de la coquille sur la microstructure des pièces coulées par centrifugation en bronze CuPb10Sn10, ont coulé des manchons avec les dimensions Ø120/ Ø30/120 mm sur une machine centrifuge avec axe verticale de rotation et rotation variable, en employant températures de préchauffage de 60°C, 220°C, 280°C et 300°C. La rotation de la coquille a été en tout cas de 900 rot/min et la température d'alliage coulé de 1180°C, afin d'éliminer l'influence de ces paramètres sur la microstructure [1].

Des pièces coulées par centrifugation ont prélevé des échantillons en trois places différentes en sectionnant longitudinalement les pièces et puis ont coupé les échantillons à 1/3 et 2/3 de l'hauteur en résultant les zones: supérieure (I), moyenne (II) et inférieure (III). Ont été étudiées les sections I-II et II-III pour éviter l'influence du couvercle et de la partie inférieure de la coquille sur la microstructure. Pour l'étude microscopique on employé une installation d'analyse de l'image, assistée par ordinateur, à l'Université Polytechnique de Bucarest.

b. Discutions

L'échantillon mS T_f 1, coulée par centrifugation dans la coquille préchauffée à 60ºC, a présenté une microstructure différente sur la direction du rayon. Dans la zone extérieure et dans les parties qui viennent en contact avec le couvercle et la partie inférieure de la coquille la vitesse de solidification a été grande, les germes de cristallisation ont été nombreux et la microstructure a eu un aspect dendritique estompé, en observant par endroits des dendrites de petits dimensions. Dans les zones moyennes, par suite de la diminution de la vitesse de solidification, la microstructure présente des dendrites de moyennes dimensions dans les zones antérieurement rappelées et dendrites de grandes dimensions dans la zone située dans la moyenne tiers d'hauteur de la pièce.

Dans les zones intérieures les dimensions des dendrites baissent un peu en général, par suite du refroidissement de la pièce du côté de la surface libre. Les plus défavorables conditions de solidification a eu la zone située dans la moyenne tiers d'hauteur de la pièce, où n'a pas éxisté l'influence du couvercle et de la partie inférieure de la coquille sur la vitesse de refroidissement. En conséquence, il s'ensuite que nous analyssons détaillé cette zone.

Dans la zone extérieure (II e), come on voit dans la figure 1, la microstructure a un aspect dendritique estompé, en présentant des dendrites très petites et isolèes de solution solide α, par suite de la grande vitesse de solidification produite par la température de préchauffage diminuée (60ºC). Dans la zone intérieure (II i) la microstructure a présenté des dendrites plus ramiffiées, avec des axes premières, secondaires et tertiaires, mais avec les dimensions en peu reduites que celles de la zone moyenne (II m).

Analysse d'image, effectuée à l'installation assistée par ordinateur, a montré l'aire individuellement occupée par les séparations de plomb (tableau 1).

Le degré de sphéroïdisation (DS) des séparations de plomb (figure 2) est plus homogène à l'extérieur en ayant valeurs de 0,5…0,72 pour 48,7% du nombre de séparations et de 0,72…0,86 pour 30,44%. Dans la zone moyenne (II m) le degré de sphéroïdisation baisse à 0,3…0,53 pour 43% des séparations, à 0,53…0,61 pour 28,7% des séparations et à 0,61…0,8 pour 28,65 des séparations.

La solidification avec une grande vitesse dans la zone extérieure a déterminé la pauvreté du liquide en Cu et Sn et l'enrichissement en Pb, mais les conditions de refroidissement plus lentes dans la zone moyenne ont favorisé l'apparition des grandes séparations de plomb. Dans la zone intérieure (II i) le degré de sphéroïdisation des séparations de plomb est plus baissé que dans les zones précédentes, en ayant valeurs de 0,32…0,54 pour 36,65% du nombre total, de 0,54…0,62 pour 16,9% séparations et 0,62…0,7 pour 15,03% du nombre total de séparations, en soulignant l'influence de la ramification plus prononcée des dendrites de solution solide α.

Tableau 1

La surface occupée individuellement par les séparations de Pb dans les pièces coulées par centrifugation à différentes températures de préchauffage de la coquille (T_c)

L'échantillon	La zone II e		La zone II m		La zone II i	
	La surface μm^2	% du nombre total des séparations	La surface μm^2	% du nombre total des séparations	La surface μm^2	% du nombre total des séparations
mS T_f 1 (T_c = 60°C)	<50 50…100 100…250	60,9 30,5 8,6	<100 100…200	96 4	<250 250..400 450..650	94 4 2
mS T_f 2 (T_c = 220°C)	<80 80…160 160…750	84,3 10,5 5,2	<70 70…130 190…310 310…600	62,5 11,2 2,7 1,3	<300 375..700	96,5 3,5
mS T_f 3 (T_c = 280°C)	<100 120…140 240…360 360…960	83,4 12,3 2,63 rest	<130 130…250 250…400	87,1 11,4 1,5	<375 375..600	99 1
mS T_f 4 (T_c = 300°C)	<120 120…200 200…400	89,4 7 rest	<175 175…350 350…675	94,2 5,16 rest	<400 400..590 590..800	95 4,4 0,6

Dans le cas d'echantillon mS T_f 2, coulé dans la coquille préchauffée à 220ºC, la microstructure a présenté un aspect dendritique sur l'entière surface de la section dans la direction du rayon (figure 3). Dans la zone extérieure (II e) la microstructure contient des dendrites de solution solide α avec des axes premières et secondaires, eutectoïde (α+δ) dans les zones interdendritiques et entre les branches des dendrites et séparations de plomb. Dans la zone moyenne (II m) les dendrites de solution solide α ont des axes premières avec la longueur de 200…300 μm et axes secondaires de 50…70 μm, et les unes des dendrites ont l'axe première grosse de 30 μm environ et des axes secondaires courtes. Dans la zone intérieure (II i) la microstructure a un aspect dendritique prononcé, avec les unes des dendrites en ayant l'axe première de

400…450 μm, un peu ramifiées et les autres plus courtes mais avec les axes premières et secondaires plus grosses.

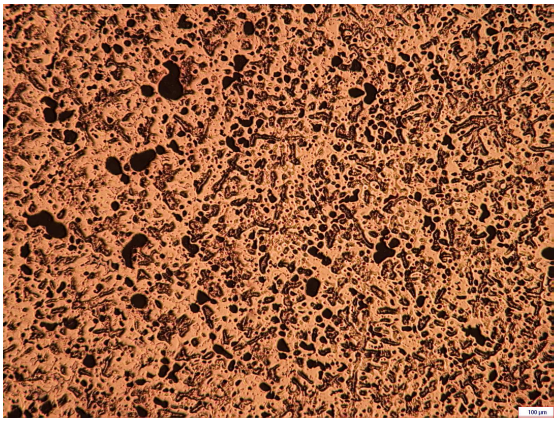

II e – la zone extérieure

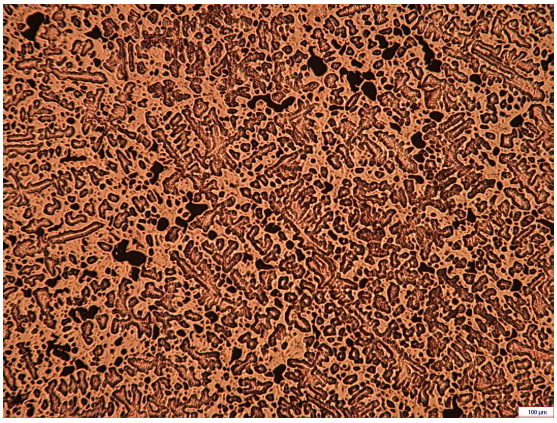

II m – la zone moyenne

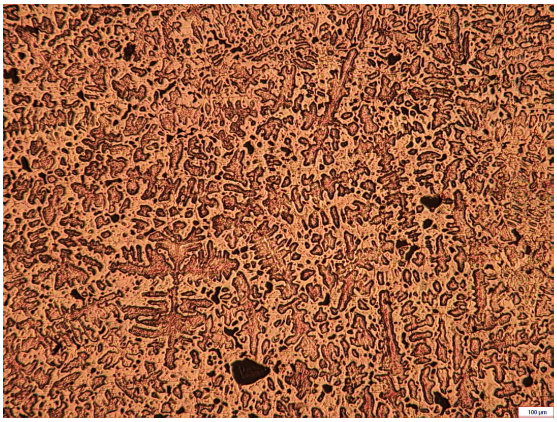

II i – la zone intérieure

Figure 1. Les microstructures de l'échantillon mS T_f 1 coulé par centrifugation dans la coquille préchauffée à 60°C
(× 50)

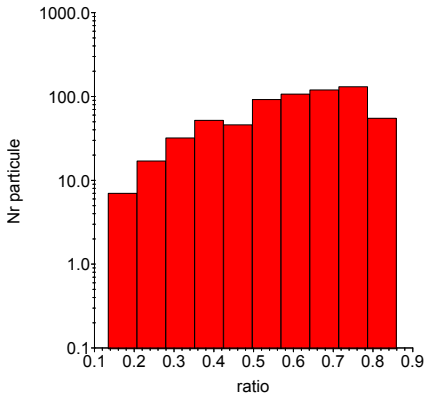

II e – la zone extérieure

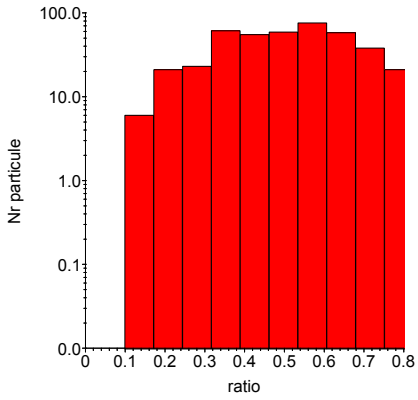

II m – la zone moyenne

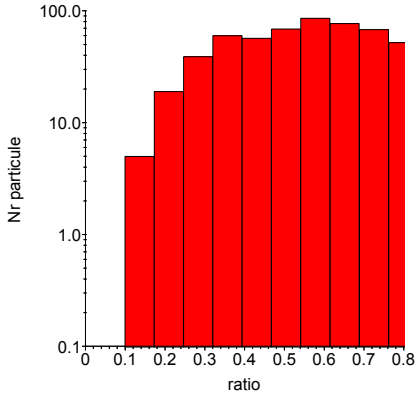

II i – la zone intérieure

Figure 2. Les degrés de sphéroïdisation des séparations de Pb dans l' échantillon mS T_f 1 coulé par centrifugation dans la coquille préchauffée à 60°C

II e – la zone extérieure

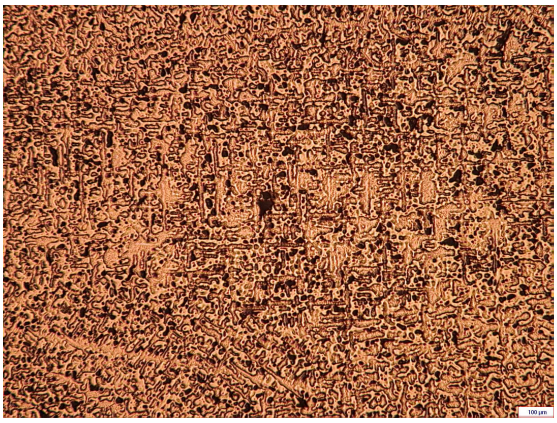

II m – la zone moyenne

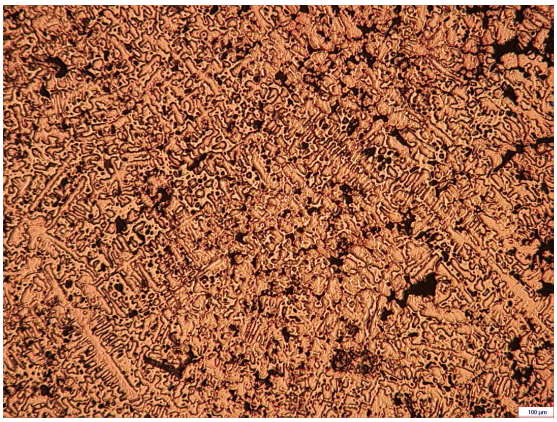

II i – la zone intérieure

Figure 3. Les microstructures de l'échantillon mS T $_f$ 2 coulé par centrifugation dans la coquille préchauffée à 220°C
(× 50)

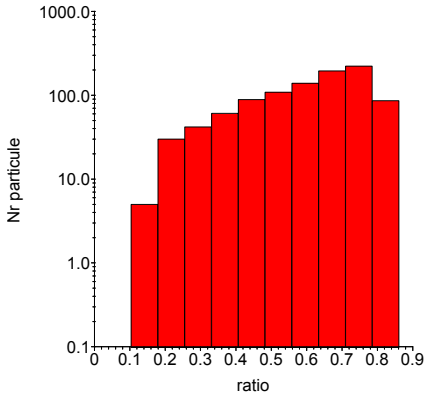

II e – la zone extérieure

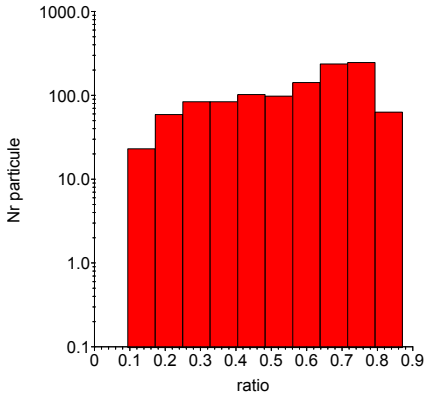

II m – la zone moyenne

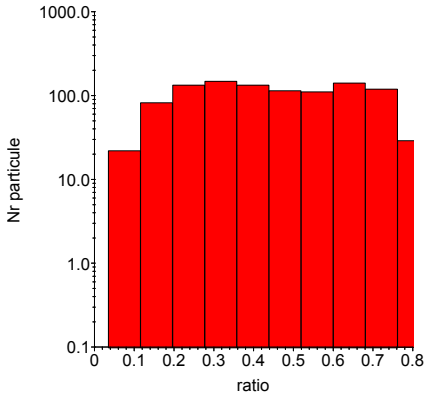

II i – la zone intérieure

Figure 4. Les degrés de sphéroïdisation des séparations de Pb dans l' échantillon mS T $_f$ 2 coulé par centrifugation dans la coquille préchauffée à 220°C

À cause de l'échange de chaleur plus lent et de la ramification des dendrites, les séparations de plomb de la zone extérieure ont occupé individuellement une ample game d'aires (voir le tableau 1).

Dans la zone intérieure (II i) les grandes séparations de plomb sont formées et developpées dans des grands microvolumes de liquide situés entre les branches rares des dendrites.

Le degré de sphéroïdisation des séparations de plomb est différent (figure 4). Ainsi, dans la zone extérieure 6,12% du nombre total de séparations ont eu DS<0,3 et 55,7% ont eu DS = 0,3…0,7 et 12,26% ont eu DS = 0,7…0,9. Dans la zone moyenne (II m) environ 35,6% du nombre total de séparations de plomb ont DS = 0,64…0,9 et 30,75 ont DS = 0,4…0,64. Dans la zone intérieure (II i) le degré de sphéroïdisation est changé, c'est-à-dire 66,3% du nombre total de séparations ont DS = 0,36…0,68 et 30% ont DS = 0,2…0,36. En comparaison avec l'échantillon coulé dans la coquille préchauffée à 60ºC, on constate une augmentation du nombre de séparations avec un petit degré de sphéroïdisation (0,1…0,2) de 4,51% jusqu'à 8,81%. Donc a baissé le nombre des séparations avec DS = 0,3…0,7 de 65,4% jusqu'à 55,7% , ainsi que celui avec DS = 0,7…0,9.

Dans le cas de l'echantillon mS T_f 3, coulé dans la coquille préchauffée à 280ºC, la microstructure a un aspect dendritique prononcé dans toutes les directions du rayon (figure 5), les dendrites de solution solide α etant plus fines dans la zone extérieure et plus developpées dans la zone intérieure. Dans la zone extérieure (II e) apparaissent des dendrites minces, à différentes orientations, en présentant des axes premières avec longueurs de 200…300 μm, des axes secondaires de 100 μm environ et des axes tertiaires de petites dimensions. Dans la zone moyenne (II m) la microstructure présent des dendrites plus grandes, avec des axes premières de 300…500 μm, des axes secondaires de 100 - 150 μm et des axes tertiaires de 50…70 μm. Dans la zone intérieure (II i) les dendrites sont plus courtes avec des axes premières de 300 μm et des axes secondaires sous 100 μm, plus ramifiées que dans la zone moyenne, en déterminant une reduction des zones d'eutectoïde (α + δ) et une meilleure distribution sur le fond métallique de la microstructure.

Le degré de sphéroïdisation des séparations de plomb dans la zone extérieure est différent (figure 6), c'est-à-dire 68% ont DS = 0,33…0,55, une quantité de 30% ont DS = 0,26…0,33, le rest ayant DS = 0,18…0,26. Dans la zone moyenne (II m), en comparaison avec la même zone d'echantillon précédent, on a constaté la même proportion de séparations avec DS = 0,4…0,7 et l'augmentation de 35,6% jusqu'à 48,93% de la quantité des séparations avec DS = 0,7…0,9. Le degré de sphéroïdisation des séparations de plomb a baissé dans la zone intérieure (II i), c'est-à-dire 28,93% du nombre total ont DS = 0,3…0,53 et 26,68% ont DS = 0,53…0,76.

Pour l'échantillon mS T_f 4, coulé dans la coquille préchauffée à 300ºC, la microstructure se maintient, en apparaissant plus accentuée dans la zone moyenne et intérieure de la pièce (figure 7). Dans la zone extérieure (II e) d'echantillon, les dendrites ont les axes premières et secondaires plus grosses que dans les échantillons précédents, à la suite de la vitesse de solidification très reduite, provoquée par la température élevée de préchauffage. Dans la zone moyenne (II m) les dendrites sont grandes en ayant les axes premières longues de 400 μm, les axes secondaires de

100…150 μm et des axes tertiaires à la suite de la largeur de la zone biphasique.

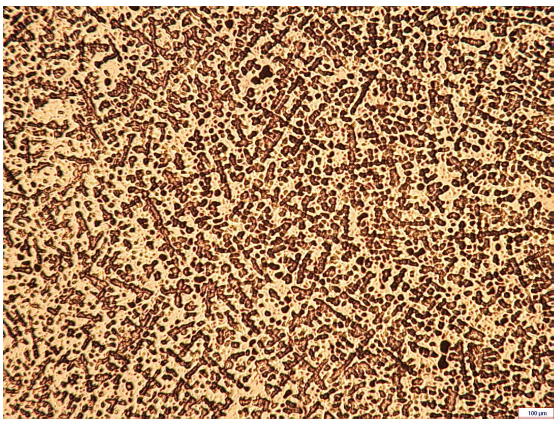

II e – la zone extérieure

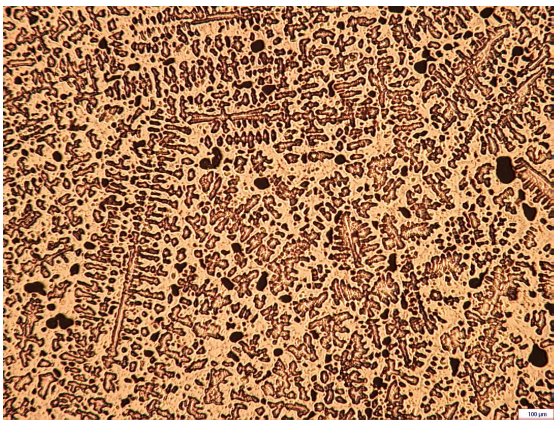

II m – la zone moyenne

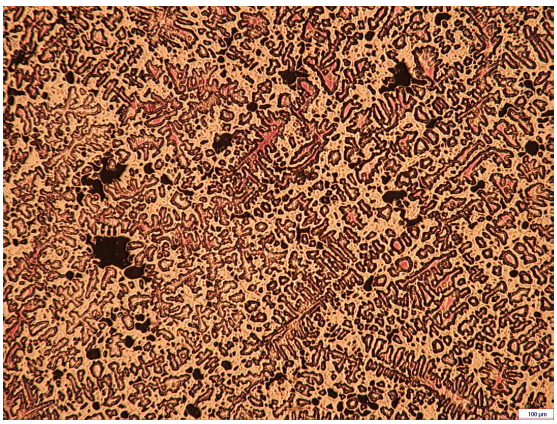

II i – la zone intérieure

Figure 5.Les microstructures de l'échantillon mST_f 3 coulé par centrifugation dans la coquille préchauffée à 280°C (× 50)

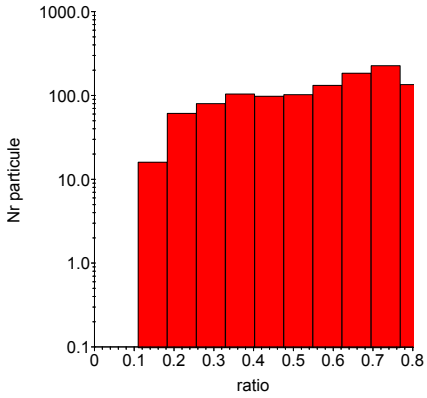

II e – la zone extérieure

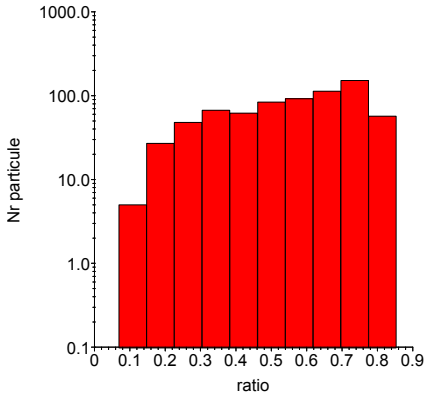

II m – la zone moyenne

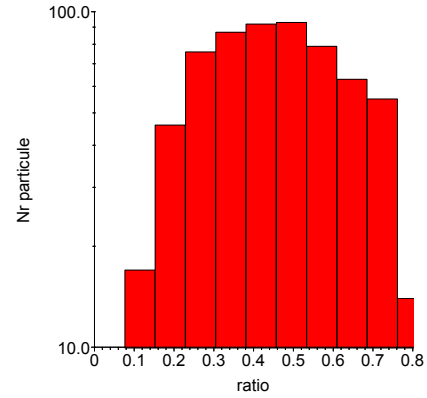

II i – la zone intérieure

Figure 6. Les degrés de sphéroïdisation des séparations de Pb dans l' échantillon mST_f 3 coulé par centrifugation dans la coquille préchauffée à 280°C

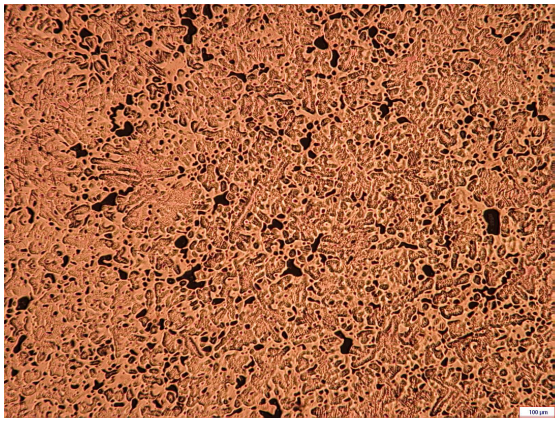

II e – la zone extérieure

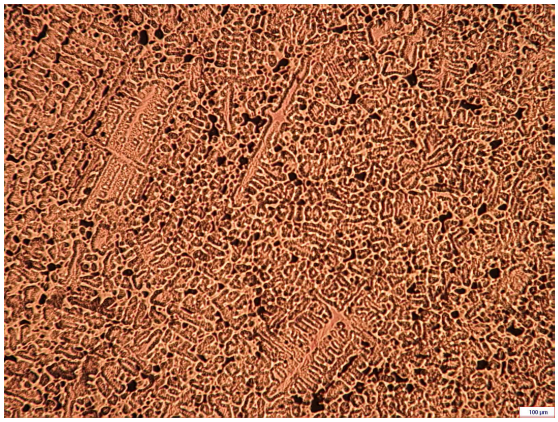

II m – la zone moyenne

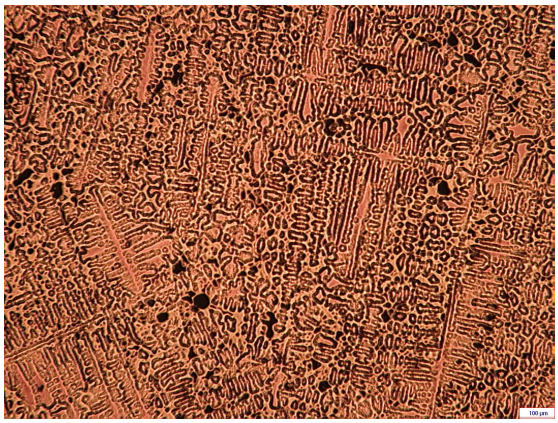

II i – la zone intérieure

Figure 7. Les microstructures de l'échantillon mST_f 4 coulé par centrifugation dans la coquille préchauffée à 300°C
(× 50)

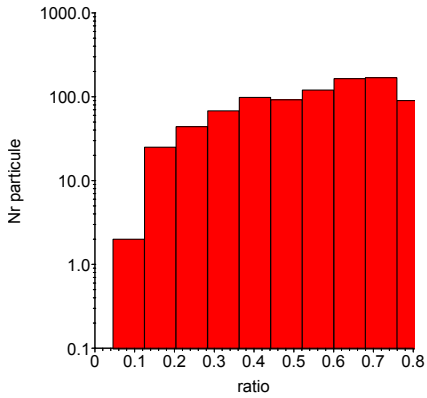

II e – la zone extérieure

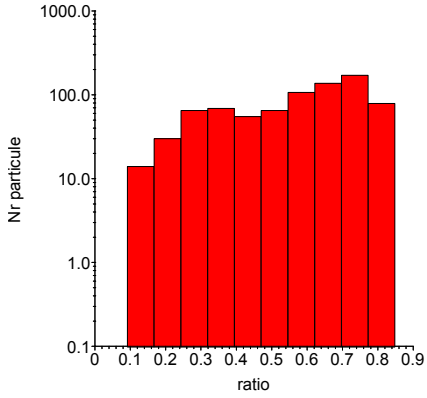

II m – la zone moyenne

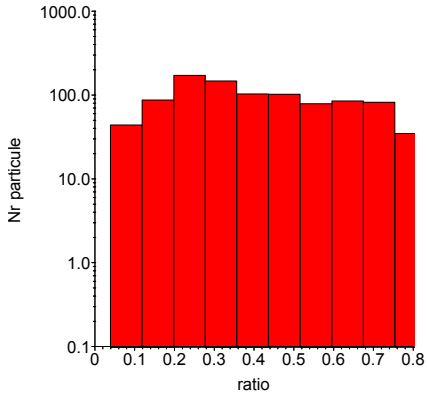

II i – la zone intérieure

Figure 8. Les degrés de sphéroïdisation des séparations de Pb dans l'échantillon mST_f 3 coulé par centrifugation dans la coquille préchauffée à 300°C

Les dendrites s'ont developpées lentement, elles ont eu la possibilité de s'accroître en dimensions et de se ramifier, mais elles ont fermé entre les branches des grands volumes de liquide, dans lequel ont apparu des zones étendues d'eutectoïde (α + δ) et des grandes séparations de plomb. Dans la zone intérieure (II. i) la microstructure a présenté un aspect dendritique grossier, avec des dendrites grandes, ramifiées, en ayant les axes premières longues de 800…1200 μm, les axes secondaires de 200…300 μm et les axes tertiaires de 50…100 μm.

Le degré de sphéroïdisation des séparations de plomb dans la zone extérieure (II e) est très différent, c'est-à-dire 24,4% des séparations ont DS < 0,36 et 55% ont DS = 0,36…0,76 mais 20,6% ont DS = 0,76…0,8 (voir la figure 8). Dans la zone moyenne (II m), le degré de sphéroïdisation des séparations de plomb est différent, c'est-à-dire 34% du nombre total ont DS = 0,24…0,55, une quantité de 51,8% ont DS = 0,55…0,77 et 8,5% ont DS = 0,77…0,85. Dans la zone intérieure (II i) le degré de sphéroïdisation est très différent, c'est-à-dire 25,4% du nombre total des séparations ont DS = 0,2…0,36 et 24,8% ont DS = 0,36…0.52 suivites de 29,8% avec DS = 0,52…0,75 et 3,72% avec DS = 0,75…0,8.

3. CONCLUSIONS

■ La température de préchauffage de la coquille exerce une puissante influence sur la microstructure des pièces coulées par centrifugation en bronze.

■ À bases températures de préchauffage (60ºC), imposées pour éviter la ségrégation du plomb, la microstructure est différente sur la direction du rayon c'est-à-dire à l'extérieur l'aspect dendritique est absent, mais dans la zone moyenne et intérieure des pièces, les dendrites ne sont pas developpées à la suite d'un transfert rapid de chaleur du côté d'alliage vers les parois de la coquille. Les séparations de plomb sont fines et uniformement distribuées sur le fond métallique de l'échantillon, en influençant d'une manière positive les propriétés antifriction.

■ À températures de 220ºC environ, habituellement utilisées dans la practique pour atténuer le choc thermique et pour la croissance de la durabilité de la coquille, les pièces présentent un aspect dendritique sur l'entière section (en direction du rayon), mais avec un différent degré de dispersion, c'est-à-dire plus grand à l'extérieur et plus reduit à l'intérieur. Dans la zone intérieure, la grosseur et la distribution des séparations de plomb peuvent affecter les propriétés antifriction.

■ À hautes températures de préchauffage (280…300ºC) la structure dendritique est plus accentueé à cause du transfert lent de chaleur du côté d'alliage vers les parois de la coquille, qui détermine l'obtention des pièces coulées avec faibles propriétés mécaniques et une reduite résistance à l'usure.

■ On resulte que pour realiser une structure fine et des propriétés mécaniques élevées il est nécessaire une baisse température de préchauffage de la coquille (60…80ºC), mais on impose de prendre des unes précautions par l'élaboration très attentive (avec le dégazage et la déoxydation avancée) pour éviter un contenu élevé d'inclusions gazeuses et oxydiques.

Bibliographie

1. Diaconescu, F. – Cercetări şi contribuţii privind influenţa parametrilor tehnologici de turnare centrifugă asupra calităţii pieselor turnate din unele aliaje neferoase, Teză de doctorat, Universitatea Tehnică „Gh. Asachi" Iaşi, 2006.
2. Sofroni, L., Brabie, V., Bratu, C. – Bazele teoretice ale turnării, Editura Didactică şi Pedagogică, Bucureşti, 1980.

FLORIN DIACONESCU
UNIVERSITÉ TECHNIQUE „GH. ASACHI" JASSY,
FACULTÉ DE SCIENCE ET GÉNIE DE MATÉRIAUX

CERCETĂRI PRIVIND INFLUENŢA TEMPERATURII DE PREÎNCĂLZIRE A COCHILEI ASUPRA MICROSTRUCTURII PIESELOR TURNATE CENTRIFUGAL DIN BRONZ CuPb10Sn10

Rezumat: În lucrare se studiază modificările microstructurale produse de diferite temperaturi de preîncălzire a cochilei, ţinând seama de efectul lor asupra schimbului convectiv de căldură şi asupra numărului de germeni de cristalizare. La temperaturi de preîncălzire înalte, din cauza schimbului lent de căldură, scade numărul de germeni de cristalizare, cresc dimensiunile dendritelor de soluţie solidă α şi microstructura devine mai grosolană. Cea mai fină microstructură se obţine la temperaturi de preîncălzire de 60…80°C.

BULETINUL INSTITUTULUI POLITEHNIC DIN IAŞI
Tomul LIII (LVII), Fasc. 3, 2007
Secția
ŞTIINȚA ŞI INGINERIA MATERIALELOR

EXPERIMENTAL RESEARCH CONCERNING THE ION-NITRIDING OF SOME CAST IRONS

BY

MIHAI ALEXANDRU and DOINA HINCU

Abstract: *The paper presents the experimental results obtained on plasma nitriding of the following cast irons Fgn 38-11, Fgn 50-7, a phosphorous gray cast iron and Fna NiCr20.2. With unalloyed nodular and lamellar cast irons a combination layer $\gamma'+\varepsilon$ is formed. The quantity of the γ' nitride type decreases with the increase of the nitriding temperature. Within the entire temperature range we have taken into consideration γ' nitrides have appeared in the diffusion layer. The alloyed cast iron Fna NiCr20.2does not form any combination layers.*
Keywords: *plasma nitriding, cast irons*

1. INTRODUCTION

The anti-friction properties of cast irons can be improved by ion-nitriding because of the existence of free carbon in their structure. Besides the enhancing of the hardness and diminishing of the friction coefficient, the ion-nitrided cast irons have a good fatigue resistance. The supplementary formation of a nitrides layer with the thickness of 5 to 10 mm, reduces more the friction coefficient, enhances the wear resistance of the parts working in hard regimes and substantially enhances the corrosion resistance.

The paper shows the results obtained at the ion-nitriding of feritic cast irons Fgn 38-11, perlitic-feritic cast iron Fgn 50-7 and of the grey, phosphorous cast iron Fna NiCr 20.2.

2. EXPERIMENTAL PROCEDURES

Treatments were done in laboratory conditions using paralelipipedic samples 18x18x25 mm. The treatment temperatures for the cast irons Fgn 38-11, Fgn 50-7 and of the grey phosphorous cast iron ranged among 500 - 580 °C and for the highly alloyed cast iron Fna NiCr 20.2 the temperature range was 500 - 600 °C. Nitriding was made using NH_3, the working pressure being 3 Torr.

They have been made hardness measurements using 0.1 kg as a weigh. each result was obtained as an average of 15 measurements for eliminating the errors due to lack of homogeneities. The determinations for the perlito-feritic cast iron Fgn 50-7 were done only in the perlitic regions having in view the fact that the ferite in mild and plastic and into the highly alloyed cast iron FnaNiCr20.2 there were avoided the carbides due to their enhanced hardness.

In view of determination of the structure of the superficial layer, the ion-nitrided samples were analyzed by an X-ray diffraction method.

3. EXPERIMENTAL RESULTS

For the establishing of the ion-nitriding parameters of the cast irons mentioned there have been taken into account the following criteria: deepness, hardness and structure of the resulted layer after nitriding (as final parameters) as well as thy initial structure of the cast iron to be nitrided, thermal stability of the structure and alloying level (as initial parameters).

At the cast irons from which there are being made parts submitted to friction, the diffusion layer plays a less important role and the obtaining of a chemical combination layer adapted to this stress is wanted. If the part is submitted to bending, the fatigue resistance grows with the condition of the obtaining of a diffusion layer thicker than the biggest size of the graphite separations. When choosing the ion-nitriding temperatures of cast irons one must take into consideration that at heating up to 500 °C, the growing of the degree of dispersion of perlite can occur leading at a modification of the mechanical properties of the part core.

Fig. 1 Fgn38-11
t= 30 h; T= 550 °C

Fig. 2 Fgn 50-7
t= 30 h; T= 550 °C

The ion-nitriding of the feritic cast iron Fgn 38-11 leads to the formation of a layer composed from a zone of chemical compounds and a diffusion layer. The diffusion layer shows two parts: towards the surface needle shape nitrides regularly developed into the ferite grains (fig. 1) and towards the interior a solid solution of N into Fe_{α}. The chemical compounds zone grows with the temperature reaching from 1-1.5 μm for nitriding temperatures of 500 °C up to 5-6 μm for the nitriding temperature of 580 °C. Also the needle shape nitrides zone grows from 50 - 60 μm for the nitriding temperature of 500 °C, up to 125 μm for the nitriding temperature of 580 °C.

the X-ray analysis of the structure puts into evidence that the combination layer is a mixture of phases $\gamma'+\varepsilon$, the quantity of the phase γ ’ decreasing substantially with the temperature enhancing. Also there could be seen that the needle shape nitrides from the diffusion layer are being made entirely from γ ’.

At the ferito-perlitic cast iron Fgn 50-7 there was obtained a layer of combinations which is thicker at higher temperatures. In the diffusion layer the needle shaped nitrides were observed at the optic microscope only in the feritic zones surrounding the nodular graphite (fig.2). The deepness of the zone with needle shape nitrides grows with the enhancing of the temperature so at 500 °C is about 45 μm and at 550 °C it reaches 125 μm.

The research made using X-rays put into evidence the fact that the combination layer is made by a mixture of phases $\gamma'+\varepsilon$. The quantity of phase ε is in a higher proportion at higher nitriding temperatures. At nitriding temperatures of 500 °C the dominant phase is γ ’. Nitrides forming in the diffusion layer are being made from γ ’ in the range of temperatures, in which test were being done.

At the ion-nitriding of grey phosphorous cast iron one can obtain layers of combination of 6-12 μm,as a function of the temperature at which the treatment was performed.

Fig. 3 Phosphorous grey cast iron
t= 30 h; T= 550 °C

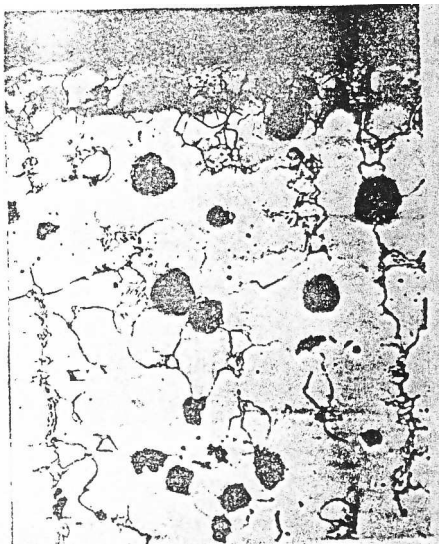

Fig. 4 Fna NiCr 20.2
t= 30 h; T= 550 °C

The X-ray structural analysis put into evidence the fact the layer of chemical combination is a mixture of phases $\gamma'+\varepsilon$. The phase ε is in very small quantity at the treatment temperature 500 °C, but is predominant at the temperature 580 °C.

The metallographic analysis performed on the grey phosphorous cast iron submitted to ion-nitriding put into evidence the trend of exfoliation of the layer during the preparation of the samples (fig.3).

This consequence is due to the presence of the lamellar graphite that because of sharpened edges creates concentration efforts, leading finally to micro-crackings.

In the case of Fna NiCr 20.2 cast iron (fig.4), on the samples treated up to 600 °C there were no observations of combination zones.

The determinations of micro-hardness in the layers of the samples nitrided at 550 °C are shown in figure 5.

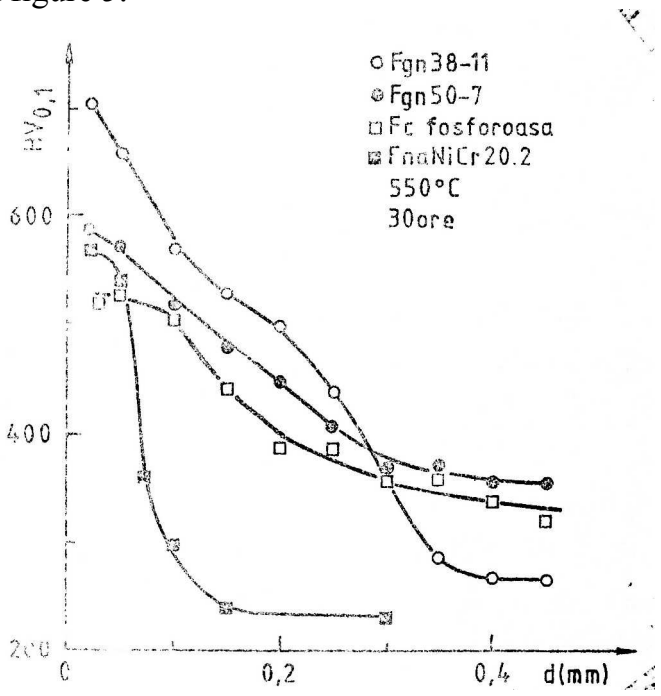

Fig. 5

It can be seen the influence of the chemical composition and of the structure of the cast iron on the hardness and its deepness. So, in the case of the Fgn 38-11 cast iron the deepness of the layer and the maximum hardness from the diffusion layer are superior to those obtained at the Fgn 50-7, at the phosphorous gray cast iron and at the highly alloyed cast iron Fna NiCr 20.2.

As a difference comparing with the nodular graphite cast irons and the non alloyed cast irons with lamellar graphite, at which one can see a uniform decrease of the hardness on the depth of the layer, at the highly alloyed cast iron with Ni and Cr, a sudden decrease of the hardness occurs at the layer boundary. The cast iron Fna NiCr 20.2 shows a much lesser depth of the nitrided layer than the other type of cast irons.

4. CONCLUSIONS

4.1. The decrease of the nitriding temperature has as a result the enhancement of the percentage of phase γ 'in the combination zone.

4.2. Referring to the diffusion mechanism of the nitrogen and of forming of the separations of γ 'phases in the diffusion layer, at the cast iron Fgn 38-11 one can formulate the hypothesis: following a ionic bombardment, in the ferrite grains of the superficial layer there are taking place processes of dislocation formation and displacement of those with their grouping at the grains boundaries. Following the dislocation grouping, dislocations channels occur, stimulating the diffusion of nitrogen and, in the same time creating the conditions of precipitation of the phase γ '.

The temperatures of ion-nitriding process, ranging among 500 – 550 °C, ensure the obtaining of a uniform and compact layer, having superior properties of hardness

and tenacity. It is preferable to work at the inferior limit of the temperature range because in this case, in the composition of the ion-nitriding layer, the phase γ ' will prevail.

REFERENCES

1. Keller, K., Ionitrierung von Gußeissenwerkstoffen, Harterei-Techn., Berlin 2002
2. Lahtin, I.M., Kogan, I.D., Azotirovanie stali, Masinostroienie, Moskwa, 2000.

Received April 2007 *District School Inspectorate*

CERCETARI EXPERIMENTALE PRIVIND NITRURAREA IONICA A UNOR FONTE

Rezumat: Sunt prezentate rezultatele experimentale obtinute la nitrurarea ionica a fontelor Fgn 38-11, Fgn 50-7, fonta cenusie fosforoasa si Fna NiCr20.2. La fontele nealiate, cu grafit nodular si lamelar se formeaza un strat de combinatie cu structura $\gamma'+\varepsilon$. Cantitatea de faza *γ ' scade odata cu cresterea temperaturii de nitrurare. Pe intreg intervalul de temperatura in care s-au efectuat experimentarile, in stratul de difuzie apar nitruriγ '. Fonta aliata* Fna NiCr20.2 nu formeaza zone de combinatie.

BULETINUL INSTITUTULUI POLITEHNIC DIN IAŞI
Tomul LIII (LVII), Fasc. 3, 2007
Secția
ŞTIINȚA ŞI INGINERIA MATERIALELOR

NON CHEMICAL TREATMENT OF WATER FOR COOLING THE INDUCTION HEATING FURNACE

BY

GHEORGHE BADARAU and IULIAN IONITA

Abstract: The paper presents the possibility of applying a non chemical way to reduce scale formation on the cooling system of the induction heating furnaces. It describes the precipitation modification of minerals in water using a pulsed-power system and the possible application of the method on specific metallurgical equipment.
Keywords: non chemical water treatment, reduce scale formation, induction heating furnace.

INTRODUCTION

Chemical water treatment can be successful at controlling scale; however, the problems associated with adding chemicals with various degrees of toxicity are factual. Chemicals in the concentrated form are often acute toxins, and their chronic toxicity in the diluted form is often uncertain. Chemicals must be added at the right time and rate or they are not as effective. Also, if improperly added to a system, they may cause severe operational problems.

The search for a nonchemical way to reduce scale formation has been the supreme goal of those seeking a "green" solution to this problem.

The pulsed-power treatment technology described in this paper has had success in a related industry (liquid food processing), and I believe that in the near future the widespread acceptance of this technology by the water treatment industry is certain.

PULSED-POWER IN WATER TRETMENT

A pulsed-power system (PPS) water treatment device is closely related to a device used for non-thermal pasteurization of food using Pulsed Electric Fields (PEFs). It aims to control with low-power pulsed electric fields the precipitation modification of minerals as calcium, magnesium, or silica compounds.

CALCIUM CARBONATE SCALE

Calcium carbonate is the most common scale-forming mineral occurring in industrial waters. Its concentration in source water varies enormously, depending on location, but in general it is the first mineral to precipitate out either by heating or by concentrating water. Control of calcium carbonate scale is therefore often the limiting item in water usage.

Calcium carbonate is a problem because when it precipitates it forms an adherent deposit (scale). This scale forms preferentially on hot surfaces (heat transfer), blocking water flow and lowering thermal efficiency.

Precipitation of calcium carbonate is not always a problem. At saturation, calcium carbonate is an effective cathodic corrosion inhibitor for mild steel. Thus, high levels of dissolved calcium carbonate in a system are often beneficial, provided that they do not form an adherent deposit [3].

Calcium carbonate does not always form a surface-nucleating scale when it reaches supersaturation; in some situations, calcium carbonate will naturally and reliably form a non-adherent powder rather than an adherent scale. At very high degrees of supersaturation, most calcium minerals, including calcium carbonate, will form non-adherent powders rather than an adherent scale [4]. This phenomenon is rarely used in practice since there is a zone of adherent scale-formation that must be passed through to reach the non-adherent zone. Although the effect is well documented, the literature contains little theoretical discussion of why it occurs.

NON-ADHERENT POWDER FORMATION

The underlying physics of the non-adherent powder phenomenon is still being debated. Most believe that this phenomenon is not an example of a switching from heterogeneous nucleation (nucleation on seed crystals) to homogenous nucleation (nucleation directly from solution) [4]. Rather, at a high degree of supersaturation small, suspended particles (colloidal-sized) in the bulk solution will act as seed crystals for precipitation, while at lower levels of saturation they will not. From this perspective, the effect is due to some interaction of the surface charge on small, suspended particles in the water with dissolved ions.

Most suspended particles in water will quickly develop a negative surface charge. The strength of this surface charge is usually described by the particle's zeta potential. Zeta potential measures the strength of the electric potential due to the surface charge on a suspended particle at the "slip point" near the particle. (The slip point is usually defined as the Stern layer/diffuse layer boundary figure 1.

The magnitude of the zeta potential depends on the strength of the surface charge on the particle and the particular composition of dissolved minerals in the

water. The electrostatic repulsion of suspended particles' zeta potential also keeps small particles from coagulating into bigger particles.

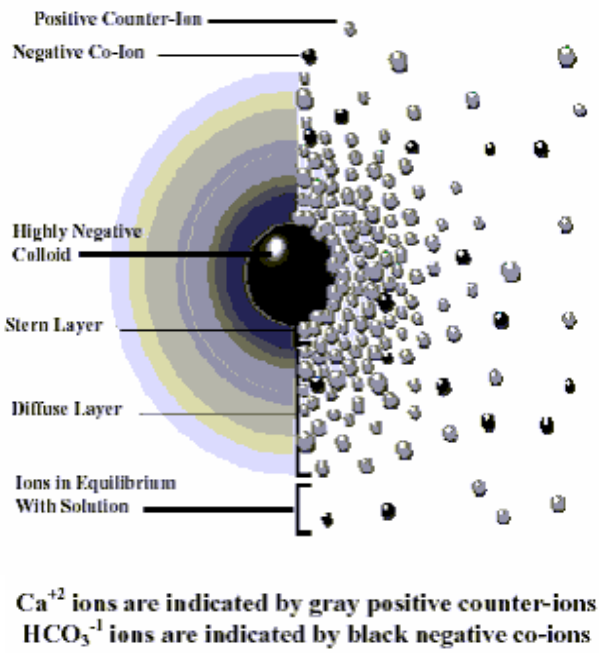

Fig. 1 Zeta potential [1]

Figure 1 shows the classical depiction of the differing charge layers around a suspended particle [5]. This drawing is not at all to scale; the suspended particle is a thousand to ten thousand times larger than dissolved ions. The exclusive presence of counter-ions (Ca+2) near the surface of the particle prevents the particle from being a seed crystal, since both co-ions and counter-ions are required to form a precipitate. When the amount of minerals in solution increases significantly, the diffuse layer will compress, bringing some co-ions close to the surface and perhaps allowing the suspended particles to act as seed crystals. However, in water concentrations typically used in industry, the electric fields surrounding suspended particles prevent the formation of a nonadherent precipitate.

SCALE CONTROL WITH PULSED-POWER

Pulsed-power systems deliver a combination of a high frequency electric pulse and a time-varying DC electric field to the water as it passes through the device. The efficacy of this device on controlling biological activity in cooling systems has been reported [6, 7, 8, 9]. This paper explores the scale mitigation properties of pulsed-power devices.

The goal of pulsed-power water treatment is to form a non-adherent powder rather than an adherent scale.

The fundamental effect of pulsed-power water treatment is the creation of nucleation sites (seed crystals) in the bulk solution. Some assert that the electric fields create a localized environment, particularly near surfaces, where seed crystals form from dissolved ions [10]. Others theorize that the electric fields and ionic currents affect the diffuse layer surrounding sub-micron suspended particles, allowing them to become nucleation sites [11].

Experiments show clearly that after passing through the PPS device precipitation will preferentially occur as a non-adherent powder rather than an adherent scale [1].

PULSED-POWERED UNITS

The units consist of two components: a transformer panel containing the electronics for pulse generation, and a coil-pipe assembly piece consisting of an unobstructed flow pipe and multiple coils outside of the flow pipe. The units usually are being constructed in pipe sizes from 1" diameter to 12" diameter. Figure 2 illustrates the orientation of the coils.

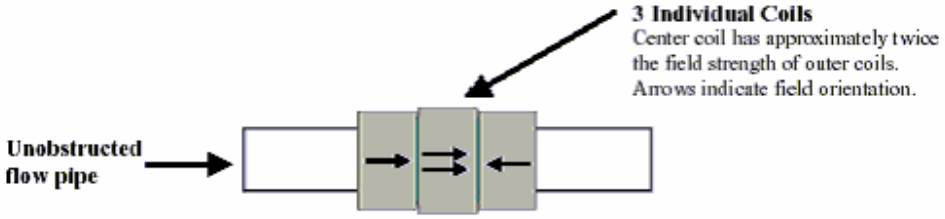

Fig. 2 Pulse power device [1]

FOULING FACTOR DETERMINATION

The fouling test technique developed at Drexel University was used to study the efficacy of PPS equipment to prevent scaling [12].

The universal heat transfer coefficient (U) is calculated from the log mean temperature difference (LMTD), which was obtained from the four temperatures measured at both the inlet and outlet of the cold and hot steams with measurements taken every 10 minutes, figure.3.

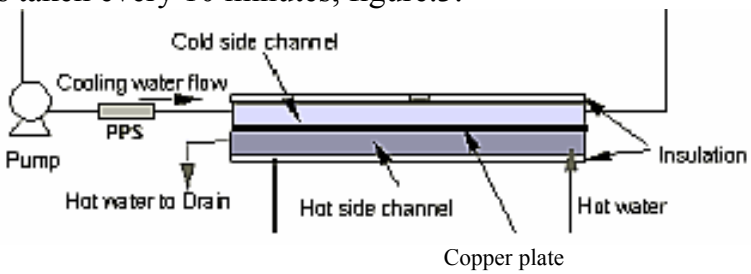

Fig. 3 Part of the installation for the determination of the fouling factor [12]

$$Q = m\, Cp(Tc,out - Tc,in) / A \quad (1)$$

$$U = Q / (A\, \Delta T_{LMTD}) \quad (2)$$

$$\Delta T_{LTMD} = \frac{(Th,in - Tc,out) - (Th,out - Tc,in)}{\ln[(Th,in - Tc,out)/(Th,out - Tc,in)]} \quad (3)$$

Q = heat transfer rate; m = mass flow rate of water; Cp = heat capacity of water; A = heat transfer surface area; Tc,in = inlet temperature of cold water; Tc,out = outlet temperature of cold water; Th,in = inlet temperature of hot water; Th,out = outlet temperature of hot water [12].

These U data are then used to calculate a fouling factor (R_f) defined by the following formula:

$$R_f = 1/U_{fouled} - 1/U_{clean} \quad (4)$$

U_{fouled} is the calculated heat transfer coefficient at a specific time, and U_{clean} is the heat transfer coefficient of a clean plate. Figure 4 shows the variation of the universal heat transfer coefficient (U) over time for the control test and how U_{clean} is determined.

The fouling factor (Rf) is a measure of the resistance to heat transfer due to fouling. Thus the higher the (Rf) value, the poorer the heat transfer.

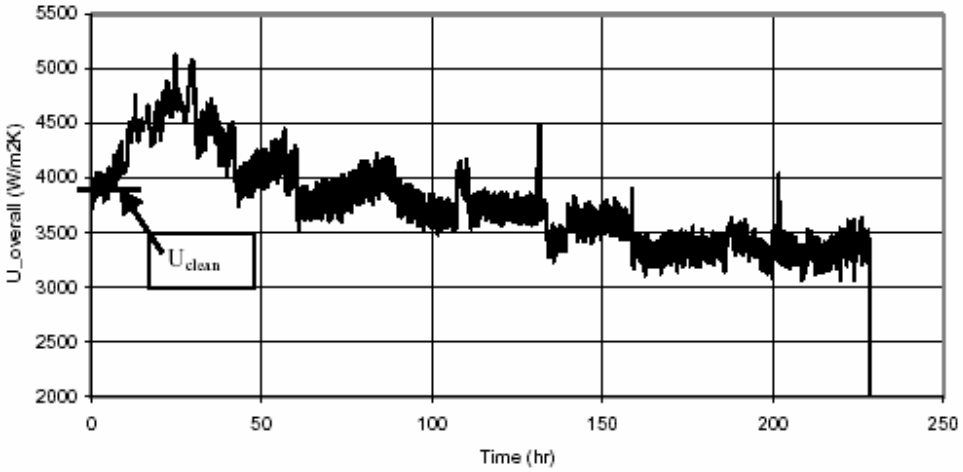

Fig. 4 Universal heat transfer coefficient (U) for no water treatment [1]

The no-treatment case, Figure 5, exhibited a typical R_f curve. For the initial period (up to 25 hours) Rf actually decreases as the heat transfer increases. The cause of this increase in heat transfer is an increase in turbulence at the surface of the plate due to the initiation of crystal growth. In a sense, the initial deposits convert a smooth heat transfer surface to an enhanced heat transfer surface.

After the first 25 hours the deposit covers enough of the surface so that the thermal insulating effect of the deposit exceeds the fluid mechanical improvement from a roughened surface.

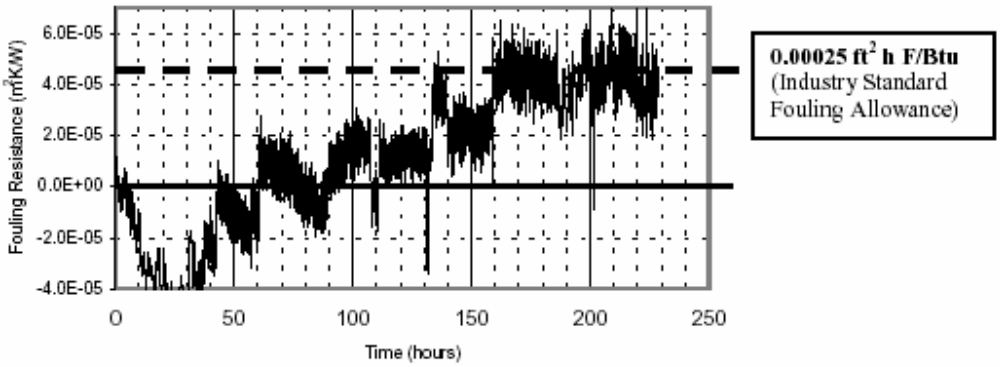

Fig. 5 Fouling factor R_f for no water treatment [1]

RESULTS ON PPS TREATMENT

The characteristic diagram of the fouling factor resulted from tests using a PPS device is shown in Figure 6.

The PPS Treatment case did not exhibit an initial drop in R_f because there were no crystals nucleating and growing from the surface of the plate.

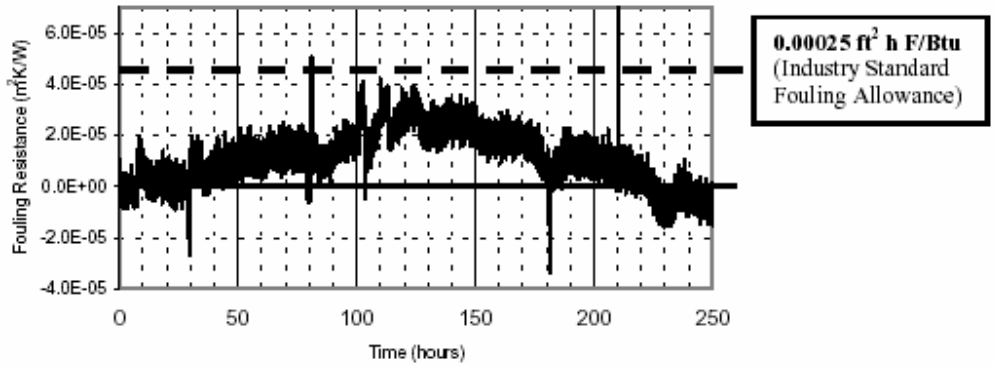

Fig. 6. Fouling factor with PPS treatment [1]

The PPS R_f curve, figure 6, has a hump in the middle.

After the test, a visual inspection of the entire heat transfer surface revealed a small area of what appeared to be impacted particles at the outlet of the channel.

It is theorized that this deposit initially caused a small increase in R_f that peaked at 125 hours. After that point, the deposit became unstable and was reduced. The removal rate of the deposit was greater than the additional deposit by impaction, resulting in R_f decreasing with time and eventually returning to (approximately) its initial start point [1].

Visual and microscopic examination of the heat transfer area at the end of the test showed that the area was completely free of deposits except for the small area at the outlet where localized turbulence (produced by 90 degree turn of flow)

caused some suspended particle deposition. This small deposit was not strongly adherent to the plate. At the end of the test, there was no measured loss of heat transfer.

THE COOLING SYSTEM OF THE INDUCTION FURNACE

An induction furnace has a simple and efficient cooling system type once-through cooling operation. The cooling device is meant to ensure the temperature for the main coil (inductor) that surrounds the crucible that sustains the melted metal. The cooling of the inductor is achieved through a coiled pipe bonded on the inductor, using low temperature bonding alloys.

For the cooling system of an induction heating furnace, scale deposition is an issue and the reduction of heat transfer following a curve similar to that depicted above means a reduction in the working capacity of the furnace. So, the engineer must be careful to not exceed the time of use of the cooling system and must do the necessary corrections in what concern the furnace loading.

If one would operate the furnace without taking into account the loss of heat transfer in the cooling system, some major problems in the work safety may occur, the main coil being overheated and, some water licks may occur because of melting of the low temperature bonding alloys. This is why, scaling deposits must be removed periodically. Using the classic chemical procedure it means the programmed interruption of the technological process.

By using the power pulsed system for preventing scale formation, several advantages are obvious: the use of the furnace at its designed capacity, the enhancing of the working time and the enhancing of the work safety.

Of course there are some expenses with the energy and with the PP device and further economic investigations must be conducted.

CONCLUSION

Pulsed-power can be an effective and environmentally responsible tool to control scale formation in industrial waters. Pulsed-power reliably alters the precipitation of calcium carbonate from an adherent, surface-nucleating scale to a non-adherent, bulk-solution powder.

This technique has been commercialized in both recirculating water of cooling towers and once-through heating operations, including low-pressure steam boilers.

I consider that the cooling system of the induction heating furnace is an installation where calcium carbonate scale formation is an issue, and pulsed-power should be considered as a green alternative to resolve it and more.

If the economical calculations will give satisfaction the introduction of this procedure could be a significant improvement of this type of furnaces.

REFERENCES

1. Lane, J., Cho, Young, Kim, Wontae, Pulsed-Power water Treatment as a Green scale Inhibitor for HVAC and Once –Through Industrial Systems, NACE International Conference 2004, poster session.
2. NACE International Publication 7K189, "Control Factors in Performance Testing of Nonchemical Water Treatment Devices," Reaffirmed 1997.
3. Betts Handbook of Industrial Water Conditioning, 9th Edition, 1991.
4. Water-Formed Scale Deposits, Cowan J. and Weintritt D., Gulf Publishing Company, 1976.
5. Zeta Potential: A Complete Course in 5 Minutes, Zeta-Meter, Inc., Staunton, VA.
6. Lane J. and Kutner G., Cooling Technology Institute Paper No. TP00-03, "A Non-Chemical Water Treatment Device," February 2000.
7. Lane J. and Opheim D., International Water Conference Paper No. IWC-01-54, "Biological Control in Cooling Towers Treated with Pulsed-Power Systems," October 2001.
8. Lane J. and Peck D., Cooling Technology Institute Paper No. TP03-21, "Condenser Water Treatment Using Pulsed Power", February 2003.
9. Kitzman K. et al, International Water Conference Paper No. IWC-03-22, "Chemical vs. Non-chemical Cooling Water Treatments – a Side-by-side Comparison", October 2003.
10. Cho, Y.I., C. Fan, and B.-G. Choi, "Theory of Electronic Anti-Fouling technology to Control Precipitation Fouling in Heat Exchangers, *Int. Comm. Heat Mass Transfer*, Vol. 24, pp 757-770, 1997.
11. Chibowski, E., L. Holysz, and W. Wojcik, "Changes in Zeta Potential and Surface Free Energy of Calcium Carbonate due to Exposure to Radiofrequency Electric Field", *Colloids and Surfaces A: Physical and Engineering Aspects*, pp 79-85, 1994.
12. Cho, Y.I., Kim W., Lee S.., ASHRAE Paper CH-03-3-3 (RP-1155) "Physical Water Treatment for the Mitigation of Mineral Fouling in Cooling-Tower Water Applications," January 2003.
13. WaterCycle Rx, French Creek Software, Inc., Kimberton, PA.

TRATAREA PE CALE NON-CHIMICA A APEI PENTRU RACIREA CUPTOARELOR CU INCALZIRE PRIN INDUCTIE

Rezumat: Lucrarea prezinta posibilitatea aplicarii unui mod non-chimic de tratare a apei pentru a reduce depunerile de piatra in sistemul de racire al cuptoarelor cu incalzire prin inductie. Se descrie modificarea precipitarii mineralelor in apa utilizand un sistem cu pulsuri electrice [i aplicatiile posibile ale metodei la utilajul metalurgic.

BULETINUL INSTITUTULUI POLITEHNIC DIN IAŞI
Tomul LIII (LVII), Fasc. 3, 2007
Secția
ŞTIINȚA ŞI INGINERIA MATERIALELOR

SOME ISSUES IN REGARD OF THE EXPERIMENTAL SHEAR MODULUS DETERMINATION FOR UNIDIRECTIONAL COMPOSITE MATERIALS

BY

MARIAN MAREŞ and BOGDAN LEIȚOIU

Abstract: The Iosipescu shear test is largely accepted as a reliable experimental method, for a wide range of composites. The "ten-degree off-axis" test is also considered as an accurate procedure for determining the shear modulus of composites with unidirectional long fibre reinforcement.
For both above-cited methods, the shear modulus value can be determined using the shear stress-strain dependence for the studied composite material. The trend line of that curve indicates an approximate value of the in-plane shear modulus (G_{12}), representing the slope of that line.
The present paper deals with a comparison of experimental data resulted from the appliance of both Iosipescu shear test and ten-degree off-axis test, on a composite based on a matrix of epoxy resin, with unidirectional carbon fiber reinforcement.
Keywords: Carbon/epoxy, unidirectional composite, shear modulus, 10° off-axis tension test, Iosipescu shear test.

The choice of a general method for studying the shear properties of composite materials is still controversial, although a large variety of experimental techniques were proposed [8]. The present paper deals with two of the most frequently used, for composites with unidirectional reinforcement.

1. Theoretical Consideration

A. About the Iosipescu Shear Test Method

Although that test was firstly introduced for metals [5], it was then developed in order to be applied on composite materials [9], and a variety of fixtures was proposed for increasing the reliability of experimental results [2]. For an accurate measurement of shear strain, special strain gage rosettes were introduced [4].

In this paper, an Iosipescu shear test is described. The experiments were done according to ASTM Standard D 5379 [13], in order to evaluate the shear modulus of the studied composite. A modified Idaho University fixture (IU fixture) (Fig. 3) was used, together with a double-side shear gage instrumentation (Fig. 2) of double-notched composite specimens (Fig. 1). The entire experimental procedure was

described elsewhere [10], together with the method that was used for analysing the experimental data.

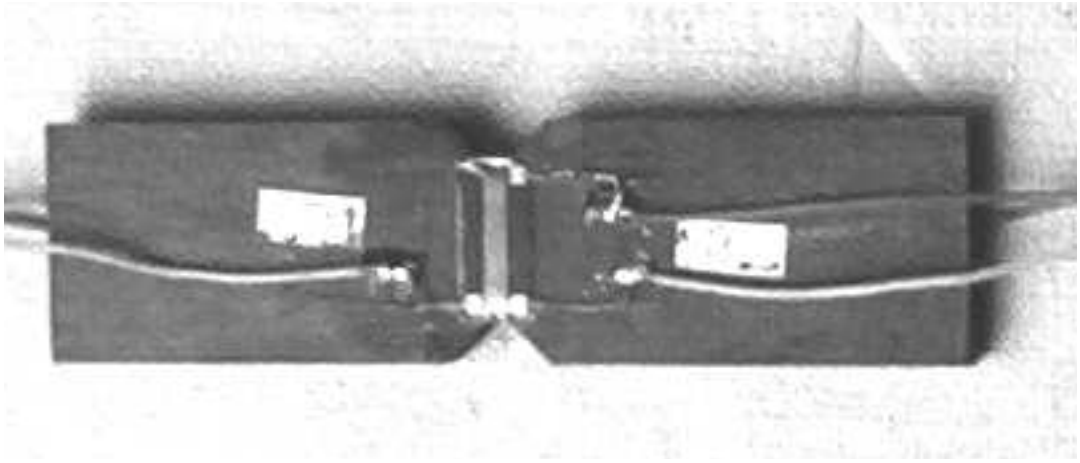

Fig. 1. The instrumented Iosipescu specimen

The shear modulus is determined as the slope of the straight line which approximates the shear stress-strain curve, in the loading stage of the experiment:

$$G_{12} = \frac{\Delta\tau_{12}}{\Delta\gamma_{12}} \tag{1}$$

where, $\Delta\tau_{12}$, $\Delta\gamma_{12}$ are the increments of shear stress and strain, respectively, for two precise levels of loading force (Fig. 4).

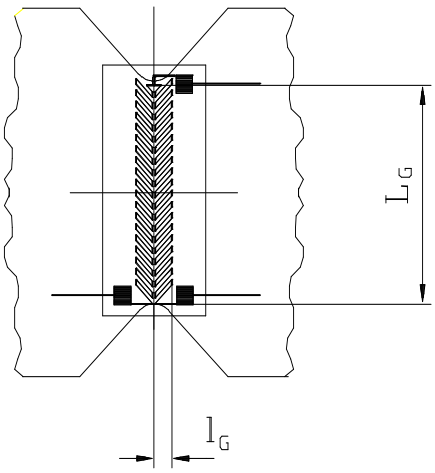

Fig. 2. Special shear gage rosette, placed in the shear section of Iosipescu specimen

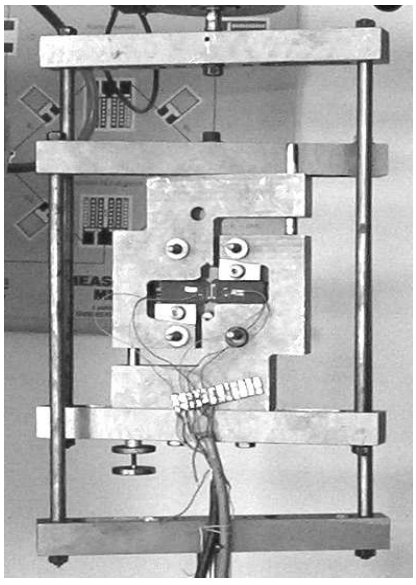

Fig. 3. The actual Iosipescu shear test fixture

For the calculus of the stress increment, the following relation is used:

$$\Delta\tau = \frac{\Delta F}{A} = \frac{\Delta F}{w \cdot h} \tag{2}$$

where ΔF is the load increment, and $A=w\cdot h$ is the gage area of the specimen.

On the other hand, the shear strain directly results from the extensional strains measured by the two transducers from the gage rosette:

$$\gamma_{12} = \varepsilon_1 - \varepsilon_2 . \tag{3}$$

B. About the ten-degree off-axis method

The ten-degree off-axis tension test (for shear properties study) was firstly introduced by Chamis and Sinclair in 1977 [Ref.1], as a specific method for testing fibrous composites.

When looking in principle, the method consists in a uniaxial tensile test of a unidirectional laminate (Fig. 4) with fibers oriented at an angle (θ) from the loading direction. Based on the previous experience about the method appliance, the 10° angle was chosen in order to minimize the effects of longitudinal and transverse stress components, σ_1 and σ_2, on the material shear response (see Ref. [3] and [11]).

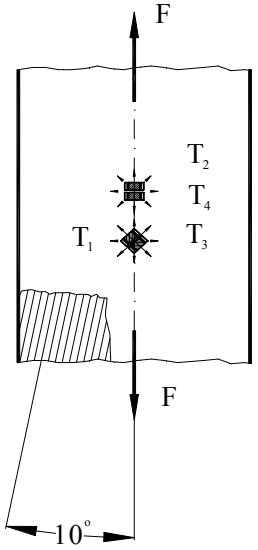

Fig. 4. Fiber direction and strain gages position on the specimen.

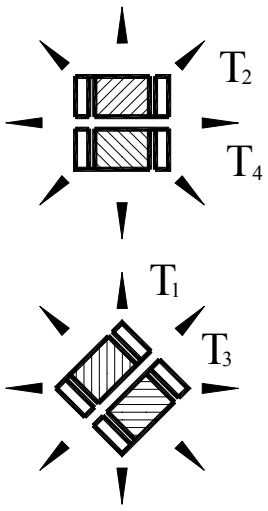

Fig. 5. The configuration of gage rosettes

It is important to note that the specimen is not properly placed into a state of pure shear stress, but under the action of a combined state of stresses. The stress on the tensile direction can be calculated from the loading force (F) and the transverse section area (A) of the specimen, as:

$$\sigma_x = \frac{F}{A} \tag{4}$$

so, the stress components, when reporting to the principal material axes, are:

$$\sigma_1 = \sigma_x \cdot \cos^2\theta , \quad \sigma_2 = \sigma_x \cdot \sin^2\theta , \quad \tau_{12} = -\sigma_x \cdot \cos\theta \cdot \sin\theta \tag{5}$$

For the present experiment, the basic component is the in-plane shear stress τ_{12}, and it can be obtained as a numerical value using the actual value θ = -10°, as follows:

$$\tau_{12} = 0{,}171 \cdot \sigma_x \tag{6}$$

On the other hand, in order to observe the shear response of the studied material, the corresponding value of shear strain is calculated as:

$$\gamma_{12} = \varepsilon_x (\sin 2\theta - \cos 2\theta) - \varepsilon_y (\sin 2\theta + \cos 2\theta) + 2\varepsilon_{45} \cos 2\theta \tag{7}$$

The strain values $\varepsilon_x=\varepsilon_1$, $\varepsilon_y=\varepsilon_2$, $\varepsilon_{45}=\varepsilon_3$ are obtained from three of the four strain gages of the rosettes that are placed on the longitudinal axis of the specimen (Fig. 5), as follows:

- T_1 and T_3 are, respectively, parallel and normal to the loading direction;
- T_2 is oriented at 45° from the same direction.

The *real value* of shear strain is obtained from the indications of the bridge instrument and its final calculus relation is:

$$\gamma_{12,TS} = -0.620295\hat{\varepsilon}_1 + 1.950524\hat{\varepsilon}_2 - 1.330228\hat{\varepsilon}_3 \tag{8}$$

where the coefficients of strain values include the two correction factors resulted from transversal sensitivity of transducers and from the level of tension voltage supply of the Wheatstone bridge, and $\hat{\varepsilon}_1, \hat{\varepsilon}_2, \hat{\varepsilon}_3,$ are the extensional stresses read as the indications of the electronic bridge.

2. EXPERIMENTAL DETAILS

A. Iosipescu Shear Tests

The studied composite is based on an epoxy resin, with unidirectional carbon fibre as reinforcement, in 68% volume content. The specimen was cut from a plate, with 3.3 mm in thickness, having 24 plies. The gage area of the specimen is:

$$A = 3{,}3\text{mm} \cdot 10{,}7\text{mm} = 35.31\text{mm}^2$$

The shear gages are produced by Micro Measurements (Vishay) and are on type N2P-08-C032A-500.

The tension voltage supply for the Wheatstone bridge was U_A=2V, in order to limit the heating of composite material, into the vicinity of transducers.

In order to obtain an accurate measurement, the shear strain on each rosette was read, separately, for an entire loading-unloading cycle, and with a previous bridge calibration at the beginning of each process.

Secondly, the shear strain was determined as the average of signals delivered by the transducers placed both on the front and back of the specimen.

The real shear strain value must be calculated on the basis of corresponding instrument indication γ_{12}^{read}, multiplied by the following two factors:

- the ratio of the standard and the real voltage supply of the bridge: 4V/2V=2
- the transverse sensitivity correction factor of transducer, determined from the producer recommendations, as

$$C_{s-tr} = \frac{1-\nu_0 K_t}{1+K_t} = \frac{1-0,285\cdot 0,019}{1+0,019} = 0,97604 \tag{9}$$

As a consequence, the effective shear strain is:

$$\gamma_{12} = \varepsilon_{+45^o} - \varepsilon_{-45^o} = 2\cdot 0,97604\cdot \gamma_{12}^{read} = 1,952\gamma_{12}^{read} \tag{10}$$

In order to be replaced into the above relation (1), the strain increment $\Delta\gamma_{12}$ is determined as the difference of the shear strains corresponding to two different level of loading force, the same values that were used at the calculus of $\Delta\tau_{12}$ (Fig. 6).

Based on experimental data, one can plot the shear stress-strain dependence for the studied material. Consequently, the shear modulus can be determined as the slope of the trend line of that curve, plotted by a mathematical program (Fig. 6).

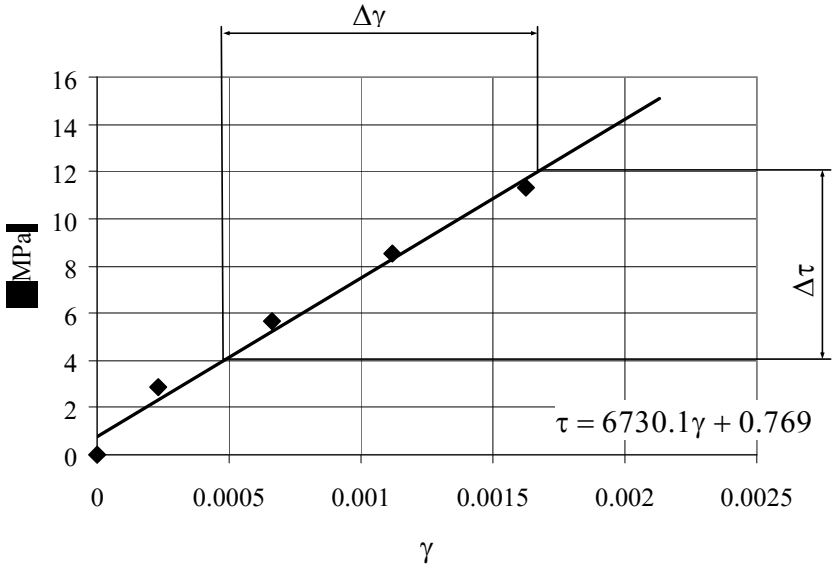

Fig. 6. The trend line for the shear stress-strain response of the 0º carbon / epoxy specimen.

On the other hand, one can observe that the shear modulus value is done by the coefficient of the shear strain term **γ**, from the trend line equation. As an example, using the experimental results that were plotted in Figure 6, the value of shear modulus is:

$$G_{12} = 6730.1 \text{ MPa}.$$

It is important to note that the method also allows establishing the shear modulus using the response of a single rosette (with the favorable effect of expenses decreasing), bonded on one face of the specimen. In this case, the experimental data leaded to an average value of $G_{av} = 6374.33$ MPa. One can suppose that the difference

of the two cathegories of results is caused by the errors induced by some imperfections of electronic device that were used in the present experiments.

The cited values of shear modulus are in good agreement with experimental data that are presented in literature for unidirectional carbon/epoxy composites, and also with the results previously obtained, by the same authors.

One can conclude that the Iosipescu shear test leads to an accurate determination of shear modulus of composite materials, on condition that one can use a precise fixture design and the experimental conditions indicated by the standard test method.

B. 10° off-axis tests

The studied composite is also based on an epoxy resin, reinforced with unidirectional carbon fibre, having a volume fraction of 68%. The specimen width is l=15.8mm=2h, with the thickness g=3.3mm and the gage length is L=90mm.

The aspect ratio of the specimen is L/h = 11.39, sufficiently high for neglecting the clamping influence on the stress state in the specimen.

The strain gage rosettes are EA-13-062TV-350 type, from Micro-Measurements Vishay, and it were bonded as indicated in Figure 5. The tension voltage supply was chosen at the level of 2V in order to prevent the local heating into the composite, near the transducer zone (see Ref.[12]).

The experiments were made on a "Textenser" testing machine, with 500N as the maximum loading force.

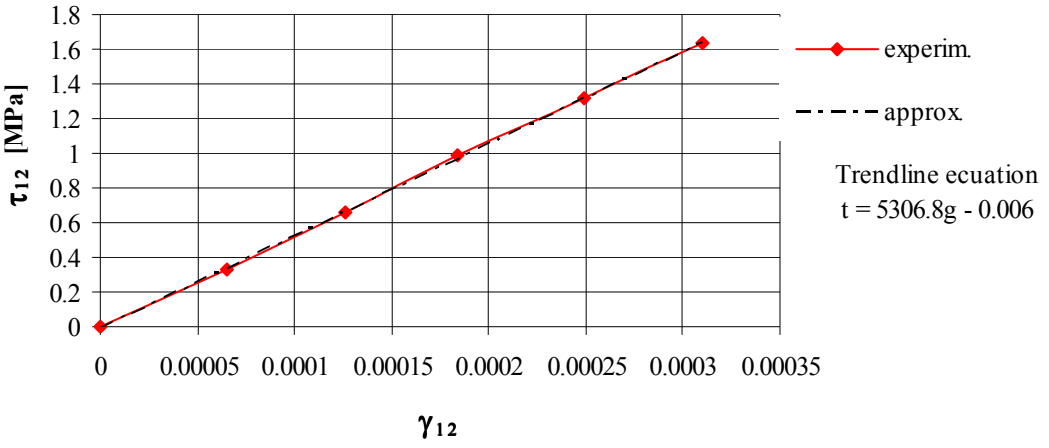

Fig. 7. The average shear response of the studied composite and the trend line of stress-strain curve.

Using the calculated values from the above-cited relations (8) and (10), corresponding to certain levels of loading force (F), one can plot the variation of shear stress-strain dependence for the studied composite material. (see Fig. 7). The trend line of that curve indicates an approximate value of the in-plane shear modulus (G_{12}), representing the slope of that line.

In fact, the resulted shear modulus value is G_{12}=5306.8MPa.

It can be observed that a different level of this value was obtained, in comparison with the value given by Iosipescu shear test. One can consider, as a reason

for that difference, the range values of shear stresses, for the two types of experiments, caused by their specific appliance. So, for the Iosipescu shear tests, a much larger range of shear stress values can be used.

3. RESULTS AND DISCUSSION

The above-described test methods were both proved as reliable for determining the shear properties of composite materials.

Based on the cited results, one can emphasize some particular issues of the two methods appliance:

- For the Iosipescu shear test, the entire applied load develops the shear stress into the gage area of the specimen. On the other hand, for the ten-degree off-axis tension test, only a small part of the applied load contributes for developing of the shear stress into the specimen. As a consequence, the Iosipescu shear test leads to a higher shear stress level, into the gage section of the specimen, than the 10° off axis tension test.
- The Iosipescu shear test allows the development of a pure shear stress state, using just a small material sample. The most important conditions for a reliable appliance of that test are related with the specimen processing precision and with the safety of the shear fixture. One can consider (based on Refs. [2], [6], [8], [10]) that the Idaho fixture is a better variant than the Wyoming fixture, although that one is agreed by the ASTM 5379-93.
- The ten-degree off-axis tension test seems to be suitable for thin plates of composite materials, containing a few layers (lamina). An Iosipescu specimen made from this kind of material could be in danger of buckling in the fixture, where it is compressed on two opposite sides. However, Ref. [7] presents an example of buckling avoidance, for thin samples, consisting in strengthening of gripped sides of the specimen.

Received April 2nd 2007

Technical University of Iassy
Department of Strength of Materials

R E F E R E N C E S

1. C h a m i s C.C., S i n c l a i r J.H., *Ten-deg. off-axis test for shear properties in fibre composites*, Exp. Mech., vol. 17, 1977, pp. 339-346.
2. C o n a n t R.N., O d o m E. M., *An Improved Iosipescu Shear Test Fixture*, Journal of Composites Technology & Research, vol. 17, 1995, pp. 50-55.
3. D a n i e l I.M., I s h a i O., *Engineering Mechanics of Composite Materials*, Oxford University Press, New York, 1994, pp. 323-324.
4. I f j u P.G., *The Shear Gage: For a Reliable Shear Modulus Measurements of Composite Material*, Exp. Mech., vol. 34, 1994, pp. 369-378.
5. I o s i p e s c u N., *New Accurate Procedure for Single Shear Testing of Metals*, Journal of Materials, vol.2, nr.3, 1967, pp. 537-566.

6. L e i ţ o i u B., *Contribuţii la îmbunătăţirea formei epruvetelor din materiale metalice şi compozite folosite la încercările metalice*, teză de doctorat, Univ. Tehn. „Gh. Asachi", Iaşi, 1998.
7. L e i ţ o i u B., A n t o h e M.E., M a r e ş M., *A Iosipescu thin specimen setting variant for shear study*, Bul. I.P. Iasi, tom LI (LV), fasc. 3, 2005, pp. 161-164.
8. M a r e ş M., L e i ţ o i u B., *Consideraţii asupra metodelor de încercare la forfecare aplicate materialelor compozite*, Construcţia de maşini, nr. 9-10, 1999, pg. 38-47.
9. M a r e ş M., L e i ţ o i u B., *Iosipescu shear test as applied to some composite materials*, Bul. I.P. Iasi, tom L (LIV), fasc. 6B, 2004, pp. 185-190.
10. M a r e ş M., L e i ţ o i u B., *The application of Iosipescu shear test for accurate determination of in-plane shear modulus, for metal matrix composites*, Bul. I.P. Iasi, tom LI (LV), fasc. 3, 2005, pp. 165-172.
11. P i e r r o n F., V a u t r i n A., *The 10° off-axis tensile test: a critical approach*, Comp. Science & Technology, vol. 56, 1996, pp. 483-488.
12. www.measurementsgroup.com, *Errors due to transverse sensitivity in strain gages*.
13. ASTM Standard D 5379-93, *Standard Test Method for Shear Properties of Composite Materials by the V-Notched Beam Method*, Annual Book of ASTM Standards, vol.15.03, 1996, pp. 235-247.

ASPECTE PRIVIND DETERMINAREA EXPERIMENTALA A MODULULUI TRANSVERSAL DE ELASTICITATE, PENTRU COMPOZITELE ARMATE UNIDIRECŢIONAL

(Rezumat)

Testul de forfecare Iosipescu este acceptat, pe plan internaţional, drept o metodă experimentală de încredere pentru studiul proprietăţilor unei game largi de materiale compozite. De asemenea, încercarea de tracţiune dezaxată este tot mai mult folosită pentru stabilirea modulului de elasticitate transversal, în cazul materialele armate cu fibre lungi, aşezate pe o singură direcţie.

Pentru ambele metode, valoarea modulului se calculează ca pantă a zonei iniţiale de pe curba caracteristică de forfecare a compozitului studiat, care se trasează folosind valorile tensiunilor şi deformaţiilor specifice obţinute prin experimente.

Lucrarea de faţă prezintă o comparaţie între datele obţinute prin încercarea de tracţiune dezaxată, respectiv prin aplicarea testului de forfecare Iosipescu, cu privire la modulul transversal al unui compozit cu matrice din răşină epoxidică şi armare cu fibre de carbon unidirecţionale.

BULETINUL INSTITUTULUI POLITEHNIC DIN IAŞI
Tomul LIII (LVII), Fasc. 3, 2007
Secţia
ŞTIINŢA ŞI INGINERIA MATERIALELOR

THE INFLUENCE OF CENTRIFUGED BALLS HARDENING ON THE WEAR RESISTANCE OF SOME CAST IRON SURFACES

BY

MARIAN MAREŞ, DORIN CONDURACHE and VASILE BULANCEA

Abstract: The centrifuged balls processing is considered as one of the best, of the many available methods that are used, for hardening the inner surfaces of different pieces.
This paper presents the use of that method in order to increase the wear resistance of some cast iron (Fc 250 on type) surfaces. The tribological tests were based on a dry-sliding shoe-on-ring tribo-model, with the contact on the inner cylindrical surface of the cast iron ring. The loss weight for the cast iron shoe was measured, after a fixed value of sliding distance.
On the basis of experimental results, one can consider that the surface hardening leads to an increase of wear resistance, for the studied material, in comparison with the unprocessed surface. On the other hand, it seams that the cited-effect tends to be insignificant, upper of a certain level of hardness increasing.
Keywords: surface hardening, plastic deformation, wear resistance.

1. INTRODUCTION

It is well known that, in principle, an increase in superficial micro-hardness directly influences the corrosion, wear and fatigue resistance of a certain material.

The cold plastic deformation is largely used, into the machine parts design and construction, in order to increase the hardness of their superficial layers. That purpose can be achieved by using various methods. One of the most reliable, mainly for be applied on the inner cylindrical surfaces, is the centrifuged balls processing [Ref. 1, 5].

The present paper deals with analyzing the influence of that type of surface hardening, on the wear resistance of some cast iron parts.

2. MATERIALS AND METHOD

Using the above-cited procedure, the cold plastic deformation of the processed parts was obtained by striking their surfaces with centrifuged steel balls [Ref. 3]. The balls are assembled in some special designed tools [Ref. 2] that are moving, in the necessary directions, on the inner cylindrical surface of the rotating processed part.

The studied material was cast iron Fc 250 (3.2% C, 1.78% Si, 0.78% Mn, 0.28% P and 0.1% S).

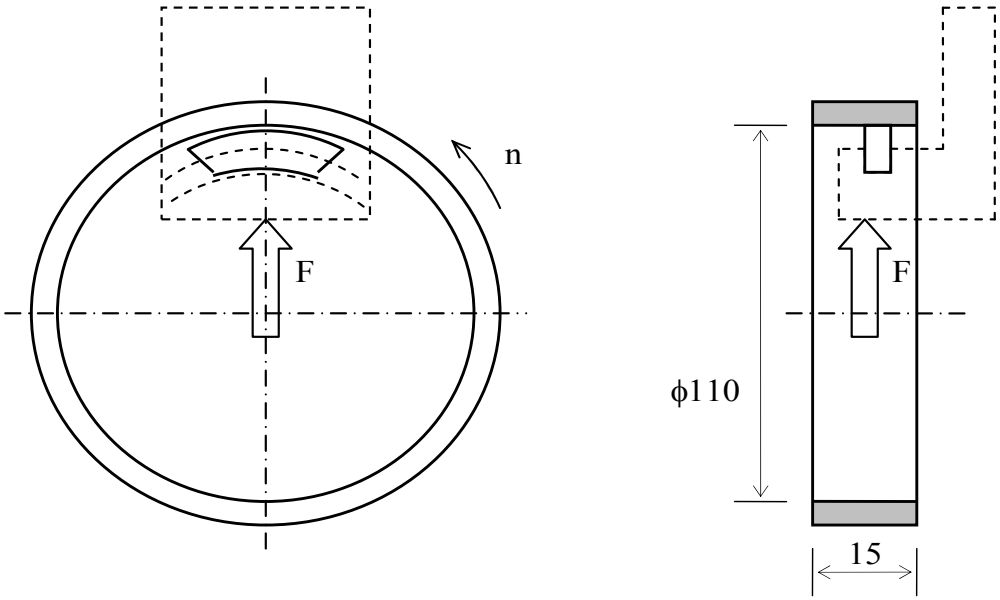

Fig.1

The cast iron rings were cut at ϕ120×ϕ110×15 mm, then their inner surfaces were processed with two sets of mechanically centrifuged balls, in different regimes, in order to obtain different values of surface micro-hardness.

Tribological behaviour of the investigated materials was evaluated in tests (see Ref. 4) that were using cast iron shoes (Fig. 1) sliding, in dry condition, against the inner surface of the rotating ring.

3. RESULTS AND DISCUSSION

For quantifying the influence of ring surface hardening on its wear resistance, three types of samples were considered (see Table 1) with increasing micro-hardness values, from 180HV to 290HV. Some rings unprocessed by inner plastic deformation were also used, in order to be compared with the processed rings.

Following each step of tribological tests, the weight-loss of the shoe was measured, after a constant value of sliding distance (L_s=250m). The data from Table 1 are the average values of weight-loss for the corresponding set of tests, and are including (inside of the brackets) the total (averaged) weight-loss of the shoe, in sliding contact with the respective type of rings.

Table 1

Type of sample	Micro-hardness [HV]	Δm_1 (Δm_t) [mg]	Δm_2 (Δm_t) [mg]	Δm_3 (Δm_t) [mg]	Δm_4 (Δm_t) [mg]
0	120	11	4 (15)	2 (17)	6 (23)
1	180	24	10 (34)	3 (37)	2 (39)
2	225	32	11 (43)	2 (45)	2 (47)
3	290	35	12 (47)	1 (48)	1 (49)

The experimental data were used for plotting the variation of total weight-loss, as a function of sliding distance (see Fig. 2). One can observe the tendency of decreasing for the distance between the curves that are corresponding to the selected types of material samples.

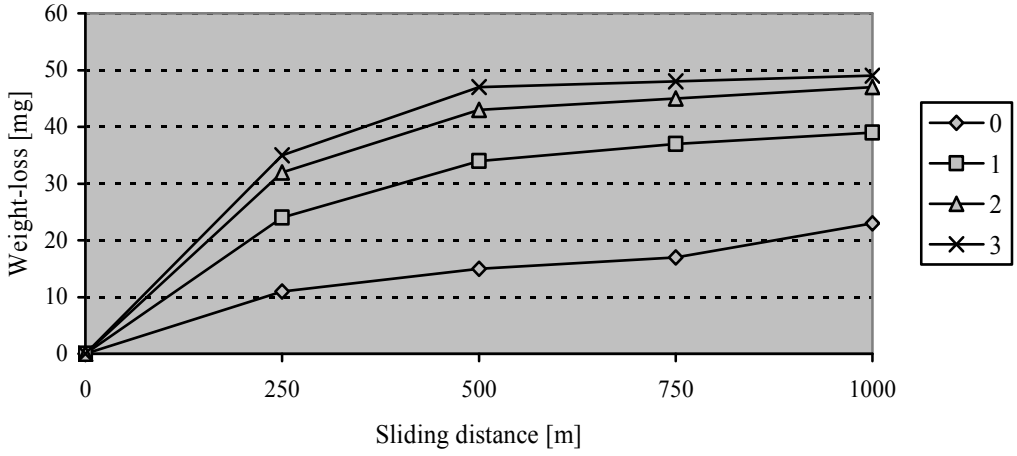

Fig. 2

4. CONCLUSIONS

The experiments that were depicted in this paper were focused on the effects of hardening made by striking with centrifuged balls, on the materials tribological behaviour.

On the basis of the above-cited results, one can consider that the superficial hardening by cold deformation has a marked influence on the wear resistance of the processed material. In fact, one can consider that the increase of micro-hardness leads to an increase of wear resistance.

On the other hand, it seams that this effect tends to be less significant, when continuing the increase of hardness, over a certain level of its value.

Received May 20th 2006

Technical University of Iassy
Department of Machine Design and Mechatronics

R E F E R E N C E S

1. B u l a n c e a D. e. a., *Aspecte constructive şi tehnologice privind ecruisarea pneumo-centrifugală cu impulsuri*, Construcţia de maşini, nr. 8-9, 1994, pg. 39.
2. B u l a n c e a D., *Contribuţii privind durificarea cu bile centrifugate a stratului superficial la suprafeţe interioare*, Ph. D. Thesis, 1997.
3. B u l a n c e a D. e. a., *Rugosity and Microhardness of Striked Metallic Surfaces Using Centrifuged Balls*, EUROMAT 97, vol. 3, p. 139.
4. C r u d u I., M a r e ş M., *The Influence of Reinforcing Particles on the Tribological Properties of Some Aluminum Matrix Composites*, BALKANTRIB 99, vol. 2, p. 49.
5. M a l u r e a n u I. e. a., *The Microstructure and Microhardness of Processed by Centrifuged Balls Cast Iron Surfaces*, Bul. I.P. Iaşi, sec. S.I.M., tom XLII (XLVI), fasc. 3-4, 1996, p. 239.

ASPECTE PRIVIND INFLUENȚA DURIFICĂRII SUPERFICIALE PRIN LOVIRE CU BILE ASUPRA REZISTENȚEI LA UZURĂ A FONTELOR CENUŞII

(Rezumat)

Una dintre cele mai eficiente metode folosite pentru creşterea durității superficiale a materialelor metalice se bazează pe lovirea semifabricatului cu bile centrifugate. Se utilizează scule de construcție specială, care se deplasează în direcțiile necesare pe suprafața interioară a piesei, aflată în mişcare de rotație.

Lucrarea de față are ca obiectiv analiza influenței acestei operații tehnologice asupra comportării la frecare a unor semifabricate din fontă cenuşie. Determinările experimentale s-au făcut pe un tribomodel de tip sabot-inel, cu contact pe suprafața cilindrică interioară.

S-a urmărit modificarea vitezei de uzură a sabotului din oțel turnat, la creşterea durității superficiale a inelelor de fontă, durificate prin lovire. S-a constatat că uzura sabotului creşte, cu intensitate moderată, la creşterea durității inelelor.

BULETINUL INSTITUTULUI POLITEHNIC DIN IAŞI
Tomul LIII (LVII), Fasc. 3, 2007
Secția
ŞTIINȚA ŞI INGINERIA MATERIALELOR

COMPARISON BETWEEN THE POLY(VINYL ALCOHOL) FILMS OBTAINED BY CROSSLINKING WITH GLUTARALDEHYDE USING DIFFERENT TECHNIQUES

BY

SILVIA PATACHIA, CATALIN CROITORU, PEDRO PAIXAO

Abstract: *Polymers crosslinking is one of the methods used for controlling the release properties of the materials applied as matrix in controlled drug delivery. In this paper we compared the sorption properties of poly (vinyl alcohol) films crosslinked with glutaraldehyde in gaseous phase and in aqueous solution, underlining those of the films crosslinked in gaseous phase, as using gaseous crosslinkers usually eliminates the possibility of unreacted toxic compound presence.*

Keywords*: Poly(vinyl alcohol), crosslinking, glutaraldehyde, solution vapours, swelling*

1. INTRODUCTION

Crosslinking is one of the factors that play an important role in the temporisation of active principle elimination in controlled drug delivery [1,4].

Controlled drug delivery occurs when a polymer, whether natural or synthetic, is judiciously combined with a drug or other active agent in such a way that the active agent is released from the material in a predesigned manner [1]. In any case, the purpose behind controlling the drug delivery is to achieve more effective therapies while eliminating the potential for both under- and overdosing.

To be successfully used in controlled drug delivery formulations, a material must be chemically inert and free of leachable impurities. It must also have an appropriate physical structure, with minimal undesired aging, and be readily processable.

A material that fulfils these properties is poly(vinyl alcohol) (PVA) [5].

As known, the temporisation of the active principle release from the polymeric matrix can be achieved by crosslinking. The higher the crosslinking is, the slower the elimination.

Glutaraldehyde [GA] is a good crosslinker for PVA, but it is a toxic compound. In medical applications it is compulsory to avoid as possible the toxic crosslinkers that could remain as unreacted traces in the polymer matrices.

Taking into account that a reaction in gaseous phase leads to a minimizing of the unreacted crosslinker in the polymer matrix, avoiding the crosslinker sorption, in

this paper we present our results concerning the crosslinking of PVA with GA in aqueous solution and with GA in gaseous phase.

We have studied the influence of the GA solution concentration and of the curing duration on the crosslinking degree of PVA film

Crosslinking degree could be appreciated by means of swelling capacity of the PVA films.

2. EXPERIMENTAL

2.1. Materials

Glutaraldehyde 45,232% wt, "Reactivul" Bucuresti

PVA 90-98 (900 polymerization degree and 98% hydrolysis degree) was purchased from Chemical Enterprises Rasnov, Romania. Glutaraldehyde of 45% wt concentration was purchased from „Reactivul" S.A. Bucharest.

2.2. PVA films preparation

The PVA films have been prepared by solution casting and solvent evaporation at room temperature (starting from 10% PVA aqueous solution). The solid content of the prepared solution was determined to be 9.8543%.

2.3. Crosslinking process

Crosslinking with glutaraldehyde was aimed to be obtained, in aqueous and in gaseous phase

Glutaraldehyde of 2,5% wt and 0,1N H_2SO_4 solutions were prepared.

Samples from the obtained films, of equal mass, were placed each in a Berzelius flask that contained 90 mL of glutaraldehyde solution and 2mL of sulphuric acid solution for 1h. The same operations were repeated at different time intervals (2h, 3h).

For crosslinking in gaseous phase the samples of film were placed each in a Berzelius flask that contained 25 mL of 0.1N sulphuric acid solution for 15 min. Then, after film surface drying, it was suspended in an isolated container, over a recipient that contained 2,5mL of 45,232% GA wt. The container was connected to a vacuum pump, as the film to be in contact with GA vapours for different time intervals (1h, 2h, 3h) (Fig. 1).

Each sample was then weight after crosslinking, washed with distilled water and dried for 24h at room temperature.

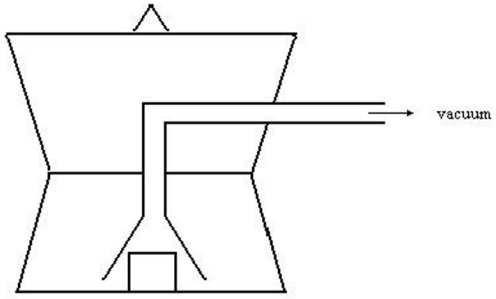

Fig.1 – Installation for crosslinking in gaseous phase

2.4. Determination of swelling isotherms

The crosslinked PVA films were placed in a Berzelius flask that contained 70 mL distilled water. At 5 minutes time interval the film was removed from the flask, superficially dried with filter paper and weight.
This operation was repeated during 1h (the film was removed, dried, weight for 12 times in the 1h interval)

3. RESULTS AND DISCUSSIONS

In figures 2, 3 and 4 respectively, the percentage of absorbed water (%) versus time (min) is plotted, for the films crosslinked in gaseous GA and in GA aqueous solution.

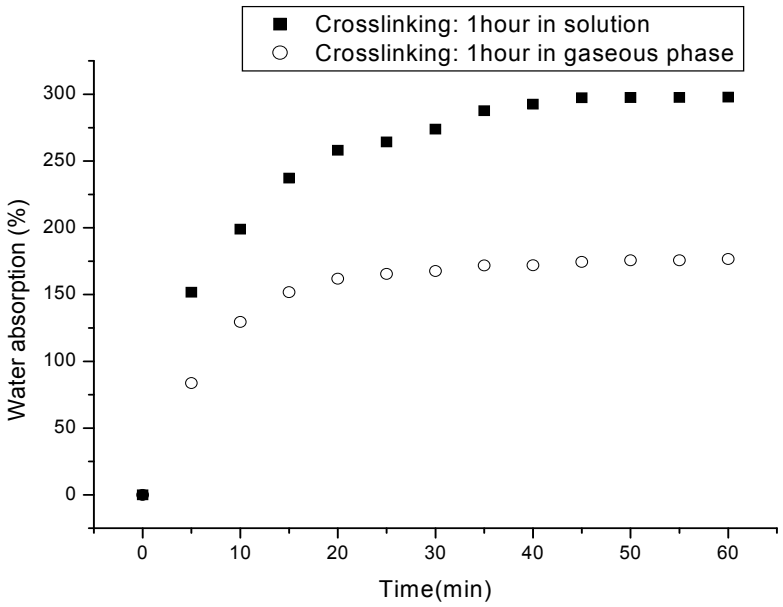

Fig.2 – Water sorption of the 1h crosslinked films in gaseous GA and in GA solution

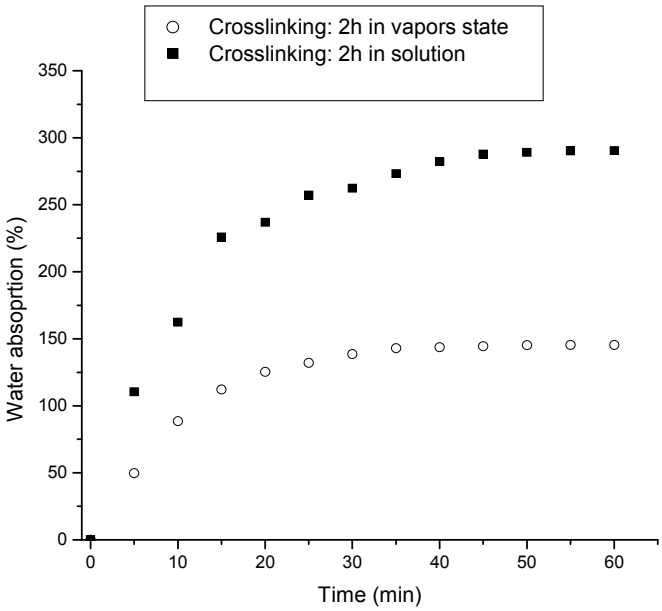

Fig..3 – Water sorption of the 2h crosslinked films in gaseous GA and in GA solution

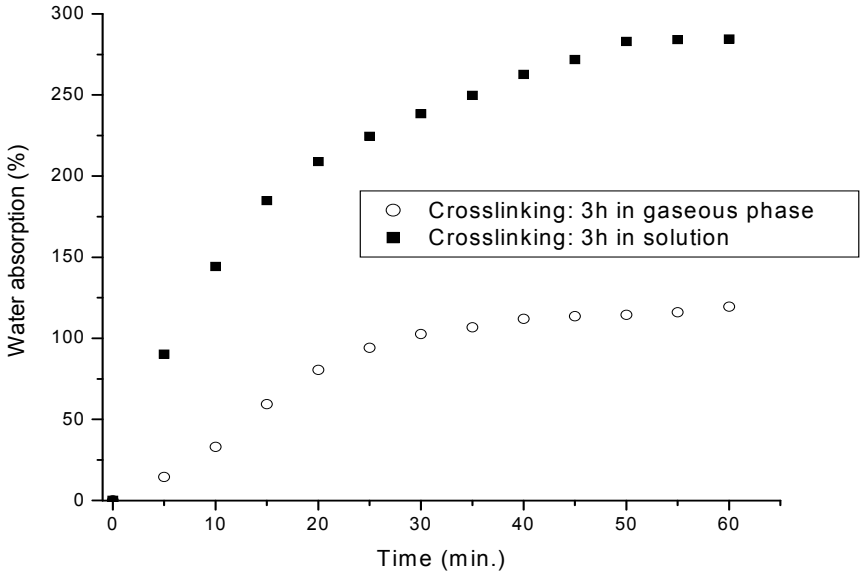

Fig..4 – Water sorption of the 3h crosslinked films in gaseous GA and in GA solution

As expected, for each time interval (1, 2, 3 h) the percentage of absorbed water is smaller in the films crosslinked with gaseous GA, which could mean a higher degree of crosslinking achieved with gaseous GA.

That could be due to the higher concentration of crosslinker in gaseous phase, by the means of vacuum and the ceiledness of the installation used.

From Fig.5 it could be seen that the crosslinking time affects the amount of water absorbed at swelling equilibrium more significant in the case of crosslinking in gaseous phase compared with the crosslinking in solution, probably due to the higher concentration of GA in gaseous phase.

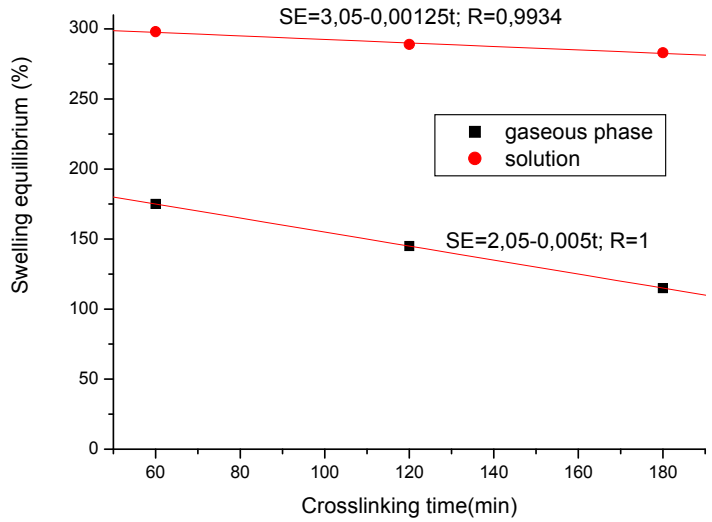

Fig..5 – Water absorbed at swelling equilibrium reaching versus the crosslinking time for crosslinked membrane in gaseous GA and in GA solution

From Fig.6 it can be seen that the time necessary for swelling equilibrium reaching is higher for films crosslinked in GA solution compared with these crosslinked in gaseous phase and also that the increasing of the crosslinking time determines the increasing of the swelling equilibrium reaching time.

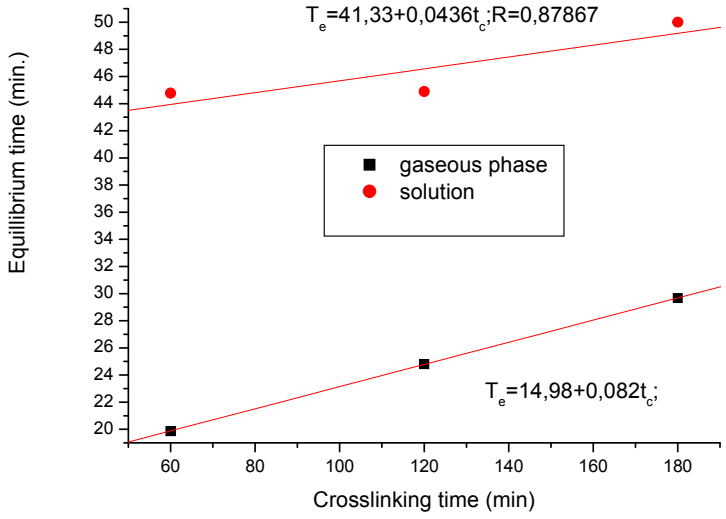

Fig.6 – Time of swelling equilibrium reaching versus the crosslinking time for crosslinked membrane in gaseous GA and in GA solution

4. CONCLUSION

In this paper we have studied the possibilities of PVA films crosslinking with glutaraldehyde in gaseous phase in order to minimize the traces of sorbed or unreacted GA from the film matrix.

We determined the influence of the crosslinking time on the swelling capacity of the PVA films and on the swelling kinetic of films.

We compared the obtained results for PVA films crosslinked in gaseous GA with those obtained for PVA films crosslinked with GA in solution.

It could be seen that the increasing of the crosslinking time leads to the increasing of the crosslinking degree in the polymer matrix and consequently to the decreasing of water sorption. The concentration of the crosslinker is also important: the higher concentration, the smaller water absorption amount.

At low pressure, in the crosslinking installation used, the concentration of GA in gaseous phase was higher than that of the concentration in diluted GA aqueous solution, leading to a higher crosslinking degree for the PVA films.

This technique could be used for crosslinking of the PVA films applied in medical or pharmaceutical fields or for sensitive compounds separation by molecular imprinting technique.

REFERENCES:

1. C.H. Hassan, N.A. Peppas. Adv. Polym. Sci. 2000;153:37.
2. N.A. Peppas, "Hydrogels in medicine and pharmacy", in "Polymers", N.A. Peppas (ed.), vol. 2, CRC, Boca Raton, FL, 1987.
3. A. Danno. J. Phys. Soc. Jpn. 1958; 13:722.
4. N.A. Peppas, E.W. Merrill. J. Appl. Polym. Sci. 1976;20:1457.
5. S. Patachia, "Blends based on poly(vinyl alcohol) and the products based on this polymer", in "Handbook of Polymer blends and composites", C. Vasile and A.K. Kulshreshtha (eds.), Chap. 8, RAPRA Technology LTD., England, Chap.8. 2003. p. 288-365.

Acknowledgement: This study has been elaborated in the frame of CEEX 148/2006 project.

PATACHIA SILVIA[1], CROITORU CATALIN[1], PEDRO PAIXAO[2]
[1]"TRANSILVANIA" UNIVERSITY OF BRASOV, CHEMISTRY DEPARTMENT, BRASOV, ROMANIA
[2]UNIVERSITY OF COIMBRA, CHEMICAL ENGINEERING FACULTY, COIMBRA, PORTUGAL

COMPARATIE INTRE FILMELE DE POLI(ALCOOL VINILIC) RETICULATE CU ALDEHIDA GLUTARICA OBTINUTE PRIN TEHNICI DIFERITE

Abstract: *Reticularea polimerilor este o metoda de control a proprietatilor de eliberare a principiilor active din materiale utilizate pentru obtinerea medicamentelor retard. In aceasta lucrare se prezinta o comparatie a filmelor de poli(alcool vinilic) obtinute prin doua tehnici de reticulare: cu glutaraldehida in solutie, respectiv in faza gazoasa. Reticularea in faza gazoasa este de preferat deoarece minimizeaza prezenta urmelor de aldehida glutarica, toxica, absorbita sau nereactionata in filmul polimer.*

BULETINUL INSTITUTULUI POLITEHNIC DIN IAŞI
Tomul LIII (LVII), Fasc. 3, 2007
Secția
ŞTIINȚA ŞI INGINERIA MATERIALELOR

MICROSTRUCTURAL EVOLUTION OF HEAVY ALLOYS BASED TUNGSTEN THROUGH SINTERING AND THERMOMECHANICAL PROCESS

BY

RADU MUREŞAN

Abstract: *The alloy is characterized by a complex multiphasical structure. The structure of the W-Ni-Fe alloy consists from a refractory phase of the solid solution rich in tungsten and a binder phase, easy inflammable, formed by the solid solution of tungsten and iron in nickel, hardened through dispersion. The behavior of the heavy alloy at plastically deformation and tempering will be determined by the crystalline nature of the phases, by their interaction and by the role of the interphasical limits which are formed at hardening. The aim of this paper is the study of the structural modification of the binder from the easy inflammable phase of the deformed alloy W-Ni-Fe.*

Keywords*: AGW, sintering with liquid phase, composite, metallic powder.*

1. INTRODUCTION

Due to the high demands for the performances of the heavy alloys based tungsten (noted from now on AGW) imposed by the enhancement of their applications, there were developed some methods of mechanical manufacture through plastic deformation, through thermal and thermo-mechanical treatments, to be applied after sintering. These methods have to improve the mechanical properties and especially the toughness and ductility of the AGW, characteristics that are reflected through their tensile; these demands were imposed by the applications from the military field [1].

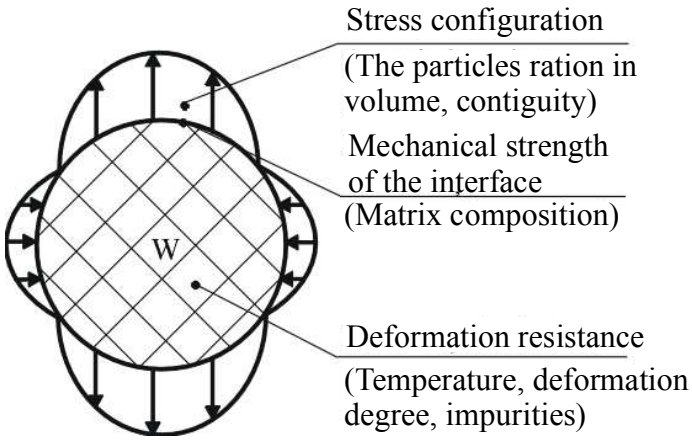

Fig.1. Representation of the stress around the tungsten grains.

Examples of the mentioned manufacturing methods are the cold and/or worm plastic deformation, (cold and/or worm forging, lamination, cold and/or worm isostatic pressing, quasi-isostatic pressing), combined or not with aging thermal treatments through deformation or precipitation

[2]. Through these manufacture methods an especially place has the dehydrogenating thermal treatment, applied to eliminate the remnant hydrogen from AGW after sintering, because his presence may be one of the causes which determine the fragilisation of the AGW with matrix based Ni-Fe. To be able to apply correctly the methods of post-sintering manufacture of AGW and to obtain maximum efficiency it is necessary to know the behaviour at plastic deformation of the two phases which compose the AGW: the hard phase from W grains and the ductile one, made from the matrix in which are included the W grains. The behaviour of the two phases together is the answer at the mechanical solicitations of these materials of composite type, which is the heavy alloys based tungsten.

After many experiments there may be said that there exists an important dependence of the yield strength of the tungsten grains by the temperature. These grains are crystallized in system cvc, while the ductile matrix crystallizes in system cfc and has a lower yield resistance, which is mostly independent by the temperature. As a result, deformation of the composite is controlled only by the deformation of the W particles, which are more resistant

. The matrix has to be able to rise his strength with the help of the hydrostatic component of the stress until a necessary level of the stress to deform the hardest phase, but to not lead to the earliest fracture of the matrix. This means that the matrix phase has to support a fast hardening through cold working, rising in this way its yield limit at that one of the tungsten grains.

On the other hand, deformation and fracture studies of the composites based tungsten, lead to the conclusions that the composite ductility and its fracture depended on many factors, which are presented in figure 1 [3]. The configuration around the tungsten grains depends on the volume ratio of the tungsten grains; the mechanical resistance of the interface depends on the matrix composition and the yield resistance of the tungsten phase depends on the temperature, deformation degree and purity [4].

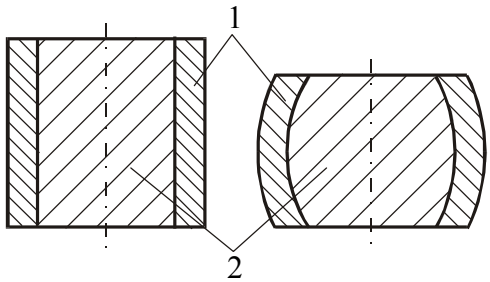

Fig. 2. Steel dies with samples:
1 - die, 2 - samples.

The studies of the behavior at deformation were done using an AGW with the nominal composition 90W-7Ni-3Fe. They shown that the deformation of the tungsten grains is very close by the global deformation of the composite in a temperature interval of –25 ^{0}C and +100 ^{0}C. The matrix deformation through cold working is bigger then that one of the tungsten grains; the last one corresponds to the double stresses compared to the nominal stress from the tungsten grains [5]. Using the obtained data it may be said that the fracture take place during the plastical deformation starting from the micro-cracks, which will be open especially between the tungsten grains, after a certain deformation, growing up with the increasing of the deformation degree.

2. THE EXPERIMENTAL PART

There were elaborated samples from the alloy W-Ni-Fe using the methods of powder metallurgy. From this mixture there were pressed samples with their exterior

diameter of 20 mm and high of 60 mm; sintering with liquid phase at 1475 ^{0}C, for 1 h, in hydrogen. After sintering the samples were manufactured through turning at an exterior diameter of 15 mm, high of 50 mm and then introduced in dies of steel; the ensembles part-die were pressed at different reducing degree, between 2-50 %, figure 2. After deformation the parts were treated at different tempering temperatures between 600 ^{0}C and 1300 ^{0}C, 1 h, to study the recrystallization of the tungsten phase, and between 300 ^{0}C and 1200 ^{0}C, 1 h, for the matrix phase. The control parameter of the material microstructure evolution was the hardness.

3. RESULTS AND DISCUTIONS

The material cold worked during the plastical deformation process is characterized by a surplus of free energy. The increasing of the free energy through deformation is tied by the material nature, by the type and repartition of the crystalline net's defects, by the conditions of the deformation process. The structure of the heavy alloy 90W-7Ni-3Fe sintered with liquid phase at 1475 ^{0}C, 1h, can be seen in figure 3.

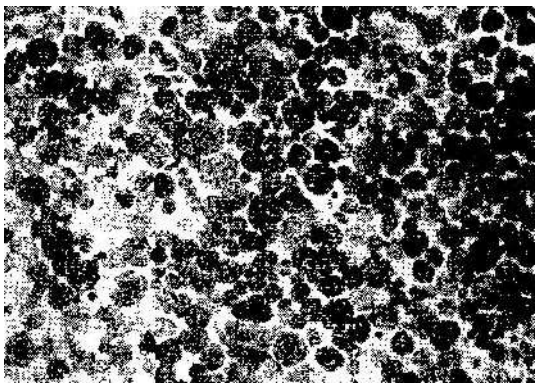

Fig. 3. Initial structure of the heavy alloy 90W-7Ni-3Fe (500 x).

In figure 4 there are presented the microhardness variations of the phase's constituents versus the deformation degree, which reveal the cold working character. The result of the microhardness measurement demonstrates that the degree of the deformation through cold working of the binder phase it is considerably greater than for the tungsten at small degree of deformation. The micro-hardness of the easy inflammable component riches, already, a deformation degree of 10 %. This value is the limit, which doesn't modify through the rising of the deformation degree. The level of the free energy is the energy of the remanent deformations and it determines the character and the speed of the structural modifications into the alloy during the tempering. Because of the interval, of the deformation degree and of the heating temperatures, there were pursued the most important steps of the structure's modifications from the alloy during the tempering.

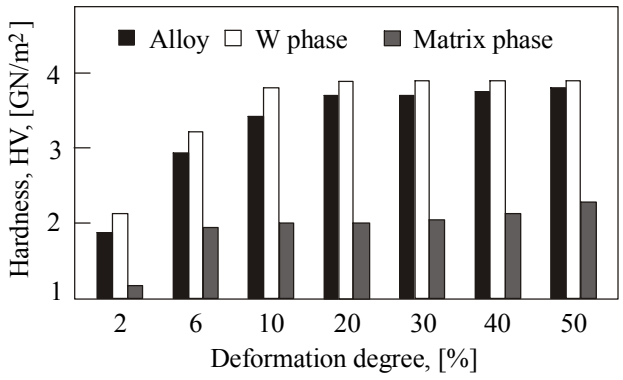

Fig. 4. The variation of AGW 90W-7Ni-3Fe hardness and phases microhardness versus the deformation degree.

As it results from the microhardness measurement, a tempering of the alloy at temperature relatively low determines a diminishing of the binder phase hardness, figure 4. The tempering process of the mechanical properties from the binder phase depends on the preliminary degree of the cold deformation and it intensify with its rising. The hardness

diminishing is determined by the relaxation degree too. The diffusion and especially self-diffusion, tied by the vacancy migration determine the relaxation. To the relaxation belongs also removal and annihilation process of the isolated vacancies, of recombination and annihilation of different vacancy aggregates.

The presence of a quantity of vacancy great enough and of the possibility of their migration through the rising of the tempering temperature permits to the dislocations to do a drag. This process generates most of the mutual annihilation actions of the dislocations with contrary sign. The dislocations with the same sign which remained in surplus rally into the walls which are perpendicular on the first slip surfaces, as called suborders, limits between the blocks of bend type which done small angles. The migration of dislocations in surplus determines the mechanism of polygonization process, which take place at high temperatures and ensure the improvement of the deformed structure.

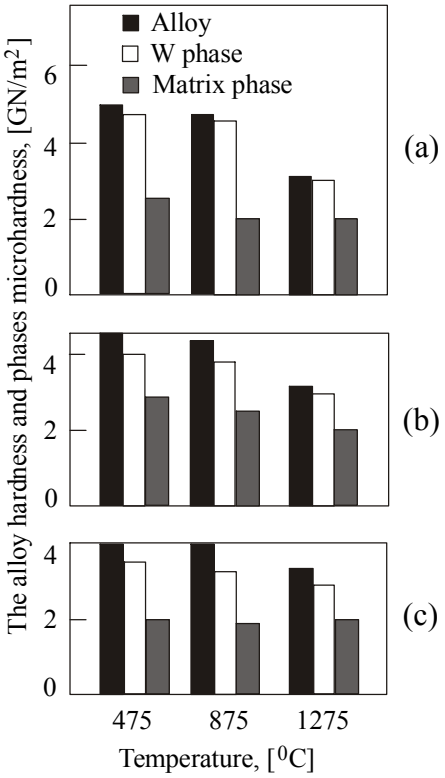

Fig. 5. The variation of the hardness and microhardness of the same AGW from fig. 4, versus the tempering temperature and different deformation degree: (a = 50 %; b =10 %; c = 2 %).

Into the samples deformed with small deformation degree (2 %), the recrystallization begins at 1000 ^{0}C. In the same time with the deformation increasing, the recrystallization beginning removes in the domain of lower temperatures, thus at a deformation of 50 % the recrystallization begins at 600 ^{0}C. At high degrees of quasi-isostatic deformation appear important gradients of free energy at the limit of the distortion and undistorted area of the crystalline net. The difference of the energetic level determines the diminishing of the recrystallization temperature. This effect may be seen on the diagram of the binder metal cold worked at the samples of heavy alloy quasi-isostatic deformed. Into the samples deformed with small degree of deformation the relaxation process may be explained through the fact that the time necessary for the disappearance of the pointshaped defects and of the dislocations at relaxation is smaller then the average period of incubation of the formation into the deformed material of the recrystallization centers. During the relaxation process, which accompany the successive modification of the mechanical properties at

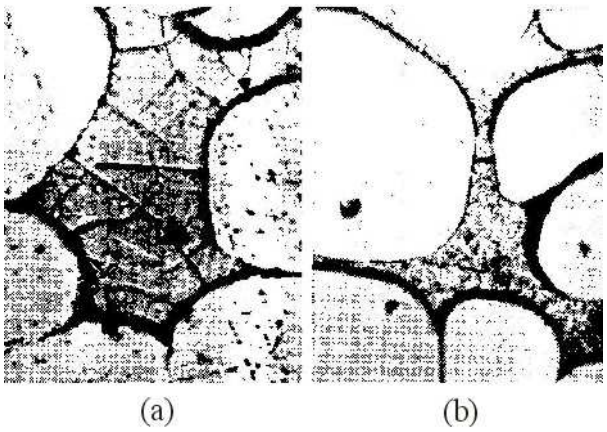

Fig. 6. The structure of the binder phase: (a) - deformation 10 %, tempering temperature 1275 ^{0}C; (b) - deformation 6 %, tempering temperature 1275 ^{0}C.

recrystallization, the hardness of the alloy diminishes suddenly, as the micro-hardness of its phase components, figure 5. For the samples strongly deformed there appears many centers of recrystallization; their rising is burdened by the intersection with other recrystallized grains. For small degrees of deformation, closely to the critical ones, appear little centers of recrystallization, which succeed to grow up until significant dimensions and intersect other recrystallized grains. For the critical deformation degree, the average size of the recrystallized grains grow up from 15 μm at 875 ^{0}C, at 35 μm at 1300 ^{0}C. Once with the growing of the tempering temperature, the size of the critical deformation removes in a lower domain. At the tempering temperature of 875 ^{0}C the deformation critical degree rich 6 % and diminish at 2 % for a tempering temperature of 1275 ^{0}C. The recrystallization for all deformation degree through tempering for 1h, ended at 1075 ^{0}C. The alloy structure with phase slow recrystallized is presented in figure 6. The growing of the recrystallized grains take place, mainly, in the limits of the initial grains (fig. 6 a) and only for the critical deformations and for that one near the critical ones, the grains dimension outruns the initial one (fig. 6 b).

4. CONCLUSIONS

The beginning temperature of the binder phase recrystallization in the heavy alloy 90W-7Ni-3Fe depends on the alloy initial cold deformation degree and it diminish from 1100 ^{0}C at 400 ^{0}C in the same time with the deformation increasing from 2 at 50 %.

- At low tempering temperatures and small deformation degree, into the phase take place, mainly, a relaxation process tied to the tempering and polygonization. For the intermediate deformation, these processes take place in the same time, overlapping.
- The size of critical deformation depends on the tempering temperature and diminishes from 6 to 2 % simultaneous with the temperature rising from 800 at1300 ^{0}C.

5. REFERENCES

1. Caldwell, S.G., Micro-hardness Variations in Tungsten-Based Heavy Alloys as a Function of Composition and Processing Variables, Progress in PM, 1985, Annual Conf. Proc., v. 41, MPIF-APMI, 1985, p. 123-138.
2. Frantsevitch, J.N., i. dr., Rekristalizatsiya wolframa w splawach wolfram-nikeli-jelezo, Por. met., 5(53), 1967, 84-91.
3. Hong, M.H. a.o., The Effect of Thermo-Mechanical Treatment on the Microstructure and Failure Behavior of Sintered W Heavy Alloy, Advanced Technology Research Center, 1994, p. 279-288.
4. *** Metals Handbook, Powder Metallurgy, v. 7, Coord. E.Klar, ASM International, USA, 1984, p. 316-320.
5. Ryu, H.J. a.o., Microstructural Control of Mechanically Alloyed Tungsten Heavy Alloy by Two Step Sintering. Proced. PM World Congr.&Exhib., v. 4, Granada, Spain, 1998, p. 520-525.

RADU MUREŞAN, Technical University of Cluj-Napoca, Faculty of Materials Science and Engineering, Muncii Av., No. 103-105, Cluj-Napoca, Romania.

EVOLUȚIA MICROSTRUCTURII PRIN SINTERIZARE ŞI PRELUCRĂRI TERMOMECANICE ÎN ALIAJE GRELE PE BAZĂ DE WOLFRAM

REZUMAT: Aliajul este caracterizat printr-o structură multifazică complexă. Structura W-Ni-Fe este compusă dintr-o fază refractară a unei soluții solide bogate in W şi o fază liant, uşor imflamabilă, formată din solutia solidă a W şi Fe în Ni durificată prin precipitare. Comportamentul aliajului greu la deformare plastică şi revenit va fi determinat de tipul rețelei cristaline (natura) a fazelor, de interacțiunea dintre ele şi de rolul limitelor interfazice care se formează la durificare. Scopul acestei lucrări este studierea modificării structurale a liantului din faza uşor durificată a aliajului de W-Ni-Fe deformat.

BULETINUL INSTITUTULUI POLITEHNIC DIN IAŞI
Tomul LIII (LVII), Fasc. 3, 2007
Secția
ŞTIINȚA ŞI INGINERIA MATERIALELOR

ABOUT INVESTIGATION FACTORS INFLUENCING THE FINAL RESULTS OF PARTS FABRICATED BY THE ELECTROMAGNETIC FORMING

BY

DORIN LUCA

Abstract. The objective of this paper was to investigate factors influencing the final results of parts fabricated by the electromagnetic forming. Investigated factors were: the discharge current that passes through the coil and the magnetic induction produced by the coil. These factors were measured because, determining the real value of work parameters of the electromagnetic forming equipment is especially important and it is recommended that the acquisition of the requested data to be performed directly from the process.

Keywords: electromagnetic forming, flat specimen, factors influencing, discharge current, magnetic induction, data aquisitions.

1. Introduction

Both in manufacturing and research activities the permanent increase of tool performance is aimed with the purpose to produce parts with energy and material consumptions as low as possible.

In case of the designing electromagnetic forming process, calculation is developed based on the adoption of an equivalent electric scheme (more properly it should be called *simplified* scheme-author's note) for the *installation-tool-part (ITS)* system. In Figure 1 the equivalent scheme of the discharge circuit of an electromagnetic forming equipment is shown.

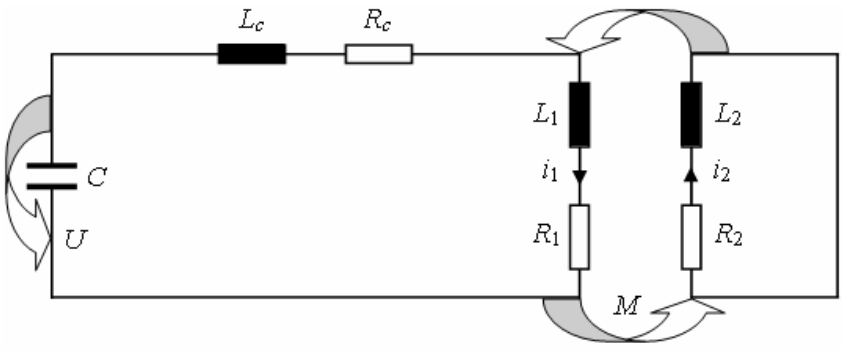

Figure 1. Equivalent scheme of the discharge circuit.

Therefore, *ITS* system is a discharge circuit consisting in: an energy stocker,

with capacity C and voltage U; the connecting lines, with inductance L_c and resistance R_c; the coil, with inductance L_1 and resistance R_1 and the specimen, with inductance L_2 and resistance R_2, being magnetically connected with the coil. This model of equivalent scheme of the discharge circuit assimilates the coil and the part to a transformer, with the mutual inductance M. Under these circumstances, the equivalent electric circuit is described by equations [1]:

$$(L_1 + L_c)\frac{\mathrm{d}i_1}{\mathrm{d}t} + \frac{\mathrm{d}}{\mathrm{d}t}(M\,i_2) + (R_1 + R_c)\,i_1 + \frac{1}{C}\int i_1\,\mathrm{d}t = 0 \tag{1}$$

$$\frac{\mathrm{d}}{\mathrm{d}t}(L_2\,i_2) + \frac{\mathrm{d}}{\mathrm{d}t}(M\,i_1) + R_2\,i_2 = 0 \tag{2}$$

where i_1 is the current passing through the coil and i_2 represents the sum of the induced currents in the specimen.

The initial conditions for equations (1) and (2) are:

$$i_1 = 0\,; \quad i_2 = 0\,; \quad (L_1 + L_c)\frac{\mathrm{d}i_1}{\mathrm{d}t} = U \tag{3}$$

where U is the initial voltage of the energy stocker.

In order to simplify the calculation, some authors [2] neglect the influence of mutual inductance M and only a total inductance L and resistance R are taken into consideration that cumulate the influences of the coil connection parameters and the coil and specimen specific parameters, according to the relationships:

$$L = L_c + L_1 + L_2 \tag{4}$$

$$R = R_c + R_1 + R_2 \tag{5}$$

In this case, the oscillating circuit equation has the form:

$$L\frac{\mathrm{d}i_1}{\mathrm{d}t} + R\,i_1 + \frac{1}{C}\int i_1\mathrm{d}t = 0 \tag{6}$$

with solution,

$$i_1(t) = I_{max}\cdot \mathrm{e}^{-\alpha t}\,\sin\omega t \tag{7}$$

where I_{max} is the maximum value (amplitude) of the discharge current, α represents the *damping coefficient* and ω is the *current pulsation*.

The damping coefficient α and the current pulsation ω are determined with the relationships:

$$\alpha = \frac{R}{2L} \tag{8}$$

$$\omega = \sqrt{\frac{1}{LC} - \left(\frac{R}{2L}\right)^2} = \sqrt{\frac{1 - D_a^2}{LC}} \tag{9}$$

where D_a is called *damping factor* and has the expressing,

$$D_a = \frac{R}{2}\sqrt{\frac{C}{L}} \tag{10}$$

For a given value of the damping coefficient D_a much lower than unit, the maximum value of the discharge current can be determined from the expression [3]:

$$I_{max} = U\sqrt{\frac{C}{L}}\left(1 - \frac{\pi R}{4}\sqrt{\frac{C}{L}}\right) \tag{11}$$

Besides discharge current intensity, the decisive influence on the electromagnetic forming manufacturing has the discharge current frequency, which is determined with the relationship:

$$f = \frac{1}{2\pi}\sqrt{\frac{1}{LC} - \frac{R^2}{4L^2}} \tag{12}$$

where L represents the total inductance of the discharge current, R is the total resistance of the circuit and C the total capacity of the energy stocker.

The discharge current frequency directly influences the deformation degree, an optimal frequency value existing for which the maximum deformation degree is obtained. Considering a solenoidal coil, its magnetic induction is determined with the relationship:

$$B(t) = B_{max} \cdot \mathrm{e}^{-\alpha t} \sin \omega t \tag{13}$$

where,

$$B_{max} = \frac{\mu_0 N I_{max}}{a} \tag{14}$$

where B_{max} is the maximum value of magnetic induction, μ_0 is the magnetic permeability of vacuum, N the solenoid number of turns and a the solenoid length.

The total pressure acting on the part equals the pressure difference on its two faces:

$$p = \frac{1}{2}\mu\,(H_1^2 - H_2^2) \quad \text{[Pa]} \tag{15}$$

where H_1, in A/m, is the intensity of the magnetic field in the space between coil and part and H_2, in A/m, is the intensity of the magnetic field on the opposite face of the specimen.

For a clearly expressed pellicular effect, pressure calculation relationship is written as:

$$p(t) = \frac{1}{2\mu_0} B_{max}^2 \cdot \mathrm{e}^{-2\alpha t} \sin^2 \omega t \tag{16}$$

Pressure calculation can be also performed with other relationships having specific forms to each specimen type.

2. Data acquisition and results

The most important parameters, in the case of manufacturing by electromagnetic forming, are the discharge current that passes through the coil and the magnetic induction produced by the coil.

Within this paper a system was designed and built, for simultaneous acquisition of data regarding discharge current and magnetic induction, which is shown in Figure 2 (*SE*-energy stocker; *GIT*-high voltage generator; *PC*-command desk; *CA*-commutation device; *DM*-electromagnetic forming device).

The acquisition of magnetic induction values required the design and manufacturing of a magnetic induction transducer, shown in Figure 3.

The turns of the transducer coil were made from enameled copper conductor with 0.09 mm diameter and were winded on a rigid thin insulating plate with the dimensions (3.39 mm × 0.31 mm).

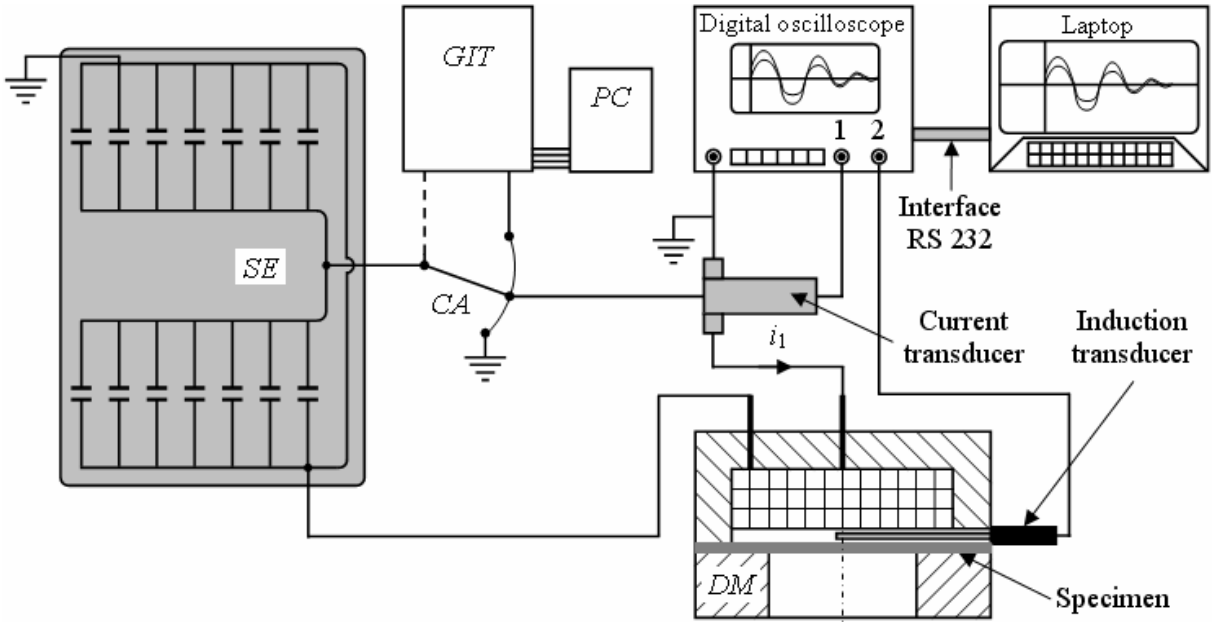

Figure 2. Designed system for data acquisition in electromagnetic forming process.

Figure 3. The induction transducer.

The obtained magnetic induction transducer was calibrated in the known uniform magnetic field of a *Helmholtz* system [4], using the constant transfer method from a first order standard.

Calibration was achieved based on the scheme shown in Figure 4.

The transducer was exactly positioned in the middle of the symmetry axis of the Helmholtz system. In this point the intensity of the magnetic field *H*, induced by the current *I* that passes through the system coils, is given by the relationship [5]:

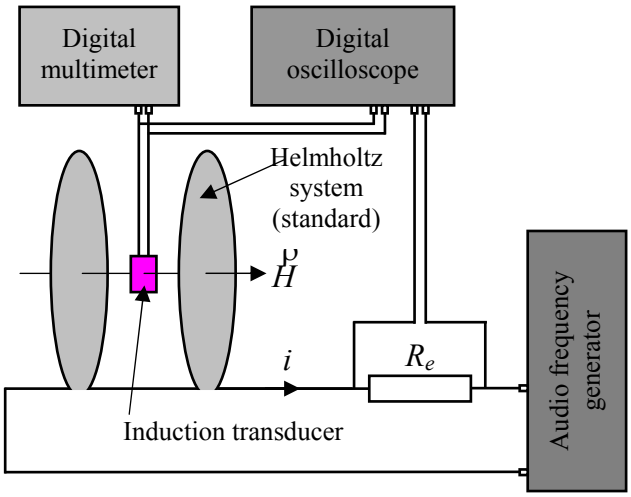

Figure 4. Calibration scheme of the induction transducer.

$$H = k_{sH}\, i \tag{17}$$

where k_{sH} is the Helmholtz system constant and has the value 477.94228 (A/m)/A.

Figure 5 shows two examples of simultaneous data aquisitions for discharged current and magnetic induction through flat coil.

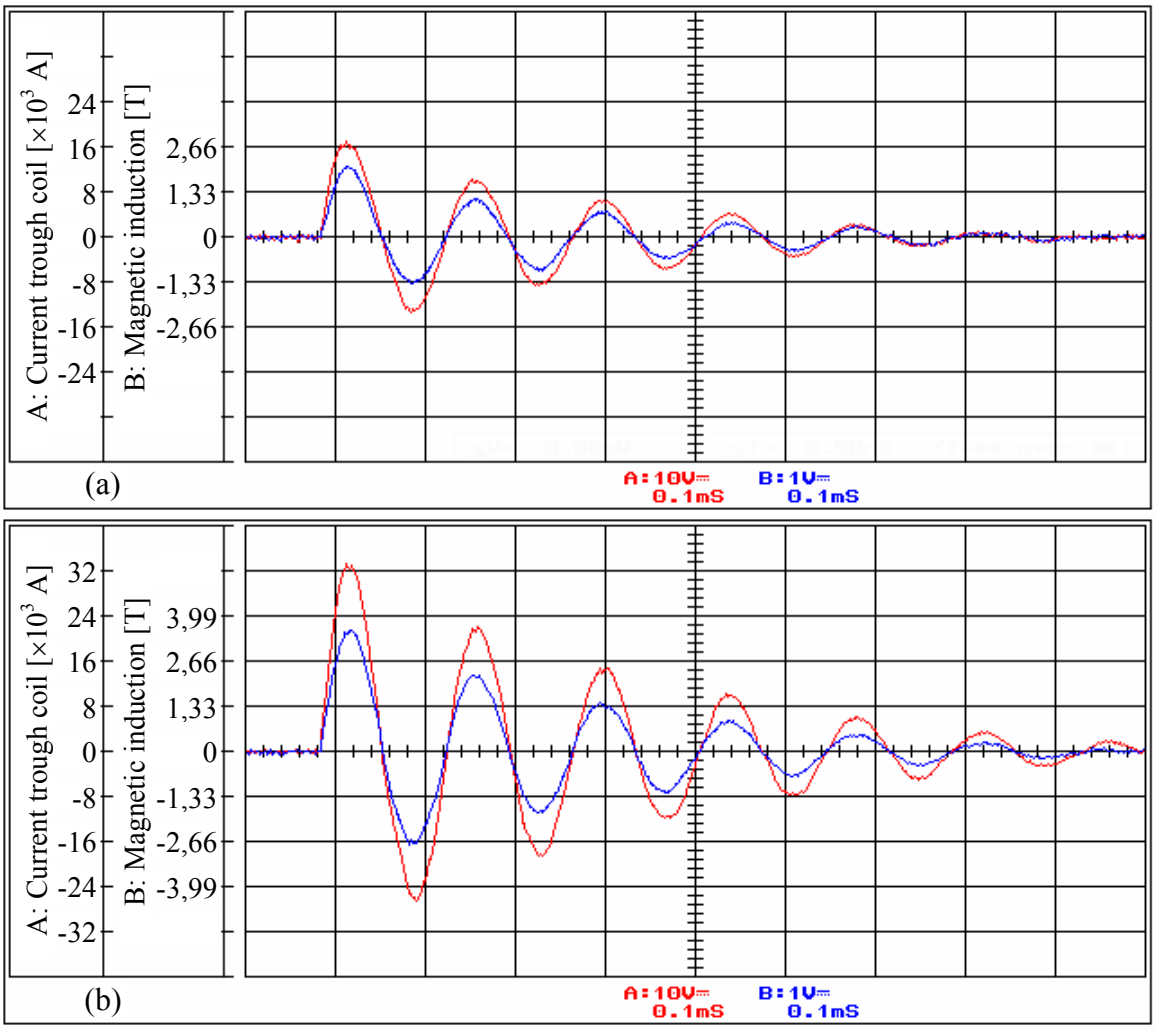

Figure 5. Examples of data aquisitions in electromagnetic forming process:
(a) $U = 2$ kV, $C = 200$ μF, $r = 30$ mm, $z = 3{,}65$ mm; (b) $U = 4$ kV, $C = 200$ μF, $r = 20$ mm, $z = 3{,}65$ mm.

Perch z shown on figures significance distance between induction transducer axis and coil turns axis used for data aquisitions (5 turns, L_1=0,910 μH, R_1=0,729 mΩ).

3. Conclusions

Calculation regarding discharge current intensity and frequency are accomplished based on the adoption of some *simplified* schemes of the installations and on some simplifying hypotheses. The discharge current intensity is significantly influenced by the damping factor value that should be as low as possible and at limit it shouldn't exceed unit. The discharge current frequency directly influences the deformation degree, which can be explained by frequency influencing the penetration depth of the magnetic field. Magnetic induction and pressure produced by the working coil depend on both the discharge current intensity and frequency, on the coil number turns as well as on its dimensional parameters. The variations of magnetic pressure magnitude and distribution are largely influenced by the ration between the voltage and the capacity of energy stocker. In order to increase the process efficiency cooling

of the electromagnetic forming devices is recommended. Based on this idea, the author even suggests to apply the cryogenic cooling of coils (for instance with liquid nitrogen passing through tubular conductors), which could exploit low temperature superconductivity of metals thus considerably increasing efficiency. Determining the real value of work parameters of the electromagnetic forming installation is especially important and it is recommended that the acquisition of the requested data to be performed directly from the process. In the present research, the acquisitioned data allowed both correct determination of the deformation pressure and obtainment by finite element modelling of some results very close to reality.

Received, May 2007 *Technical University "Gh. Asachi" Jassy*

REFERENCES

1. TAKATSU, N.; KATO, M.; SATO, K.; TOBE, T. - High-Speed Forming of Metal Sheets by Electromagnetic Force. *JSME International Journal*-Series III, 1988, vol. 31, nr. 1, p. 142-148. ISSN 1340-8062.
2. MIRONOV, V.A. - *Magnitno-impul'snoe pressovanie poroškov*. Riga: Izdatel'stvo Zinatne, 1980. 194 p.
3. BAUER, D. - Dimensionarea optimă a sculelor şi instalaţiilor pentru deformare în câmpuri magnetice (traducere). *Prelucrarea metalelor prin tehnologii neconvenţionale*, 1973, nr. 1, p. 26-30.
4. JILES, D. - *Introduction to Magnetism and Magnetic Materials*. London; Weinheim; Tokyo; Melbourne; Madras: Chapman & Hall, 1996. 440 p. ISBN 0-412-38640-2.
5. LUCA, D. - *Research and Contributions Regarding Plastic Processing by the Electromagnetic Forming Proceeding,* PhD Thesis (in Romanian). Iaşi: Technical University, 2000.

DESPRE INVESTIGAREA FACTORILOR CE INFLUENTEAZA REZULTATELE FINALE A PIESELOR FABRICATE PRIN MAGNETOFORMARE

(Rezumat)

Obiectivul acestei lucrari a fost sa investigheze factorii ce influenteaza rezultatele finale a pieselor fabricate prin deformare electromagnetica (magnetoformare). Factorii investigati sunt: curentul de descarcare care trece prin bobina si inductia magnetica produsa de bobina. Acesti factori au fost masurati deoarece, determinarea valorii reale a parametrilor de lucru a instalatiei de deformare electromagnetica este foarte importanta si se recomanda ca achizitia datelor necesare sa se realizeze direct din proces.

BULETINUL INSTITUTULUI POLITEHNIC DIN IAŞI
Tomul LIII (LVII), Fasc. 3, 2007
Secția
ŞTIINȚA ŞI INGINERIA MATERIALELOR

EXPERIMENT OF IRON INOCULATING BY TWO STAGES, IN MOULD

BY

VASILE COJOCARU-FILIPIUC, SERGIU STANCIU and GELU BARBU

Abstract: An iron inoculating mould prepared for inoculating by two stages was experimented.Configuration of inoculant second chambers has determined high sintering of inoculant − Mg master alloy.

Iron was inoculated very uniform according to an inoculant consumption of 0.75% with 10% Mg.

One estimates changing of inoculant second chambers geometry and tangential feeding of reaction chamber.

Keywords: mould inoculating, reaction chambers, fine graphite

1. GENERAL CONSIDERATION

Advantages and disadvantages of iron inoculating in mould are known, remarking advantage which consists in eliminating of uninoculating risk caused of big duration between beginning of inoculating and beginning of crystallization and disadvantage which consists in ununiform inoculating caused of fact that at beginning of pouring iron is inoculated more and to final of pouring iron is inoculated less, [1], [2], [3], [4], [5].

Inoculants are introduced in liquid iron, usually, as ferro-alloy and master alloy, metallic materials which contain impurities, impurities which are transferred, partially, to inoculated iron, too. That's why one searches inoculating methods which to provide bigger inoculants assimilating efficiency and which to determine less consumption of inoculants.

This paper presents experimenting of an inoculating technology in mould, [6], by inoculating system equipped with four second reaction chambers which to determine inoculating in two stages.

2. EXPERIMENTS

In figure 1 it is presented draught of mould which is used for iron inoculating.

Inoculating manner, according to figure 1, consists in placing of inoculant (18) in reaction chamber (4). Before pouring, the feeding of the mould cavity is blocked by obturating core (17). After pouring, inoculating, chemical-thermical homogenizing

and non-metallic inclusions separating at the metallic bath surface from the reaction chamber, the feeding of the mould cavity is unobturated.

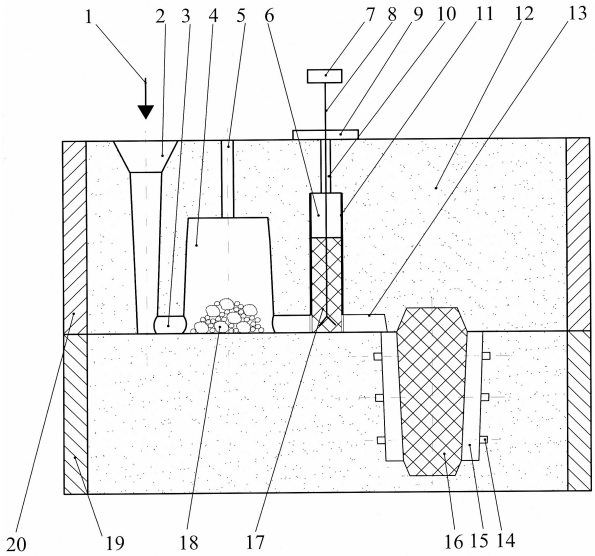

Fig.1.Draugh of inoculating mould for iron, equipped with simple reaction chamber. 1 − pouring sense; 2 − downgate; 3 − reaction chamber feeding; 4 − reaction chamber; 5 − ventilating canal; 6 − slot of obturating core; 7 − acting device; 8 − acting bar; 9 − bar blocking device; 10 − bar canal; 11 − graphite blocking; 12 − foundry sand; 13 − feeding of the mould cavity; 14 − samples cavities; 15 − casting cavity; 16 − core; 17 − obturating core; 18 − master alloy with Mg; 19 − inferior flask; 20 − superior flask.

According to experiment, reaction chamber is equipped with four second inoculant reaction chambers, as in figure 2.

Volume of the reaction chamber is about 1550 cm^3 and corresponds to a weight of 10.9 kg.

Volume of mould cavity is about 1360 cm^3.

Size of the reaction chamber is ϕ 110x158 mm.

Size of a second inoculant chamber is ϕ 34x35 mm.

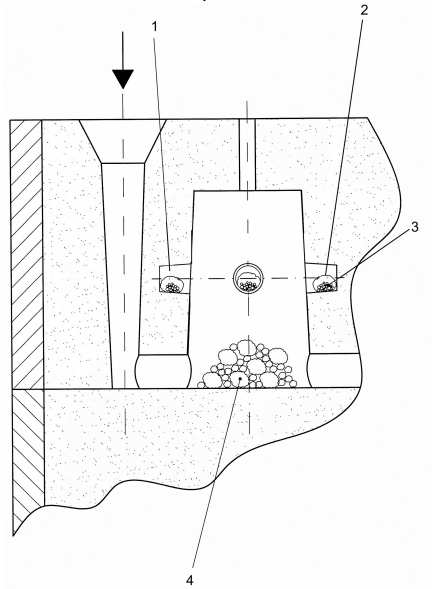

Fig.2. Draugh of reaction chamber equipped with four second inoculant reaction chamber: 1 − second inoculant reaction chamber; 2 − paper; 3 − second inoculant; 4 − main inoculant.

Mould was preheated, superficially, by a butane burner − a mobile one.

Iron was elaborated in an induction furnace equipped with a graphite crucible, having capacity of 30 kg of iron and frequency of 20000 Hz.

Manufactured iron had next chemical composition: 3.83% C; 2.98% Si; 0.67% Mn; 0.152% P; 0.43% S.

Oligoelements from manufactured iron had following concentrations: 0.064% Cr; 0.013% Mo; 0.035% Ni; 0.006% Al; 0.004% Co; 0.056% Cu; max.0.003% Nb; 0.024% Ti; 0.016% V; max. 0.007% W; 0.004% Pb; 0.015% Sn; 0.008% As; max. 0.001% Zr; 0.002% Ca; max. 0.003% Ce; 0.002% B; max. 0.001% Zn; max. 0.001% La; max. 92.073% Fe.

Metallic charge had 100% high purity pig iron with following chemical composition: 3.9% C; 1.75% Si; 0.75% Mn. One used for increasing of Si content FeSi75. To inoculate, one used a ferro-alloy with Mg and Mischmetall having following chemical composition: 10% Mg; 1.5% Mischmetall; 42% Si; 1.5% Al.

One was used 1.5% inoculant placed by the following set-up: 0.75% on the base of the reaction chamber (placed in central zone) and 0.19% in very second inoculant reaction chamber.

Iron evacuating temperature from furnace was of 1490^0, temperature determined by a optical pyrometer. The feeding of the reaction chamber was perpendicular on this one. An experiment was realized, only.

Duration between pouring finishing and dezobturating of cavity mould feeding was of 5 seconds.

3. RESULTS OBTAINED

Inoculant from second inoculant reaction chamber was sintered. So, for inoculating 0.75% of inoculant participated. On the surface of the reaction chamber a crust with thickness of 1.5…2.0 mm was solidified.

Figure 3 shows metallographic structure of those 12 samples placed in mould cavity as in figure 1, on three planes and by four a plane, placed equidistantly (at. 90^0). Putting down of samples is done by two figure separated by a point, the first figure representing the placing plane (1 − above plane; 2 − average plane; 3 − bottom plane) and second figure representing position given the feeding of the mould cavity (1 − sample next to feeding; 2, 3 and 4 − considerate by positive trigonometric sens given the sample 1).

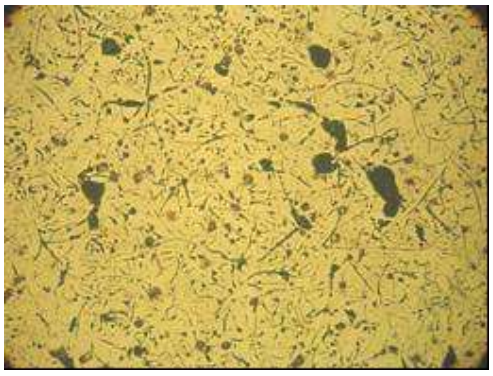

sample 3.1

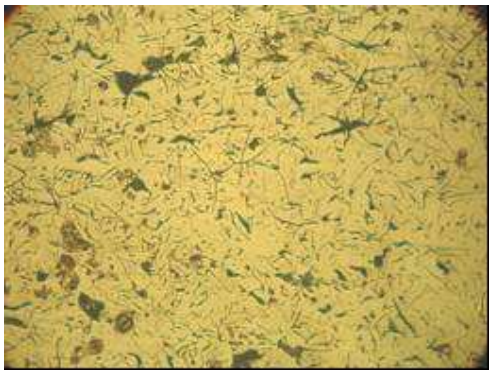

sample 3.2

Fig.3. Metallographic structure of samples. Aggrandizement of 100.To be continued.

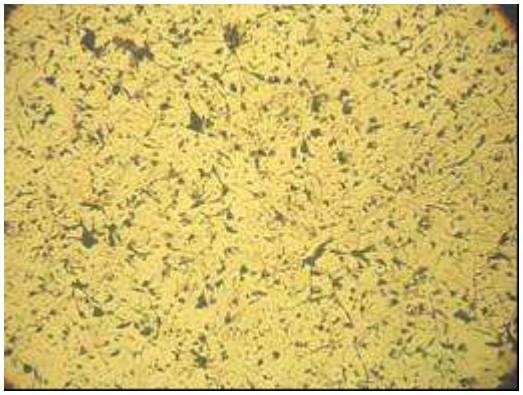

sample 3.3.

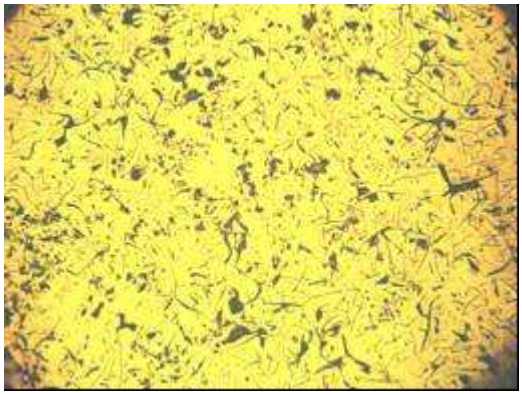

sample 3.4.

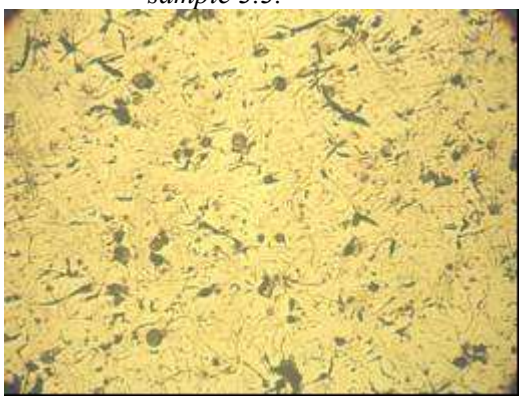

sample 2.1

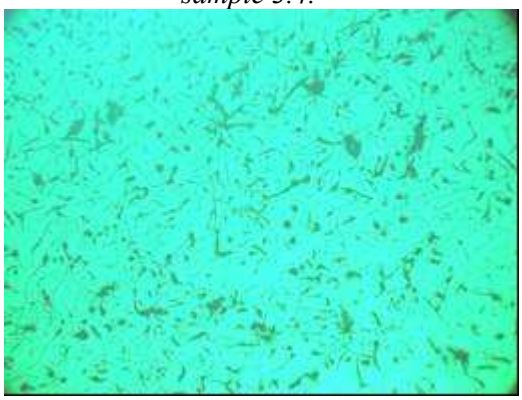

sample 2.2

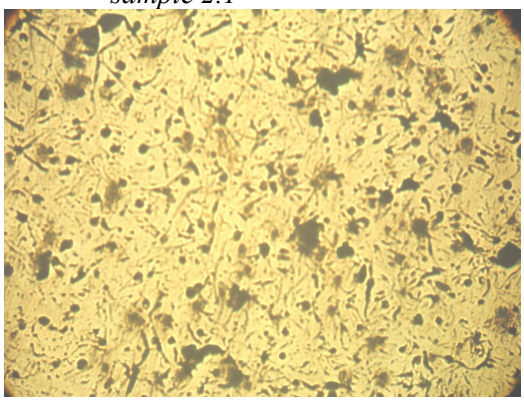

sample 2.3

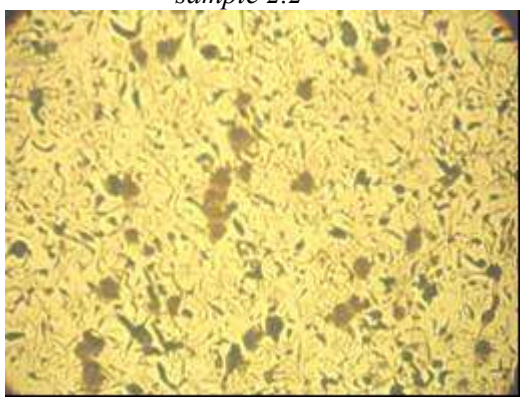

sample 2.4

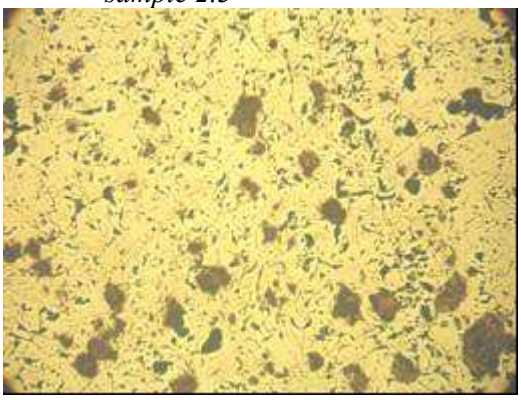

sample 1.1

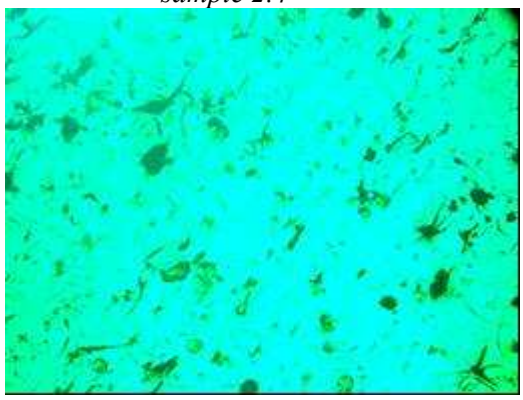

sample 1.2

Fig.3. Metallographic structure of samples. Aggrandizement of 100.To be continued.

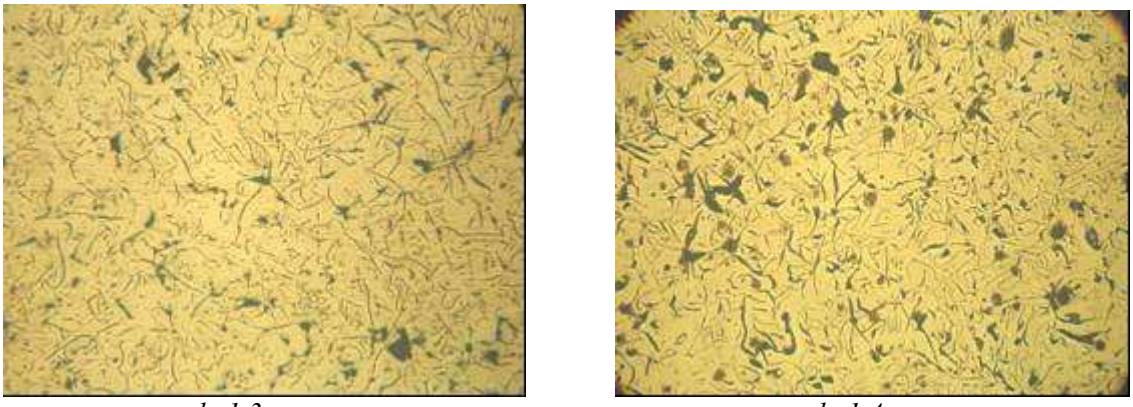

sample 1.3 *sample 1.4*

Fig.3. Metallographic structure of samples. Aggrandizement of 100. Continued from another page

Remanent magnesium content was of 0.002%.
Magnesium assimilating efficiency was about 60%.

4. RESULTS − INTERPRETATIONS

Because of inoculant sintering in second inoculant reaction chambers, one recommends that second inoculant reaction chamber to be realize as in figure 4. So, inoculant from second inoculant reaction chambers will be involve by liquid iron to superior part of the reaction chamber. In addition, one recommend that the feeding of the reaction chamber to be tangential given the reaction chamber.

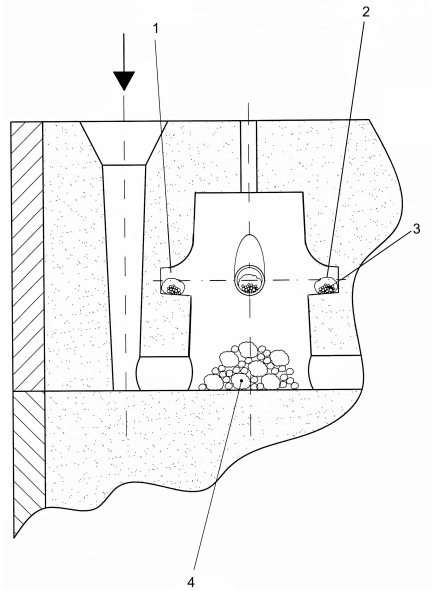

Fig. 4. Draught of the reaction chamber equipped with four second inoculant reaction chamber whose geometry is changed given the variants from figure 2.

Because of inoculant sintering in second inoculant reaction chambers, practically, iron was inoculated by 0.75% inoculant, that is less that value indicated by technical literature. So, one explains why graphite was inoculated a little .

Graphite inclusions from all 12 samples are fine, between fine lamellar inclusions being little graphite nodules and rarely bigger graphite nodules, too.

Geometry of graphite inclusions from those 12 samples is relative very uniform. That's why on considers that in mould inoculating technology experimented determined a good chemical homogenizing.

Technical University "Gh. Asachi" from Jassy.

REFERENCES

1. Cojocaru-Filipiuc, V. *Nodular graphite obtainment by modification in the mould*. Kohászat.1997.5-6.p.183...185.
2. Cojocaru, V. *Fonte−obținere*. Iaşi. Editura "**Samia**". 2003;
3. Sofroni, l., Ripoşan, I., Brabie, V. and Chişamera, M. *Turnarea fontei*. Bucureşti. **Editura Didactică şi Pedagogică**. 1985.
4. Sofroni, L., Ştefănescu, D.M., and Vicenz, C. *Fonta cu grafit nodular*. Bucureşti. **Editura Tehnică**. 1978;
5. Sofroni, L. and Ştefănescu, D.M. *Fonte modificate cu proprietăți superioare*. Bucureşti. **Editura Tehnică**. 1971;
6. Cojocaru, V. and Oprinca, S. *Rețea de turnare*. **Brevet România**. nr. 107 574. 1993.

Note

The present paper is based on data obtained by research elaborated within the Contract of Scientific Research no. 63GR/19.05.2006, theme 6, cod 630 and theme 12/2007, financed by C.N.C.S.I.S. from the Ministry of Education and Research.

EXPERIMENT DE MODIFICARE A FONTEI ÎN FORMĂ, ÎN DOUĂ TREPTE

Rezumat: S-a testat o formă de modificare a fontei pregătită pentru modificarea în două trepte.

Configurația camerelor secundare ale modificatorului a determinat sinterizarea modificatorului pe bază de Mg şi dezactivarea lui.

Fonta s-a modificat foarte uniform, corespunzător unui consum de modificator de 0,75% cu circa 10% Mg.

Se estimează schimbarea geometriei camerelor secundare ale modificatorului şi alimentarea tangențială a camerei de reacție.

BULETINUL INSTITUTULUI POLITEHNIC DIN IAŞI
Tomul LIII (LVII), Fasc. 3, 2007
Secția
ŞTIINȚA ŞI INGINERIA MATERIALELOR

THERMODYNAMIC ACTIVITY OF CARBON − DECISIVE FACTOR FOR GRAPHITE GEOMETRY IN GREY CAST IRON

BY

VASILE COJOCARU-FILIPIUC

Abstract: Nodular graphite nuclei are constituted, thanks to critical values of carbon thermodynamic activity, on surface of thermodynamic phases created by inoculant elements in liquid elements in liquid iron, thermodynamic phases as gas bubbles or drops.

Chemical elements introduced in liquid iron which are solved in liquid iron cannot be inoculants to constitute nodular graphite .

During eutectic transformation, complex phenomena which occur, under influence of chemical composition of iron, can degenerate graphite geometry − inoculation degeneration.
Keywords: nodular graphite nuclei; thermodynamic activity of carbon; phases inoculant of elements in liquid iron.

1. GENERAL CONSIDERATIONS

There is carbon, in case of grey cast irons, like graphite, for the most part, and like solid solution (ferrite, austenite and metallographic constituents, except thermodynamic equilibrium, conformable to reality) fastened cementite in perlite or in metallographic constituents, except thermodynamic equilibrium Fe-C, conformable to reality, [1].

Graphite, in irons, but in other alloys, too, can have divers shapes (geometries), from point-like one, to divers shapes, in plane being as lamellar, vermicular/compact, coral − lake, chunky, nests, nodular etc.

Graphite shape, weight of graphite inclusions, volume of a graphite inclusions and quantity of graphite determine significantly values of mechanical and physical characteristics.

According as factors which determine graphite (geometry, weight and quantity) and activating manner of those ones are known it results that iron proposed to obtain characteristics can be obtained from the graphite influence point to of view.

In this paper it is presented influence of carbon thermodynamic activity on graphite geometry.

Graphite from iron which is constituted during iron cooling arises from liquid solution and solid solution as result of diffusion of carbon particles through those ones.

Therefore, it is a matter of carbon thermodynamic activity in a solution because the thermodynamic activity involves diffusion process.

2. CARBON THERMODYNAMIC ACTIVITY IN LIQUID IRON

An iron in liquid state is a liquid solution which has carbon content, definited.

When energetic parameters involve "associating" of more carbon particles which are put in order according to a crystallographic system, there is reality of constituting of a crystallographic nucleus − graphite nucleus.

To increase the graphite nucleus, it must that carbon particles to diffuse through liquid solution − through liquid metallic matrix − that is those ones must diffuse from zones where carbon concentration is less, to zone where carbon concentration is bigger − at beginning to graphite nuclei and then to graphite inclusions. This situation might constitute an example given the impossibility to explain diffusion phenomenon by Fick laws. Therefore, factor which determines carbon diffusion through liquid solution is thermodynamic activity − not content.

According to [2], thermodynamic activity of carbon can be to define by two manners − carbon rational thermodynamic activity (relation (1)) and carbon practical thermodynamic activity (relations (2) and (3)).

$$a_C' = f_C \cdot X_C, \tag{1}$$

where a_C' is carbon rational thermodynamic activity; f_C − carbon thermodynamic activity coefficient; X_C − molar fraction of carbon.

$$a_C'' = f_C \cdot C_C^*, \tag{2}$$

where a_C'' is carbon practical thermodynamic activity; C_C^* − molal concentration of carbon (molality)

$$a_C''' = f_C \cdot C_C, \tag{3}$$

where a_C''' is carbon practical thermodynamic activity too; C_C − molar concentration of carbon.

There are convertion factors between X_C, C_C^* and C_C − they are known.

During liquid iron cooling, one estimates that carbon content and pressure above metallic bath are constant.

Thermodynamic activity coefficient depends of chemical composition of iron, iron temperature and pressure above metallic bath.

[1] and [3] bibliography sources show nodular graphite constituting during liquid iron cooling, between temperatures 1350…1320^{0}C. So, conclusion is nodular graphite nuclei are constitutes at same temperatures.

In the case of hypoeutectic iron, nodular graphite is constituted between 1350…1320^{0}C and lamellar graphite is constituted during eutectic transformation. So, nodular graphite nuclei and lamellar graphite nuclei are constituted at different temperature. Well, in this moment, one estimates that the factor which explains different temperature for constituting nodular and lamellar graphite nuclei is carbon thermodynamic activity.

It is known that carbon thermodynamic activity is big, so carbon particles diffusing through liquid solution to graphite nuclei and inclusions and through solid solution (austenite), to graphite inclusions.

Taking into consideration that pressure above metallic bath is constant, usually, it follows that carbon thermodynamic activity depends of carbon quantity, iron chemical composition and iron temperature.

Bibliography shows that temperature − big values − is an important factor for inoculating.

Source [4] shows that, in case of hypereutectic irons, nodular graphite nuclei are constituted between 1350…1320^{0}C and during eutectic transformation.

Indifferently of inoculant nature it is certain that difference between hypoeutectic iron and hypereutectic iron is carbon content − more precisely, value of carbon equivalent. Well, a bigger carbon quantity involves constituting of nodular graphite nuclei during eutectic transformation in the case of hypereutectic iron.

In relation (1), (2) and (3), f_C depends of temperature, too, so, "appearing" idea that carbon thermodynamic activity is factor which explains constituting of nodular graphite nuclei.

The temperature is less, the carbon thermodynamic activity is bigger − is bigger carbon thermodynamic activity coefficient. For example, in the case of Fe-C binary system, there is relation (4).

$$\lg f_C = \frac{4370}{T}[1 + 4 \cdot 10^{-4}(T - 1770)](1 - N_{Fe}^2), \tag{4}$$

where T is temperature and N_{Fe} is molar fraction of iron.

Liquid iron temperature, to inoculate, must be big, but thanks to implicating of divers factors − for example, endothermic dissolving of inoculant, decreasing of iron temperature thanks to elimination of big magnesium bubbles from liquid iron etc.

One estimates that during liquid iron cooling, there is a temperature when carbon thermodynamic activity determines constituting of nodular graphite nuclei.

In case of hypoeutectic grey iron uninoculated, graphite nuclei are constituted during eutectic transformation and they represent lamellar graphite. Well, if iron is not inoculated, by normal conditions of pressure, in the case of technical iron, graphite nuclei which are constituted represent lamellar graphite.

To constitute a graphite nucleus, carbon particles must have a certain thermodynamic activity.

In case of a technical iron, thermodynamic activity depends of chemical composition of iron according to relation (5).

$$\lg f_C = \%C \cdot e_C^C + \%E_1 \cdot e_C^{E_1} + \%E_2 \cdot e_C^{E_2} + ... + \%E_m \cdot e_C^{E_m}, \tag{5}$$

where E_1, E_2,…E_m represent chemical element from chemical composition of iron; $e^{C, E_1, E_2, ..., E_m}$ − interaction coefficient of chemical elements from chemical composition, of carbon too, on carbon.

In the case of a technical iron, when pressure is constant, although temperature decreases during iron cooling and although carbon quantity can be increased, these ones increasing carbon thermodynamic activity, however graphite is constituted lamellar. Thus, to constitute nodular graphite nuclei − nodular graphite − it must inoculate iron, that is it must introduce inoculant in liquid iron.

Inoculant is introduced in liquid iron in small quantities − for example, 0.15…0.60%, so, influence on certain characteristics being little. Concretely, e_C^{Mg} has value + 0,07, [5], well, very little, that is carbon thermodynamic activity coefficient

does not increase so much. Well, it's about another factor which involves constituting of nodular graphite nuclei and increasing of graphite nodularly.

Although Mg and Si have, relatively, same interaction coefficient on carbon, Mg is inoculant, only.

Difference between Mg and Si that Mg constitutes a thermodynamic phase − Mg bubbles.

In Mg bubbles, Mg particles shift chaotically, and so, carbon particles have increasing conditions − distances between Mg particles from Mg bubbles are big. Well, there are energetical conditions that carbon particles to constitute graphite nuclei on surface of Mg bubbles. Graphite nuclei can increase into Mg bubbles.

What happend with another inoculants? Which is state of those one in liquid iron? In table 2 fusing temperature, boiling temperature and thermodynamic phases nature of inoculants in liquid iron are represented, [6].

Table 1. Boiling temperatures, fusing temperatures and thermodynamic phases nature of inoculants in liquid iron

Nodulizing inoculant for graphite	Temperature, in ^{0}C, at atmospheric pressure		Nature of thermodynamic phases of inoculants in liquid iron
	fusing	boiling	
Mg	650.0	1107	gas bubbles
Ca	838.0	1440	drops and gas bubble
Ce	795.0	3468	drops
Y	1509.0	2927	drops and solide inclusions
Li	108.5	1330	drops and gas bubbles
Na	97.8	892	gas bubbles
Ba	714.0	1640	drops

Practically and rarely, Mg is used like inoculant, only, another inoculant elements to nodulize graphite using oneselves as ferro-alloys and master alloys, when values of fusing and boiling temperature are another − nature of thermodynamic phases of ferro-alloys and master alloys being another than those of inoculant elements. Well, it is possible, that all inoculant to involve thermodynamic phases as gas bubbles and drops.

If inoculant element is in liquid iron gaseous state and as bubbles, increasing conditions of graphite in inoculant bubbles are better than in case when inoculant element is in liquid iron as drops thanks to bigger distances between inoculant particles from gas bubbles.

Graphite increasing of graphite in gas bubbles and drops of inoculante elements determine that inoculant elements particles to diffuse to and in liquid solution.

Well, it must that inoculant elements to be in liquid iron as gaseous or liquid state and as gas bubbles and as drops − not as solution.

In case magnesium, magnesium bubbles becomes bigger at the same nearing of surface of metallic bath, so, distance between magnesium particles becoming bigger, and graphite increasing easier. Conclusion is that when inoculation is done in ladle, graphite nodules have a bigger size given the mould inoculation where graphite nodules have a less size.

As carbon particles diffuse through liquid solution and deposit oneselves in inoculant bubbles on graphite, carbon concentration decreases in liquid solution, so,

decreasing carbon thermodynamic activity, too. As a result, in case of hypoeutectic iron is not possible constituting of nodular graphite nuclei till liquids line. In addition, during crystallization, austenite is crystallized including carbon, so, carbon thermodynamic activity from liquid solution decreasing till eutectic temperature − eutectic transformation. Therefore, it is not possible to constitute nodular graphite nuclei during eutectic transformation in case of hypoeutectic iron. So, small carbon quantity from liquid solution does that inoculant elements particles from gas bubbles to diffuse easily in liquid solution and to disappear little inoculant elements bubbles.

In case of hypereutectic irons, bigger carbon content than in case of hypoeutectic irons, determines that at eutectic temperature − eutectic transformation − to increase carbon thermodynamic activity, to constitute nodular graphite nuclei on surface of little inoculant elements bubbles, and finally, to constitute nodular graphite. So, little graphite nodules are obtained between big graphite nodules (constituted at big temperatures). In addition, during crystallization austenite is not constituted − carbon concentration in liquid solution (between graphite nodules) is constant. Inoculant elements particles from little gas bubbles does not diffuse through liquid solution because of big carbon content.

Phenomena which occur in case when inoculant is in liquid iron as gas bubbles are as in case when inoculant is in liquid iron as drops.

During eutectic transformation, complex phenomena which occur, under influence of chemical composition of iron, can degenerate graphite geometry, this subject being object of another paper.

3. CONCLUSIONS

1.Nodular graphite nuclei are constituted when carbon thermodynamic activity has a critical value.

2. Nodular graphite nuclei are constituted on surface of thermodynamic phases created by inoculant elements in liquid iron − thermodynamic phases as gas bubbles or drops, only, not as solution.

3. At big temperatures, nodular graphite nuclei are constituted on surface of big gas bubbles and drops of inoculant elements.

4. In case of hypereutectic irons, nodular graphite nuclei are constituted on surface of little gas bubbles or drops, during eutectic transformation, thanks to big values of carbon thermodynamic activity.

5. Because of austenite separating crystallization of iron, in case of hypoeutectic iron, carbon thermodynamic activity decreases very much and, so, is not possible constituting of nodular graphite nuclei during eutectic transformation.

Technical University “Gh. Asachi” from Jassy.

REFERENCES

1. Cojocaru, V. *Fonte−obținere*. Iaşi. Editura "**Samia**". 2003;
2. Vermeşan, E., Ionescu, I. and Urseanu, A. *Chimie metalurgică*. Bucureşti. **Editura Didactică şi Pedagogică**. 1981;
3. Sofroni, L., Ştefănescu, D.M., and Vicenz, C. *Fonta cu grafit nodular*. Bucureşti. **Editura Tehnică**. 1978;
4. Sofroni, L. and Ştefănescu, D.M. *Fonte modificate cu proprietăți superioare*. Bucureşti. **Editura Tehnică**. 1971;
5. Dragomir, I. *Teoria proceselor siderurgice*.Bucureşti. **Editura Didactică şi Pedagogică**. 1985;
6. Sofroni, l., Ripoşan, I., Brabie, V. and Chişamera, M. *Turnarea fontei*. Bucureşti. **Editura Didactică şi Pedagogică**. 1985.

Note

The present paper is based on data obtained by research elaborated within the Contract of Scientific Research no. 63GR/19.05.2006, theme 6, cod 630 and theme 12/2007, financed by C.N.C.S.I.S. from the Ministry of Education and Research.

ACTIVITATEA TERMODINAMICĂ A CARBONULUI − FACTOR DETERMINANT PENTRU GEOMETRIA CARBONULUI, ÎN FONTELE CENUŞII

Rezumat: Germenii de grafit nodular se formează datorită valorii critice a activității termodinamice a carbonului pe suprafața fazelor termodinamice create de elementele chimice modificatoare în fonta lichidă, faze termodinamice sub formă de bule gazoase sau picături. Elementele chimice introduse în fonta lichidă care se dizolvă în fonta lichidă nu pot fi modificatori pentru formarea grafitului nodular.

În timpul transformării eutectice, fenomenele complexe care au loc, sub influența compoziției chimice a fontei, pot degenera geometria grafitului până la compromiterea modificării.

BULETINUL INSTITUTULUI POLITEHNIC DIN IAŞI
Tomul LIII (LVII), Fasc. 3, 2007
Secția
ŞTIINȚA ŞI INGINERIA MATERIALELOR

SENSITIZATION ASSESSMENT OF DUPLEX STAINLESS STEEL USING CRITICAL PITTING TEMPERATURE CPT METHOD - ASTM G48

BY

FUAD M. KHOSHNAW and RAMADHAN A. GARDI

Abstract: Generally, the effect of various fabrication processes, such as welding, in stainless steel alloys can be translated properly with applying specific heat treatments. In this study the influence of this treatment on pitting susceptibility of the stainless steel was evaluated by $FeCl_3$ test according to ASTM standard G48, which is originally dedicated for determination the pitting resistance of austenitic stainless steel.
In this study the influence of heat treatments on pitting corrosion of two stainless steels SAF 2304 and AISI 316L was studied. The stainless steels were given aged treatment in the temperature of 400^{o}C, 500^{o}C, and 600^{o}C for various times. The results showed that with increasing the aging temperature from 400^{o}C to 500^{o}C the pitting corrosion rate of stainless steel alloys are increased at all aging times. At 600^{o}C and when aging time equal to 24 hours both types of stainless steels subjected to minimum critical pitting temperature among other aging temperatures and times selected in this study.
These results are attributed to the metallurgical aspects like carbide precipitation, forming other intermetallics and phases, secondary austenitic, etc, which had significant effects on the corrosion behavior in stainless steel alloys. Increasing the amount of these aspects encourages the pitting corrosion.
Keywords: Stainless steel, sensitization range, critical pitting temperature (CPT), carbide precipitation.

Introduction

Duplex stainless steels are Fe-Cr-Ni alloys with a microstructure consisting initially of ferrite and austenite with approximately 1:1 ratio at room temperature. These steels possess a combination of properties high strength and corrosion resistance that can not be attainable readily using conventional single phase of austenitic or ferritic stainless steel. Compared to the austenitic alloy, duplex alloys have better local and stress corrosion resistance particularly in hot corrosion environment containing chloride ions [1, 2]. Compared to the ferritic stainless steels they can offer improved formability, weld-ability and toughness [3]. Because of these properties duplex stainless steels are used increasingly in some petrochemical industries and oil refineries [1, 3-5]. As mentioned above although they were developed since 1930s, they were not become popular before development of high alloy duplex stainless steel because of difficulties in hot workability and their susceptibility to intergranular corrosion after welding and specific heat treatments, especially in what called sensitization range [2,6].

A range of temperature between 400-600^{o}C is called a "sensitization range". During heat treatment of stainless steels within this range, various transformation occurs involving precipitation of sigma (σ), chi (x), intermetalic phases (R), body centered cubic (α), etc. These transformations seriously affect the localized corrosion

resistance such as pitting and intergranular corrosion in stainless steel alloys [2, 3, and 5].

Since duplex stainless steel generation is relatively new, international standard methods for this group of alloys have not been well-known yet. Therefore, in order to determining the effect of heat treatments, and subsequently the metallurgical aspects, on this group of alloys, the critical pitting temperature (CPT) method, ASTM G48, has been used [2,7]. In spite of, originally, this standard method is originally dedicated and used for austenitic stainless steel.

The object of this work is to study the effect of heat treatments, within the sensitization range, on pitting corrosion of SAF 2304 and AISI 316L.

EXPERIMENTAL WORK

Two types of stainless steels have been selected, SAF 2304 and AISI 316L. All test specimens, 20mm x 25mm, were cut from a sheet 50 x 25 cm with 4 mm thickness for SAF 2304, and 2mm thickness for AISI 316L, with refinishing the sheared edges. The 25mm dimension had been parallel to the longitudinal direction. Before and after heat treatments the specimens were mechanically finished with the aid of 120 and 220 grid abrasive paper, subsequently with using the water to avoid over heating .The specimens degreased using soap and acetone then dried by hot air [7].

To evaluate the influence of the sensitization range temperatures, 400-600^{o}C, on duplex alloys, the CPT method, according to ASTM G48 [8, 9], has been used in this study. To investigate the effect of metallurgical aspects on pitting corrosion of the alloys, three different temperatures, within the sensitization range, have been selected, which were 400^{o}C, 500^{o}C, and 600^{o}C and for each of these temperatures five different times 0.5 hr, 1.5 hr, 10 hrs, 24 hrs and 72 hrs were selected. The specimens stayed in the furnace at the specified temperatures and times. After, they were cooled in the air.

Each specimen is placed inside 0.5-liter Erlenmeyer flask. After pouring 250 ml of 10% $FeCl_3$ solution into the container housed in a constant temperature water bath. After exposure for 24 hours at appropriate temperature the specimens were removed, rinsed with water and scrubbed with nylon bristle brush under running water, dried with hot air and examined for pitting with necked eye. If the pits had not appeared, the same conditions were repeated with a higher temperature by 2.5^{o}C, with using a fresh solution, and so on until the pits appeared [2, 8, and 9].

To investigate the metallurgical aspects like carbide precipitation, brittle phases, etc, beside any specimens for a given condition, another specimen (10 x 10) mm was inserted into the furnace to proceed and take the same variations. The investigations were carried out by either optical microscope, or naked eye. After each heat treatment the specimens were mounted to give more facilities of preparation stages (grinding, polishing and etching). Polishing has been done using diamond slurry on a medium-nap cloth [7].

RESULTS

As received condition

The experiments showed that the CPT for received alloys, without heat treatments, was equal to 32.5°C, and 40°C for austenitic and duplex alloys respectively. This can be easily attributed to the chemical composition for each alloy, especially the 3% of Mo in duplex alloy [1, 2, 5, and 6]. This amount of Mo element would restrain the decomposition and would stabilize the microstructure at specific temperatures [2, 5].

Heat treatments at 400°C

Table 1 illustrates the results of CPT test for both SAF 2304 and AISI 316L at 400°C. The Table showed the CPT values for SAF 2304 specimens remained as for received specimen, at 40°C for 30 minutes and 1.5 hour, however it is decreased to 30°C for AISI 316L at same conditions. This resistance of CPT of SAF 2304 can be attributed to higher chromium and nitrogen content. Increasing such elements would adhesive the chromium oxide (passive film) that formed on the stainless steel alloys.

Table 1 Critical pitting temperature for SAF 2304 and AISI 316L at 400°C

Time	SAF 2304	AISI 316L
0.5 hr	40.0	30.0
1.5 hr	40.0	30.0
10 hrs	37.5	30.0
24 hrs	37.5	27.5
72 hrs	37.5	27.5

With increasing the aging time to 10, 24 and 72 hrs, the CPT is decreased by 2.5°C and became 37.5°C, i.e. the pitting corrosion resistance is decreased with increasing the aging time, and this may be attributed to the more precipitation of chromium carbide along the ferrite austenite boundaries which resulted on the expense of Cr depletion [2, 6].

However, in the practical side, these results could be considered as a good indication, i.e. remaining duplex alloy for longer than 1 hour would not affect badly on pitting corrosion. In the other mean, 1 hour was enough time to create all the metallurgical aspects, such as carbide precipitation.

Table 1 showed that the CPT of AISI 316L specimen aged at 400°C for 0.5, 1.5 and 10 hrs is reduced by 2.5°C compared with as received condition, 32.5°C. Moreover, further reducing in CPT is observed for specimens aged for 24 hours and 72 hours, which reaches 27.5°C. In general the temperature 400°C has little influence on pitting characteristic of duplex stainless steel type SAF 2304, while this

temperature has more effects on AISI 316L. This might be attributed to the fact that AISI 316L could easily be sensitized but SAF 2304 requires higher temperature.

Heat treatments at 500°C

Table 2 shows that the CPT of SAF 2304 and AISI 316L aged at 500°C. The Table showed that duplex specimens aged for 0.5 hour, 1.5 hours, 10 hours and 24 hours subjected to pits at a temperature lower than as received condition by 2.5°C i.e. (37.5°C). As a general view, the results showed that duplex alloy would not affected largely by aging at 500°C, except in the longest time. However, a marked decrease in CPT produced by increasing aging time to 72 hours which reaches 32.5°C. This may be attributed to decomposition of ferrite phase to secondary phases which revealed darkness, as shown in Figure 1. The decomposition of ferrite to secondary phases "probably σ phase-which usually needs longer time", means more Cr dissolution in these new phases, and this resulted in depletion of Cr at grain boundaries, thus caused lowering the CPT [2, 3, and 6].

Table 2 Critical pitting temperature for SAF 2304 and AISI 316L at 500°C

Time	SAF 2304	AISI 316L
0.5 hr	37.5	27.5
1.5 hr	37.5	27.5
10 hrs	37.5	27.5
24 hrs	37.5	25.0
72 hrs	32.5	25.0

Table 2 showed the AISI 316L specimen exhibited to a continuous decreasing in CPT with increasing the aging times at 500°C. The CPT for austenitic alloy, as a first aged time, 30 minutes, was less than 400°C by 5 degree centigrade. This can be explained that the austenitic alloy is much susceptible to sensitization at 500°C, rather than 400°C compared to duplex alloy.

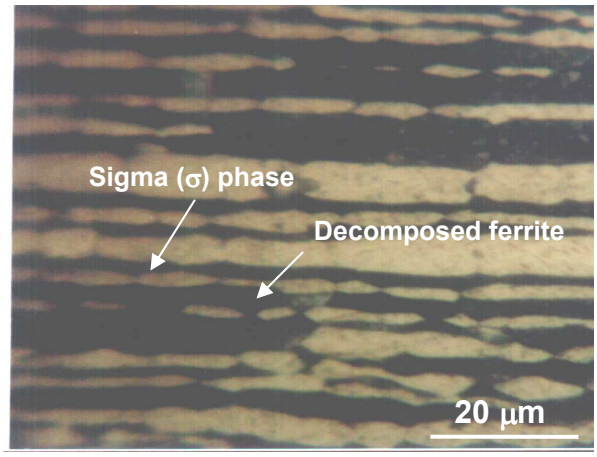

Figure 1 The microstructure of SAF 2304 aged at 500°C for 72 hours.

With increasing the aged time, i.e. 24 and 72 hours, the CPT of the alloy is decreased, and reached 25°C. The reason of this phenomenon can be attributed to possibility of the carbides and phases that need a longer time. Precipitation such phases, means increasing the preferential sites, which helping pit initiations and subsequently lowering the CPT.

Heat treatments at 600°C

Table 3 shows the CPT for SAF 2304 and AISI 316L aged at 600°C. The results showed that the duplex specimens aged at 600°C exhibited to the lowest CPT than the specimens aged at 500°C and 400°C in the same aging times.

Table 3 Critical pitting temperature for SAF 2304 and AISI 316L at 600°C

Time	SAF 2304	AISI 316L
0.5 hr	35.0	25.0
1.5 hr	32.5	25.0
10 hrs	30.0	<20.0
24 hrs	27.5	<20.0
72 hrs	27.5	<20.0

The Table showed that the duplex specimens aged at 600°C for 0.5 hour, is subjected to pitting at a temperature 5°C lower than that for received specimen, i.e. 35°C. Increasing the aging times led to further decreases in CPT and reached its minimum values for the specimens aged for 24 hours and 72 hours which equals 27.5°C for both aged times. In the other side, Table 3 showed that the austenitic specimens aged at 600°C were exhibited to continuous reducing in CPT and reached minimum value for the specimens aged for 10 hours, 24hours and 72 hours which is less than, or equals, 20°C i.e. at least 12.5 °C lower than that exhibited of as received condition.

Decreasing in CPT for the specimens aged at 600°C, for both alloys, can be attributed to the precipitation of chromium carbides along ferrite austenite phase boundaries, in austenitic alloy as shown in figure 2, and the ferrite phase decomposed to sigma phase, in duplex alloy as shown in figure 3. This secondary austenite and sigma phase caused a lower pitting resistance because they are acting as a preferential site for pitting.

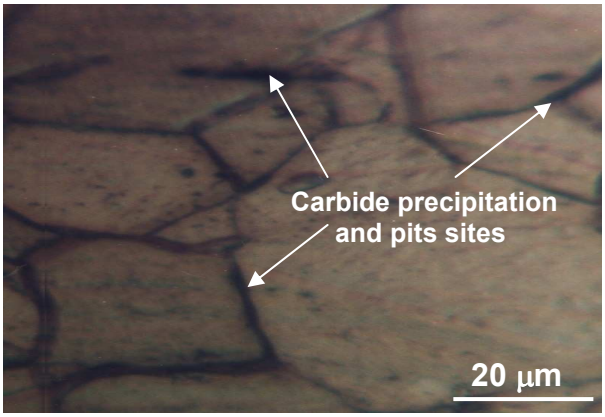

Figure 2 The microstructure of aged austenitic alloy at 600°C for 24 hours

Figure 4 showed the visual formation of pits of both types of stainless steels. Large number of pits with great size can be evident on the surface of SAF 2304 specimens aged at 24 hours and 72 hours. Also dense pits with smaller size on the surface of AISI 316L specimen aged for 72 hours can be evident.

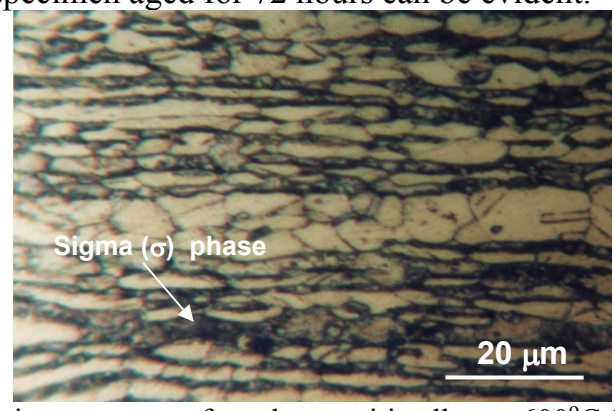

Figure 3 The microstructure of aged austenitic alloy at 600°C for 24 hours

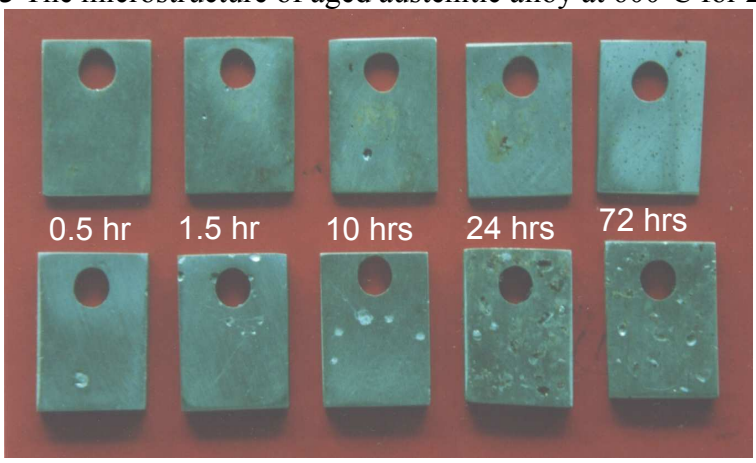

Figure 4 Visual investigation of the pits created at 600°C, at different aged times; the upper specimens AISI 316L, the lower = SAF 2304

DISCUSSION

Table 1 showed that the duplex stainless steel SAF 2304 specimens aged at 400°C for 0.5 and 1.5 hours have an equal CPT, 40°C, as in received condition, i.e. The aging temperature at 400°C for aging times 0.5 and 1.5 hours had no effects on pitting resistance of SAF 2304. However, austenitic specimens showed a noticeable decrease with increasing similar aged times.

This investigation shows that creation and changing the metallurgical aspects in austenitic stainless steel is much time sensitive than duplex, which is practically means austenitic stainless steel need higher cooling rate, after welding or heat treatments to avoid precipitation of carbide or other hard phases [3, 6]. However, it seems that 400°C is not a worst temperature for sensitizing the austenitic alloy, because aging for 72 hours at that temperature only caused decreasing 2.5°C, and 5°C comparing with 0.5 hr and not treated specimens respectively.

Austenitic stainless steel showed that 500°C is the worse temperature for sensitization than 400°C, because it was only need 30 minutes, and may be less, to

decreasing the CPT by 5 degree centigrade, compared with un-treated specimen. However, at 400^{o}C the CTP was decreased only 2.5^{o}C, for the same time. The same approach could be applied on duplex alloy, because CPT was not affected at 400^{o}C in 30 minutes aging time, however 500^{o}C is decreased CPT by 2.5^{o}C in similar aged time.

Regarding a temperature 600^{o}C, the results showed that both alloys subjected to sensitization in a very early aging time, 30 minutes, or less. Table 3 showed that CPT values decreased noticeably with longer aged times. This means that this temperature is a worst comparing with other lower temperatures, 400 and 500^{o}C, in all aged times, for both alloys. This means, in engineering applications, such as welding and heat treatments [4], such type of alloys should not remained in this sensitization range, especially 600^{o}C.

Because, this sensitizing temperatures are encouraging the stainless steel alloys for metallurgical phase transformations, that act as pit triggers. Therefore, high cooling rates at these temperatures are necessary to avoiding precipitation carbide and second phases, in stainless steel alloys, that have harmful effects on pitting corrosion [3, 6].

CONCLUSIONS

1- The range of temperature 400^{o}C to 600^{o}C is located within a sensitization range of duplex stainless steel alloy.

2- With increasing the aging temperature from 400^{o}C to 600^{o}C, the susceptibility of SAF 2304 and AISI 316L to pitting corrosion increased.

3- The CPT of duplex stainless steel SAF 2304 reached minimum values 30^{o}C at 600^{o}C for 24 hours. While AISI 316L reached minimum, 20^{o}C, at the same temperature beginning with 10 hours.

* Loughborough University, UK Wolfson School of Mechanical and Manufacturing Engineering, Loughborough University, Loughborough, LE11 3TU, Leicestershire,UK
**, Salahaddin University-Hawler, Kurdistan-Iraq

REFERENCES

1. J. Olsson, and M. Snis, Duplex – A new generation of stainless steels for desalination plants, Desalination, (2007) Vol. 205 pp. 104–113.
2. F. M. Khoshnaw, and R. A. Gardi, Effect of some metallurgical aspects on intergranular and pitting corrosion of stainless steel alloys SAF 2205 and SAF 2304, Stainless steel world conference, (2003) Holland, , pp. 56-61.
3. J. Nowacki, and P. Rybicki, Influence of heat input on corrosion resistance of SAW welded duplex joints, Journal of achievements in materials and manufacturing engineering, (2006) Vol. 17 Issue 1-2, pp. 113-116.
4. E. Evangelista, H.J. Mcqueen, M. Niewczas. and M. Cabibbo, Hot workability of 2304 and 2205 duplex stainless steels, Canadian metallurgical quarterly (2004) Vol. 43, No 3, pp. 339-354.
5. J. J. Dunn and D. S. Bergstrom, AL 2003 LDSS (UNS S32003) as a Substitute for Type 316L, Presented at the stainless steel world 2006 Conference, Houston, Texas.

6. Khoshnaw F. M. and Hamakhan, I. A., "Determination of the mechanical properties of austenitic stainless steel weldments by using stress strain microprobe" Materials science and engineering A, (2006) Vol. 426, No, 1-2, pp. 1-3.
7. ASTM E3, Standard test method for metallugraphy of metals, Annual Book of ASTM standard, Vol. 0.3-0.02, Philadelphia, 2006.
8. ASTM G 48, "Standard practices for detecting critical pitting temperature in stainless steels", Annual book of ASTM standards, Vol. 0.3, 0.2, Philadelphia, 2006.
9. P. Hummelgaard, K. Vilpponen, Improved method for ASTM G48 corrosion testing of welds, Nordic innovation centre, 2004, project number: 1639-03.

STABILIREA SENSIBILITATII OTELURILOR INOXIDABILE DUPLEX UTILIZAND METODA TEMPERATURII PUNCTULUI CRITIC – ASTM G48

Rezumat: In general, efectul diferitelor procese de fabricatie, cun ar fi sudarea otelurilor inoxidabile pot fi transferate in mod correct utilizand tratamente termice specifice. In acest studiu a fost evaluate influenta acestui tratament asupra susceptibilitatii la pitting prin testarea cu FeCl3 conform standardului G48 - ASTM, carea esete dedicate determinarii rezistentei la pitting a otelurilor inoxidabile austenitice. In acest studio a fost abordata influenta tratamentului de coroziune tip pitting pentru doua marci de oteluri SAF 2304 si AISI 316L. Otelurilor li s-a facut un tratamente de imbatranirela 400^{o}C, 500^{o}C, si 600^{o}C pentru diferite perioade. Rezultatele au aratat ca odata cu cretserea temperaturii de tratament de la 400^{o}C la 500^{o}C rata coroziunii prin pitting la otelurile inoxidabile creste indifferent de timpul de mentinere. La 600^{o}C si la timpi de imbatranire de 24 de ore ambele oteluri s-au gasit la punctual critic de pitting pentru combinatiile temepratura timp selectate in studio. Aceste rezultate sunt atribuite aspectelor metalurgice ca: precipitatrea carburilor, formarea fazelor intermetalice sau austenitei secundare etc, cu effect semnificativ asupra comportarii la coroziune si anume, de crestere a acesteia.

BULETINUL INSTITUTULUI POLITEHNIC DIN IAŞI
Tomul LIII (LVII), Fasc. 3, 2007
Secţia
ŞTIINŢA ŞI INGINERIA MATERIALELOR

A SUSTAINABLE INDUSTRIAL DEVELOPMENT OF MATERIAL SCIENCE AND ENGINEERING

BY

ADRIAN DIMA[1], ALINA ADRIANA MINEA[1], IULIA MARGARETA DIMA[2]

ABSTRACT: *Protecting the environment became, at this time, a major problem of all humanity. In this context, regarding Romania's integration in European community we must show that one of the main chapters that were negotiated for time extension is environment.*

In the article, based on the new scientifically ways to board the "TO KNOW HOW" area, we are proposing for analysis another way to board the sustainable development concept. The paper also presents the field of material science and engineering and its importance in sustainable development. Materials Science and Engineering represent a science in full evolution in concordance with the necessities of a modern society. Without modern materials and without European integration we cannot conceive a society development at the needed level.

KEYWORDS: *industrial development, European integration, materials science, sustainable development.*

1. INTRODUCTION

Protecting the environment became, at this time, a major problem of all the humanity. The irrational industrial developments, the excessive chemicals of agriculture, town extension are the factors of pollution, with high negative impact on environment. This chaotic development cannot contribute to a sustainable development; it goes to a present development with negative effects in future times.
In the actual economical situation of our society, economical increasing must remain the principal objective for our integration in European community.

Economical increasing cannot be concrete without protecting the environment, because a chaotically economical development it is going to ruin the life conditions with non-recoverable repercussions in time.

Sustainable development, the concept that clearly define that it must establish the present necessities without compromising the ability of future generations to satisfy their own needs, represent the only way to progress.

In addition, there are many opinions that this concept, of sustainable development is a utopia, that this concept cannot be imposed to transition and poor countries, because of their impossibility to apply and respect these principles.

Therefore, it is necessary a stagnation of economical development if we do not want to affect the environment.

The outstanding results in area of materials science and engineering from the last 10 years, on the basis of developing non polluting technologies and constant re-

using of scraps is creating the premises to affirm that the materials science and engineering development permit the discovery of non polluting technologies, that are using non conventional fuels, ecological technologies for scraps reusing.

These facts are contribution to realize an effective economical increasing based on sustainable development.

2. DISCUSSIONS

We must remark that, in the present, are many studies that show that a brutal action under environment will damage the ecological equilibrium that goes, finally, to disasters. These ecological disasters will negatively influence not only the further development, but the life possibilities in safe conditions, too.

As follows, near United Nations Organizations take place an International Commission of Development and Environment. This commission is supervising the evolution of environment quality and monitor economical activities that could damage the earth ecological equilibrium.

In this context, regarding Romania integration in European community, we must show that one of the main chapters that were negotiated for time extension is Environment.

Making a step back to International Commission of Development and Environment we can show that its activity until now is concretized in creation and consolidation of a new concept called Sustainable Development Concept.

The concept is promoting that way of economical development that assure the rational use of conventional energetic resources that assure the use of non conventional energetic resources and regenerative ones, along with protection and conservation the environment.

This concept shows that for assuring the welfare of the present and future generations it is highly recommended to preserve and conserve the existing patrimonies.

Therefore, by practically applying this concept, we must find the optimum solutions regarding economical dimensioning in all area in order to discover, to apply the non-polluting technologies, and to develop an ecological agriculture.

The concept of sustainable development can be defined like the developments that accomplish the present necessities without compromising the needs of the future generations.

The sustainable development concept is creating lots of disagreement in opinions moving to dangerous ideas regarding stopping the economical development and generalization of environment role.

In this idea, in the report of Rome Club regarding human economical development is pointed that it is not normal to absolute the environment role in the disfavor of economical development. In addition, in this report is shown that sustainable development must sustain human progress on the entire planet for as longer as it can. In this context, there are many comments regarding principal objectives, priorities and concrete actions.

In the article based on the new scientific ways to board the "TO KNOW HOW" area, we are proposing for analysis another way to board the sustainable development concept, as shown in figure 1.

Economical development on industrial basis it is strictly connected with development of materials engineering, environmental protection and its resources because of using the minerals resources (bringing out, working out, processing) in industrial processes that are producing industrial gases that have a high degree of pollution and affects the environment.

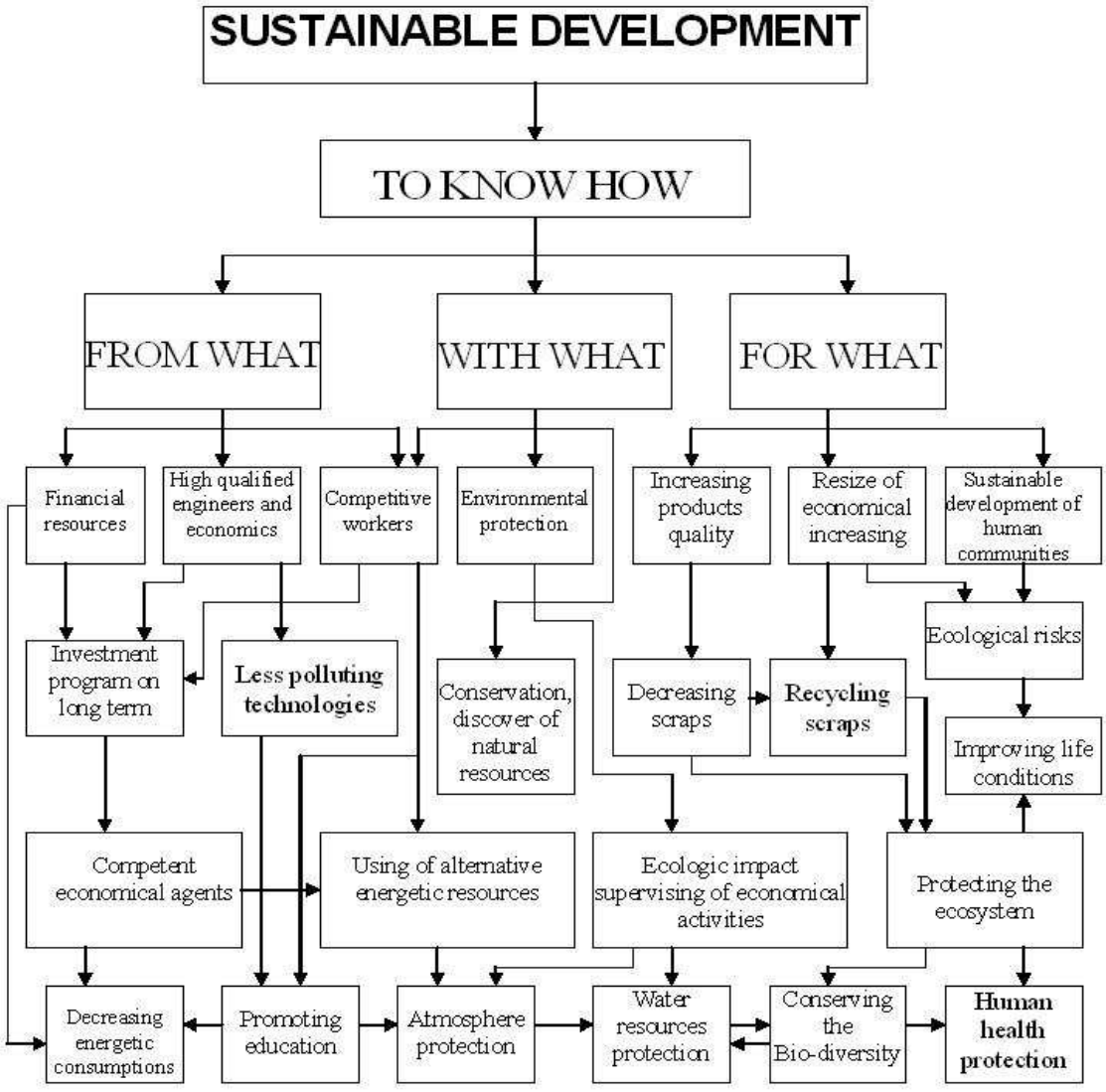

Figure 1. Scheme for illustrating the influence sustainable development concept

For decreasing these negative aspects, the materials obtaining and processing technologies must concentrate on reducing the consumptions of materials and energy, on decreasing the technological losses and minerals resources and on minimizing of polluting emissions and scraps.

In highly developed countries it was imposed a legislation regarding pollution, a legislation that is needed to be applied in our country, too. These laws are referring at

the designing in the same time with the destruction (at the end of the life cycle) of technologies or products. This project of designing (with the project of destruction) must contain elements and possibilities of recovery of some parts of the initial project. The implementation of non-polluting or with a low degree of polluting technologies (ecological technologies) is very expensive and need important material resources. The economical agents, in their majority, do not have enough capital and financial assets to apply these technologies, so authorities must interfere to support these initiatives to introduce the non-polluting technologies and to minimize the negative effect of industrial activity over environment. The chaotically industrial development, massive forestland clearings, water courses deviations, brutal modifications of ecosystems, intense exploitation of natural deposits are important risk factors that cannot be avoided.

For underlining the importance of some economical and industrial category as a subject of sustainable development, in assuring environmental quality conditions, these have the eco suffix. Eco-material and eco-product represent, in the context, categories that have an ecological performance, as:

- to respect the norms of environmental quality, product norms and emissions norms;
- to have a high degree of recyclables to justify big expanses for storing or neutralization.

It could be said that a sustainable material, processed in a sustainable industry is the result of an industrial process characterized through:

- have eco material characteristics and it is also an performing material;
- have the substitution of diverse assets: natural, economical, human etc.;
- metallurgical processes and technologies are transforming into social engineering;
- represents the success of scientifically and technological progress, in industrial globalization conditions;
- integration of environmental engineering in scientifically science is as part of socio-economical theory.

Steel has an important place in the industrial metallic materials area. In this context, we can say that, in present, steel can be considered as a sustainable material, made in a sustainable siderurgy.

The arguments for sustaining this idea are:

- steel is and will be the main metallic vector for developing high research areas, with direct implications in life quality;
- siderurgy represents an auto-performing area through increasing the technical and scientific assets;
- siderurgy has a process of translating the quality of material giver to industrial system giver;
- steel evolution is based on industrial fitness, defined as the way found by an industrial area stays always in actual trend.

Industrial fitness represents the procedure in which an industrial area stays young for its workers. This is not a biological age issue; it is the expression of an interior attitude.

3. CONCLUSIONS

Applying the concept in the concrete case of our country it can be said that sustainable development consist in the capacity of the national system and the authorities to realize a perfect equilibrium between social, technical and economical conditions and environment quality that are contributing to the welfare of our country.

In order to apply the ways and programs that are going to a sustainable development are necessary important financial and human resources and to understand that, now, it is necessary to minimize our profits to accomplish large benefits later.

Material Science represents a science in full evolution in concordance with the necessities of a modern society. In conclusion, to this area, of materials science and engineering it is assigned the mission to find technical and technological solutions for reducing the negative aspects of other activities, for reducing the environmental pollution and to contribute with scientific researches to invigorate the polluted areas.

REFERENCES

1. T. Rusu, L. Moldovan, SE Avram (2003) Managementul activitatilor pentru protectia mediului, Ed. Mediamira, Cluj Napoca;
2. A. Nicolae (2004) Dezvoltare durabila in siderurgy prin valorificarea materialelor secundare, Ed. Printech, Bucuresti;
3. V. Nistreanu (1999) Elemente de ecologie, Ed. Bren, Bucuresti;
4. M. Bordea (2006) Consideratii si cercetari privind informatizarea proceselor metalurgice din unele agregate moderne pentru elaborarea otelurilor, teza de doctorat, Cluj Napoca;
5. A. Dima, A.A. Minea (2004) Durable development – way to progress, welfare and European integration, Buletinul IPI, trom XL, Iasi.

Received April 12, 2007

[1] *"Gh. Asachi" Technical University of Iasi, Romania*
[2] *Tutora School, Tutora, Romania*

DEZVOLTAREA DURABILA IN STIINTA SI INGINERIA MATERIALELOR

REZUMAT: Protectia mediului a devenit, la ora actuala, o problema majora, de o deosebita importanta, cu care se confrunta omenirea.
In acest context, privind integrarea romaniei in comunitatea europeana, trebuie sa aratam ca unul din principalele capitole la care s-a negociat prelungirea timpului de rezolvare si dupa integrarea propriu-zisa este Mediul.
In prezenta lucrare, pe baza perceptelor noii modalitati stiintifice de abordare a domeniului „TO KNOW HOW", va propunem spre analiza o alta modalitate de abordare a conceptului dezvoltarii durabile.

BULETINUL INSTITUTULUI POLITEHNIC DIN IAŞI
Tomul LIII (LVII), Fasc. 3, 2007
Secția
ŞTIINȚA ŞI INGINERIA MATERIALELOR

EXPERIMENTAL INSTALLATION FOR THE STUDY OF THERMO MECHANICAL FATIGUE IN MEMORY SHAPE ALLOYS

BY

DRAGOS ACHITEI, CARMEN NEJNERU, DAN GELU GALUSCA, ROXANA-GABRIELA CARABET, ION HOPULELE

Abstract: *The paper shows the installation for the experimental study of thermal fatigue in shape memory alloys, type AlCuZn. The installation contains some systems: the mechanical stress system, the command system of the mechanical stress, thermal command system, the measurement system of the thermal cycles.*
Keywords*: shape memory alloys, thermal fatigue, mechanical fatigue.*

1. INTRODUCTION

The memory shape alloys are sensitive to fatigue. In addition, towards the phenomena met in classical crystalline materials like the formation of the dislocations arrangements and the densities of dislocations, the presence of the link between the grains in polycrystalline materials which are supplementary sources of initializing the cracks, the memory shape alloys present supplementary link mechanisms to phase change which is characteristic to them.

These mechanisms are grouped in a thermal fatigue way and three mechanical fatigue ways.

Table 1

Thermal and mechanical fatigue ways in memory shape alloys.			
	$T < M_f$	$A_f < T < M_s$	$T > M_s$
Mechanical	Reorientation of the martensite	realization of martensite through contraction	classical fatigue in austenite phase
Thermal	Thermal cycling between the stability domains of those two phases.		

Most practical times, the different mechanisms interfere and the phenomenon becomes very complex. Thermal fatigue depends on the following factors:
- temperature ;
- applied stress ;
- imposed deformation ;
- transformation temperature M_s.

In case of a device where the memory element makes memory shape effect in double sense within the work system (to reestablish it is used spring coupling), the modulus of fatigue defines through the cycle number until recovery stress decreases to a minimum value (circa 70% from the initial one).

According to the cycling type to which a memory shape alloy is submitted, this can present irreversible deterioration phenomena of the microstructure which define specific categories of fatigue.

In case of cycling through double memory shape effect the applied stress is maintained constant and the thermal fatigue appears and in cycling through simple memory shape effect appears thermo mechanical fatigue.

The mechanical fatigue implies the rupture after the next stages:
- the defects storage (which create cyclic cold hardening);
- cracks formation;
- cracks spreading first in stationary state then non-stationary until final rupture.

The mechanical fatigue resistance of the memory shape alloys depends on the value of M_s Temperature namely as M_s is smaller as fatigue resistance is weaker.

2. THE EXPERIMENTAL INSTALLATION

The installation has a complex configuration in order to realize the experimental study of thermal fatigue in memory shape alloys.

To serve the proposed purpose, the installation will be formed from two work posts with the same stress type, to shorten the time necessary to the asked determinations into the work plan because the number of cycles which is necessary to a solicitation is 10^4-10^5 cycles implicitly the function time for realizing the cycles is dozens of day order.

The standard samples, of memory shape alloy, will be submitted to traction being caught between the dies and the solicitation is made through a lever system to whose end it would be attached a plate where different weights were put on.

Figure 1. Standard sample, CuZnAl shape memory Alloys, for thermal fatigue test

The dies used for traction strain are toggled into the metallic enclosure, fitted with eyehole, which would be heated with a device which would blow warm air towards the sample.

According to the weights putted on the plate, the sample would be submitted to a strain that is directly proportional with the weight; the proportionality is obtained with the help of the lever system.

During experiments the memory shape alloy sample will suffer an elongation which could be determined by a dial comparator.

The installation will cyclic function, the number of heating – cooling cycles will be recorded by an electromechanical counter.

The installation contains the following systems:

a) the command system of the mechanical stress for thermal fatigue study;
b) the mechanical stress system;
c) thermal command system for the thermal fatigue installation;
d) the measurement system of the cycles in memory shape alloys.

a) The mechanical stress system is formed of:

- levers system;
- catch dies of the sample;
- transducers to determine the force and the displacement.

The map of the mechanical stress system is shown in figure 2.

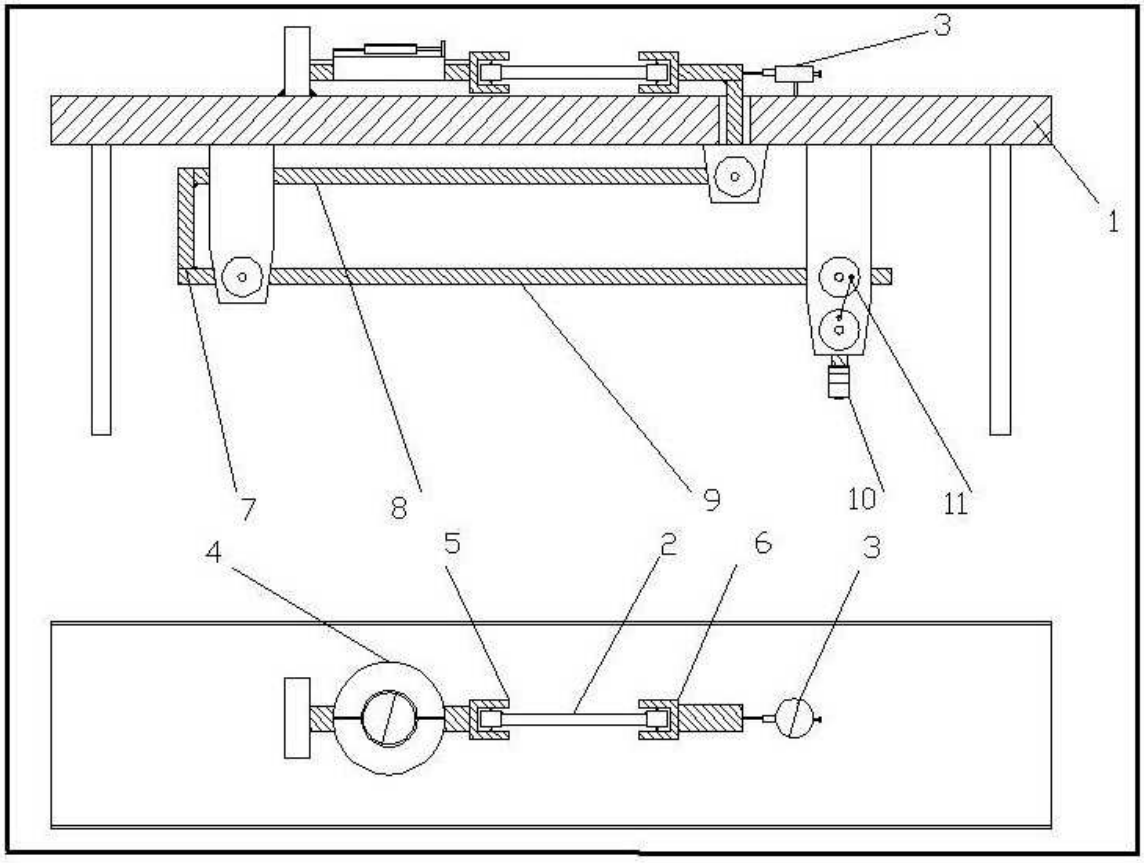

Figure 2. The mechanical stress system for the study of thermo-mechanical fatigue of the shape memory alloys: 1 – bed frame; 2 – sample; 3 - shift transducer; 4 – force transducer; 5, 6 – catch arms of the sample; 7, 8, 9 – stress levers; 10 – weights for stress; 11 – loading and unloading mechanism.

b) The command system of the mechanical stress for thermal fatigue study is shown in figure 3.

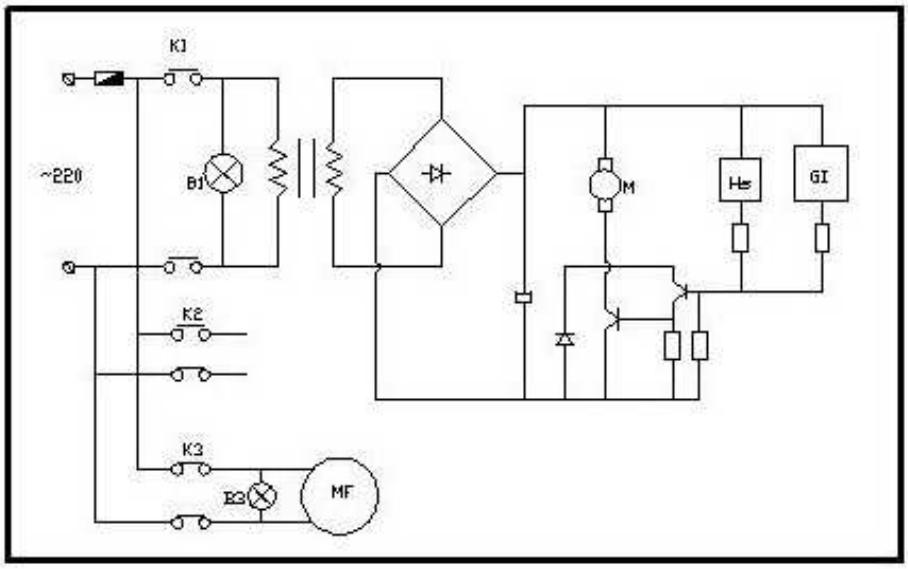

Figure 3. The command system of the mechanical stress for fatigue study of the memory shape alloys: K1 – tappet switch; K2 – heating switch; K3 – ventilator switch; Hs – position transducer (Hall); GI – impulse generator (time).

c) Thermal command system for the thermal fatigue installation is shown in figure 4.

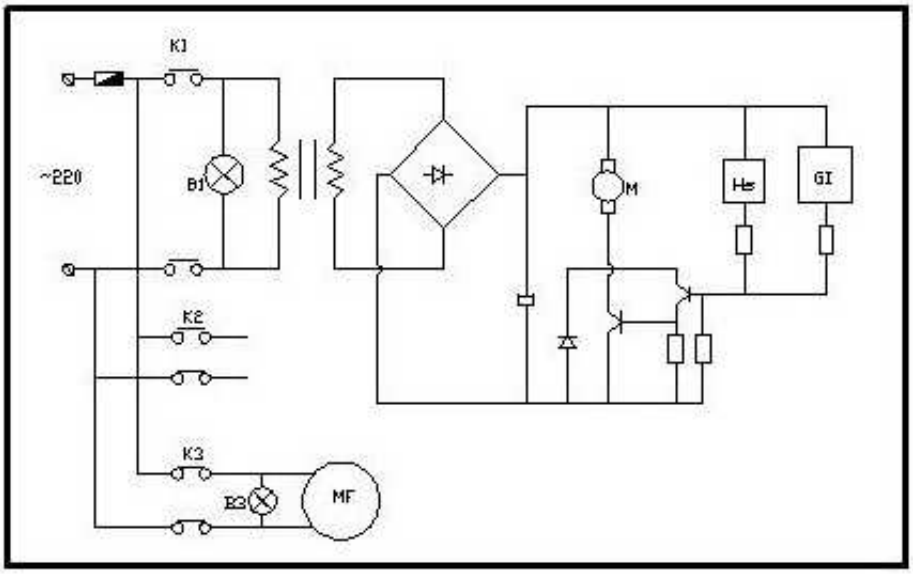

Figure 4. Thermal command system for the thermal fatigue installation of the memory shape alloys

d) The measurement system of the cycles in memory shape alloys.

An extremely important problem of this installation is the synchronization of thermal cycle with mechanical cycle.

This thing is import in shape memory alloys in order to determine the thermo mechanical fatigue during the material education which can be done to materials which present a double memory shape effect.

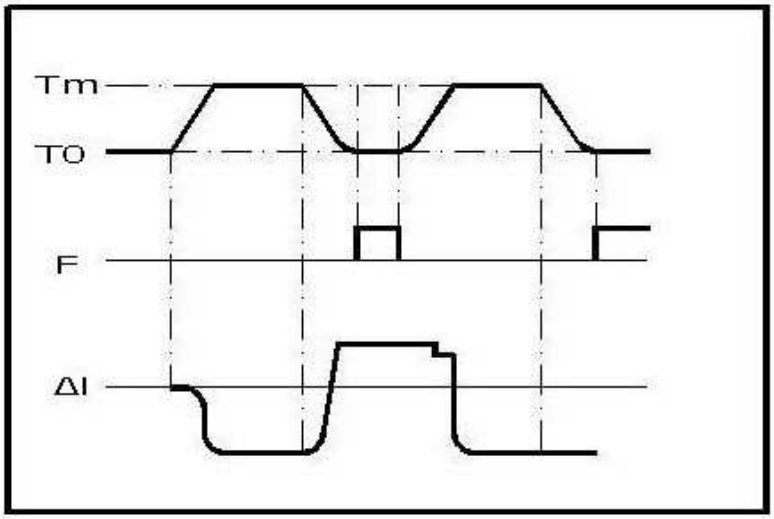

Figure 5. The map of the stress for thermo mechanical fatigue on memory shape alloys in the education process (through in-sequence traction).

The planning of the experimental study on the thermal fatigue of each alloy takes into consideration the procurement stages of the memory (education cycle) and the stress type to which it can be used (free reversion, retained reversion, with production of work, with pseudo elasticity).

There are four testing states:

- the fatigue in education process (reduced number of cycles);
- mechanical fatigue in austenite state;
- mechanical fatigue in martensite temperature;
- mechanical fatigue in transition temperature.

CONCLUSIONS

So we can conclude that the installation must satisfy all the conditions for the two types of tests:

a) mechanical fatigue in different temperature;
b) thermal fatigue through heating-cooling cycles with constant stress.

REFERENCES

[1]. Stanciu S., Cercetari privind influenta unor factori metalurgici asupra proprietatilor aliajelor cu memoria formei pe baza de Cu, Teza de doctorat , Iasi, 1998.

[2]. Dia V., Studiu documentar cu privire la tehnologiile si utilajele de prelucrare metalurgica a aliajelor cu memoria formei, Referatul nr. 1 din cadrul pregatirii Tezei de doctorat, Iasi, 2000.

[3]. Dia V., Dispozitive si instalatii experimentale pentru studiul parametrilor de prelucrare metalurgica a aliajelor cu memoria formei, Referatul nr. 2 din cadrul pregatirii Tezei de doctorat, Iasi, 2002.

[4]. Achiţei D., Studiul influentei oboselii termice/mecanice asupra proprietatilor de memorie a formei la unele aliaje metalice cu baza cupru, Proiect de cercetare stiintifica, Iasi, 2006.

Receiced april 2007 *Technical University "Gh.Asachi" Iasi*

INSTALATIE EXPERIMENTALA PENTRU STUDIUL OBOSELII TERMO-MECANICE LA ALIAJELE CU MEMORIA FORMEI

Rezumat :

Lucrarea prezinta instalatia pentru studiul experimental al oboselii termice la aliajele cu memoria formei, de tipul CuAlZn. Instalatia cuprinde mai multe sisteme : sistemul mecanic de solicitare, sistemul de comanda a solicitarii mecanice, sistemul de comanda termica si sistemul de masurare a cicluirlo de oboseala termica.

BULETINUL INSTITUTULUI POLITEHNIC DIN IAŞI
Tomul LIII (LVII), Fasc. 3, 2007
Secția
ŞTIINȚA ŞI INGINERIA MATERIALELOR

EXPERIMENTAL HEAT TREATMENT INSTALLATION FOR CYCLIC AGEING OF THE ALUMINUM ALLOYS

BY

CARABET ROXANA-GABRIELA, NEJNERU CARMEN, DIMA ADRIAN, ROTARU GINU, HOPULELE ION

Abstract: The paper presents the concept of a precipitation treatment installation, type cyclic for the aluminum alloys. The project of the installation take into consideration all the inconveniences which appear in the heat treatment of the aluminum alloys caused to their sensibility to the irregularity of the heating.
Keywords: aluminum alloy, cyclic heat treatment, ageing, solution treatment

1. INTRODUCTION

The importance of studying the heat treatments of the aluminum alloys is due to their large use in different domains such as transport, constructions, power industry, and medicine and food industry as well as for their difficulties caused to aluminum alloys sensibility to the irregularity of heating.

There have been mainly studied the treatment and the behavior of aluminum alloys for air industry (type duralumin).

The heat treatment of these alloys is solution treating followed by ageing.

The alloys that support solution treatment must fulfill the following conditions:

- to admit the variation of solubility within solid state;
- to admits a high percent of secondary phases.

The solution and precipitation mechanism is:

- the structure of aluminum alloys presents precipitates to the grains limit and once the material is heated over the solidus line these dissolve getting a solid solution to the temperature of the heat treatment. After sudden quench, the structure „freezes" and it is obtained a supersaturated solid solution that is soft and plastic.

The final operation – ageing takes through warming under the solidus line and non-shock chilling to the procurement of a secondary phase disperses in the mass of the solid solution so that the material would become tough.

The explanation of material hardness through the appearance of the precipitates is that the precipitates block the movement of the dislocations in the material so that as finer and more disperse the precipitates are as powerful the blockage of the dislocations is and such the material is tougher.

Thereby it is welcomed a theoretic and experimental study on the structural transformations that appear in the aluminum alloys during ageing and the test of some new ageing methods besides those well-known: natural ageing, artificial ageing.

The new proposed to study type of ageing is cyclic ageing.

In case of a cyclic ageing it is followed to reach the following objectives:

- a bigger structural stability;
- the procurement of a greater precipitation germs;
- the formation first of the clusters which are favorable to hardness (which block the dislocations).

2. THE DESCRIPTION OF THE INSTALLATION

The aluminum alloys present intense heat transfer so that any heating irregularity leads to heats on different parts of the pieces compromising the heat treatment. Under these conditions, the heat treatment installations for aluminum alloys must respect the uniformity conditions of temperature in the entire space of the treatment enclosure.

It is recommended the heat treatment in salt baths or oil baths.

The proposed installation for the cyclic precipitation treatment represents a system with two troughs with oil at two different temperatures. The telescopic arm, which with the help of two engines can move the sample into an oil bath or in another one to a time range mechanically, established. A counter (the general scheme of the installation is in figure 1) records the number of cycles.

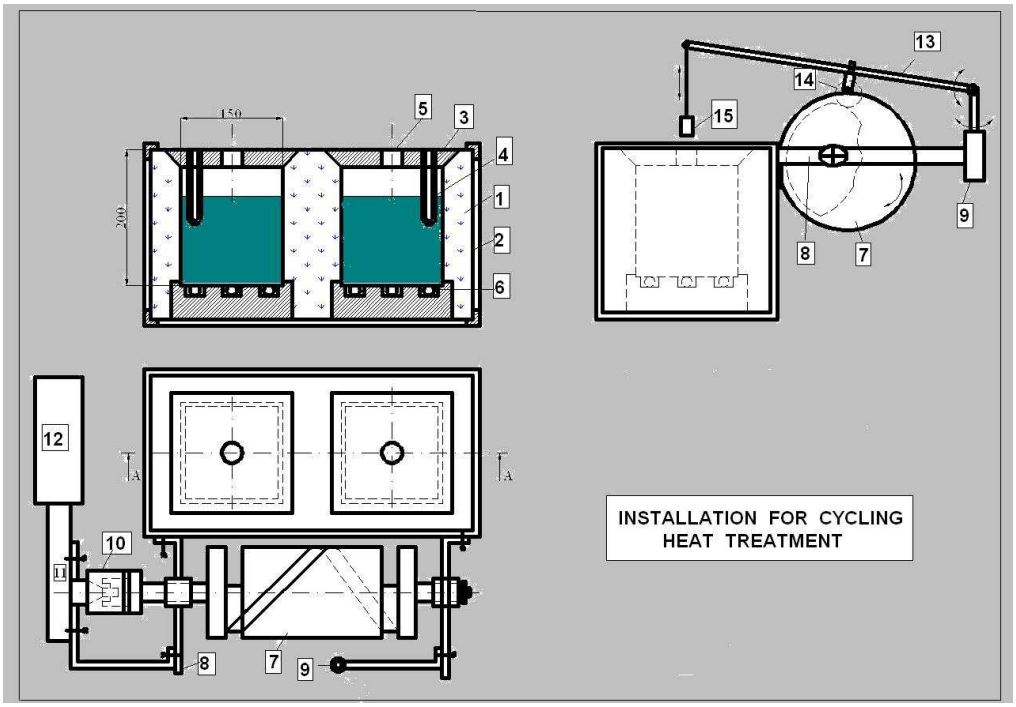

Figure 1. Installation for cycling heat treatment

Where:

1. Thermal insulation;
2. Metallic frame;
3. Thermal insulation cap;

4. Thermowell;
5. Sample inlet;
6. Electric heating system;
7. Spatial cam to maneuver the sample;
8. Support holders of the cam;
9. Support holders of the arm;
10. Rotation coupler;
11. Reductor;
12. C.c. electric engine.
13. Arm;
14. Cam roll follower;
15. Sample.

The installation includes the following systems:
1 – heating system;
2 – command and control system;
3 – driving system of the arm.

a) The heating system includes:
   - Two stainless steel through $150 \times 150 \times 200$ mm;
   - Two kantal resistors with ceramics insulation fitted in two firebricks.

b) The command and control system includes:
   - Two thermocouples type Cromel-Alumel to measure the temperature within the two oil baths;
   - Cycles counter;
   - Electric heating system

The electric heating system from figure 2 contains:
1) Command circuit of the heating resistors;
2) Power supply;
3) Antistatic filter.

2) the power supply ensures the integrated circuit supply and the stabilization of reference supply for the thermal probe;
3) the filter protects the montage by ensuring its stability and protecting it from the static from 220 V net.

The thermal command system includes two stages:
– The first stage: the detection part of the temperature variation in the through is realized with an integrated specialized circuit. In addition, it is used a thermocouple as a sensor.
- The second stage: the command part of the heating resistors of the through realized with a controlled rectifier diode.

The operation of the heating system of the troughs

The variation of the temperature in the through is permanently observed by the integrated circuit which realizes the necessary correction to maintain the temperature constant.

Thus, if the temperature rises over the reference value, the integrated circuit commands the interruption of the power from the controlled rectifier diode opening

the circuit of the heating resistors. If the temperature decreases under the reference value, the integrated circuit commands the opening of the controlled rectifier diode straining all the heating resistors.

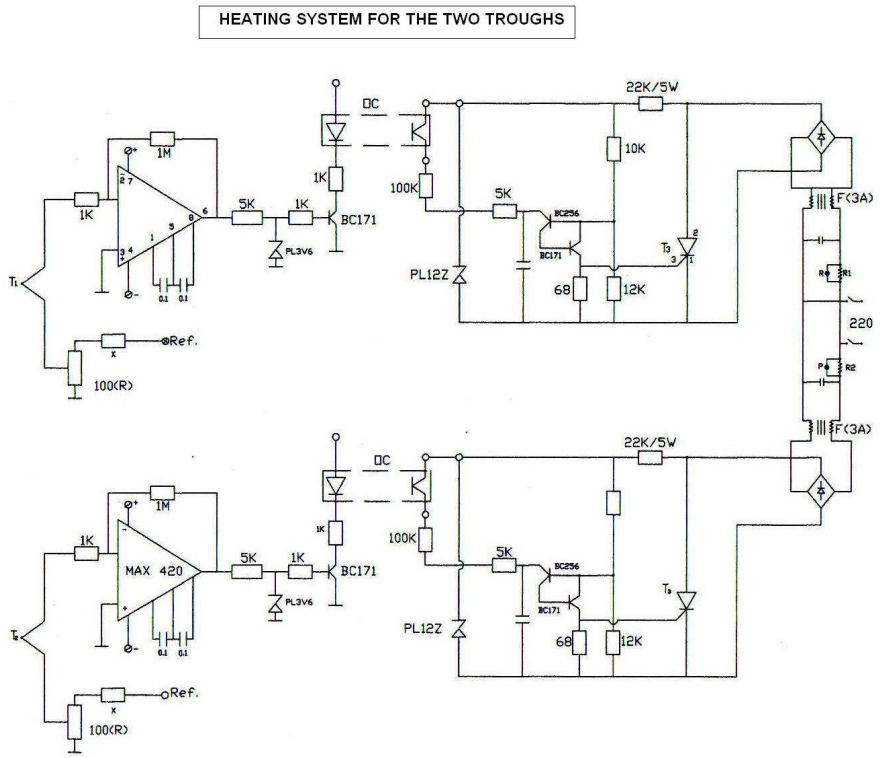

Figure 2. Heating system for the two troughs

c) The driving system of the arm includes:

The engine and a spatial cam can realize the driving movement of the arm upwards, downwards and laterally from a through to another one.

3. CONCLUSIONS

With the help of the installation, there can be done experiments for aluminum alloys:

- it can be varied the proposed cycle types such as modifying the two cycling temperatures, varying the maintain time in each oil baths and the symmetry degree of the proposed treatment;
- it can be tested the efficiency of the ageing treatment realized in the experimental installation by making a comparison with other samples realized in classical conditions of ageing treatment.

The efficiency of the ageing treatment can be emphasized with the help of determining the mechanic properties like hardness and mechanic resistance.

Received March 12, 2007

Technical University „Gh. Asachi" Iasi

REFERENCES

1. Carabet Roxana Gabriela - Conceperea si realizarea unei instalatii de tratament termic pentru imbatranirea aliajelor de aluminiu folosind cicluri termice, Lucrare de disertatie 2006;
2. Suzana Gadea, Maria Petrescu – Metalurgie fizica si studiul metalelor, partea a-III-a, Editura Didactica si Pedagogica, Bucuresti, 1983.

INSTALAȚIE EXPERIMENTALĂ PENTRU TRATAMENTUL TERMIC DE ÎMBĂTRÂNIRE A ALIAJELOR DE ALUMINIU UTILIZÂND CICLURILE TERMICE

Rezumat: Lucrarea prezinta conceptia unei instalatii de tratament termic de imbatranire varianta ciclica pentru aliajele de aluminiu. Proiectul instalatiei tine cont de inconvenientele ce apar la tratamentul termic al aliajelor de aluminiu datorita sensibilitatii acestora la neuniformitatea incalzirii.

BULETINUL INSTITUTULUI POLITEHNIC DIN IAŞI
Tomul LIII (LVII), Fasc. 3, 2007
Secția
ŞTIINȚA ŞI INGINERIA MATERIALELOR

WASTE REVALUATION FROM THE ALUMINUM RECYCLING INDUSTRY

BY

MARGINEAN IOAN[1], TARCOLEA MIHAI[1], MIREA VASILE[1], MARIA ROMAN[2], COCOLAS ADRIAN[1]

Abstract: *In production process of primary aluminum, over1000 kg of aluminum obtain, result as waste, other 2880 kg of solid compound. Through the replacement in process of production frame of primary aluminum and secondary aluminum, it's possible to remove these quantities of sub-product.*
The waste with higher aluminum percent can be directly recycled, for removal this one through recasting and those with lower aluminum percent of the dross (ashes) can be use as refractory material, in the frame of other industrial process. This study it propose an alternative method, viable economically specking, to generate auxiliary substance and stockpile the waste of process proceeded for industry of aluminum.

1. MOTIVATION OF THE CONCERNS IN THE RECYCLING AREA COMPLETE OF ALUMINUM WASTE (GENERAL PRESENTATION OF ALUMINUM WASTE)

Waste revaluation from aluminum waste describe a series of technical and economical barrier, being in some case waste generating of waste which have negative effect over the environment. It's the case of waste gathered from mixed flux, where it's necessary the introduction of auxiliary operation of removing the contaminate. It has in picture the cost of these operations, in order to not exceed the production cost of primary aluminum. Recycling rate of primary aluminum it grows progressively, it will be a growth of ~35 %, for the year 2010.

2.ALUMINUM WASTE CLASSIFICATION.

Aluminum destined to recycling can be separated in two categories: new waste and old waste.

New wastes represent technological waste generated by the casting process, thermic or mechanic processing and materials with lower percent of residual aluminum. They are returning directly in the recasting circuits, has chemical composition known and may be processed, and it's require a little preparation. Approximate 100 % of fabrication waste are recasting in aluminum industry.

Old waste*s are* those are which proceed of product or articles out of use, at the end of their life cycle. In this way the waste are fag, auto vehicle components, metallically carpentry, old lead wire, domestic apparatus, etc. Old waste proceeds of

collecting unit, which are gifted with shredders, magnetically separators, installation of detaching in dense environment.

3. THE CHARACTERISTICS OF THE RESIDUE RESULT BY EACH PHASE OF PROCESSING OF ALUMINUM ALLOYS WASTE.

Processors of secondary aluminum can be integrated in big aggregate works of products of aluminum or can work as independent unit. Through rapid price changes of the waste aluminum and the primary aluminum, as well as the fluctuation by the market regarding the alloys demanding from aluminum cast or warped, the processing must be very flexible. The wastes are generally received at the independent collecting unit. As a rule, these wastes are processed through casting, along with internal waste. Before the elaboration stage, from waste are removed the impurities through centrifugal action and washed for removal of the oil, water magnetically separated of ferrous components witch can be present.

The stage of elaboration-refinement consists from casting, refinement, allying, and pours the aluminum recovered from waste.

This process is used for transformation the waste of aluminum in product, after the flow sheet as well the one describe in fig. 1.

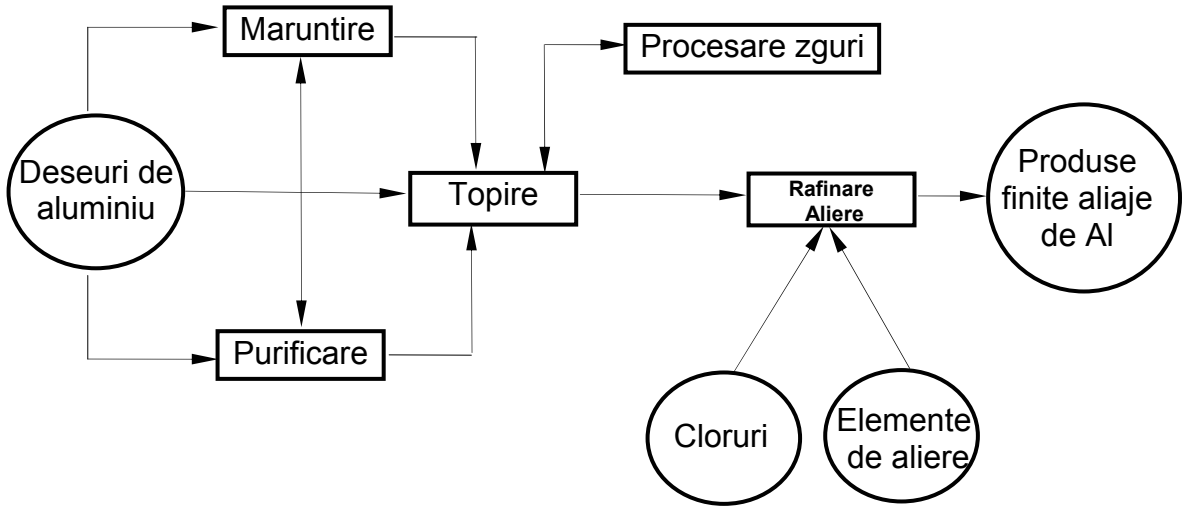

Fig. 1. Typical flow sheet for processing the waste of secondary aluminum

4. CHEMICAL COMPOSITION OF WASTE AND DROSS.

The waste can be classified by chemical composition:

- *waste with simple chemical composition* so called "white dross"
- *waste with complex chemical composition* so called " black dross”

Chemical composition and quantity of wastes can be determinate by physical and chemical characteristics of the materials witch compose the loading, the type of the elaboration aggregate used, the work atmosphere and the work technology and technology of elaboration applied, table 1.

Table 1. Waste chemical composition

Chemical composition, %	Sample											Total average
	1				2				3			
	1.1	1.2	1.3	Average of sample	2.1	2.2	2.3	Average of sample	3.1	3.2	3.3	Average of sample	
Aluminum	50,100	47,700	50,000	**49,267**	68,600	64,500	59,400	**64,167**	72,200	69,500	23,830	**55,177**	**56,203**
Silicon	6,800	8,240	7,240	**7,427**	7,000	5,870	7,200	**6,690**	3,500	4,700	4,600	**4,267**	**6,128**
Magnesium	2,060	2,290	2,060	**2,137**	0,950	0,950	0,960	**0,953**	1,180	1,190	0,600	**0,990**	**1,360**
Iron	1,830	2,020	2,000	**1,950**	1,200	4,000	9,500	**4,900**	0,750	0,970	0,420	**0,713**	**2,521**
Manganese	0,150	0,130	0,150	**0,143**	0,150	0,170	0,340	**0,220**	0,130	0,120	0,120	**0,123**	**0,162**
Titan	0,630	0,720	0,600	**0,650**	0,170	0,160	0,150	**0,160**	0,290	0,270	0,070	**0,210**	**0,340**
Copper	1,060	1,000	0,930	**0,997**	1,030	10,200	1,000	**4,077**	0,870	0,130	0,800	**0,600**	**1,891**
Plumb	0,250	0,320	0,240	**0,270**	0,110	0,130	0,130	**0,123**	0,084	0,150	0,016	**0,083**	**0,159**
Zinc	0,740	0,610	0,550	**0,633**	0,500	0,540	0,520	**0,520**	0,340	0,360	0,094	**0,265**	**0,473**
Tin	0,040	0,043	0,038	**0,040**	0,037	0,028	0,028	**0,031**	0,023	0,030	0,005	**0,019**	**0,030**
Nickel	0,025	0,060	0,024	**0,036**	0,050	0,033	0,039	**0,041**	0,025	0,030	0,009	**0,021**	**0,033**
Phosphor	0,050	0,055	0,047	**0,051**	0,016	0,020	0,020	**0,019**	0,055	0,020	0,007	**0,027**	**0,032**
Calcium	1,000	0,700	0,840	**0,847**	0,460	0,330	0,370	**0,387**	0,250	0,360	0,210	**0,273**	**0,502**
Chrome	0,028	0,020	0,030	**0,026**	0,014	0,015	0,026	**0,018**	0,014	0,013	0,004	**0,010**	**0,018**
Potassium	0,520	0,640	0,520	**0,560**	0,640	0,400	0,480	**0,507**	0,200	0,500	0,320	**0,340**	**0,469**
Sodium	1,700	2,110	2,060	**1,957**	1,620	1,070	1,800	**1,497**	1,500	1,750	1,400	**1,550**	**1,668**
Borine	0,011	0,013	0,007	**0,010**	0,005	0,005	0,007	**0,006**	0,005	0,005	0,005	**0,005**	**0,007**
F	1,780	1,880	1,030	**1,563**	0,840	1,040	1,410	**1,097**	0,930	0,970	2,020	**1,307**	**1,322**
Cl^-	1,500	1,330	1,490	**1,440**	0,180	1,280	0,530	**0,663**	0,450	0,500	0,490	**0,480**	**0,861**
CO_3^{2-}	2,130	1,900	2,500	**2,177**	4,140	1,280	1,160	**2,193**	0,870	3,770	1,350	**1,997**	**2,122**
SO_4^{2-}	0,050	0,050	0,050	**0,050**	0,050	0,050	0,050	**0,050**	0,050	0,050	0,050	**0,050**	**0,050**
NO_3^-	2,480	2,540	1,740	**2,253**	1,360	2,042	1,610	**1,671**	1,610	2,090	2,035	**1,912**	**1,945**

Table 2. Dross chemical composition ALMET SA

Chemical composition, %	Sample												Total average
	2.1				2.2				2.3				
	2.1.1	2.1.2	2.1.3	Average of sample	2.2.1	2.2.2	2.2.3	Average of sample	2.3.1	2.3.2	2.3.3	Average of sample	
Aluminum	69,900	68,270	65,700	67,957	63,900	63,500	68,200	65,200	33,300	32,800	34,100	33,400	55,519
Silicon	2,280	3,450	3,140	2,957	3,580	3,480	3,360	3,473	3,580	3,580	3,600	3,587	3,339
Magnesium	0,860	0,820	0,780	0,820	1,140	1,020	1,020	1,060	2,040	2,050	2,040	2,043	1,308
Iron	2,000	1,180	1,066	1,415	1,380	2,100	2,400	1,960	2,000	1,940	1,880	1,940	1,772
Manganese	0,160	0,160	0,180	0,167	0,160	0,180	0,160	0,167	0,100	0,100	0,098	0,099	0,144
Titan	0,200	0,270	0,260	0,243	0,390	0,450	0,380	0,407	1,300	1,300	1,280	1,293	0,648
Copper	1,030	1,018	0,790	0,946	0,820	1,140	0,800	0,920	0,560	0,560	0,560	0,560	0,809
Plumb	0,820	0,160	0,120	0,367	0,260	0,350	0,240	0,283	0,360	0,280	0,300	0,313	0,321
Zinc	0,640	0,780	0,580	0,667	0,600	0,680	0,660	0,647	0,700	0,680	0,660	0,680	0,664
Tin	0,018	0,038	0,034	0,030	0,046	0,084	0,070	0,067	0,060	0,060	0,056	0,059	0,052
Nickel	0,034	0,036	0,032	0,034	0,030	0,032	0,032	0,031	0,022	0,220	0,220	0,154	0,073
Potassium	0,240	0,230	0,240	0,237	0,380	0,410	2,220	1,003	0,830	0,840	0,740	0,803	0,681
Sodium	2,000	1,800	1,760	1,853	2,240	2,060	7,200	3,833	3,200	3,000	2,084	2,761	2,816
Borine	0,007	0,015	0,009	0,010	0,007	0,018	0,009	0,011	0,015	0,021	0,025	0,020	0,014
F	0,850	0,950	0,900	0,900	1,230	0,710	1,040	0,993	1,420	1,170	1,350	1,313	1,069
Cl^-	0,710	0,540	0,390	0,547	0,750	0,850	0,590	0,730	2,080	2,130	1,710	1,973	1,083
CO_3^{2-}	2,250	1,600	1,170	1,673	1,740	2,900	1,780	2,140	2,240	3,560	2,530	2,777	2,197
SO_4^{2-}	0,050	0,050	0,050	0,050	0,050	0,050	0,050	0,050	0,050	0,050	0,050	0,050	0,050
NO_3^-	3,840	2,480	3,590	3,303	2,640	4,090	2,540	3,090	2,110	2,110	2,230	2,150	2,848

5. WASTE AND DROSS UTILIZATION AS REFRACTORY MATERIALS AND EXOTHERMIC AT DIE CAST CONFECTION

Tested materials (generally dross from process) has been included in a series of 14 die basis of siliceous sand (in witch the core sand for the model was form dross binded with manifold binder of foundry), used for casting of measuring mark as "cone of blowhole".

The die of this event is that of cylindrical pyramid, with peak semi-spherical, with a diameter of 40 mm, going from a base with a diameter of 70 mm, extended with a border in steps with a diameter of 100mm. As cast proceeding it chose using the direct and rain cast. The first two die 1/0 and 2/0 was as type "witness", and to the execution of them it use only siliceous sand, and in booth use direct cast. The dies 1/1, 1/1.1, 2/1 and 2/1.1 have a layer of thermal insulator binded with furan resin. At the first two die it used bolter slag on bolter of 1 mm, and in next two die it used a batch base of dross. As in witness case we use direct casting, see figure 2 and 3.

Fig. 2. Die aspect before casting (Washed dross)

Fig. 3. Die aspect with refractory batch of slag and dross binded with furan resin (3/6…. 6/6) and sodium silicate (1/4 …. 4/4). (Unwashed dross)

Fig. 4. Die aspect with batch dross binded with resin after 48 hours from execution (Washed dross)

Fig. 5. Die aspect with batch binded with resin after 48 hours from execution (Unwashed dross)

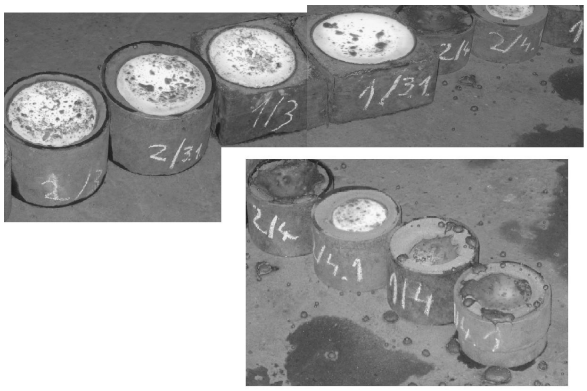

Fig. 6. Cast alloy in course of solidification (Washed dross)

Fig. 7. Cast alloy in course of solidification (Unwashed dross)

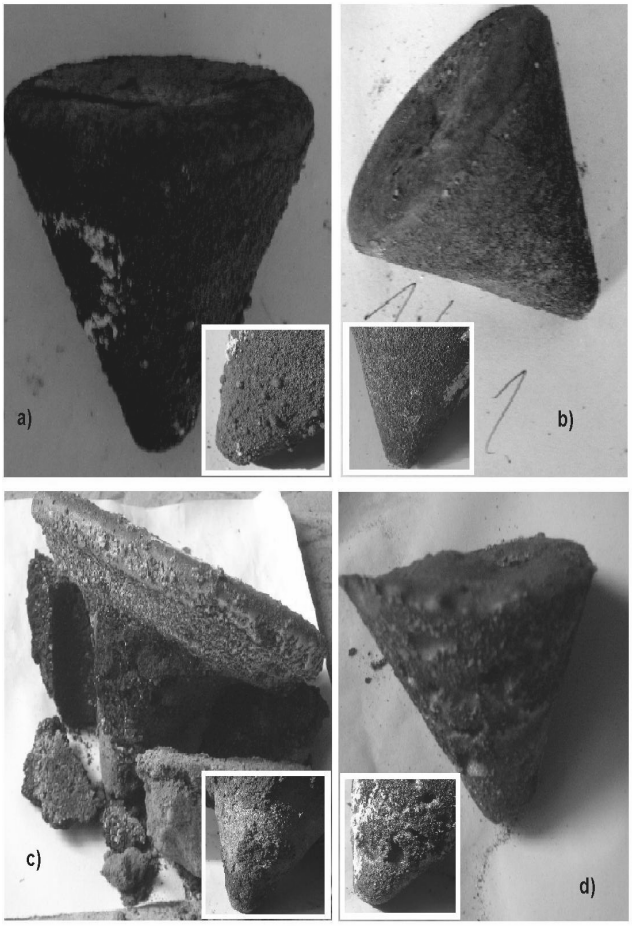

Fig. 8. Die cast and debated, function by the batch used a) Classical batch; b) Furan resin 4%; c) Sodium silicate with Fortusil 7%; d) Monophosfat of Al (Washed dross)

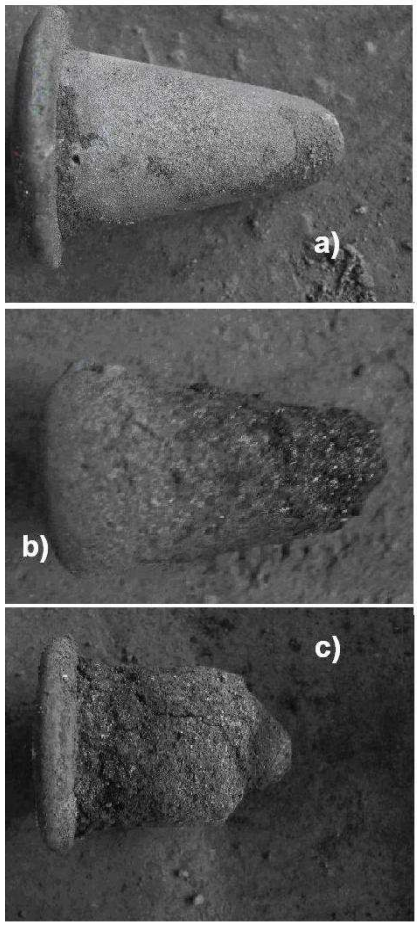

Fig. 9. Die cast and debated, function by the batch used a) Classical batch; b) Furan resin 4%; c) Sodium silicate with Fortusil

(Unwashed dross)

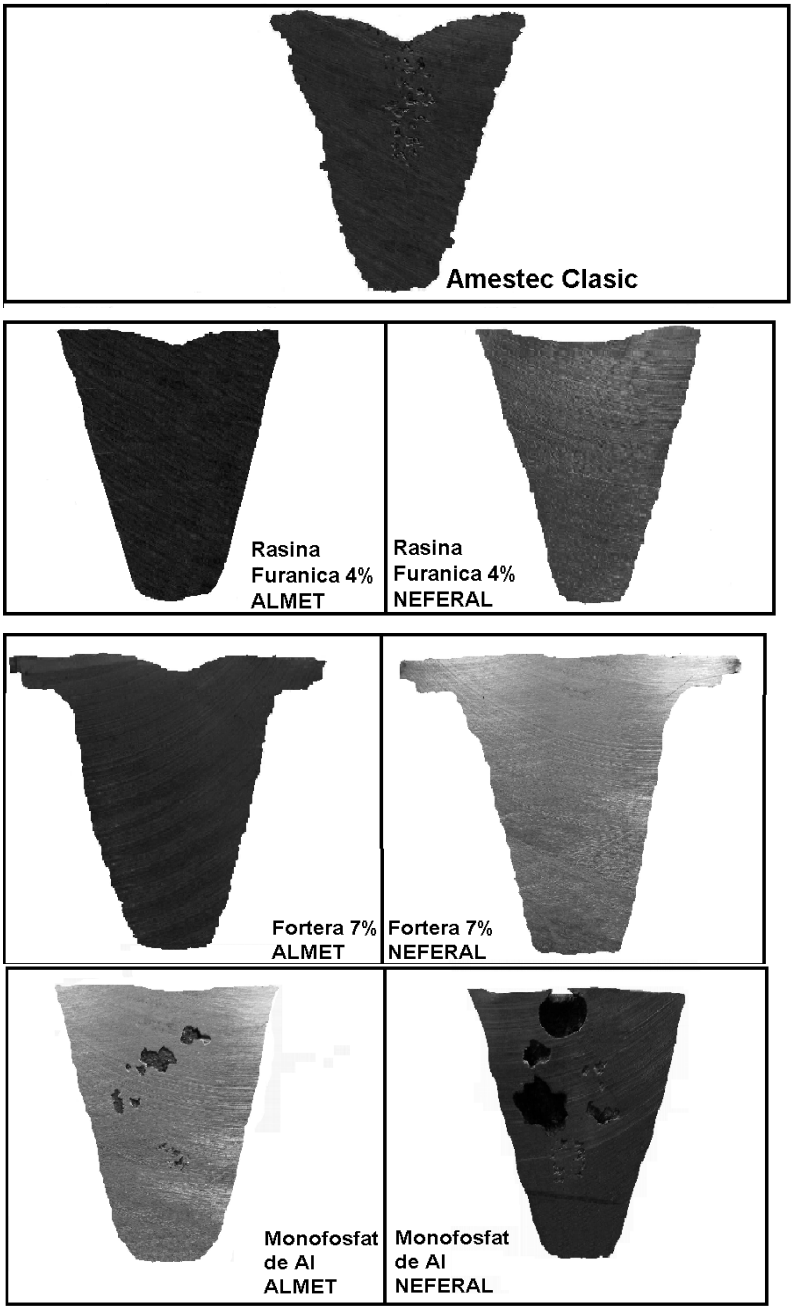

Fig. 10. Cut samples (Washed dross)

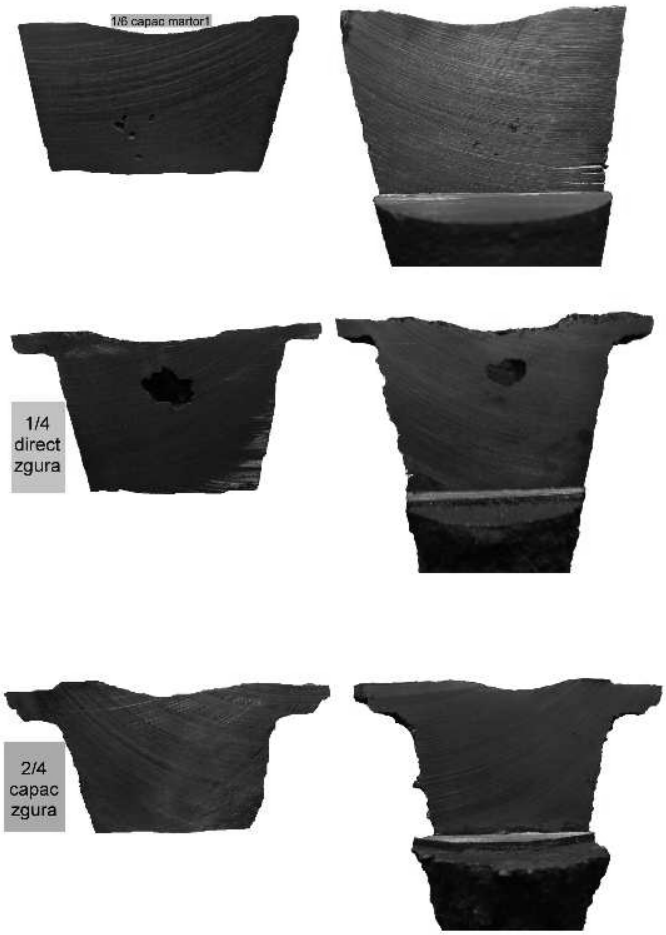

Fig. 11. Cut samples (Unwashed dross)

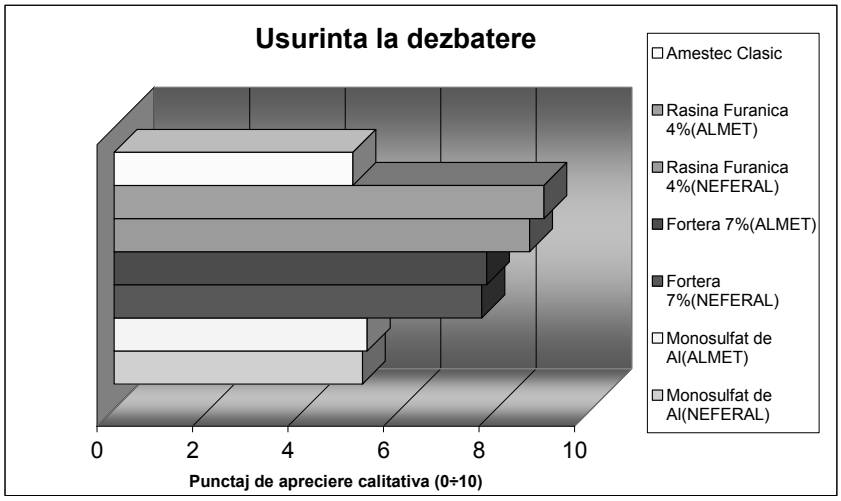

Fig. 12. Easiness of debating

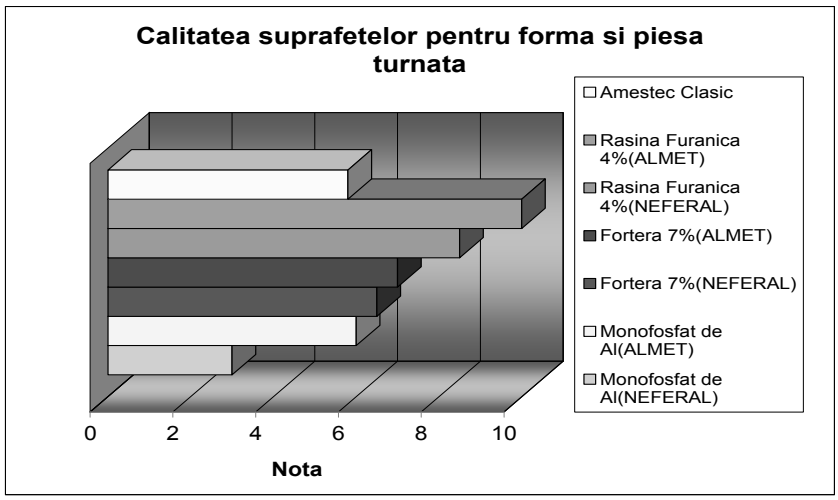

Fig. 13.Surface quality for the die and cast piece

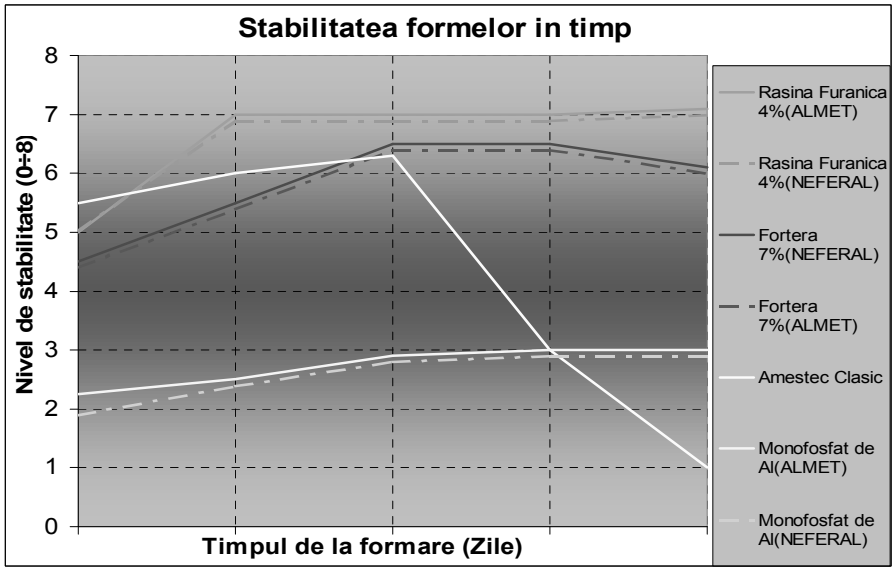

Fig. 14. Die stability in time

6. CONCLUSION REGARDING THE UTILIZATION OF THE SLAG AND DROSS AS REFRACTORY MATERIALS.

Prequesit wash of the dross in water at high temperature (30-60˚C) enlarge the degree of solubilization of soluble salts. Washing at temperature of 40˚C lead on at lower content of soluble salt Na and K in washed material and it's recommended the using of warm water at stage of washing.

For die cast used in gap 1-3 days, using of the washed dross it is favorable if the bending it is made with furan resin or with binder base on oligomer compound (Fortera; oligomer – through thermo destruction they put in liberty pyro carbide (carbon flocks).

For classical die cast in gap 1-3 days, using of the washed dross it is unfavorable for binders as sodium silicate or aluminum monophosfate which are dependents by the atmospheric condition, temperature, humidity, atmospheric

pressure. Humidity excess from this (un-dried) generates gas inclusion. The presence of the organic compound binded for this type of batch(base on washed or unwashed dross)favorable for quality of casting process and quality of cast die.

As final observation, the batch form all die with furan resin did not enlarge his volume, didn't have place the chemical reaction as in case of the study accomplish on unwashed dross, the difference was the type of the dross used, unwashed dross having salts. It can make a recommendation for using furan resin, having the best stability in time, having a die surface quality even and the cast piece superior than the classical batch, and the piece where it used as binder sodium silicate with fortusil - oligomeric compound.

The dross used from ALMET was superior then the dross from NEFERAL, having a superior cast piece quality in dies made with different binder.

In table 3 are systematically result regarding the experiments of using the slag/dross at loam.

Table 3 Characteristics of the loam with slag/dross proceeded for recycling the aluminum base of the binder utilization:

Characteristics*	**Loam**				
	Classic**	**Washed dross and binded with:**			
		Furan	**Sodium silicate**	**FORTERA**	**Monophosphate aluminum**
Branch point length, min	1÷5	15÷30	15÷60	10÷30	30÷120
Strengthen time, min	180÷480	30÷180	60÷480	60÷180	60÷480
Time stability	good	From mediocre at week	good	good	good
Stripping behavior	good	Very good	From god to satisfactory function by the ambient temperature and atmospheric humidity	Very good	Mediocre
Cast behavior	good after 8 hours from making	Very good after 60 min from making	Very good for 24 hours until 72 hours form making after this period appears the phenomenon of hygro scopic	Very good after 8 hours from making	Good after at least 24 hours from making
Debating characteristic	relatively good	Very good	good	V. very good	From satisfactory at good
Quality of the raw cast piece	Satisfactory	good	Satisfactory	Very good	good

**For surface of hollow mould unpainted, wall thickness ≈ 50 mm; ** Argil or bentonite*

OBSERVATION: The slag and dross can be used in foundry, combined with loam based on siliceous sand for realization die cast.

In this way it can revaluation the using of slag in utile way, so you don't have to throw them to the waste dump, so the slag and dross can be usable for loam at die casting from steel or cast iron with minimum costs, since these slag and dross can take the place in some limits the exothermal material in or thermo-insulating enough costing and showing a deficit in foundries of ferrous alloys (steel foundry) and big piece.

Bibliography:

1. "Aluminum Recycling", www.epagov/radiation/cleanmetals/does/tsd
2. "Secondary Aluminum Operations", www.epa.gov/ttn/chief/ap42/ch12/final
3. Sofroni.L, Elaborarea şi turnarea aliajelor, Editura Didactică şi Pedagogică, Bucureşti 1976
4. An Introduction to aluminium recycling process www.eaa.net/environment/recycling.asp
5. CeEx 53/2003 „ Metode de procesare a cenusilor reziduale din industria aluminiului secundar cu scopul prevenirii poluarii mediului si a conservarii resurselor naturale”

[1]-Univ. Politehnica Bucharest
[2]-INCDMNR, Bucharest

VALORIFICAREA DESEURILOR DIN INDUSTRIUA DE RECICLARE A ALUMINIULUI

Rezumat: In procesul de productie a aluminiului primar la fiecare tona de aluminiu obtinuta rezulta deseuri de compus solide de 2,88 tone. Prin inlocuirea in cadrul procesului de productie a aluminiului primar si aluminiului secundar este posibil sa se indeparteze aceste cantitati de sub-produs. Deseurile cu cantitate mare de aluminiu poat fi reciclate direct, pentru indepartarea lui prin returnare iar cele cu un procent mai mic de aluminiu, cenusile, pot fi utilizate ca material refractar in cadrul altor procese industriale. Acest studio propune o metoda alternative, viabila din punct de vedere economic, pentru a genera substante auxiliare si a diminua haldele de deseuri din industria de aluminiu.